Investigating The Role Of Aviation Fuels Hydrocarbon Chemistry On Its Autoxidation

Matthew Dwyer

December 2019

Investigating The Role Of Aviation Fuels Hydrocarbon Chemistry On Its Autoxidation

Matthew R. Dwyer

A thesis submitted in partial fulfilment of the requirements for the degree of Doctor of Philosophy

Department of Mechanical Engineering
The University of Sheffield

Supervisors
Dr Simon G. Blakey, Dr Ehsan Alborzi, Prof Anthony J.H.M. Meijer
and Dr Robert Woolley

December 2019

Acknowledgements

Completing this thesis would not be possible without the help and support of so many people.

Firstly, my thanks must go to my supervisors; Simon, Ehsan and Anthony for the opportunity to do this PhD. I have grown as a scientist and an engineer through their examples.

I would like to thank my group members in chemistry. Theo, for all his insight and for providing an exceptional example. Eren, for sharing every step with me and providing friendship through out. Heather, for bringing a much needed female influence to our group and providing so much support and friendship towards the end, it would have been a nightmare without you.

Much thanks also goes to my group members in the LCCC for providing so much experience, encouragement and engineering know how. Yousef and Charlie for making sure I wasn't the only PhD student. Thanks to Dmitry, Dave, Tim, Richard and Simon for providing all their technical support. Thanks also goes to Kevin Hughes, for providing access to another PetroOxy device.

A big thank to the tea crew for the laughs and advice. Phil, Tom, Maria, Simon and Andy for being terrible influences and expensive therapists. Mike, Quoc and Jonny for giving me time away from the PhD and Harris for putting up with me for the longest time.

I would like to thank my siblings: James, Abi, Siân, Megan and Michael (as well as David and baby Henry), for their encouragement, support and for being a sounding board for all of my complaints.

Finally I would like to thanks my parents, Mick, Kim and Leanne, for their love and for giving me the work ethic and ambition to finish the PhD, as well as for raising me with the curiosity needed to begin one in the first place.

Abstract

Advancements in jet engine design have led to improvements in efficiency and power output. As a result the operating temperature of the engine has steadily increased over the years. To counter this increased thermal load on the engine, aviation fuel is used as a heat sink, which leads to it becoming thermally stressed. The increase in temperatures in the fuel causes it to undergo autoxidation. In these conditions, insoluble material, such as gums and sediments, are formed in the fuel systems. eventually this build up of insoluble material leads to in-service issues and an increase in operating costs for engine manufacturers and airlines. Not all fuels behave the same in thermally stressed conditions, with the fuels chemical composition affecting this property, referred to as thermal stability. The importance of environmental concerns and security of supply issues have led to numerous alternative fuels to be exploited in recent years. However, the effect that their chemical composition has on their autoxidation behaviour is not well understood, as these novel fuels can have very different chemistry to historical stocks.

These novel fuels are chemically purer than conventionally derived fuels with lower concentrations of polar and sulfur species. As such, it is important to understand the role that an aviation fuels hydrocarbon composition has on its thermal stability, as this will become the dominant factor effecting their thermal stability. The work in this thesis focuses on understanding the mechanisms that govern the radical autoxidation of hydrocarbons and how their chemical and electronic structure affects these processes. Aviation fuels with well defined chemical composition, as well as individual hydrocarbon components, such as n-alkanes, cycloalkanes and aromatics are investigated in this study.

This thesis uses computational and experimental techniques to investigate the role that hydrocarbon composition has on the thermal stability of an aviation fuel. The PetroOxy oxidation stability tester is demonstrated as an

effective research tool for investigating the oxidation mechanism, with good repeatability of the data collected, and can study three distinct regimes of hydrocarbon oxidation. The induction period, rapid radical oxidation and slower oxidative coupling regimes are studied for fuels and mono-component hydrocarbons, with the results linked to findings in the literature. From this study, it is clear that aromatic hydrocarbon can act as antioxidants in the fuel by increasing the induction period, but eventually led to bigger issues with deposition in the fuels tested. As such, cycloalkanes offer an alternative, as they can alter the density of the fuel without sacrificing the thermal stability properties.

Density functional theory (DFT) has been used to construct pseudo-detailed mechanisms for the initial oxidation of three distinct classes of hydrocarbons, n-alkanes, cycloalkanes and mono-aromatics. These mechanism are able to demonstrate the fundamental differences between the three classes of hydrocarbons, and how these structural and electronic differences affect the kinetics of their autoxidation. However, this work also highlighted the need to correctly describe these radical reaction mechanism, as single reference method like DFT fail to model the bi-radical nature of many of these reactions. This phenomena is investigated further, by applying multi-reference and unrestricted electronic structure methods to the reactions of peroxides and peroxyl radicals. These reactions are shown to be vital to understand autoxidation, and the inclusion of computational calculated rate parameter for these reactions into pseudo-detailed mechanisms, allows them to be able to predict the oxidation rate of an industrial solvent in an isothermal tube reactor.

A key finding of this thesis is the importance of using multi-reference computational chemistry methods to investigate the radical reactions that occur in the autoxidaiton process, and using these calculations to construct a pseudo-detailed kinetic mechanism, in order to correctly model thermal stability and better understand the fundamental chemistry at play. This also offers an interesting challenge, as this work is at the cutting edge of applications for theoretical chemistry, and can provide a link from first principles to real world applications.

Contents

List of Figures

List of Tables

Glossary

Terminology

Thermal stability - The ability for a chemical or material to resist breakdown and change at increased temperatures.

Autoxidation - Oxidation that occurs spontaneously in presence of oxygen, usually at increased temperatures.

Fuel specification - Documents released by the standards agencies which control the production and properties of aviation fuel.

PetroOxy - PetroOxy thermal stability tester device, a small scale static tester.

Ab initio - From first principles.

Quantum chemistry - The use of quantum mechanical theories to investigate chemistry.

Wave function - Mathematical description of a quantum state.

Eigenvalue equation - An equation where a function is applied to an eigenvector to give a set of eigenvalues, i.e. the Schrödinger equation.

Electron correlation - Interactions between electrons in a quantum mechanical system, often used to refer to the error in this description.

Electronic structure - Description of the motion and position of the electrons in a system. Such as, a molecule.

Abbreviations

OEM - original equipment manufacturer

HiReTS - High Reynolds number Thermal Stability Tester

JFTOT - Jet Fuel Thermal Oxidation Tester

QCM - Quarz-Crystal Microbalance

DFT - density functional theory

PT - Perturbation theory

MCSCF - Multi-configuration self consistent field theory

CASSCF - Complete active space self consistent field theory

CASPT - Complete active space perturbation theory

CI - Configuration interaction

HF - Hartree-Fock

CCSD(T) - Coupled Cluster Single Double Triple

AtJ - Alcohol to Jet

HEFA - Hydroprocessed Esters and Fatty Acids

CHCJ - catalytic hydrothermal conversion jet

GC-MS - Gas Chromatography Mass Spectrometry

FTIR - Fourier-transform infrared spectroscopy

BAS - Basic Autoxidation Scheme

SMORS - Soluble Macromolecular Oxidatively Reactive Species

Introduction

The world is reliant on oil and petroleum products. Their chemical composition is vital for its uses in modern applications and has a dramatic effect on its performance properties. Petroleum is used for energy generation, pharma-ceuticals, chemical feed-stocks, and in construction. The biggest demand for oil comes from the transport sector, with road vehicles contributing to most of that demand. However, aviation is requiring a larger and larger share of the oil every year.[1] This can be seen in the change in oil use since 1973 in figure 1.1, as well as the growth in the overall use of oil in that time.
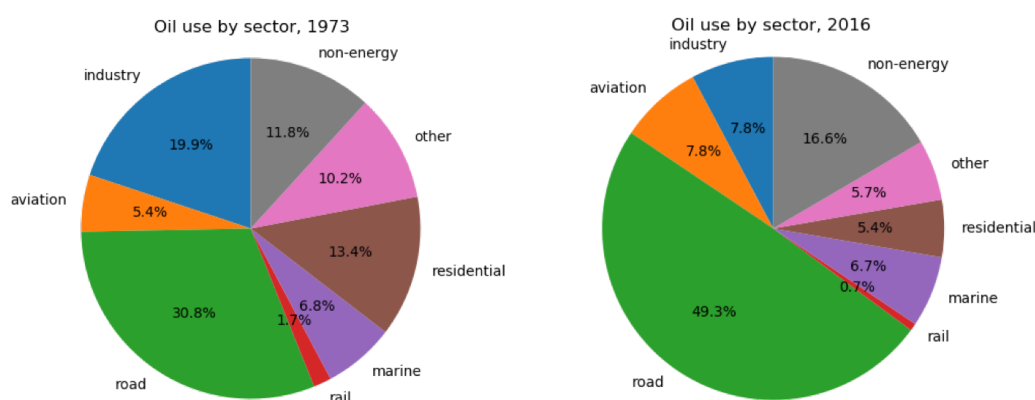
Fig. 1.1: Change in use of oil from 1973-2016. 2251 million tonnes of oil equivalent (mtoe) of oil was used in 1973 and an estimated 4650 mtoe was used in 2016.[1]

Until recently the chemical composition of the oil products used in transport has only been considered in terms of the fraction of the distillate that is used, as this affects the combustion behaviour and physical properties of the fuel. With greater understanding of the impact that the combustion products have on the environment, sulfur has been limited in most fuels, due to legislation imposed on the automotive sector. However, the effect that any fuel's specific chemical composition has on its properties is only just beginning to be under-stood. This thesis will focus particularly on how the chemistry of the major hydrocarbon component of oil effects the properties of aviation fuel. Namely one property, its thermal stability.[2]

1.1 History of aviation and fuel

The majority of modern aircraft operate using the jet turbine engine. Early work developing the engine began in the years following the First World War. However, it was not until the leaps in development taken by necessity, due to the Second World War that they entered production in 1944. These early jet engines developed further over the following decades, increasing in efficiency and performance and power output, leading to the rapid expansion of global air travel for both passenger and freight uses. This expansion has continued unabated since the 1970s, in spite of oil price spikes caused by wars in the Middle East or the market collapse of the commercial aviation sector after the 9/11 attacks.[3] The sector is expected to continue its expansion, at a rate of 2.5-4.4 % per annum, despite climate change and measures aimed at controlling its effects. Figure 1.2 demonstrates the results that these potential increases can have on the demand for fuel. On the current technology, If aviation's expansion is limited to 2.5 % per annum then an estimated 580 mtoe of fuel could be used by 2037, compared to the 362 mtoe used in 2016. However if it expands by 4.4 % on the current technology then 910 mtoe will be used by the aviation sector.[1, 3]

One driver is the economic growth and expansion of the middle classes in the developing regions of the globe, leading to expectations for greater access to air travel and trade. To meet this expansion in capacity, airplanes have generally increased in size and load since the 1970s and thus the jet engines used as propulsion have also been developed further. Technical developments to improve the engine have included the turbo-prop, increasing the by-pass ratios, turbo-jet and the move towards the high Mach number ramjet engines.[4] This means that jet engines have increased in power output, in-line with the improvements in combustion and fuel efficiency. The gains in performance have resulted in an increase in the operating temperatures of the jet engines. To ensure that there is no drop in performance this excess heat needs to be removed. The current solution is that the fuel is used as a heat sink.

The requirements for the fuel to act as a heat sink, in addition to its primary function as an energy source, has meant that not every hydrocarbon fuel is appropriate for use in aviation. In the early days of aviation, a wide cut of kerosene was used, as it was widely available and had suitable physical
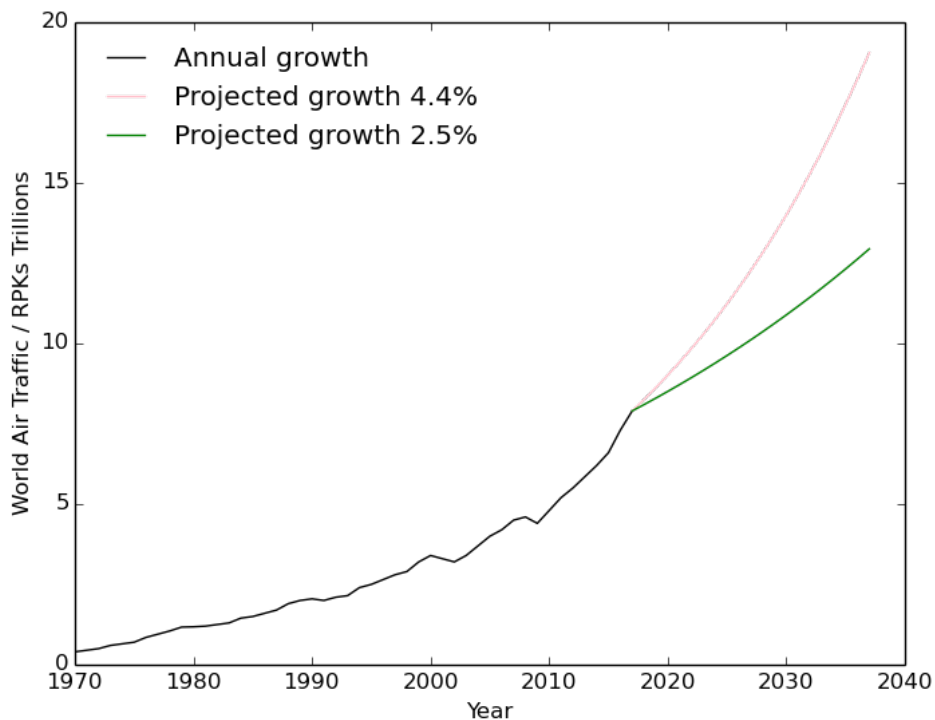
Fig. 1.2: Growth of air travel since 1970 in revenue passenger kilometers (RPK), with expected growth forecast up to the 2037, adapted from ICAO data.[3]

properties. However, due to increased development and specialisation of jet engines this is no longer true. As such, specialised aviation fuels have developed, which require specific properties to meet the demands of aviation. The fuel requires good combustion characteristics and high energy density to ensure its primary application as an energy source are met. Good lubricity, low volatility, and the correct distillation profile are also required to aid its handling and safety. To meet these specific requirements the fuels in service have specialised as discussed in the section below.

Environmental concerns and security of supply are new drivers for both engine efficiency and alternatively derived fuels, pushing operating temperatures even higher and requiring the fuel to take higher thermal loads.[5] As will be discussed below, this has lead to novel fuels to be derived from synthetic means or though use of non-petroleum hydrocarbon sources, with some finding their way into circulation as blends with the conventionally derived fuel Jet-A1.[6]

1.2 Fuel specification

The properties of aviation fuel and methods of production are controlled and regulated by the fuel specification documents released by a number of regulation bodies around the world. The most utilised fuel specifications are controlled by the American Society for Testing and Materials international (ASTM) in the USA, the Defence Standard (DEFSTAN) in the UK, GOST in Russia, as well as separate Chinese standards.[7, 8] Primary physical properties are controlled by the fuel specification documents including freezing point, appearance, distillation curves, and density. These requirements have an impact on the types of fuels that can be used and as a consequence the chemical compositions of such fuels. An example of this can be seen in the property of freezing point as straight-chain alkanes have freezing points too high for use at cold temperatures in polar regions and at high altitudes. However, branched alkanes have energy densities which are too low to meet specification. As such, for an aviation fuel to be within the specification, it is required have a mixed hydrocarbon composition.

The fuel specifications also provide controls on the concentrations of specific species in the fuel. The volume of aromatic hydrocarbons allowed in a fuel is limited to 25% and the volume of naphthalenes, which are multi-ring aromatics molecules, being limited to 3%. The fuel specifications also limits the concentration of impurities which can be found in the fuel, such as sulfur species, as they have a number of negative effects on the fuels properties or detrimental environmental impacts.

The aviation sector is likely to undergo changes in the near future caused by both internal growth and external pressures. The African and Asian markets are currently under-exploited, with expansion expected, driven by demand from the growing middle classes in those regions. This means that the sector will take up a greater share of the available oil. There is likely to be more differentiation in the types of aviation fuel available, due to the proliferation in the number of alternative fuels, with the rate of change in engine architecture unlikely to keep pace. There is also the rising concern about aviation's impact on climate change and pressure for strategies to combat it. This means changes in the engine to make them cleaner and more efficient, with the fuels expected to follow suit, particularly looking at the exclusion of sulfur from the fuels. Aviation fuel is currently treated as a commodity, purchased for use in

the sector at the lowest price, with its affect on the performance properties and thermal stability not being of the greatest concern. On top of the strong motivation to make alternative fuels for environmental reasons, they also offer an opportunity for the improvement in the fuel to become an enabler of new engine technologies, which would be limited with current fuels. These changes mean that a greater understanding of the affect that the chemistry of a fuel has on its properties is required.

1.3 Thermal stability, oxidation chemistry and mechanisms

One of the properties that the fuel specification documents controls is thermal stability.[9] Thermal stability is the property of a chemical to resist irreversibly breaking down, through oxidation or other decomposition mechanism, at high temperatures. The higher a chemical's thermal stability the greater its resistance to decomposition. These mechanisms of breakdown are treated separately, and happen at 2 different temperatures, as can be seen in figure 1.3. This thesis will focus on the thermal stability of aviation fuel with respect to oxidation.
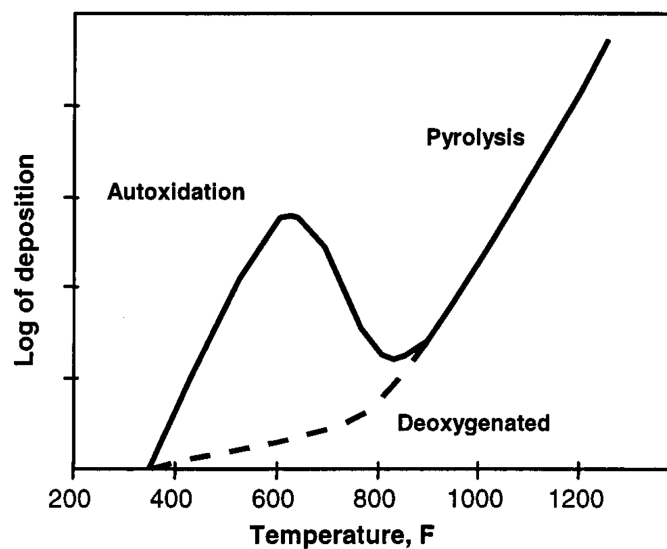
Fig. 1.3: The log of the deposit growth in the autoxidation and pyrolysis region, adapted from a figure by Spadaccini *et al* .[10]

Because the engines operate at higher temperatures, and the fuel is expected to remove this heat, the fuel is pumped around at increased temperatures.

This leads to in-service issues, as the fuel starts to form insoluble gums and deposits, which foul the fuel system. This reduces the effectiveness of the fuel as a heat exchange fluid and increases the temperature of the aircraft systems. To avoid this problem the airlines have to service the aircraft more frequently. Accordingly, decreasing the time between shop visits has an effect on the running costs of an OEM. This issue has other negative consequences as current engines are pushing at the temperature limit that they can put into current fuels. Increasing the efficiencies and power output of the engines further will greatly increase the risk of engine malfunction.

To ensure the quality of aviation fuel from a thermal stability perspective, the fuel is tested using the jet fuel thermal oxidation tester (JFTOT), to measure its breakpoint. The breakpoint is the highest temperature that a fuel still passes the specification pressure differential and deposit colour requirements.[7, 9] The test pressure differential rating is 25 mm Hg and the colour of the deposit is compared to the ASTM colour standard. These tests take quantitative and qualitative measures of the deposit, recording not only the colour and thickness of the deposit, but also the uniformity of the deposit. Additionally, the deposit thickness can be measured using the interferometric or ellipsometric methods. The minimum breakpoint temperature required for a conventional fuel to be suitable for use in flight is 260 °C.

Gums and deposits are formed in the fuel due to the increased temperature causing the fuel to oxidise at a rapid rate. The oxidation occurs as the hydrocarbons in the fuel react with the dissolved oxygen forming oxidation products such as alcohols, aldehydes, ketones and esters.[11] The oxidised products can react with the heteroatomic species naturally present in the fuel to form larger more polar products. This is in addition to the heteroatomic species reacting directly with the oxygen during oxidation. These oxidised products are more polar than the hydrocarbon fuel and as such will fall out of solution, forming the insoluble gums that remain in the bulk and deposits that can form on the wall, which lead to fouling and in-service issues. There can also be material formed that is partially or completely soluble, but which changes the physical properties of the fuel. The nature of the oxidised products will be discussed further in the literature review in chapter 3.

This highlight an important distinction to be made, the difference between thermal stability and oxidative stability. Thermal stability is the irreversible change of a chemical which leads to its properties changing and in aviation

fuel results in the formation of insoluble species. Oxidative stability is the ability of a chemical species to resist oxidation. Poor thermal stability can be caused by poor oxidative stability but they are not always interchangeable. An example would be the case of the phenols found naturally occurring in the fuel. They are thought to act as antioxidants in the fuel as they are preferentially oxidised instead of the bulk fuel. However, this is desirable in the fuel as it has been shown to improve the thermal stability of a fuel, and synthetic antioxidants are added to fuels with low phenol concentrations. The distinction between oxidative and thermal stability will be important later when reviewing the literature, and in the studies carried out in this thesis, as there are fuels that have can have a high thermal stability but be oxidised very quickly.
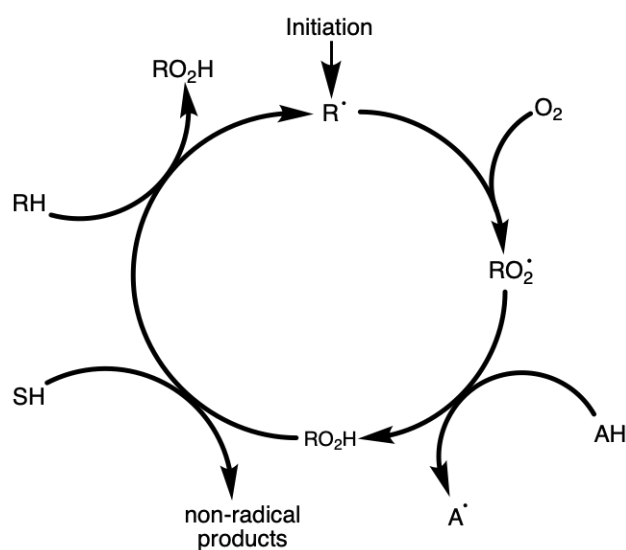
Fig. 1.4: The Basis Autoxidation Scheme (BAS) proposed by Bolland and Bateman, applied to aviation fuel by Zabarnick *et al*. This acts as a starting point for most hydrocarbon oxidation mechanisms.[12–14]

Returning to autoxidation, it is generally assumed to occur though radical reaction mechanisms. A radical refers to a chemical species with an unpaired electron. This results in radicals reacting rapidly through chain reactions. The reason for this is that each electronic orbital has a preference to be doubly occupied, by electrons of opposite spin. The reason for which will be covered in more detail in chapter 2. The hydrocarbons in the fuel undergo radical initiation at increased temperature. A number of possible mechanisms are proposed to initiate the oxidation of hydrocarbons. These routes include the abstraction of a hydrogen from the hydrocarbons in the fuel, by dissolved metals or peroxides in the fuel, or homolytic fission of the carbon-hydrogen bond.[14] This means that it can react with the dissolved oxygen rapidly,

forming peroxyl radicals, which are highly reactive species. A general mechanism for Basic Autoxidation Scheme (BAS) can be seen in figure 1.4, with the initiation step omitted, but the exact mechanism hasn't been determined yet.

The oxidation mechanism then progresses through a number of radical pathways. As radicals are unstable species, and thus very reactive, they allow for the formation of products which would otherwise not be possible in an apolar medium. Addition, disproportionation, elimination, and hydrogen transfer reactions occur until the alcohols, aldehydes, ketones, acids, and ester oxidation products are formed. These are the primary oxidation products. They affect the physical properties of the fuel and increase its acidity. However, they are not large enough or polar enough to form the gums themselves, as they are partially soluble in the fuel.

These primary oxidation products are more polar than the bulk fuel and as such they will start to aggregate together. This is driven by the decrease in the free energy of the system, in-spite of the entropic penalty, as the unfavoured polar-apolar interactions are minimised through this process. These aggregated oxidation products will then react further, allowing them to form larger molecular weight species, which are more extensively oxidised. These species are even more susceptible to oxidation, and will eventually become too polar to be soluble in the hydrocarbon fuel and will fall out of solution. This leads to insoluble sediments to form, which at higher temperatures can bind to the metal surfaces causing deposition. A number of suggested mechanisms have been suggested, including the SMORS mechanism proposed by Beaver *et al*, which can be seen in figure 1.5.
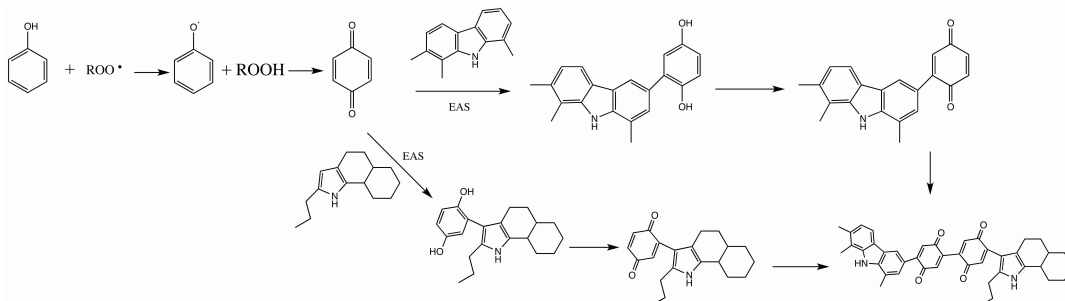
Fig. 1.5: SMORS mechanism proposed by Beaver *et al*, a possible route to the polar products to form insoluble material.[15]

The reason that the initial fuel cannot react directly with the dissolved oxygen directly is because of quantum mechanical selection rules. The ground state electronic structure of oxygen is a diradical triplet spin state. It is because of this diradical nature, that oxygen can only slowly oxidise species in the air, as reactions between the diradical oxygen and non-radical species are spin forbidden. Incidentally, it is for this reason that life on earth is able to occur.

1.4 Fuel composition, oil fields and production methods

As has been discussed previously in the introduction, a number of petroleum and alternatively derived products are suitable for use as jet fuels. Fuel produced from petroleum sources are referred to as conventional fuels. However, they can have varied chemical composition depending on the origin of the oil and the production methods employed. Understanding the composition of the fuel that is extracted from each oil field is important, because as different oil fields are being exploited, the chemistry of the final jet fuel can change. As an example, fuels derived from Brent crude or west Texas sources demonstrate superior thermal stability to those from Venezuelan or Indonesian sources because the latter two sources have high concentrations of heteroatomic impurities in them.

Conventional fuels are formed from the middle-distillate fraction of the oil and have an average carbon chain length of ten to sixteen. They can also have high concentrations of iso-alkane and aromatic compounds in the fuel, which alter the chemical composition, physical properties and thermal stability of the fuel. The breakdown of the oil products obtained from the major oil fields of the world can be seen in figure 1.6. The concentration of heavy oil waxes and sediments found in the oil is usually a good indication of the concentration of minor heteroatomic species in the fuel, which contribute to lower thermal stability. These minor components include sulfur and phenolic species, as well as some aromatic nitrogen species.

These minor components can be removed from the fuel to improve the thermal stability by hydrotreating the straight run distillate using a heterogeneous catalyst. Hydrogenation can be used to chemically reduce the heteroatomic species found in the fuel into hydrocarbons and gaseous product, with these
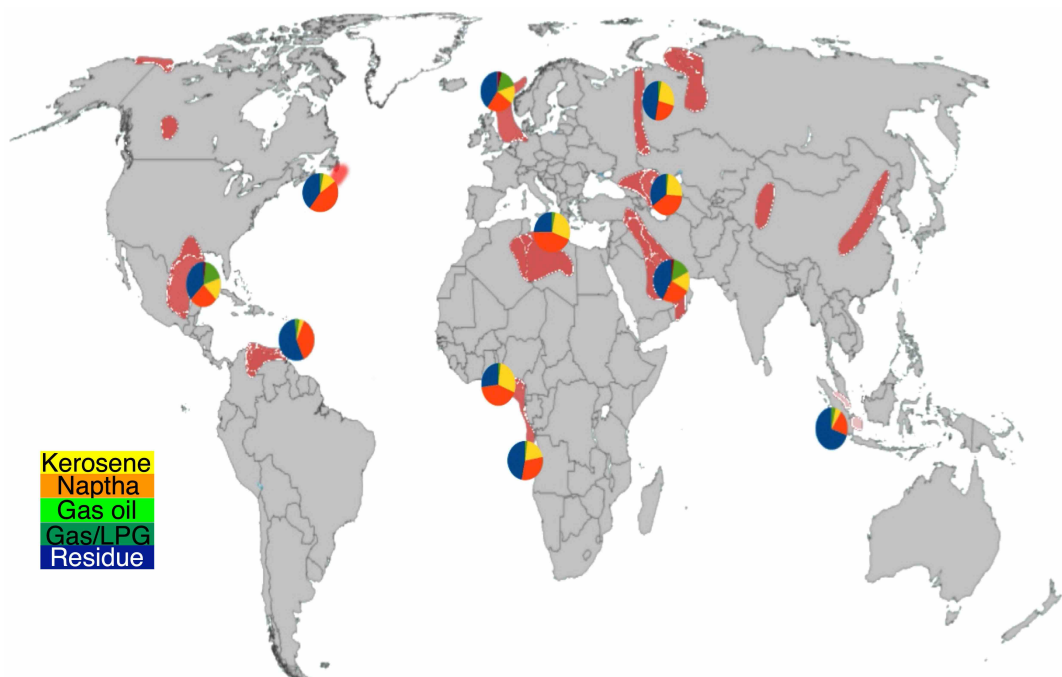
Fig. 1.6: Breakdown of the oil products obtained the worlds major oil fields. The yellow segment indicates kerosene, and the orange segment is the naphtha. the dark green segment is gas/LPG and the light green is gas oil. The dark blue segment indicates the amount of residue in the atmospheric distillate.[16–18]

reactions summarised in figure 1.7. Separate processes exist for sulfur, nitrogen and oxygen species. Previous studies have shown that changing the extent of hydrotreatment of a straight run fuel impacts its thermal stability.[2] Mild hydrogenation to remove the polar species improved the breakpoint of a reference fuel used in the study by 68 °C to 354 °C. This is a significant increase, so clearly these heteroatomic species which form a minor component in the fuel, make a major contribution to the thermal stability of a fuel.

To improve control over the chemical composition of the fuel even further, and thus provide improvements of its thermal stability, further hydrotreatment can carried out. More specialised catalysts are used to further alter the fuel. They hydrogenate the unsaturated hydrocarbons, such as alkenes and aromatics, to alkanes. These processes have the effect of producing a fuel which is more chemically pure and demonstrates improved thermal stability. This more severe hydrotreatment increased the breakpoint of the same reference fuel in the previous study to >371 °C.[2] It can be deduced from this, that while the minor components have the main contribution to a fuel thermal stability properties, the hydrocarbon composition also has an important role in
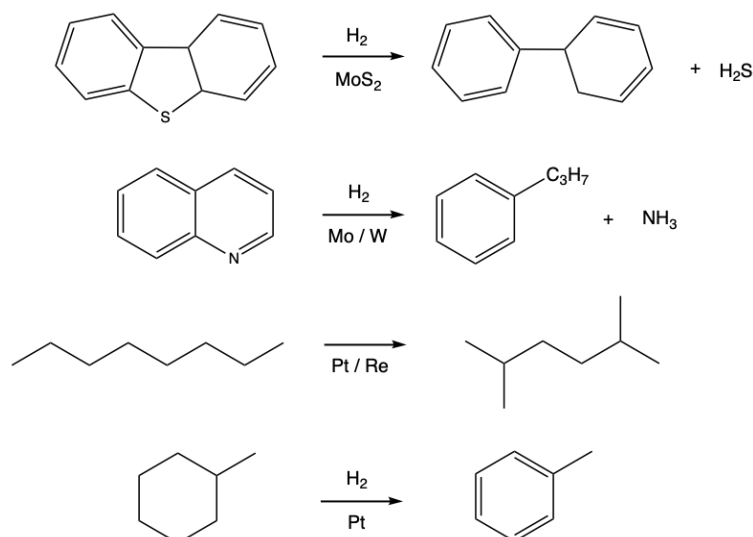
Fig. 1.7: Example of hydrogenation, dehydrogenation and isomerization processes used in refineries.

determining this behaviour. There is some logic to this, as the hydrocarbons form the oxidation products and insoluble gums, so changing composition should affect these mechanisms. This is demonstrated by the behaviour of the single fuel that was used in this study.[2]

There are other processes that are employed in the production of conventional fuel. These convert oil from natural gas condensates, heavy oil residues and shale and oil sands into aviation fuel. To do this the feed-stock is cracked and catalytically reformed into alkanes and aromatic hydrocarbons with the correct physical properties for use in aviation. Despite the high processing, changing the feed-stock has an affect on the thermal stability and chemical composition of the fuels derived from them. For example, fuels manufactured from the heavy oil residues left over after the distillation process generally have more sulfur and oxygenated polar species in them, reducing the thermal stability, or requiring a large amount of post-production processing to remove them. These production methods lead to improvements in the fuels thermal stability. However, they increase the cost of production and the fuel. These processes can also have the result of negatively effecting other physical properties such as reducing the lubricity of the fuel. This increased processing can also lead to higher metal contamination from increased contact with metal catalysts. which can further exacerbate the thermal stability problem.

Compounding this is the increased utilisation of shale and oil sand derived fuels, and all of the issues being reported in relation to their use, means that these in-service issues are likely to increase in the future even using the current engine architecture. However, the use of heavy oil residues, shale and oils sands is only going to increase as the economic drive for oil requires their exploitation. A summary of the production processes used in an oil refinery can be seen in the figure 1.8.
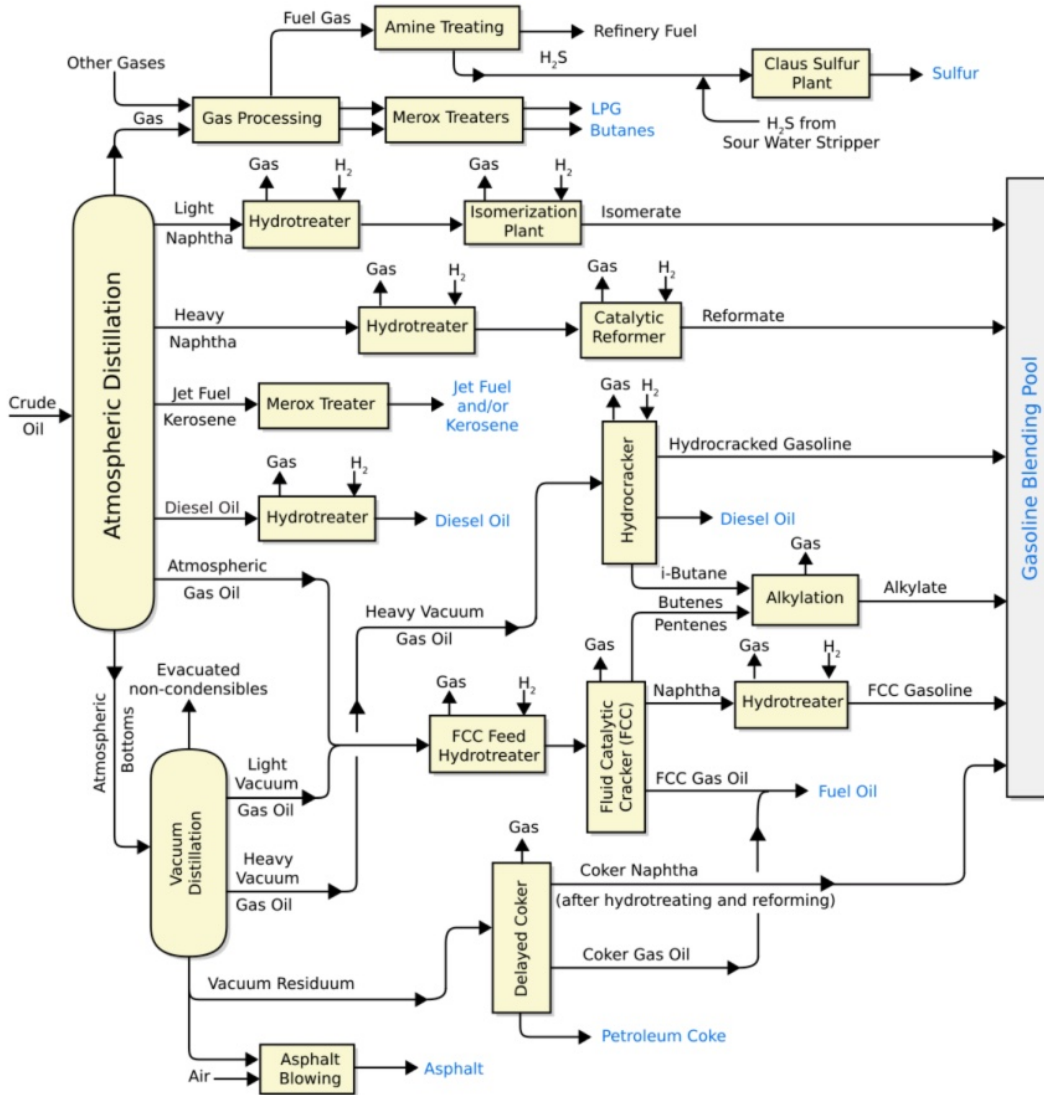
Fig. 1.8: Flow diagram of the typical processes carried out in an oil refinery. Adapted with permission from a figure on Wikipedia commons. [19]

Aviation fuel can also be produced from hydrocarbon sources other than petroleum. These fuels are referred to generally as alternative, or synthetic fuels. There is currently four commonly used approved methods for the production of these synthetic fuels.[20] These are:

1. Fisher-Tropsch synthesised paraffinic kerosene (FT-SPK).

2. Synthesised paraffinic kerosene from hydroprocessed esters and fatty acids (SPK-HEFA).

3. Synthesised iso-paraffin's from hydroprocessed fermented sugars (SIP-HFS).

4. Alcohol-to-Jet synthetic paraffinic kerosene (ATJ-SPK).

Because of this wide variety of hydrocarbon sources these fuels can have varied compositions. However, synthetic fuels generally undergo post-production processing. This improves the chemical purity of these fuels by removing the polar species found in the feedstocks. Alternative fuels can potentially have very high thermal stability compared to straight-run kerosene. However, this is dependent on the feedstock and manufacturing processes used.

Fisher-Tropsch fuels are the most utilised alternative fuels currently in production. They are produced from hydrocarbon sources, such as coal and natural gas, which are converted into syngas using the steam-reforming reaction. For this process any hydrocarbon source can be used, but these fuels have developed in regions where oil is not readily available. As such, coal is usually used as the hydrocarbon source. The syngas is used in the Fisher-Tropsch reaction to form long chain hydrocarbons, known as Fisher-Tropsch waxes. The Fisher-Tropsch waxes are hydrocracked to form kerosene suitable for use in aviation. The composition of the fuel produced can be controlled by the selection of catalyst. Fisher-Tropsch fuels are chemically very pure and demonstrate high thermal stability. However, the reduced polar and aromatic concentrations in the fuel can have a detrimental effect on its other physical properties. This can be solved by the use of fuel additives to improve lubricity. Despite the potential performance improvements from using Fisher-Tropsch fuels, there is a high cost involved in their production because of the number of processes, high operating temperatures and expensive catalysts needed. This has limited their use to this point, outside of areas where political situations have made oil alternatives a necessity.

The other alternative fuels approved for use in blends are derived from bio-sources. These can be animal fats, crops cultivated for use, sugars and farming waste, which can be converted into into hydrocarbons suitable for

use in aviation. A number of production routes are used for converting the biological feedstock into aviation fuel. For the production of SPK-HEFA oil and fats undergoes trans-esterification with alcohols, which converts these highly branched carbohydrates into smaller straight chain molecules. These esters are usually hydroprocessed into hydrocarbons with the correct molecular weight for use as an aviation fuel. Their thermal stability and impurity levels are heavily linked to the feedstock, and the level of post production processing, such as hydrotreatment. If they are from a clean source, with low metal and polar contamination, and undergo hydrotreatment these fuels can show very high thermal stability. Synthetic fuels have been approved for use in blends with conventional fuels. As such, this can reduce the overall production cost for a synthetic source to a final fuel, but because of the ratios of blending they can have properties indistinguishable from conventional fuels and fall under D1655.[7]

Other methods for the production of bio-fuels, include the production from iso-paraffin's from hydroprocessed fermented sugars and Alcohol-to-Jet fuels. The synthesised iso-paraffins originate from the production of farnesene, a branched alkene, which can then be hydroprocessed into saturated iso-alkanes. The farnesene is produced from fermenting sugars from agricultural waste. The final method for the production of synthetic fuel is to use ethanol and iso-butanol from crop cultivation as a feedstock. The feedstock then undergoes dehydration, oligomerisation and hydrogenation to produce hydrocarbons in the jet range. These bio-fuels have very high chemical purity, and thus demonstrate good thermal stability properties. However, because of the need to cultivate crops for their production, they can effect food security and have environmental impacts. because of this increased demand for sustainability in the aviation sector a number of new production routes are in various stages of development. These routes include the utilisation of waste carbon from the waste of agricultural and industrial processes, as well as converting carbon dioxide in the air to fuel.

1.5 Aims and thesis outline

As aviation develops and expands thermal stability is becoming a more significant issue. The fuels used for jet engines will become more specialised to extract greater performance from the fuel and improve the efficiency of the engines. However, this requires a more detailed understanding of the role a

fuels specific chemistry has on its properties than is currently available. It is clear that not all fuel is the same, and as such not only the minor components affect it thermal stability, but the bulk hydrocarbon component matters greatly as well. This is particularly true with the expansion of the use of synthetic routes to jet fuel, which have little to no heteroatomic species due to the rather harsh production pathways, and as such the thermal stability of these novel fuel will be dominated by the hydrocarbon component. However, it is currently not clear what role each hydrocarbon class has on its thermal stability properties and the development of the jet engine is being stifled by this lack on knowledge. With a greater understanding of how a fuels chemical composition affects its properties, they can be tailored for a specific purpose, and help facilitate future improvements.

As such the overriding aim of this thesis will be to demonstrate that an aviation fuels hydrocarbon composition matters, it should be considered when selecting fuels for test programs and use in service, and that it can negatively affect its performance and thermal stability. The hope would be that this leads to synchronised improvements in the engines and fuels, leading to faster advancements.

A more specific aim of this thesis will be to challenge the assumption that a fuels thermal stability originates solely from the minor components, and that the bulk hydrocarbon chemistry plays no part. The classes of hydrocarbon discussed in this thesis have different physical properties, utilised to the fuels advantage, but also very different chemistries available to them. Aromatic hydrocarbon undergo electrophilic substitution reactions a class of reactions unique to them. Electronic conjugation and conduction effects also determine a hydrocarbons reactivity. This thesis will investigate the hydrocarbon chemistry and attempt to highlight their differences, showing that they must be taken into account when trying to understand thermal stability, and the oxidation mechanism which govern the process.

This thesis will take a multi-disciplinary approach to investigate the problem of thermal stability in aviation and the oxidation mechanisms that cause the insoluble products to form. An aim of the thesis is to demonstrate the usefulness of computational chemistry methods and show their power as a tool to aid in the understanding of thermal stability. This thesis will also attempt to link these fundamental quantum chemistry calculations to experimental work. This is to validate the fundamental work carried out and allow for these

oxidation models to aid in the development of future fuels. These methods will be used to understand the detailed reactions mechanisms that take place in the oxidation aviation fuel. Peroxide species are thought to play a crucial role in the formation of oxidation products. However, it is still not clear what that role is, with a number of intermediates and reaction routes suggested, all encompassing complex electronic spin configurations. As such this thesis will investigate these reactions and mechanisms in the hope of providing clarity on these processes.

The fuels being used in the future will have an increasingly higher synthetic and chemically purer composition, hence they will be less like what is currently found in service, and historical knowledge will be less valid. For this reason it is of particular importance to carry out this work now, as the fuel is likely to change rapidly due to environmental concerns and supply changes, so we need to understand how these changes will affect its properties. This thesis will focus particularly on the changes to thermal stability that having chemically purer synthetic and hydrotreated fuels has on the fuel through a study of the response of the hydrocarbon composition to thermal stressing.

The outline of this thesis is as follows:

1. Chapter 2 gives an introduction to the important quantum mechanics and electronic structure concepts needed for the rest of the thesis. This is intended to be a self-standing piece of work and not require the reader to have to consult electronic structure and quantum mechanics textbooks in order to understand the arguments being made within.

2. Chapter 3 is a literature review, focusing on the role of that the chemical components in the fuel has on its thermal stability, the existing mechanisms that govern this thermal stability and previous methods modelling the process. A brief amount of time will dedicated to the physical phenomena that affect this chemistry.

3. Chapter 4 presents the main experimental and modelling results of this thesis. The experimental studies will investigate the thermal stability of fuels and surrogate hydrocarbon blends in the PetroOxy static thermal stability tests, and analysis the products formed using GC-MS, FTIR and UV-Vis. The modelling work will focus on the development of detailed

kinetic mechanisms for specific classes of hydrocarbon, namely: n-alkanes, cyclic alkanes and mono-aromatic.

4. Chapter 5 studies the chemical reactions of peroxides and peroxyl radicals found in the fuel using multi-reference electronic structure methods. This chapter will provide fundamental understanding of the quantum mechanical phenomena that allow for these reactions to progress rapidly and inclusion of the results allows for the improvement kinetic predictions.

5. Chapter 6 offers a general discussion on the results methodology presented in this thesis, the implications on the thermal stability field, and to the understanding of the autoxidation mechanism.

6. Chapter 7 provides some conclusions originating form this study and makes recommendations for future work.

7. Chapter 8 is a list of published work originating from this thesis at the time of submission.

Theoretical Methods 2

Quantum mechanics, and thereby computational chemistry techniques used in this thesis, has its origins from the beginning of the 20th century. This development started with the need to find solutions to the black body and photoelectric problems in classical physics. Planck achieved this through the quantization of the treatment of energy, and subsequently, with Einstein postulation that light had particle-like properties and matter having wave-like properties. These early theories of quantum mechanics culminated in the concept of wave-particle duality, with de Broglie proposing in 1924 that the wavelength of light is related to its momentum,

$$\lambda = \frac{h}{p}. \tag{2.1}$$

This means that atoms and molecules can be treated as having wave-like properties.[21] This had important consequences for how scientists viewed chemistry and the physical description of the atom.[22, 23] The current model of the atom has the electrons in "orbitals" surrounding the nucleus. These orbitals represent the probability amplitude of finding the electron. For an extended system such an atom or molecule, the set of orbitals is referred to as the electronic structure. We can characterise the electronic structure by the quantum numbers of the orbitals, particularly for atoms and linear molecules.

For atomic systems the principal quantum number, n, denotes the electronic shell the orbital is in. The azimuthal quantum number, l, denotes the sub shell. It is also called the angular quantum number, as it causes the shape of the orbital i.e. s, p, d and f orbitals. The magnetic quantum number, m_l, gives the projection of the orbital. All of these quantum numbers have analogies in classical mechanics. However, quantum mechanical particles also have a spin quantum number, m_s, which is intrinsic to quantum mechanics and has no classical description. The allowed values for the electrons spin are $+\frac{1}{2}$ and $-\frac{1}{2}$ since electrons are fermions. Molecular systems are more complex and can not easily be described using this set of quantum numbers.

Electronic spin is vital to chemistry in general and the radical reactions investigated in this thesis in particular. Two electrons of the same spin cannot occupy the same orbital, as is stated by the Pauli exclusion principle. This means that they cannot form a new bond. When radicals react together, they must therefore pair up and have opposite spin. This will be of particular importance to the reactions of peroxides and peroxyl radicals investigated in chapter 5.

The application of quantum mechanics to chemistry presented new problems and required new methods for investigating the electronic structure of atoms and molecules. This started in 1925 with Heisenberg's development of matrix mechanics and with Schrödinger developing wave mechanics in 1926.[24–31]

2.1 Schrödinger equation

In 1926 Schrödinger developed solutions to quantum mechanical problems through wave mechanics and applied it to a non-relativistic and time-dependent system,

$$\hat{H}\Psi(t) = i\hbar\frac{\partial\Psi}{\delta t},\tag{2.2}$$

where, Ψ, is the wave function of the system.[32, 33] The wave function completely describes a system of particles, but has no physical meaning and cannot be measured. However, $|\Psi|^2$, is the probability density of the system, which gives the probability of finding a quantum mechanical particle, and is a measurable value of the function within a finite space. $\hbar$ is the reduced Planck's constant and i indicates that this problem is complex. $\hat{H}$ is the Hamiltonian operator. If $\hat{H}$ does not depend on time the time-independent Schrödinger equation can be extracted from this time-dependent equation. This is done by separating the wave function into its spatial, (r), and temporal, (t), components, also known as its space and phase components

$$\Psi(r, t) = e^{-\frac{iEt}{\hbar}}\psi(r).\tag{2.3}$$

This separation of the wave function allows for the time-dependent Schrödinger equation to be rewritten as

$$\hat{H} e^{\frac{-iEt}{\hbar}} \psi(r) = i\hbar \left(\frac{-iE}{\hbar} \right) e^{\frac{-iEt}{\hbar}} \psi(r). \tag{2.4}$$

As the wave function is not a measurable property of the system, and only the $|\Psi|^2$ has physical meaning, the phase component of the time-dependent Schrödinger equation can be cancelled out. This means that if the Hamiltonian applied to the system does not depend on time, the Schrödinger equation becomes independent of time

$$\hat{H} \psi(r) = E \psi(r). \tag{2.5}$$

Equation 2.5 is only true if the Hamiltonian for the system is not time-dependent, and has stationary states which do not alter as a function of time, such as low energy minima on the surface. These stationary states are related to properties that chemists are interested in, such as orbitals, equilibrium geometries and the energies associated with them. Thus, for most properties of interest to the chemical sciences, the simpler time-independent Schrödinger equation can be used.

Equation 2.5 is an eigenvalue equation, where the Hamiltonian operator acts on the the eigenfunction $\psi(r)$, to give a set of eigenvalues for that eigenfunction. Solving this equation for a many-body system is not a trivial problem, and can only be achieved exactly for simple systems such as the hydrogen atom, without the problem becoming intractable. For more complex systems, such as the ones of interest to us in this thesis, approximations must be made, both in the implementation of the Hamiltonian and the wave function.

2.2 Hamiltonian operator

The Hamiltonian is an operator, which acts on a set of eigenstates, to give a corresponding set of eigenvalues, also known as its spectrum.[22, 34, 35] It contains the kinetic, $\hat{T}$, and the potential energy, $\hat{V}$, operators

$$\hat{H} = \hat{T} + \hat{V}. \tag{2.6}$$

The kinetic component can be further broken up into the movement of the electrons and nuclei described by some set of electronic and nuclear coordinates, i and A, in the system. As a consequence it's solution wiil be,

$$\hat{T} = -\sum_i \frac{\hbar^2}{2m_e}\Big(\frac{\partial^2}{\partial x_i^2} + \frac{\partial^2}{\partial y_i^2} + \frac{\partial^2}{\partial z_i^2}\Big) - \sum_A \frac{\hbar^2}{2}\Big(\frac{1}{M_A}\frac{\partial^2}{\partial x_A^2} + \frac{\partial^2}{\partial y_A^2} + \frac{\partial^2}{\partial z_A^2}\Big), \tag{2.7}$$

where m_e is the mass of an electron, and M_A is the mass of the nuclei. This can be rewritten more concisely as

$$\hat{T} = -\frac{\hbar^2}{2m_e}\sum_i \hat{\nabla}_i^2 - \frac{\hbar^2}{2}\sum_A \frac{1}{M_A}\hat{\nabla}_A^2, \tag{2.8}$$

where $\hat{\nabla}^2$ is the laplacian and represents a 3-dimensional partial differentiation,

$$\hat{\nabla}^2 = \Big(\frac{\partial^2}{\partial x^2} + \frac{\partial^2}{\partial y^2} + \frac{\partial^2}{\partial z^2}\Big). \tag{2.9}$$

The potential energy operator, $\hat{V}$, describes the interactions between the particles in the system. This includes repulsive nucleus-nucleus and electron-electron interactions, as well as an attractive interaction between the electrons and the nuclei

$$\hat{V} = +\frac{e^2}{4\pi\varepsilon_0}\Big(\sum_{A>B}\frac{Z_A Z_B}{R_{AB}} + \sum_{i>j}\frac{1}{r_{ij}} - \sum_{A,i}\frac{Z_A}{r_{Ai}}\Big), \tag{2.10}$$

as described through Coulomb's law. The entire Hamiltonian operator can be written as

$$\hat{H} = -\frac{\hbar^2}{2m_e}\sum_i \nabla_i^2 - \frac{\hbar^2}{2}\sum_A \frac{1}{M_A}\nabla_A^2 + \frac{e^2}{4\pi\varepsilon_0}\left(\sum_{A>B}\frac{Z_A Z_B}{R_{AB}} + \sum_{i>j}\frac{1}{r_{ij}} - \sum_{A,i}\frac{Z_A}{r_{Ai}}\right).$$

<div align="right">(2.11)</div>

This expression can be simplified by setting the physical constants, e, m_e, $\hbar$ and $4\pi\varepsilon$, where ε_e is the electrical permeability of free space, to 1. As follows in 2.12

$$\hat{H} = -\frac{1}{2}\sum_i \nabla_i^2 - \frac{1}{2}\sum_A \frac{1}{M_A}\nabla_A^2 + \sum_{A>B}\frac{Z_A Z_B}{R_{AB}} + \sum_{i>j}\frac{1}{r_{ij}} - \sum_{A,i}\frac{Z_A}{r_{Ai}}. \qquad (2.12)$$

In this system of units the energy associated with the Schrödinger equation is now the given in the units of Hartrees, which is 2625 kJ mol^{-1} or 631 kcal mol^{-1}. The Schrödinger equation is exact until this point, but can be simplified even further by applying the Born-Oppenheimer approximation.

2.3 Born-Oppenheimer approximation

All methods used in this thesis rely on the Born-Oppenheimer approximation, which states that the kinetic energy terms of the electrons and the nuclei can be decoupled from each other. This idea originates from the simple concept that the nucleus is far heavier than the electron, $\sim$1800 times more in the case of the hydrogen atom. As such the kinetic energy terms of the electrons operate on very different scales to those of the nuclei. The Born-Oppenheimer approximation was proposed in a paper by Born and Oppenheimer in 1927, where they demonstrated that the wave function can be separated into a nuclear and electronic component, leading to equation 2.13.[36, 37] Here, $\Phi(r; R)$ is the electronic wave function for a set of electronic coordinates in a fixed nuclei framework and $\chi(R)$ is the nuclear wave function for this set of coordinates

$$\Psi(r, R) = \Phi(r; R)\chi(R). \qquad (2.13)$$

The way that the Born-Oppenheimer approximation is implemented in electronic structure calculations, is through the clamped nucleus approach, where the electronic Schrödinger equation is solved for a series of stationary nuclear coordinates. The nuclear coordinates can then be re-optimised for this new electronic potential. The clamped nuclear electronic Schrödinger equation is written as

$$\hat{H}_{el}\Phi(r;R) = E(R)\Phi(r;R). \tag{2.14}$$

Here the electronic energy for a single set of nuclear coordinates, $E(R)$, is obtained with the electronic wave function at this set of coordinates. The electronic Hamiltonian has the nuclear kinetic operator omitted, and the nuclear-nuclear potentials is treated as constant, when written in atomic units the Hamiltonian has the form

$$\hat{H}_{el} = -\frac{1}{2}\sum_i \nabla_i^2 + \sum_{A>B} \frac{Z_A Z_B}{R_{AB}} + \sum_{i>j} \frac{1}{r_{ij}} - \sum_{A,i} \frac{Z_A}{r_{Ai}}. \tag{2.15}$$

This can be written more compactly as

$$\hat{H}_{el} = \hat{T}_e(r) + \hat{V}_{eN}(r;R) + \hat{V}_{NN}(R) + \hat{V}_{ee}(r). \tag{2.16}$$

From equation 2.16 a few important points should be made. The first being that due to the $\hat{V}_{eN}(r;R)$ term, the electronic and nuclear components of the Hamiltonian cannot be fully separated. Thus, the wave function cannot be separated either, which increases the complexity of the problem. The second important point to note is that the $\hat{V}_{NN}(R)$ term is a constant, which shifts the energy, but does not perturb the solution. Applying the electronic Hamiltonian allows for the eigenvalues for a set of stationary nuclear coordinates to be calculated. The second step is to optimise the nuclear coordinates to reduce the repulsive nuclear-nuclear potential terms for the electronic potential calculated using the electronic Schrödinger equation. This allows the full eigenvalue equation to be written as

$$\hat{H}_{el} \sum_i \Phi_i(r; R)\chi_i(R) = E(R) \sum_i \Phi_i(r; R)\chi_i(R). \qquad (2.17)$$

The motion of the nuclei in the electronic potential can be calculated using the nuclear Schrödinger equation in 2.18. In this equation the kinetic energy of nuclei is calculated in a field potential casued by the movement of the electrons. This field potential originates from solving the electronic Schrödinger equation, and from solving the nuclear Schrödinger equation, the vibrational levels for a specific electronic state can be calculated.

$$\hat{H}_{nucl}\chi(R; r) = E(r)\chi(R; r). \qquad (2.18)$$

From solving the electronic and nuclear Schrödinger equations we can get the equilibrium molecular geometry, ground state electronic structure, as well as the spectroscopic and thermodynamic properties of a molecule can be determined from first principles. Solving the electronic Schrödinger equation for a set of coordinates results in a potential energy surface, which is a powerful tool for investigating chemical reactions, and will be discussed in more detail later in the chapter.
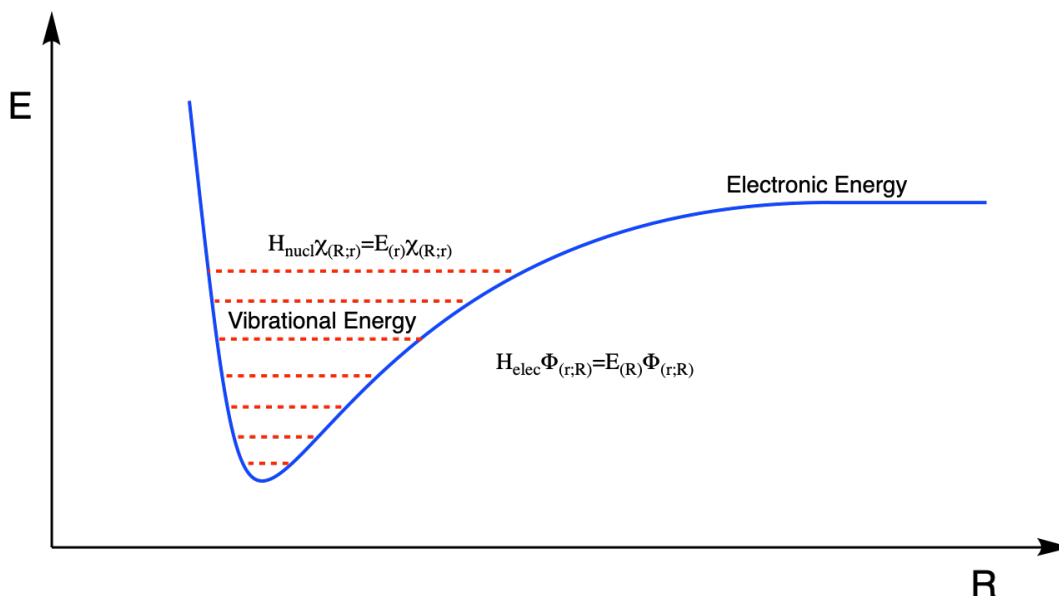
Fig. 2.1: Potential energy surface of a diatomic molecule, generated from solving the electronic and nuclear Schrödinger equations.

2.4 The variational principle

The central aim of the electronic structure theory is to solve the eigenvalue equation, namely the Schrödinger equation. To do this, a trial set of eigenvalues is calculated, and must be able to be minimised to the true minimum energy. To do this, the variational principle is used, which states that for a normalised wave function the expectation value of the Hamiltonian is larger than or equal to the true ground state energy of the system. To demonstrate this and discuss quantum mechanics theories further, we must first introduce Dirac's bra-ket notation.[38]

Bra-ket notation allows for the wave function and operator to be described in an n-dimensional space, known as the Hilbert space. If we take the example below the left hand term, the bra, is usually a column vector, with the right hand term, or the ket, being a row vector. This makes the solution, or action, a scalar product of the 2 vectors,

$$\langle \Phi_a | \Phi_b \rangle, \tag{2.19}$$

$$\langle \Phi_a | \Phi_b \rangle = \begin{pmatrix} a_1^* & a_2^* & \cdots & a_n^* \end{pmatrix} \begin{pmatrix} b_1 \\ b_2 \\ \vdots \\ b_n \end{pmatrix} = \sum_{i=a}^{n} a_i^* b_i \tag{2.20}$$

The closed bra-ket in equation 2.19 also represents the integral of the wave function over the Hilbert space,

$$\langle \Phi_a | \Phi_b \rangle = \int \Phi_a^* \Phi_b dr. \tag{2.21}$$

If we write the eigenvalue equation in bra-ket notation we get equation 2.22

$$\hat{H} | \Phi_a \rangle = \varepsilon_a | \Phi_a \rangle. \tag{2.22}$$

If we assume that eigenfunction $|\Phi_a\rangle$ is orthonormal to another eigenfunction $|\Phi_b\rangle$, in that they are orthogonal to each other and normalised over all Hilbert space then the overlap is

$$\langle\Phi_a|\Phi_b\rangle = \delta_{ab}. \tag{2.23}$$

The δ_{ab} is the Kronecker delta and it equal 1 if $a = b$ the 0 if $a \neq b$. How orthonormality is imposed on a wave function will be discussed in the next section. When Kronecker delta is equal to 1 their is full overlap of the wave functions. If the $\langle\Phi_b|$ is applied to equation 2.22 then we get

$$\langle\Phi_b|\,\hat{H}\,|\Phi_a\rangle = \varepsilon_a\delta_{ab}. \tag{2.24}$$

We can use equation 2.24 to prove that solutions to the eigenvalue equation satisfy the variation principle. If we have a normalised trial wave function then the expectation value can be used as the upper bound of the true ground state energy

$$\langle\tilde{\Phi}|\,\hat{H}\,|\tilde{\Phi}\rangle \geq \varepsilon_a. \tag{2.25}$$

Where we only achieve equality if the trial wave function is the true wave function, $|\tilde{\Phi}\rangle = |\Phi_0\rangle$. This can be proven by taking a trial function, which is written as a linear combination of eigenfunctions. Thus, we get equation 2.26

$$\langle\tilde{\Phi}|\tilde{\Phi}\rangle = 1 = \sum_{ab}\langle\tilde{\Phi}|\Phi_a\rangle\langle\Phi_a|\Phi_b\rangle\langle\Phi_b|\tilde{\Phi}\rangle = \sum_{ab}\langle\tilde{\Phi}|\Phi_a\rangle\,\delta_{ab}\,\langle\Phi_b|\tilde{\Phi}\rangle$$
$$= \sum_{a}\langle\tilde{\Phi}|\Phi_a\rangle\langle\Phi_a|\tilde{\Phi}\rangle = \sum_{a}|\langle\Phi_a|\tilde{\Phi}\rangle|^2. \tag{2.26}$$

If we apply this into equation 2.24 then we get

$$\langle \tilde{\Phi}|\hat{H}|\tilde{\Phi}\rangle = \sum_{ab} \langle \tilde{\Phi}|\Phi_a\rangle \langle \Phi_a|\hat{H}|\Phi_b\rangle \langle \Phi_b|\tilde{\Phi}\rangle = \sum_a \varepsilon_a |\langle \Phi_a|\tilde{\Phi}\rangle|^2. \qquad (2.27)$$

If the wave function is normalised we get $\varepsilon_a \geq \varepsilon_0$. This leads to equation 2.28

$$\langle \tilde{\Phi}|\hat{H}|\tilde{\Phi}\rangle \geq \sum_a \varepsilon_0 |\langle \Phi_a|\tilde{\Phi}\rangle|^2 = \varepsilon_0 \sum_a |\langle \Phi_a|\tilde{\Phi}\rangle|^2 = \varepsilon_0. \qquad (2.28)$$

As the expectation value of the approximate wave function is always higher than the true wavefucntion, the energy can be used to determine the quality of the trial function, the trial function is altered until the energy is minimised. The most common way of presenting this is

$$\tilde{E} = \frac{\langle \tilde{\Phi}|\hat{H}|\tilde{\Phi}\rangle}{\langle \tilde{\Phi}|\tilde{\Phi}\rangle} \geq \varepsilon_0. \qquad (2.29)$$

2.5 Hartree products and the Slater-Condon rules

Until this point electronic structure theory and the Schrödinger equation have been discussed in a general terms. However, for these theories to be useful, we need to be able to apply them to obtain approximate solutions to the many-body Schrödinger equation. The first step to achieving this is being able represent the wave function in a way that is easy to understand and use.[39] If all of the electrons in the wave function are treated as independent particles in an N electron wave function, then it can be written as a product of the one electron functions.

$$\Phi(r_1, r_2, r_3, ...r_N) = \psi_1(r_1)\psi_2(r_2)\psi_3(r_3)...\psi_N(r_N) = \prod_i^N \psi_i(r_i). \qquad (2.30)$$

This is the Hartree product of the wave function, Φ_{HP}, with each one electron function having spatial coordinates in Hilbert space $r_i = \{x_i, y_i, z_i\}$.[40–45] These one-electron functions are independent of each other and ignore the

electron-electron interactions. This is called the *orbital approximation*. In addition to spatial coordinates, quantum mechanical particles also have spin coordinates. As electrons are fermions, this takes the form of $\pm\frac{1}{2}$ or α and β. This is means that the coordinates can be split into a spatial and spin component and the Hartree product can also be split into space and spin parts

$$\tau_i = \{r_i, \sigma_i\} = \{x_i, y_i, z_i, \sigma_i\}, \tag{2.31}$$

$$\Theta(\tau) = \Phi(r)\Xi(\sigma). \tag{2.32}$$

Thus the Hartree product is a product of a set of single particle space-spin functions, presented in 2.33,

$$\theta(\tau) = \phi(r)\xi(\sigma). \tag{2.33}$$

Thus, equation 2.30 can be written as

$$\Theta_{HP}(\tau_1, \tau_2, \tau_3, ...\tau_N) = \theta_1(\tau_1)\theta_2(\tau_2)\theta_3(\tau_3)...\theta_N(\tau_N) = \prod_i^N \theta_i(\tau_i). \tag{2.34}$$

In this expression, electronic spin introduces an issue, as fermions are required to be indistinguishable due to the Pauli antisymmetry principle. This requires that the wave function changes sign when two electrons coordinates are exchanged, such as in 2.35

$$\theta_1(\tau_1)\theta_2(\tau_2) = -\theta_1(\tau_2)\theta_2(\tau_1). \tag{2.35}$$

However this is not true for the Hartree product as the electrons can be exchanged with no affect on the sign of the product

$$\Theta_{HP}(\tau_1, \tau_2) = \Theta_{HP}(\tau_2, \tau_1). \tag{2.36}$$

This representation of the wave function thus is incorrect. This problem was solved in 1929 when Slater introduced a normalised determinant as an approximation of the wave function. This satisfies both the antisymmetry principle and the requirement for the electrons to be indistinguishable.[46] This leads to the Hartree product being expressed as

$$\Theta_{HP}(\tau_1, \tau_2) = \frac{1}{\sqrt{2!}} \begin{vmatrix} \theta_1(\tau_1) & \theta_2(\tau_1) \\ \theta_1(\tau_2) & \theta_2(\tau_2) \end{vmatrix} = \frac{1}{\sqrt{2!}} [\theta_1(\tau_1)\theta_2(\tau_2) - \theta_1(\tau_2)\theta_2(\tau_1)], \tag{2.37}$$

$$\begin{aligned} \Theta_{HP}(\tau_1, \tau_2) &= \frac{1}{\sqrt{2!}} \begin{vmatrix} \theta_1(\tau_2) & \theta_2(\tau_1) \\ \theta_1(\tau_1) & \theta_2(\tau_2) \end{vmatrix} = \frac{1}{\sqrt{2!}} [\theta_1(\tau_2)\theta_2(\tau_2) - \theta_1(\tau_1)\theta_2(\tau_1)] \\ &= -\frac{1}{\sqrt{2!}} [\theta_1(\tau_1)\theta_2(\tau_2) - \theta_1(\tau_2)\theta_2(\tau_1)]. \end{aligned} \tag{2.38}$$

The other strength of the Slater determinant is that it easily allows for an N electron wave function to be written. However this can become quite cumbersome, so an alternative and convenient way of enforcing antisymmetry on the wave function is to use the antisymmetrizer $\hat{A}$

$$\hat{A} = \frac{1}{\sqrt{N!}} \sum_{\hat{\pi} \epsilon S_n} \epsilon_\pi \hat{\pi}. \tag{2.39}$$

The $\hat{\pi}$ is the permutation operator, which exchanges the coordinates of the particles in a symmetry group S_n, for a given number of particles n. The ϵ_π is the sign change that would accompany that permutation. $\hat{A}$ is a Hermitian operator. A Hermitian operator is one which is a square matrix with complex component, and is equal to its own conjugate transpose,

$$\hat{A}_{ab} = \hat{A}_{ab}^\dagger. \tag{2.40}$$

This allows us to write the complex elements of the matrix as a set of real 2×2 matrices. Thus, the operator has a spectrum of real eigenvalues. The antisymmetrizer is also an idempotent operator. Idempotence means that once the operator has been applied once, subsequent applications have no affect on the operation, a simple example of this is multiplication by 1. The antisymmetrizer being idempotent means that when it is applied to an antisymmetric wave function, or antisymmetric elements in the wave function, it leaves it unperturbed. The use of the antisymmetrizer allows for an N electron Slater determinant to be rewritten as

$$\Theta_{HP}(\tau_1, \tau_2, ...\tau_N) = \sqrt{N!}\hat{A}\theta_1(\tau_1)\theta_2(\tau_2)...\theta_N(\tau_N). \tag{2.41}$$

The benefits of using the antisymmetrizer can be seen when we use it to get the electronic energy of a system in Dirac notation

$$E_e = \langle\Theta|\hat{H}_e|\Theta\rangle = \langle\Theta|\sum_a \hat{h}_a + \sum_{a>b} \hat{v}_{ab})|\Theta\rangle . \tag{2.42}$$

Where $\hat{h}_a$ are the one electron terms from the Hamiltonian and $\hat{v}_{ab}$ are the two electron terms. The antisymmetrizer gives us the same results as that obtained from determinants but in a more succinct notation. The nuclear kinetic energy term and the nuclear-nuclear potential terms have been ignored at this point.

We can greatly simplify the problem by applying the Slater-Condon rules, which state that a wave function constructed from Slater determinants of orthonormal orbitals can be expressed as a sum of the integrals of the one and two-body operators acting on the individual orbitals.[46–48] This allows us to separate the N-electron wave function into a sum of one and two-electron integrals, thus, the problem becomes more tractable. For the one-body operator the Slater-Condon rules are,

$$\langle\Theta|\hat{H}|\Theta\rangle = \sum_{i=a}^{N} \langle\theta_a|\hat{h}|\theta_a\rangle , \tag{2.43}$$

$$\langle\Theta|\hat{H}|\Theta_a^b\rangle = \langle\theta_a|\hat{h}|\theta_b\rangle\,, \tag{2.44}$$

$$\langle\Theta|\hat{H}|\Theta_{ab}^{cd}\rangle = 0. \tag{2.45}$$

In these expressions for the one-body operator, when there is no change in the wave function, the integral over the wave function become a sum of the one-electron integrals. The integral of the Hamiltonian over a wave function with 1 orbital difference between the bra and ket becomes a single 1-electron integral. All other terms disappear. This rule applies to our kinetic energy operator. For the two-body operators, such as the electron-electron repulsion operator, the following rules apply.

$$\langle\Theta|\hat{H}|\Theta\rangle = \frac{1}{2}\sum_{a=1}^{N}\sum_{\substack{b=1\\b\neq a}}^{N}\Big(\langle\theta_a\theta_b|\hat{h}|\theta_a\theta_b\rangle - \langle\theta_a\theta_b|\hat{h}|\theta_b\theta_a\rangle\Big), \tag{2.46}$$

$$\langle\Theta|\hat{H}|\Theta_a^c\rangle = \sum_{a=1}^{N}\Big(\langle\theta_a\theta_b|\hat{h}|\theta_c\theta_b\rangle - \langle\theta_a\theta_b|\hat{h}|\theta_b\theta_c\rangle\Big), \tag{2.47}$$

$$\langle\Theta|\hat{H}|\Theta_{ab}^{cd}\rangle = \langle\theta_a\theta_b|\hat{h}|\theta_c\theta_d\rangle - \langle\theta_a\theta_b|\hat{h}|\theta_d\theta_c\rangle\,. \tag{2.48}$$

When the operator is applied to a wave functions with one or less orbital differences the integral is a sum of two-electron integrals. When the the bra and ket are different by two orbitals, the integral becomes a two-electron integral, and if the bra and ket differ by more than two orbitals the integral vanishes. These rules allow for the electronic structure problem to be simplified.

2.6 Hartree-Fock theory

We can use the Slater-Condon rules in conjunction with the antisymmetrizer to get our one and two-electron terms in Hartree-Fock theory. If we examine the one electron term first for a system where a is an electron and $a \neq b$, this term can be written as

$$\langle\Theta|\sum_a \hat{h}_a|\Theta\rangle = \langle\Theta|\hat{h}_1|\Theta\rangle + ..., \tag{2.49}$$

using the antisymmetrizer we get

$$\langle\Theta|\hat{h}_a|\Theta\rangle = \sqrt{N!}\Big(\langle\hat{A}\theta_1\theta_2...|\hat{h}_1|\hat{A}\theta_1\theta_2...\rangle + ...\Big). \tag{2.50}$$

Due to the antisymmetrizer being Hermitian and idempotent, it means that this can be rewritten so that the antisymmetrizer only has to be applied to the bra or the ket

$$= \sqrt{N!}\Big(\langle\hat{A}\theta_1\theta_2...|\hat{h}_1|\theta_1\theta_2...\rangle + ...\Big). \tag{2.51}$$

When the antisymmetrizer is applied to equation 2.51 and the permutation operator is applied we get the following expressions

$$\langle\Theta|\sum_a \hat{h}_a|\Theta\rangle = \frac{1}{\sqrt{N!}}\Big(\langle\theta_1\theta_2...|\hat{h}_1|\theta_1\theta_2...\rangle + \langle\theta_2\theta_1...|\hat{h}_1|\theta_1\theta_2...\rangle + ...\Big), \tag{2.52}$$

$$= \frac{1}{\sqrt{N!}}\Big(\langle\theta_1|\hat{h}_1|\theta_1\rangle + \langle\theta_2|\hat{h}_1|\theta_2\rangle + ...\Big), \tag{2.53}$$

$$= \sum_a \langle\theta_a|\hat{h}|\theta_a\rangle . \tag{2.54}$$

Equation 2.54 contains only the one electron terms for the electronic energy. This simplifies the problem, as solution now relies on N terms rather than $N! \times N!$ terms. If this is carried out for the two-electron terms we get equation

$$\langle\Theta|(\sum_{a>b} \hat{v}_{ab}|\Theta\rangle = \frac{1}{2}\sum_{ab}\Big(\underbrace{\langle\theta_a\theta_b|\hat{v}_{ab}|\theta_a\theta_b\rangle}_{\substack{J_{ab}\\ \text{coulombic integral}}} - \underbrace{\langle\theta_a\theta_b|\hat{v}_{ab}|\theta_b\theta_a\rangle}_{\substack{K_{ab}\\ \text{exchange integral}}}\Big). \tag{2.55}$$

The first term is the Coulombic term, and has analogies in classical mechanics. However, the second term is the exchange term. This does not have a classical physics interpretation, as it originates from the requirement for the electrons to be indistinguishable and obey the antisymmetry principle. If we rewrite equation 2.42 in this way we get

$$E = \sum_a \langle \theta_a | \hat{h} | \theta_a \rangle + \frac{1}{2} \sum_{ab} \Big(\langle \theta_a \theta_b | \hat{v}_{ab} | \theta_a \theta_b \rangle - \langle \theta_a \theta_b | \hat{v}_{ab} | \theta_b \theta_a \rangle \Big). \qquad (2.56)$$

The one-electron functions can now be selected variationally to minimise the energy of the N electron system. This equation is exact within the Born-Oppenheimer approximation Schrödinger equation. However, it is intractable due to the two electron terms. To solve this issue in Hartree-Fock theory the Hamiltonian can be simplified by using the following pseudo 1-electron operators,

$$\hat{F} = \hat{h} + \sum_a (\hat{J}_a - \hat{K}_a). \qquad (2.57)$$

Here $\hat{h}$ is the one electron operator, $\hat{J}_a$ is the Coulomb operator and $\hat{K}_a$ is the exchange operator. The $\hat{J}_a$ and $\hat{K}_a$ operators are described as acting on single one electron space-spin functions $\theta_a(\tau_1)$, giving the equations

$$\hat{J}_a \theta_b(\tau_1) = \int \theta_a^*(\tau_2) \hat{v}_{12} \theta_a(\tau_2) d\tau_2 \cdot \theta_b(\tau_1) \qquad (2.58)$$

and

$$\hat{K}_a \theta_b(\tau_1) = \int \theta_a^*(\tau_2) \hat{v}_{12} \theta_b(\tau_2) d\tau_2 \cdot \theta_a(\tau_1). \qquad (2.59)$$

The $\hat{J}_a$ operator describes the average repulsion experienced by one electron space-spin function by all of the other electrons, and the $\hat{K}_a$ operator similarly does this, but for changing permutations. For this reason Hartree-Fock theory is described as a mean-field approach. If we use the Fock operator on one of the one electron space-spin functions we get an eigenvalue equation

$$\hat{F}\,|\theta_i\rangle = \varepsilon_i\,|\theta_i\rangle. \tag{2.60}$$

This is exact for each one electron eigenfunction, $|\theta_i\rangle$, and eigenvalue ε_i. The eigenfunctions used in 2.60 are the electronic orbitals within a system, and the eigenvalues are the orbital energies. Solving equation 2.60 can can be carried out, but it is still very difficult and computationally expensive to do. This means that the orbitals, and thereby the wave function, must be represented as a set of simple functions. This is done by expanding them in some basis functions,

$$\theta_i = \sum_\mu c_{\mu i}\varphi_i, \tag{2.61}$$

where $c_{\mu i}$ is some coefficient describing the weighting of the basis functions φ_i. The choice of basis functions for use for this purpose will be discussed in more detail in the next section. When this expansion is inserted into the Fock equation we get

$$\hat{F}\sum_\mu c_{\mu i}\,|\varphi_\mu\rangle = \varepsilon_i\sum_\mu c_{\mu i}\,|\varphi_\mu\rangle. \tag{2.62}$$

When the bra $\langle\varphi_k|$ is applied to equation 2.62 it can be solved

$$\sum_\mu c_{\mu i}\,\langle\varphi_k|\hat{F}|\varphi_\mu\rangle = \varepsilon_i\sum_\mu c_{\mu i}\,\langle\varphi_k|\varphi_\mu\rangle. \tag{2.63}$$

This can be written in the matrix form

$$\mathbf{Fc} = \varepsilon\mathbf{Sc}. \tag{2.64}$$

Equation 2.64 is the Hartree-Fock-Roothaan equation. $\mathbf{c}$ is the matrix coefficient and ε is the diagonal matrix of the orbital energies. $\mathbf{F}$ is the Fock matrix and $\mathbf{S}$ is the overlap matrix which have the form,

$$\mathbf{F}_{k\mu} = \langle \varphi_k | \hat{F} | \varphi_\mu \rangle \, , \tag{2.65}$$

$$\mathbf{S}_{k\mu} = \langle \varphi_k | \varphi_\mu \rangle \, . \tag{2.66}$$

The Hartree-Fock-Roothaan equation allows for us to minimise the energy systematically and iteratively.[49–53] This is because our overlap matrix and Fock matrix depends on the quality of our trial wave function, and thus depends on our trial coefficients. We can solve the Hartree-Fock-Roothaan equations, or the Secular equation version 2.67, to get new energies. We can alter the coefficient matrix to lower the energy variationally until we reach convergence

$$(\mathbf{F} - \varepsilon \mathbf{S})\mathbf{c} = 0. \tag{2.67}$$

2.7 Representation of the wave function

As shown in equation 2.68, our trial wave function is an expansion of some basis functions, using the orbital coefficients.

$$\theta_i = \sum_\mu c_{\mu i} \varphi_i, \tag{2.68}$$

This leads us to the question, how do we represent our unknown wave function best. In computational chemistry, 1-electron basis functions are built as a linear combination, into molecular orbitals and the trial wave function. Often a basis set will be formed of a number of basis functions. For this, any set of functions that allows for efficient manipulation and implementation can be used, for instance point grids are used in solid state electronic structure calculations. It was found that the best set of basis functions to represent the atomic orbital were Slater-type orbitals derived from the hydrogenic atomic orbtals.[23] They perform well, because they have a cusp at the nucleus and decay exponentially. However, they are computationally expensive when numerous functions are used a basis set, as they cannot be integrated efficiently.

As a consequence, usually Gaussian-type orbitals are used to form the basis sets. They do not have the correct cusp at the orbital, nor do they decay exponentially, but they are much computationally cheaper to integrate.[23, 54–57] The difference between a Slater orbital and a Gaussian orbital can be seen in figure 2.2.
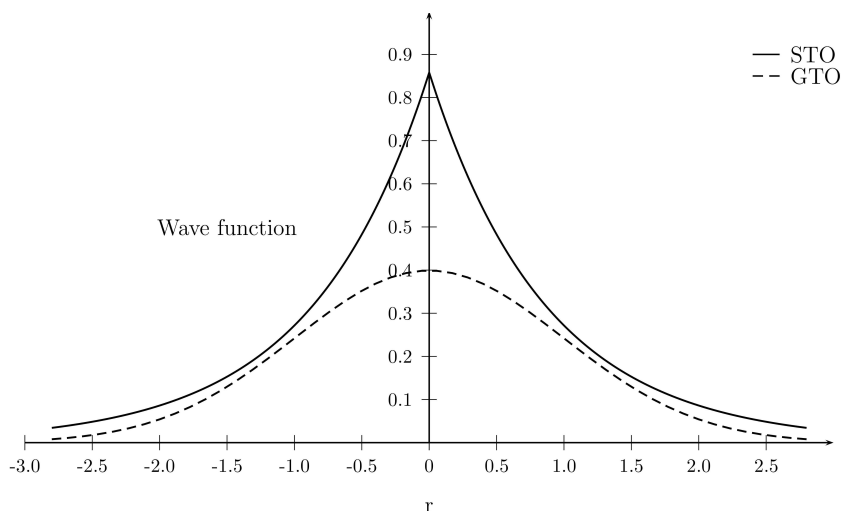
Fig. 2.2: Comparison of Gaussian and Slater type orbital functions (taken from [58, 59]

Although Gaussian functions are not a good representation of the wave function. They are computationally cheaper to use because a product of two Gaussian functions is also a Gaussian. Thus, more Gaussian functions can be combined together and contracted to form a function which looks like a Slater orbital. This allows for larger basis sets, with polarisation and diffuse functions included in them to improve the description of the wave function and get higher chemical accuracy. Gaussian basis sets are what are used in this thesis.[60–66]

To make the basis functions of use in chemistry they are required to have a principal quantum number, some function for their angular momentum, so that they can form the s, p, d, f and g atomic orbitals. This angular momentum function must also have projection so that can act in Hilbert space. It is common practice to include functions with higher angular momentum (polarisation functions), in order to improve the description of bonding orbital, and diffuse function to improve the description of inter-molecular forces and non-bonding interactions. To cause the functions to collapse to 0 at distance, they have an exponential term, with some exponent which effects the shape

of the basis function. The form of the Gaussian type function can be seen in equation 2.69

$$\varphi_n = N_{nl} m_l e^{-\alpha r^2}.$$ (2.69)

The quality of the basis set is determined by the number of basis functions it contains (its size). This directly influences the accuracy of the results of the calculations. However, even with an infinite-sized basis set (a complete basis, the energy obtained from Hartree-Fock would still not be the true ground state energy of the system. To understand this further and improve on Hartree-Fock we need to introduce electron correlation.

2.8 Electron correlation and perturbation theory

Hartree-Fock theory is one of the simplest methods for solving the approximate Schrödinger equation. However, it has a number of issues with its description of the electrons, which lead to errors in the calculated energy. The difference between the true energy of the system calculated from the full Schrödinger equation and the Hartree-Fock equations is called the correlation energy.[67] The correlation energy is a direct consequence of the Hartree-Fock treatment of the electrons i.e. the mean field approach, where an electron interacts with the average potential of the other electrons in the system, rather than interacting with the individual electrons.[68–70] This has the effect of increasing the energy of the system, as the potential energy will be artificially high in places where there should be an electronic hole. This can be seen in figure 2.3. This poor description of electron-electron interactions is called dynamic correlation.

Dynamic correlation is important to describe a number of interesting properties, including inter-molecular forces, and leads to errors in the energies obtained. Therefore, a number of post Hartree-Fock methods have been developed to recover this dynamic correlation energy and improve accuracy. Therefore, a number of post Hartree-Fock methods have been developed to recover this dynamic correlation energy
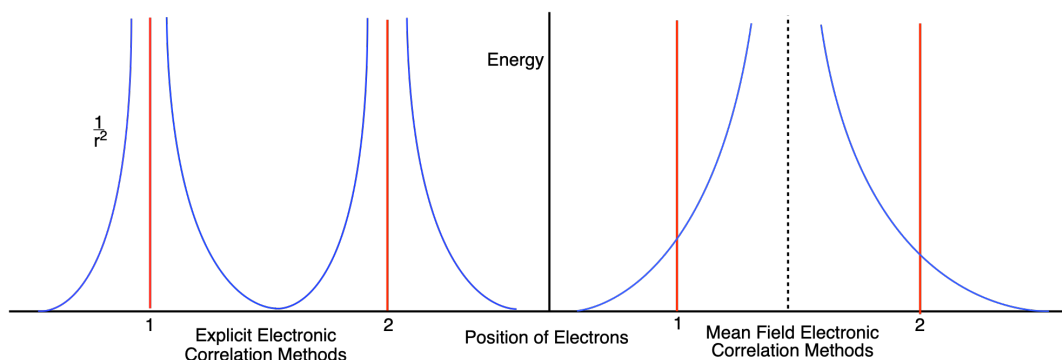
Fig. 2.3: Potential energy of a system when a third electron is introduced, the red lines are the position of the electrons and the blue are the potential energy. In the mean field method, the energy is artificial high between the two electrons.

The simplest improvement to Hartree-Fock theory is Møller–Plesset or Rayleigh–Schrödinger Perturbation theory, which are a subset of the wider mathematical field of perturbation theory.[71, 72] In this thesis Rayleigh-Schrödinger perturbation theory will be used. The reason for using perturbation corrections is that it makes improvements to the description of dynamic correlation at short and long ranges, which are particularly important for calculating bond breaking and forming reactions. Perturbation theory makes this improvement by making a small change to the reference Fock wave function, the perturbation. The effect it has on the solution of the Fock operator are the corrections to improve the accuracy and description of the system. Perturbation theory only works if this perturbation is not too large and the effects not too great. If this is not the case, the description of the system can break down. In the case of the breaking the hydrogen-hydrogen bond this effect is quite dramatic.

We can apply this perturbation to the Hamiltonian

$$\hat{H} = \hat{H}^0 + \lambda \hat{V}, \tag{2.70}$$

where $\hat{H}^0$ is our Hartree-Fock reference and λ some perturbation parameter which we apply to the operator $\hat{V}$. This can then be applied to our Schrödinger equation to get

$$(\hat{H}^0 + \lambda \hat{V}) |\Phi_a\rangle = E_N |\Phi_a\rangle, \tag{2.71}$$

With $|\Phi_a\rangle$ and E_a being perturbed

$$|\Phi_a\rangle = |\Phi_a \lambda\rangle, \tag{2.72}$$

$$E_a = E_a \lambda. \tag{2.73}$$

If we expand the wave function and energy through a Taylor series we get equations 2.74 and 2.75 respectively

$$|\Phi_a\rangle = |\Phi_a\rangle|_{\lambda=0}, + \left.\frac{\partial |\Phi_a\rangle}{\partial \lambda}\right|_{\lambda=0} \lambda + \left.\frac{\partial^2 |\Phi_a\rangle}{\partial \lambda^2}\right|_{\lambda=0} \frac{\lambda^2}{2!} + ..., \tag{2.74}$$

$$E_a = E_a|_{\lambda=0}, + \left.\frac{\partial E_a}{\partial \lambda}\right|_{\lambda=0} \lambda + \left.\frac{\partial^2 E_a}{\partial \lambda^2}\right|_{\lambda=0} \frac{\lambda^2}{2!} + ... \tag{2.75}$$

This allows us to express the wave function and energy to the nth term as

$$|\Phi_a^{(n)}\rangle = \frac{1}{n!} \left.\frac{\partial^n |\Phi_a\rangle}{\partial \lambda^n}\right|_{\lambda=0}, \tag{2.76}$$

and

$$E_a^{(n)} = \frac{1}{n!} \left.\frac{\partial^n E_a}{\partial \lambda^n}\right|_{\lambda=0}. \tag{2.77}$$

When this is expansion is substituted into the Schrödinger equation and simplified we get

$$(\hat{H}^0 + \lambda \hat{V})(|\Phi_a^{(0)}+\rangle + \lambda |\Phi_a^{(1)}\rangle + \lambda^2 |\Phi_a^{(2)}\rangle + ...)$$
$$= (E_a^{(0)} + \lambda E_a^{(1)} + \lambda^2 E_a^{(2)} + ...)(|\Phi_a^{(0)}+\rangle + \lambda |\Phi_a^{(1)}\rangle + \lambda^2 |\Phi_a^{(2)}\rangle + ...). \tag{2.78}$$

The zeroth order perturbation is the standard Schrödinger equation, and the first and second order perturbation Schrödinger equation can be written as

$$\text{first order } \hat{H}^0 \ket{\Phi_a^{(1)}} + \hat{V} \ket{\Phi_a^{(0)}} = E_a^{(0)} \ket{\Phi_a^{(1)}} + E_a^{(1)} \ket{\Phi_a^{(0)}}, \tag{2.79}$$

$$\text{second order } \hat{H}^0 \ket{\Phi_a^{(2)}} + \hat{V} \ket{\Phi_a^{(1)}} = E_a^{(0)} \ket{\Phi_a^{(2)}} + E_a^{(1)} \ket{\Phi_a^{(1)}} + E_a^{(2)} \ket{\Phi_a^{(0)}}. \tag{2.80}$$

We can then used these equations to get our first and second order energy correction. If we apply the zeroth order wave function $\bra{\Phi_a^{(0)}}$ to equation 2.79 we get

$$\bra{\Phi_a^{(0)}} \hat{H}^0 \ket{\Phi_a^{(1)}} + \bra{\Phi_a^{(0)}} \hat{V} \ket{\Phi_a^{(0)}} = \bra{\Phi_a^{(0)}} E_a^{(0)} \ket{\Phi_a^{(1)}} + \bra{\Phi_a^{(0)}} E_a^{(1)} \ket{\Phi_a^{(0)}}. \tag{2.81}$$

This makes our first order perturbation energy

$$E_a^{(1)} = \bra{\Phi_a^{(0)}} \hat{V} \ket{\Phi_a^{(0)}}. \tag{2.82}$$

If we consider this perturbation, the reference wave function is still a valid state, but no longer had valid eigenvalues attached to it as the energy differs by $\bra{\Phi_a^{(0)}} \hat{V} \ket{\Phi_a^{(0)}}$. This is caused by our perturbed wave function $\bra{\Phi_a^{(0)}} \neq \ket{\Phi_a^{(0)}}$. As such we have improved our solution to the Schrödinger equation by applying this first order perturbation, but to get more of the correlation energy and improve further, higher order corrections are needed.

When the same process is applied to equation 2.80 we get

$$\begin{aligned}
&\bra{\Phi_a^{(0)}} \hat{H}^0 \ket{\Phi_a^{(2)}} + \bra{\Phi_a^{(0)}} \hat{V} \ket{\Phi_a^{(1)}} \\
&= \bra{\Phi_a^{(0)}} E_a^{(0)} \ket{\Phi_a^{(2)}} + \bra{\Phi_a^{(0)}} E_a^{(1)} \ket{\Phi_a^{(1)}} + \bra{\Phi_a^{(0)}} E_a^{(2)} \ket{\Phi_a^{(0)}},
\end{aligned} \tag{2.83}$$

and we can write the second order perturbation energy as

$$E_a^{(2)} = \langle \Phi_a^{(0)} | \hat{V} | \Phi_a^{(1)} \rangle . \tag{2.84}$$

From the second order correction we recoup more of our correlation energy. The perturbed wave function can be constructed from a linear combination of unperturbed wave functions using a perturbation coefficient

$$|\Phi_N^{(n)}\rangle = \sum_{\mu} C_{\mu}^n |\Phi_{\mu}^{(0)}\rangle . \tag{2.85}$$

The utilisation of second order Rayleigh-Schrödinger perturbation theory allows most of the dynamic correlation energy to be recovered. Even if we went to the nth order of perturbation and recouped all of the dynamic correlation energy, there is still inaccuracies present in our description of the electronic structure of molecules. Another contribution to the correlation energy comes from the use of a single Slater determinant in Hartree-Fock and post Hartree-Fock methods. The use of a single determinant leads to the electronic structure being described qualitatively incorrectly in situations far from equilibrium, such as for breaking bonds. In such cases the electronic configuration not being correctly described with a single Slater determinant. This is called static correlation, due to it being caused by the electrons having the wrong orbital configuration. To solve this issue, configuration interaction and multi-reference methods need to be used.

2.9 Configuration Interaction and multi-reference methods

The problem of correctly describing the electronic configuration of a system can be seen clearly if we take a system of two bonded atoms, A-B, which share a pair of electrons in the bond. When we extend the distance between the two atoms, we start to break the bond homolytically. Thus, the atoms are pulled further away from each other, the electrons should be shared equally between each atom, and we form two radicals. However, in Hartree-Fock theory as the bond is extended, we actually form a mix between 2 neutral

atoms and an ion pair. In the ion pair one of the atoms keeps both electrons and there is an electron hole on the other atom. This is qualitatively incorrect. It also leads to quantitative errors, as the coulombic interactions will continue to rise as the two ions are pulled apart. As such, we never achieve the situation where the two atoms are non-interacting particles and the potential reaches its asymptotic value.

What we should see is that one electron is placed in one orbital that is centred on A and the other electron should be in an orbital which is centred on B. However as electrons have spin, we can write this configuration in two different ways, in one where the A orbital has α spin and the other, where the B orbital has α spin. This is why using a single Slater determinant can not describe the system correctly, as in that case the wave function will be a combination of both of these electronic configurations, as well as the two ionic configurations. To describe this system completely we will need four configurations, and to achieve this we will need four Slater determinants. This can be seen visually below in figure 2.4. To solve this problem, we need to introduce configuration interaction theory, from which we can extract Multi-configuration SCF theory.[73–78]
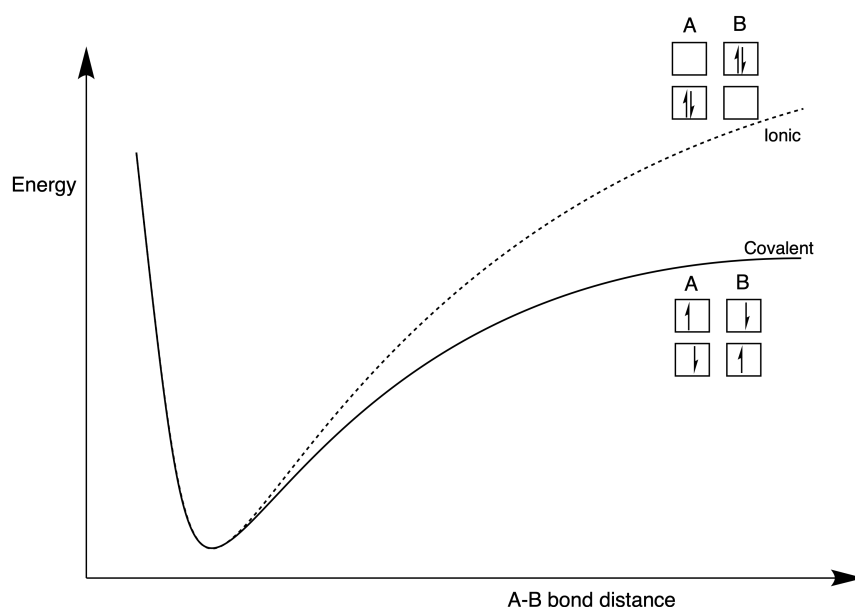
Fig. 2.4: Possible electronic configurations and potential energy surfaces for two electrons as the A-B bond is broken.

Configuration interaction theory solves the non-relativistic Schrödinger equation, within the Born-Oppenheimer approximation. If we assume we have a

complete set of basis function for a single variable, x_1, the wave function has the form

$$\Phi(x_1) = \sum_i a_i \varphi_i(x_1). \tag{2.86}$$

If we then expand our wave function as a function of two variables, x_1 and x_2, which share the same domain and fix x_2 we get the following expression

$$\Phi(x_1, x_2) = \sum_i a_i(x_2) \varphi_i(x_1). \tag{2.87}$$

Each of these expansion coefficients, $a_i(x_2)$, is a function of a single variable and thus can be expanded to give

$$a_i(x_2) = \sum_j b_{ij} \varphi_j(x_2). \tag{2.88}$$

When equation 2.87 and 2.88 are combined we get the following expression

$$\Phi(x_1, x_2) = \sum_{ij} b_{ij} \varphi_i(x_1) \varphi_j(x_2). \tag{2.89}$$

If we did this for an N electron system, using space-spin orbitals we get equation 2.90

$$\Phi(x_1, x_2, ...x_N) = \sum_{ij...N} b_{ij...N} \varphi_i(x_1) \varphi_j(x_2)....\varphi_N(x_N). \tag{2.90}$$

We need to enforce Pauli antisymmetry on the system, so that

$$\Phi(x_1, x_2...x_M, x_n) = -\Phi(x_2, x_1...x_N, x_M) \tag{2.91}$$

meaning that $b_{ij} = -bji$ and $b_{ii} = 0$. This can alternatively written as

$$\Phi(x_1, x_2, ...n_M, n_N) = \sum_{ij..N} b_{ij...M,N}[\varphi_i(x_1)\varphi_j(x_2)...\varphi_M(x_M)\varphi_N(x_N)$$
$$-\varphi_j(x_1)\varphi_i(x_2)...\varphi_N(x_M)\varphi_M(x_N)], \quad (2.92)$$

This simplifies to

$$\Phi(x_1, x_2, ...n_M, n_N) = \sum_{j>i} 2^{\frac{1}{2}} b_{ij} \ket{\varphi_i\varphi_j}. \quad (2.93)$$

For a N-electron wave function, it can be expressed as a linear combination of all possible N-electron Slater determinants for a complete basis of space-spin orbitals. If we solve the Schrödinger equation in a complete basis set, we get a complete set of electronic eigenstates of the system. If our complete set of N-electron basis functions are described by

$$\ket{\Phi_i} = \sum_i a_i \ket{\varphi}. \quad (2.94)$$

The the eigenvectors of the Hamiltonian $\hat{H}$ are described by

$$\ket{\Phi_j} = \sum_i^I c_{ij} \ket{\varphi_i}. \quad (2.95)$$

If the Hamiltonian is constructed so that is satisfies equation 2.96 for a system where $i, j = 1, 2, ...I$,

$$\hat{H}_{ij} = \bra{\Phi_i}\hat{H}\ket{\Phi_j}, \quad (2.96)$$

then we can use Slater's rules to write $\hat{H}$ as a set of one and two electron integrals. Similarly to how we used it in Hartree-Fock theory.[46, 47] For the one electron terms we get

$$\langle i|\hat{H}|j\rangle = \int \varphi_i^*(r_1)\hat{h}(r_1)\varphi_j(r_1)dr, \tag{2.97}$$

and the two electron terms we get,

$$\langle ij||kl\rangle = \langle ij|kl\rangle - \langle ij|lk\rangle. \tag{2.98}$$

Where

$$\langle ij|kl\rangle = \int \varphi_i^*(r_1)\varphi_j^*(r_2)\frac{1}{r_{12}}\varphi_k(r_1)\varphi_l(r_2)dr_1dr_2 \tag{2.99}$$

and

$$\langle ij|lk\rangle = \int \varphi_i^*(r_1)\varphi_j^*(r_2)\frac{1}{r_{12}}\varphi_l(r_1)\varphi_k(r_2)dr_1dr_2. \tag{2.100}$$

To take advantage of Slater's rules, the Slater determinant must be rearranged to maximise the similarity, or coincidence between the Slater determinants. This means that when

$$\langle \Phi_1|\hat{H}|\Phi_2\rangle \tag{2.101}$$

where,

$$\begin{aligned} |\Phi_1\rangle &= |abcd\rangle \\ |\Phi_2\rangle &= |crds\rangle \end{aligned} \tag{2.102}$$

if we interchange the columns to increase this coincidence, obeying the Pauli antisymmetry principle, we get

$$|\Phi_2\rangle = |crds\rangle = -|crsd\rangle = |srcd\rangle\,. \tag{2.103}$$

Once we have done this we apply Slater's rules and determine how many space-spin orbitals differences there is between the Matrices. This leads to the following expressions

$$\text{0 differences } \langle\Phi_1|\hat{H}|\Phi_1\rangle = \sum_m^N \langle m|\hat{h}|n\rangle + \sum_{m>n}^N \langle mn||mn\rangle\,, \tag{2.104}$$

$$\text{1 difference } \langle\Phi_1|\hat{H}|\Phi_2\rangle = \langle m|\hat{h}|p\rangle + \sum_n^N \langle mn||pn\rangle\,, \tag{2.105}$$

$$\text{2 differences } \langle\Phi_1|\hat{H}|\Phi_2\rangle = \langle mn||pq\rangle\,, \tag{2.106}$$

$$\text{>2 differences } \langle\Phi_1|\hat{H}|\Phi_2\rangle = 0. \tag{2.107}$$

Equation 2.104 describes the ground state configuration, equation 2.105 describes a single excitation, and equation 2.106 describes a double excitation. When there are more than two differences, then the term becomes zero and can be ignored. This allows us to write our wave function as an expansion by a set of excitation's function of a reference determinant, which we will take to be the Hartree-Fock determinant,

$$|\Phi\rangle = A_0\,|\Phi_{HF}\rangle + \sum_{ra} A_a^r\,|\Phi_a^r\rangle + \sum_{\substack{a<b,\\r<s}} A_{ab}^{rs}\,|\Phi_{ab}^{rs}\rangle + \sum_{\substack{a<b<c,\\r<s<t}} A_{abc}^{rst}\,|\Phi_{abc}^{rst}\rangle + \dots \tag{2.108}$$

This gives us a set of variational coefficients, A_i, which we can use to optimise to the ground state energy. The terms in the equation describes the Slater

determinants where we have replaced space-spin orbital a in the reference determinant with orbital r. We can combine a set of Slater determinants together to make them eigenfunctions of the spin operators $\hat{S}_2$ and $\hat{S}^2$. These eigenfunctions are often referenced as the configuration state functions (CSFs) and can have any variation of allows spin configurations. The CSFs allow us to study excited states or bond breaking systems, where no single CSF can describe the system fully, so linear combination of a set of CSFs. This theory is ferred to as Configuration Interaction theory.

Configuration Interaction (CI) theory has a number of issues when using it to solve these multi-configurational problems. This originates from the fact that to carry out a Full CI calculation, where every possible CSF is included would be computationally unfeasible. Therefore, truncated CI expansions are used, which introduces errors into the calculation. We are not only failing to recover all of the correlation energy due to limiting the size of the basis set and the number of CSFs, but size consistency problems are introduced into the problem. Size consistency refers to the properties of a quantum chemistry method describing the electronic structure and energy of a system consistently at any separation.

An example would be if we separated two atoms to an infinite distant. If a double excitation was taken from the the dimer of the two atoms when separated to infinite distance then the system will behave correctly. However, if the two atoms are calculated separately, with a double excitation carried out on both individual fragments, then the system is incorrectly described with a quadruple excitation being carried out in total on the system. This is not true for closed shell methods such as Hartree-Fock. This is particularly important when trying to describe the process of bond breaking. As a consequence, we need a method that can describe this problem in a size-consistent and computationally feasible way.

Multi-configurational SCF (MCSCF) or complete active space SCF (CASSCF) is one method of solving these problems. In this method, only the configurations where the electrons of interest are involved are included in the final solution, if they have the correct spin state and symmetry.[79–83] This allows one to limit the size of the expansion to something which is manageable. We can extract the MCSCF equations from CI, starting by writing the MCSCF wave function and energy in terms of the CI expansion

$$\Psi_{MCSCF} = \sum_i^{CI} A_i \Phi_i, \tag{2.109}$$

$$E = \sum_{IJ}^{CI} c_I^* c_J H_{IJ}. \tag{2.110}$$

H_{IJ} is the matrix elements of the electronic Hamiltonian between two determinants $|\Phi_i\rangle$ and $|\Phi_j\rangle$. Due to Slater's rules, these can be written as one and two electron integrals. The simplest way to do this is with unitary group generators, with equation 2.110 as,

$$E = \sum_{IJ}^{CI} c_I^* c_J \left[\sum_{pq} \lambda_{pq}^{IJ} h_{pq} + \frac{1}{2} \sum_{pqrs} \Gamma_{pqrs}^{IJ} \langle pq|rs \rangle \right]. \tag{2.111}$$

If we sum over the CI coefficients we can write the energy as

$$E = \sum_{pq} h_{pq} \lambda_{pq} + \frac{1}{2} \sum_{pqrs} \Gamma_{pqrs} \langle pq|rs \rangle, \tag{2.112}$$

with

$$\lambda_{pq} = \sum_{IJ}^{CI} c_I^* c_J \lambda_{pq}^{IJ}, \tag{2.113}$$

and

$$\Gamma_{pqrs} = \sum_{IJ}^{CI} c_I^* c_J \Gamma_{pqrs}^{IJ}. \tag{2.114}$$

These are our one and two electron density matrices, which gives a convenient form of our MCSCF energy. This allows us to variationally optimise the energy

as a function of the configurations and the orbital coefficients. The MCSCF equations are written as

$$\Psi_{MCSCF} = \sum_i^{CI} A_i \Phi_i, \qquad (2.115)$$

$$\Phi_i = A\Big\{ \prod_{j<i} \phi_j \Big\}, \qquad (2.116)$$

$$\phi_j = \sum_\mu c_{\mu j} \varphi_\mu. \qquad (2.117)$$

Here, A_i are our CSF coefficients and $c_{\mu j}$ are our orbital coefficients. The number of CSF coefficients increases with the number of states. We can get the energy from equation 2.110. MCSCF differs from CI in that both the CSF coefficients (2.115) and the orbital coefficients (2.116) are optimised simultaneously in MCSCF to get the ground state energy of the system, whereas in CI only the CSFs are optimised. Moreover, each CSF consists of Slater determinants which consist of orbitals, ϕ_j. These orbitals are expressed as a set of basis functions in equation 2.117. MCSCF also differs from CI as the user can determine the CSFs used by constricting the number of active electrons and active orbitals in the configurations and restricting the optimisation to a specific spin state and symmetry.[84]

To explain the consequences of this, consider the following. If we take our example of A-B from before, and this time say our dummy atoms have the 3 electrons each i.e. Li. If we take the ground state of the bonded system, then we have 3 doubly occupied molecular orbitals. This system is a singlet, as the α and β electrons are paired up in the orbitals. As we break the bond, to correctly describe the system, the α and β electrons need to be able to occupy different orbitals. We could include all of our electrons in the active space, which would allow electrons in the lowest occupied orbital to be excited to a higher orbital. If we assume that 6 orbitals are active in the bond breaking then the number of configurations will be 175. As the system gets larger the number of configurations becomes unmanageable. But we do not need to include every electron and as many orbitals in the calculation, as the core electrons are unlikely to be important in the bond breaking, and high energy

unoccupied orbitals are unlikely to be involved. Thus, we can limit our active space, to include only important electrons and orbitals. This should mean that all important configurations are included in the solution.
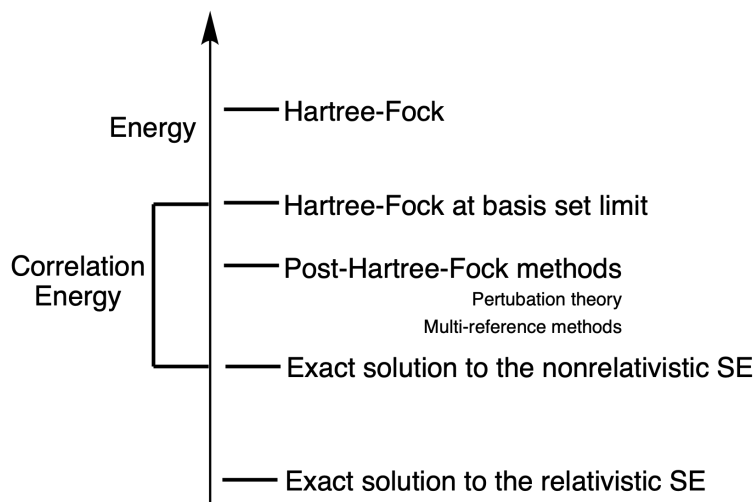
Fig. 2.5: Improvements to the electron correlation energy through the use of different levels of theory.

MCSCF with the second order Rayleigh-Schrödinger perturbation correction has been used extensive in chapter 5 of this thesis. The active spaces selected and reasoning for selecting them will be in that chapter in more detail.[71−74]

2.10 Density Functional Theory

While the wave function methods discussed up to this point are very effective at solving electronic structure problems, they offer one major drawback, namely that the solutions become increasingly complex as the size of the system increases. Thus, they become computationally prohibitively expensive. This means that another approach must be taken to finding solutions to the many-body problem. An alternative methodology to find the approximate solution to the electronic Shrödinger equation is Density Functional Theory, or DFT.

The origins of DFT can be found in Thomas-Fermi (TF) theory, developed in the 1920s, to find the distribution of electrons in atoms.[85, 86] Instead of using the wave function, TF theory finds solutions to the electronic structure problem using the electron density, $n(r)$, as a function of the nuclear potential, $V(r)$, in a finite volume in phase space

$$n(r) = \frac{8\pi}{3h^3} p_f^3(r). \tag{2.118}$$

Here $p_f^3(r)$ is the Fermi momentum. When equation 2.118 is solved for the Fermi momentum and substituted into the kinetic energy equation gives the TF kinetic energy

$$t_{TF}[n] = \frac{p^2}{2m_e} \propto \frac{(n^{\frac{1}{3}})^2}{2m_e} \propto n^{\frac{2}{3}}(r), \tag{2.119}$$

$$T_{TF}[n] = C_F \int n(r) n^{\frac{2}{3}}(r) d^3r = C_F \int n^{\frac{5}{3}}(r) d^3r, \tag{2.120}$$

where C_F is given by

$$C_F = \frac{3h^2}{10m_e} \left(\frac{3}{8\pi}\right)^{\frac{2}{3}}. \tag{2.121}$$

The potential energy can also be derived. However, TF theory has a number of issues with its description of the electronic structure problem. The first is that it approximates that electrons are evenly distributed in phase space. This is a poor description of electrons in an atom. It is also only correct when the nuclear charge is infinite. Thus, it is particularly poor in describing light atoms. However, even for systems where these conditions are met, it does still not correctly describe the system, as it is a purely classical theory. In particular it does not include exchange, nor does it does it take the correlation of the electrons into account. This made it unsuitable for anything of chemical interest.

Despite these limitations, Walter Kohn and Pierre Hohenberg turned to TF theory, when they were looking at metal alloys in 1963. They used TF theory to derive a solution to their problem, as it described interacting electrons in an external potential

$$n(r) = \gamma(\mu - v_{eff}(r))^{\frac{3}{2}}. \tag{2.122}$$

Here μ is the chemical potential. The effective potential, v_{eff}, and γ are given by

$$\gamma = \frac{1}{3\pi^2}\left(\frac{2m}{\hbar^2}\right)^{\frac{3}{2}} \quad \text{and} \quad v_{eff}(r) = v(r) + \int \frac{n(r')}{|r - r'|}dr'. \qquad (2.123)$$

Equation 2.122 represents an alternative way of thinking about the electronic structure problem. The effective potential is the nuclear charge, and γ relates to the kinetic energy of an electron in the potential. This is used as the starting point of Density Functional Theory.[87] Hohenberg-Kohn DFT is based on the lemma that the ground state density, $n(r)$, of a bound system of interacting electrons in an external potential, $v(r)$, determines the potential uniquely. This can be seen below if we take a non-degenerate ground state density, $n(r)$, in a potential, $v_1(r)$

$$E_a = \langle \Psi_a | \hat{H}_a | \Psi_a \rangle = \int v_a(r)n(r)dr + \langle \Psi_a | \hat{T} + \hat{U} | \Psi_a \rangle . \qquad (2.124)$$

Where $\hat{T}$ is the kinetic operator and $\hat{U}$ is the electronic interaction operator. If we now assume there is a second potential, $v_b(r)$, with the same density, but is not equal to $v_a(r)$ plus some constant

$$E_b = \langle \Psi_b | \hat{H}_b | \Psi_b \rangle = \int v_b(r)n(r)dr + \langle \Psi_b | \hat{T} + \hat{U} | \Psi_b \rangle . \qquad (2.125)$$

When Kohn, Levy and Lieb used the Rayleigh-Ritz minimal principle for Φ_a and Φ_b, then the inequalities below are given.[88–90]

$$\begin{aligned} E_a < \langle \Psi_b | H_a | \Psi_b \rangle &= \int v_a(r)n(r)dr + \langle \Psi_b | T + U | \Psi_b \rangle \\ &= E_b + \int (v_a(r) - v_b(r))n(r)dr, \end{aligned} \qquad (2.126)$$

and

$$E_b < \langle \Psi_a | H_b | \Psi_a \rangle = \int v_b(r) n(r) dr + \langle \Psi_a | T + U | \Psi_a \rangle$$

$$= E_a + \int (v_b(r) - v_a(r)) n(r) dr, \tag{2.127}$$

by adding the two equations together, you get the relationship below

$$E_a + E_b < E_a + E_b. \tag{2.128}$$

As this is absurd, the density $n(r)$ cannot describe both potentials $v_a(r)$ and $v_b(r)$. Therefore, it must describe the potential uniquely, and the lemma is correct.

Hohenberg-Kohn DFT has two central theorems. The first is that the external potential, and hence the total energy, is a unique functional of the electron density. If $v_a(r)$ and $v_b(r)$ have the same ground state density, $n(r)$, then $v_a(r) - v_b(r)$ = constant. This means that a functional of the ground state $n(r)$ uniquely determines the potential and all other properties. This is the Hohenberg-Kohn functional

$$F[n] = T[n] + U[n]. \tag{2.129}$$

The second Hohenberg-Kohn theorem states that the functional, $F[n]$, only gives the ground state energy of the system if the density is the true ground state density for and N electrons and potential $v(r)$

$$E_{(v,n)}[n] = F[n] + \int v(r) n(r) d^3 r. \tag{2.130}$$

This is analogous to the variational principle used in wave function methods discussed previously in the chapter. For 2.130 to be useful for electronic structure problems, it needs to be variational so that it can be optimised to the true ground state. This was shown by Levy and Lieb using the constrained search method.[89, 90] They applied the Rayleigh-Ritz minimal principle

$$E = min_{\Psi} \langle \tilde{\Psi} | H | \tilde{\Psi} \rangle . \tag{2.131}$$

This is where the $\tilde{\Psi}$ is the trial wave function, as the trial density is a function of the trial wave function, the minimisation can be carried out for the trial density. The trial density, $\tilde{n}(r)$, if fixed for a set of trial functions, $\tilde{\Psi}_n$

$$E_v[\tilde{n}(r)] = min \langle \tilde{\Psi}_n | H | \tilde{\Psi}_n \rangle$$
$$= \int v(r)\tilde{n}(r)dr + F[\tilde{n}(r)]. \tag{2.132}$$

Here, $F[\tilde{n}(r)]$ is the universal functional and has the form

$$F[\tilde{n}(r)] = min \langle \tilde{\Psi}_{n(r)} | T + U | \tilde{\Psi}_{n(r)} \rangle . \tag{2.133}$$

When the energy is minimised over all possible trial densities, we get equation 2.134, which demonstrates that the minimum is found when the true ground density is obtained

$$E = min_{\tilde{n}(r)} E_v[\tilde{n}(r)] = min_{\tilde{n}(r)} \int v(r)\tilde{n}(r)dr + F[\tilde{n}(r)]. \tag{2.134}$$

The power in this, is that now finding the approximate solution to the Shrödinger equation is optimising to the minimum energy as a function of the 3-dimentional electron density, rather than the complex task of finding the minimum as a function of $\tilde{\Psi}$. Which is a function of all n-electrons.

Thus, Hohenberg-Kohn DFT offers a way of getting to the true ground state density of a system, and thus the minimum energy variationally. In 1965 Kohn and Sham attempted to extract the Hartree equations from Hohenberg-Kohn DFT to make it iterative and to improve the description of the kinetic energy operator.[91] The Hartree equations for a set of spatial and spin coordinates j can be seen below

$$v_H(r) = -\frac{Z}{r} + \int \frac{n(r')}{|r - r'|} dr', \qquad (2.135)$$

$$-\frac{1}{2}\nabla^2 + v_H(r)\psi_j(r) = \varepsilon_j\psi_j(r), \qquad (2.136)$$

$$n(r) = \sum_{j=1}^{N} |\psi_j(r)|^2. \qquad (2.137)$$

Equation 2.135 describes the potential due to the nuclear charge and the mean density of the electrons. Equation 2.136 is the Shrödinger equation for a single particle and 2.137 gives the new density as a function of the trial $\psi_j(r)$.

The Hartree equations use the density of the system to generate new potentials and trial wave functions. The Hartree equation 2.136 is for a set of non-interacting electrons in an external potential, analogous to The Hohenberg-Kohn variational equation, which can be seen in 2.138. As the number of electrons in the system is not changing, and we are searching for a stationary point in the change in $n(r)$, the Euler-Lagrange equation for this system is 2.139

$$E_{v(r)}[\tilde{n}(r)] = \int v(r)\tilde{n}(r)dr + T_s[\tilde{n}(r)] \geq E, \qquad (2.138)$$

$$\delta E_v[\tilde{n}(r)] = \int \delta\tilde{n}(r)\{v(r) + \frac{\delta}{\delta\tilde{n}(r)}T_s[\tilde{n}(r)]|_{\tilde{n}=n} - \varepsilon\}dr = 0. \qquad (2.139)$$

Now for a non-interacting system the ground state density and energy can be calculated

$$(-\frac{1}{2}\nabla^2 + v(r) - \varepsilon_j)\psi_j(r) = 0, \qquad (2.140)$$

$$n(r) = \sum_{j=1}^{N} |\psi_j(r)|^2, \qquad (2.141)$$

$$E = \sum_{j=1}^{N} \varepsilon_j. \qquad (2.142)$$

However, this formulation of DFT has some issues. The first of these being that it is for non-interacting electrons. It also fails to take correlation or exchange into account. For an interacting system the Hohenberg-Kohn functional is equation 2.143

$$F[\tilde{n}(r)] = T_s[\tilde{n}(r)] + \frac{1}{2} + \frac{\tilde{n}(r)\tilde{n}(r')}{|r - r'|} dr dr' + E_{xc}[\tilde{n}(r)], \qquad (2.143)$$

and the variational equation has the form 2.144

$$E_v[\tilde{n}(r)] = \int v(r)\tilde{n}(r) dr + T_s[\tilde{n}(r)] + \frac{1}{2} \int \frac{\tilde{n}(r)\tilde{n}(r')}{|r - r'|} dr dr' + E_{xc}[\tilde{n}(r)] \geq E. \qquad (2.144)$$

The $E_{xc}[\tilde{n}(r)]$ is the exchange-correlation functional, and turns the system from an non-interacting classical system into an interacting quantum mechanical one. The Euler-Lagrange equations are

$$\delta E_v[\tilde{n}(r)] = \int \delta\tilde{n}(r)\{v_{eff}(r) + \frac{\delta}{\delta\tilde{n}(r)}T_s[\tilde{n}(r)]|_{\tilde{n}=n} - \varepsilon\}dr = 0, \qquad (2.145)$$

$$v_{eff} = v(r) + \int \frac{\tilde{n}(r)\tilde{n}(r')}{|r - r'|} dr' + v_{xc}(r), \qquad (2.146)$$

$$v_{xc}(r) = \frac{\delta}{\delta\tilde{n}(r)}E_{xc}[\tilde{n}(r)]|_{\tilde{n}(r)=n(r)}. \qquad (2.147)$$

The equations can now be solved and give the self-consistent Kohn-Sham equations which can be solved iteratively to the true density, or some desired cut off

$$(-\frac{1}{2}\nabla^2 + v_{eff}(r) - \varepsilon_j)\psi_j(r) = 0, \tag{2.148}$$

$$v_{eff}(r) = v(r) + \int \frac{n(r')}{|r - r'|}dr' + v_{xc}(r), \tag{2.149}$$

$$n(r) = \sum_{j=1}^{N} |\psi_j(r)|^2, \tag{2.150}$$

$$E = \sum_{j=1} \varepsilon_j + E_{xc}[n(r)] - \int v_{xc}(r)n(r)dv - \frac{1}{2}\int \frac{n(r)n(r')}{|r - r'|}. \tag{2.151}$$

The Kohn-Sham equations require some set of orbitals to be used during the optimisation. These are called the Kohn-Sham orbitals. However, unlike orbitals used in wave functions methods where they are one electron eigenfunctions of the system, the Kohn-Sham orbitals do not have the same physical meaning.[92, 93] But, the sum of the orbitals energies is related to the total energy *via*

$$E = \sum_{j=1}^{N} \varepsilon_j - E_H[n(r)] + E_{xc}[n(r)] - \int \frac{\delta E_{xc}[n(r)]}{\delta n(r)}n(r)dr, \tag{2.152}$$

$$E[n(r)] = T_s[n(r)] + \int v_{ext}(r)n(r)dr + E_H[n(r)] + E_{xc}[n(r)]. \tag{2.153}$$

Here, E_H is the Hartree energy and the kinetic energy has the form

$$T_s[n(r)] = \sum_{j=1}^{N} \int \phi_j^*(r)(-\frac{\hbar^2}{2m}\nabla^2)\phi_j dr. \tag{2.154}$$

The v_{ext} is the nuclei-electron interaction and can be substituted into equation 2.149 instead of the $v(r)$ term and the exchange-correlation potential, $v_{xc}(r)$ can be substituted for

$$v_{xc}(r) = \frac{\partial E_{xc}[n(r)]}{\partial n(r)}. \tag{2.155}$$

This allows the Kohn-Sham potential to be constructed from a sum of the external potentials of the inter-electronic interactions and the effective potential. This is done through a chosen set of Kohn-Sham orbitals to give the one-electron Kohn-Sham equation

$$\left(-\frac{1}{2}\nabla^2 + v_{ks}(r) - \varepsilon_j\right)\psi_j(r) = 0. \tag{2.156}$$

Kohn-Sham DFT and orbitals allow for a basis set to be selected and a solution to the Kohn-Sham equations to be found in an iterative and variational procedure. The solution should be exact, if the trial density used to construct the potential is close enough to the true density. However, for that to be correct the true functional, $F[n(r)]$ or $E_{xc}[n(r)]$ needs to be used. This is problematic, since the Hohenberg-Kohn theorems do not offer a description of the functional. As such a number of approximations for the functional have been made. This thesis will present the approximations to the Kohn-Sham $E_{xc}[n(r)]$ functional as that is the most common implementation of DFT. Moreover, it is the one used in this work.

The first approximation for the Kohn-Sham $E_{xc}[n(r)]$ functional was the local density approximation. This used the density from the uniform electron gas, in a finite set of space

$$E_{xc}^{LDA} = \int e_{xc}(n(r))n(r)dr. \tag{2.157}$$

The energy e_{xc} can be split into it constituent parts of exchange and correlation, which were calculated by Ceperley and Wigner for the homogeneous gas cloud

$$e_x(n) = -\frac{0.458}{r_s},$$ (2.158)

$$e_c(n) = -\frac{0.44}{r_s + 7.8},$$ (2.159)

r_s is the one-electron radius. It allows the potential to be constructed from the sum of these one electron terms.[94–96] There are a number of problems with the local density approximation. The most important of these is that it underestimates the exchange component in the system and overestimates the correlation part. This is because it is constructed from the homogeneous electron gas cloud, and as such is inherently mean field. Where this approximation is not appropriate, such as for any system of chemical interest, this leads to poor description of the systems. The approximation does work for some systems, where the errors cancel. However, such as predicting for solid state calculations.

The local density approximation treats the electrons in the system as being non-interacting. However, this is not a true reflection of the system.[97–99] If we take a system with an electron at some position r_i, then the density at position r_j can be given by

$$\int n_{xc}(r_i, r_j)dr_j = -1.$$ (2.160)

This is known as the exchange-correlation hole and transforms the system into one of an interacting set of electrons. It describes the reduction in electron density at r_j due to the electron being present at position r_i. This is sometimes called screening. To develop density functional theory further, screening needs to be incorporated into the functional. The way this is done is by introducing a Hamiltonian that depends on the λ, where $\lambda = 0$ represents the Kohn-Sham system and $\lambda = 1$ is the true physical system. This allows the density to be written as

$$n_{xc}(r_i, r_j) = \int_0^1 n_{xc}(r_i, r_j; \lambda)d\lambda.$$ (2.161)

Equation 2.161 can be solved exactly to give the exchange-correlation functional

$$E_{xc} = -\frac{1}{2}\int n(r)\bar{R}_{xc}^{-1}(r[n(\tilde{r})])dr,$$ (2.162)

where $\bar{R}_{xc}^{-1}(r[n(\tilde{r})])$ has the form

$$\bar{R}_{xc}^{-1}(r[n(\tilde{r})]) = \int \frac{-\tilde{n}_{xc}(r_i, r_j[n(\tilde{r})])}{|r_i - r_j|}dr.$$ (2.163)

As $\bar{R}_{xc}^{-1}(r[n(\tilde{r})])$ is expected to drop off rapidly with distance, we can expand the term and integrate to give

$$E_{xc} = E_{xc}^{LDA} + \int G_2(n)(\nabla n)^2 dr + \int [G_4(n)(\nabla^2 n)^2]dr + ...,$$ (2.164)

G_2 is a functional of the density. However this expression gives poor results, but resummation can leads to a useful sequence

$$E_{xc}^0 = \int \epsilon(n(r))n(r)dr(LDA),$$ (2.165)

$$E_{xc}^1 = \int f^1(n(r)|\nabla(r)|)n(r)dr(GGA).$$ (2.166)

The GGA, or generalised gradient approximation, depends not only on the density but the gradient of the density hence the name.[100–102] Most modern functionals are variants of GGA functionals, and they offer improvements in the calculated energies and thermodynamic data compared to LDA functionals. Another class of functional is the hybrid functional, most of which are GGA hybrid functionals. hybrid functionals make improvements to the functional by taking some contribution from the Hartree-Fock exchange energy. The inclusion of a better description of exchange results in improvements in the equilibrium bond length and vibrational frequencies. As such, they allow for

more accurate calculation of stationary point properties, compared to pure GGA functionals.

The most popular modern functional in use is the B3LYP functional developed by Becke, Lee, Yang and Perdew.[103, 104] It has some exhange contribution from the Hartree-Fock energy, and some contribution from the LDA exchange and correlation energy. This functional has 3 parameters which were optimised against the G1 molecule set. More recent functionals have undergone more byzantine parameterisation against data sets. Due to the inclusion of components from the LDA exchange-correlation energy, as well as the Hartree-Fock exchange, B3LYP offers excellent results for the equilibrium bond distances, Thus can give good starting geometries for higher level wave function methods.[103, 104] The benefit to using density functional theory is that due to its low computational expense, it allows hundreds of atoms to be treated using electronic structure methods, something that would be very hard with wave function methods beyond Hartree-Fock theory, without considering advances in linear scaling methods.[105–107]

2.11 Potential energy surfaces and chemical kinetics

As we have seen in this chapter computational chemistry allows us to calculate the energy of a system at a set geometry. This would in principle allows us to calculate the energy of the system at every geometry related to a reaction of interest. These energy points would be connected to each other through the change in coordinates along some vector, and thus we would be generating a potential energy surface (PES) of the reaction of interest. In chemistry this allows us to determine how likely a reaction is to happen, through kinetics, as well as calculate the energetics of the reaction, through thermodynamics. The power of this *ab initio* approach is that it allows us to understand fundimentally why reactions happen, as the surface depends on steric and electronic factors.

However, it becomes clear that doing this presents a number of challenges. The first is how to interpret and present the PES in a convenient and understandable manner. It is clear that the energy as a function of a few sets of coordinates could be presented as a 3-dimensional graph or as a contour

plot. However, it is not clear how it could be shown as a function of every coordinate in the system. The second issue is an even more fundamental one. If no other forces are acting on the system, then a non-linear system has 3N-6 degrees of freedom where N is the number of atoms. It would be unfeasible to calculate the energy at every point as a function of all these degrees of freedom for any system of interest. It is also not likely that all of these degrees of freedom are of interest to the reaction. If we take the reaction of peroxyl-dodecane (known as 1-oxidooxydodecane) abstracting a hydrogen from dodecane then in principle we have to calculate a surface dependent on 225 degrees of freedom. However, as this reaction is going to be most effected by the coordinates that pertain to the R-H bond breaking and O-H bond forming, we assume that it is not necessary to calculate all the other coordinates.

Most quantum chemistry software packages allow us to carry out a constrained optimisation of a system. This means that a single point on a reaction surface can be calculated, where all the other degrees of freedom are unrestricted, and can be optimised to the lowest energy point for that point of interest. This allows us to take a slice of the PES, fixing only the most important coordinate, while keeping the others free. If we consider this idea further, to determine whether a reaction is going to take place, and the rate at which it takes place. We can see that it is not even necessary to calculate every point along this reaction pathway. The most important states for determining the kinetic of a reaction are the low energy reactants, products and the transition state linking the two states, seen in figure 2.6.

The transition state in figure 2.6 is the highest energy point on a low energy reaction pathway. Other points on the full potential energy surface may be higher in energy, i.e. if all the bond lengths are extended by 1 Ångström, but these states are physically unlikely to be formed. This transition state can also be called an activated complex, and is the conceptual highest energy state in a single step reaction, and thus is the rate limiting state.[108–110] The concept of the transition states give a physical meaning to the Arrhenius rate equation and allows us to use quantum chemistry to investigate chemical reactions from first principles.

This thesis will construct a kinetic mechanism by using the kinetic and thermodynamic parameters calculated from the *ab initio* calculations in Gaus-
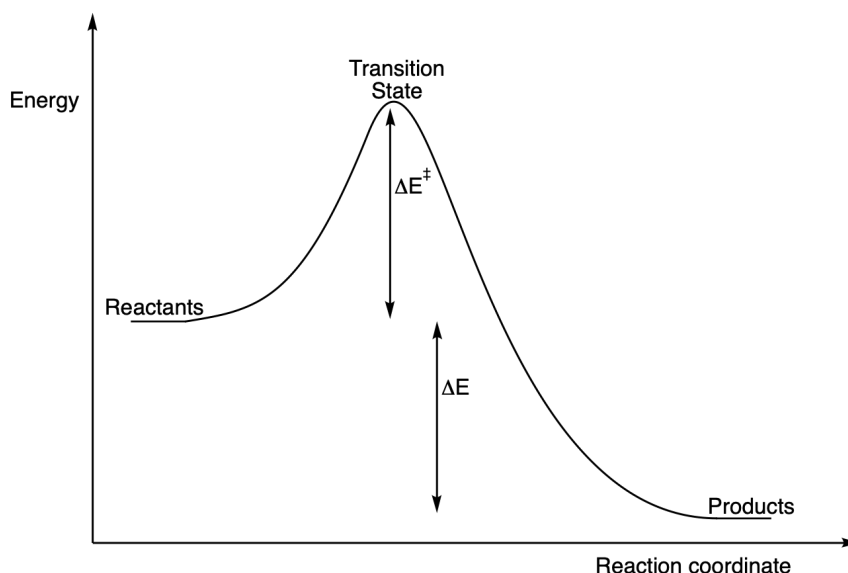
Fig. 2.6: A theoretical 1-dimensional potential energy surface between some reactants and products through a transition state.

sian.[111–119] The kinetic and thermodynamic data can be used to generate Arrhenius parameters from the Arrhenius rate equation seen in 2.167

$$k(T) = Ae^{\frac{-E_a}{RT}}. \tag{2.167}$$

In equation 2.167, E_a is our energy of activation, R in the gas constant, T is the temperature and A is the pre-exponential factor. Alternatively the Arrhenius equation can be rewritten as 2.168 through the transition state theory (TST) interpretation proposed by Eyring *et al.*[108, 109, 120] In this form the Arrhenius equation can be written as

$$k(T) = \frac{k_B T}{h} e^{\frac{-\Delta G^\ddagger}{RT}}, \tag{2.168}$$

with the pre-exponential factor being replaced by a term including the Boltzmann constant, k_B. As the Gibbs energy can be separated into its component parts, equation 2.168 can be rewritten as

$$k(T) = \frac{k_B T}{h} e^{\frac{\Delta S^\ddagger}{R}} e^{\frac{-\Delta H^\ddagger}{RT}}. \tag{2.169}$$

In condensed systems, as the $P\Delta V$ term will be small, this is the equivalent to

$$k(T) = \frac{k_B T}{h} e^{\frac{\Delta S^{\ddagger}}{R}} e^{\frac{-\Delta E^{\ddagger}}{RT}}. \qquad (2.170)$$

As such we see that our Arrhenius parameters can be derived from first principles, with $H^{\ddagger}$ being our energy of activation, and 2.171 being our pre-exponential factor

$$A = \frac{k_B T}{h} e^{\frac{\Delta S^{\ddagger}}{R}}. \qquad (2.171)$$

This gives us a physical interpretation of the pre-exponential factor from the Arrhenius equation. It can also be called the frequency factor, and in collision theory it depends on how likely a reaction between two species is to happen if they collide, determined by the orientation of the molecules. In transition state theory this is interpreted as the entropy of activation. This is more rigorous, as it can tell more about nature of the transition state, and the reactions kinetics. The internal energy of the transition state is now included in the pre-exponential factor using transition state theory. This allows molecular vibrations and rotations that couple to the reaction coordinate, which could stabilise or destabilise the transition state, to be included. The thermodynamic data generated from Gaussian, and particularly the entropic contribution of the Gibbs energy, can be improved through the use of the GoodVibes program.[121] In this program, improvements are made to the thermodynamics by correcting the description of the low frequency rovibrational modes by introducing a quasi-harmonic approximation to the vibrational modes.[122–126] The correction to the entropic terms can be done in two ways, either the more simple approach of cutting of the contribution from all mode bellow 100 wavenumbers, or by dampening these modes. Improvements are also made to the enthalpic description of the rovibrational modes allowing for better descriptions of the vibrations and rotations that effect the reaction coordinate.

It is important to remember that Arrhenius reaction rate theory was developed as an empirical theory. Thus, in its original formulation, a multi step mechanism had a single set of reaction rate parameters. This means that when

constructing a mechanism using quantum chemistry to study the autoxidation of aviation fuels, care must be taken to construct it from single step processes. The entire mechanism may have a rate determining step, or rate determining state, which we will be able to identify using quantum chemistry.[110] These discussions will be based not only on the kinetics parameters calculated from the frequency calculations carried out in Gaussian, which takes the second derivatives of the wavefunction to calculate the thermodynamics of the systems, but also from the electronic energy of the systems.

There are some limitations to the interpretation of transition state theory that are being used in this thesis. It is assumed that when the transition state is formed, the reaction goes to completion, and products are formed. This is not always true if the transition state is very short lived and the vibrational modes in the transition state do not have time to reach a Boltzmann distribution. Standard transition state theory also does not include quantum tunnelling into its description of a reaction. This is of particular importance for cold temperature reaction. Therefore, it is unlikely to be in effect during autoxidation. However, transition state theory can be modified with WKB theory to include it. As can be expected, at higher temperature the theory also breakdown, as it does not fully describe the role of vibrational modes in stabilising and destabilising transition states.

Literature Review 3

The literature review in this thesis focuses on the previous work carried out in the field of thermal stability. The main purpose of this literature review will be to cover the effect that a fuels chemical composition has on autoxidaiton, and its role in the deposition mechanisms. This includes the implication that the origin and production methods have on the chemistry and composition of aviation fuel. However, this is just one aspect of the field of thermal stability, with physical and flow issues also affecting thermal stability, and will be covered in this review. This review will also summarise and critique the literature investigating the modelling approaches used to predict the thermal stability of aviation fuels. Finally a summary of the literature will be presented and future directions to fill gaps in the literature will be discussed.

3.1 Chemical composition and thermal stability

Before commencing the review of the literature into the role that a fuels chemical composition has on its thermal stability, it is important to discuss what chemical species are present in the fuel, and how they alter the properties of the fuel. The major component of all aviation fuel is the hydrocarbon component, but as discussed in chapter 1, the nature of this component can be varied while still meeting the property requirements set out in the fuel specification documents. The hydrocarbon species found in jet fuel include straight chain n-alkanes, branched iso-alkanes, cyclic alkanes of various sizes, mono and poly-aromatics rings. These hydrocarbons all have different effects on the fuel properties. The n-alkanes and iso-alkanes form the majority of the hydrocarbon fuel, they have high hydrogen to carbon ratios, increasing the fuels heat to weight ratio. They offer good combustion properties for the fuel, reducing the polluting emissions, and the fuels negative environmental impacts. However, due to n-alkanes uniform structure they have high freeze points, as they can pack tighter, and form strong Van der Waals forces between the chains. They also have high viscosity at low temperatures which can reduce the ability to pump the fuel to the engines. To combat this issue, the ratio of iso-alkanes can be increased to reduce the freezing point of the fuel, and improve their viscosity. However, this can reduce the energy density

and the maximum range of the fuel. To improve the energy density of the fuel, aromatic hydrocarbons can be added to the fuel. They are hydrogen deficient compared to saturated hydrocarbons, meaning they have very poor combustion properties, and form a lot of smoke and carbon particulates when burned. Example chemical structures of these classes of hydrocarbon can be seen in figure 3.1.
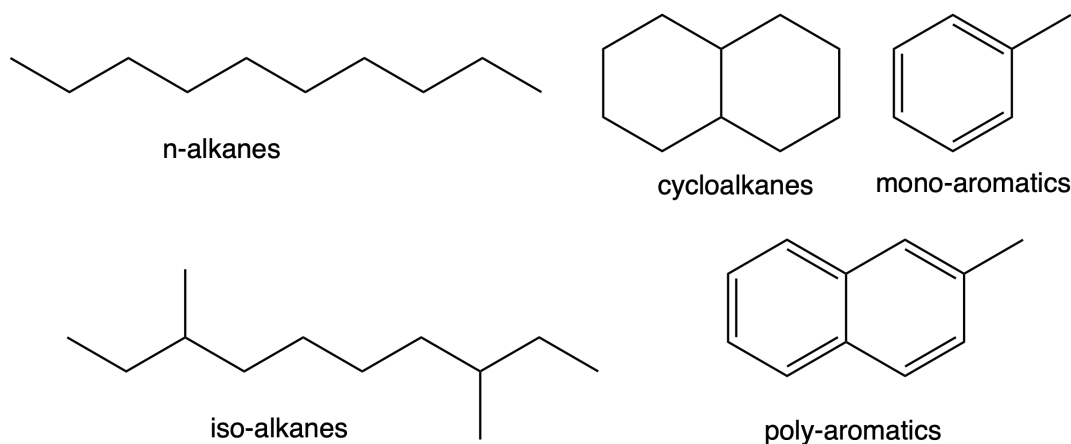
Fig. 3.1: Common chemical structures of classes of the hydrocarbon components found in aviation fuel.

The hydrocarbon component of the fuel is known to control its bulk properties. However, aviation fuel has trace components and impurities, with their concentration being limited by the fuel specification as they affect some properties of the fuel. These include the fuels lubricity and cleanliness. These minor components of the fuel include polar oxygenated species, sulfur and nitrogen containing compounds and metal impurities. An example of the species which can be found in the fuel can be seen in figure 3.2. The exact composition and concentrations of these species can be affected by the a number of factors such as the feedstock and the post-production processing that the fuel is subjected to. Oxygen and nitrogen containing species, particularly heteroatomic aromatic species, have been suggested to have negative effects on the fuels thermal stability and cleanliness. However, they can act as antioxidants in the fuel, with particularly phenolic species found in the fuel thought to improve the storage and thermal stability. Sulfur species are found in high concentrations in fuels originating from heavy oils sources, and have been suggested to improve the lubricity of the fuel by binding to the metal surfaces and increasing the slip between the fuel and the surface. However, all of these species have been linked to reduce the thermal stability of a fuel, as sulfur,

oxygen and nitrogen have been found in the deposits in high concentrations. This will be discussed later in this review in more detail.
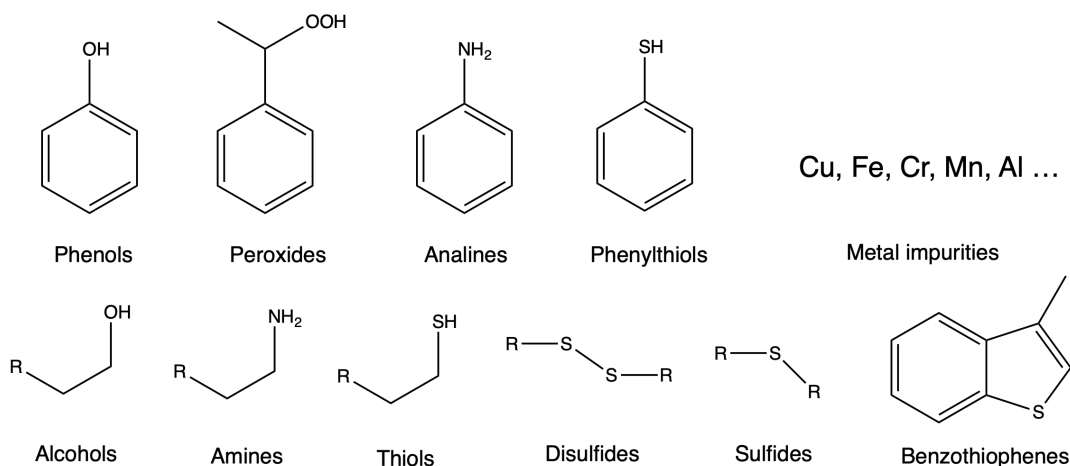
Fig. 3.2: Example chemical strucutres of trace impurities commonly found in aviation fuel.

A number of additive packages are also used in the fuel to alter it properties, with these having heteroatomic species in them, and are found in low concentrations in the fuel. However, they can affect the thermal stability of the fuel, which will discussed in greater detail in the relevant section.

3.1.1 Hydrocarbon composition

This review will start by investigating the affect that hydrocarbon composition has on the thermal stability of a fuel and the oxidation rate and mechanism. Early studies into the affect of the hydrocarbons structure has on its oxidation was focused not only in relation to the thermal stability of these chemicals, but also on their use as monomers for polymerisation. The work by Mayo *et al*, Howard *et al* and Taylor *et al* investigated the rate of oxidation of a number of saturated and unsaturated hydrocarbons including aromatic species.[127–137] The authors found in separate studies that alkenes, particularly styrene, were very reactive to radical oxidation and radical species, and formed higher molecular weight products. Under oxidative conditions these products would also have high amounts of oxygen present in them. However, the authors were unclear if the styrene monomers are oxidised prior to polymerisation or if the extended oligomer system, are oxidised post polymerisation. Due to the fast rate of polymerisation of the styrene monomers once initiated, and high aromatic stabilisation of oxidisation products, it would be suggested that the

oligomer is oxidised after formation. The literature indicates that all alkenes have a very poor effect on the thermal stability of aviation fuel as they can form oligomers in the fuel. Alkenes are also easily oxidised, as the hydrogen next to unsaturated double bond can be easily abstracted and the radical formed is stabilised by conjugation with the double bond. The product of these reactions, and the alkenes themselves are facile towards addition reactions with the oxygenated products of the fuel, yielding extended oxygenated compounds. For this reason alkenes are seen as undesirable in the fuel, as they do not provide any benefits to the other fuel properties, and are excluded from the fuel through hydrotreatment.

Alkanes fall into two branches, cyclic and noncyclic, which can be branched or unbranched. These classes of alkanes are also referred to as cycloalkanes, n-alkanes and iso-alkanes. Previous work investigating the affect that branching has on the abstraction has shown that tertiary carbons react quicker, forming the radical.[138] This is caused by the adjacent carbons donating electron density to the electron deficient radical centre, stabilising the radical through inductive effects. Experimental work carried out at IFPEN found that increasing chain length caused a reduction in the induction period of the fuel.[138, 139] This continued up to a plateau reached at 12 carbons chains and longer. The authors also found that a mixtures of hydrocarbon with various chain lengths showed a linear response behaviour, indicating that the rate of their autoxidation is caused by the ratio of terminal and chain carbons in the hydrocarbon. This would provide evidence in support that its the stabilisation of the radical through inductive effects that affects the rate of hydrogen abstraction.

The roles that cycloalkanes have on the thermal stability is open to debate. They increase the density of a fuel when compared to iso-alkanes, which means that they offer the benefit of improving the range of aircraft when used if their thermal stability can be understood. Previous work at IFPEN indicates that they do not increase the induction period and as such the authors stated that they are not acting as an antioxidant in the fuel.[140] The work by IFPEN indicates that they do not increase the induction period or the total deposit formed when compared to aromatic species. This is important as they would improve the thermal stability of a fuel, when compared to aromatics, meaning they can be used to increase energy density of a fuel without decreasing thermal stability. If cyclic hydrocarbons increase the range without affecting thermal stability, then synthetic fuels can be developed to take advantage of

this. However the work from IFPEN and Dayton point to the fact that not all aromatics and cyclic-alkanes are the same, with toluene behaving differently to methyl-naphthalene, and decalin to tetralin.

Wong and Bittker investigated the deposition of four hydrocarbons over a temperature range of 150-450 °C.[141] In this study it was found that 1-hexene was the most autoxidatively unstable and formed the most deposits, this is unsurprising, because as discussed due to the unsaturated double bond it is particularly reactive to radical addition. Cyclohexane caused the next most deposits, with decane and benzene exhibiting much less deposition. The authors said that this was due to decane and cyclohexane having much stronger C-H bonds, and as such initiating the oxidation reactions was more difficult.

Aromatics

Aromatic hydrocarbons that occur naturally in aviation fuel help to improve the energy density both in terms of by volume and weight. However, they have a negative effect on the combustion properties of the fuel, hence limits are imposed. Their affect on the thermal stability of aviation fuel is complex and not completely understood. The literature indicates that the aromatic hydrocarbons can improve the stability of the fuel, by reducing the rate of the deposition, while increasing the amount of deposit formed overall. Work carried out at IFPEN indicated that the addition of aromatic increased the induction period of the oxidation of the fuel.[140] This increased induction period was found to be particularly effective for larger aromatic hydrocarbons with benzylic carbons. This supports the earlier work carried out by Igarashi *et al* and Taylor *et al*.[134, 142, 143] That work showed that 1-methyl-naphthalene (1-MN) had a dramatic affect in increasing the induction period of the fuel. It is suggested that this is caused by the stabilisation of the radical formed on the benzylic carbon by conjugation through the two aromatic rings. The effect was seen by Taylor *et al* in a number of aromatic hydrocarbons, with the increased aromaticity of the hydrocarbon used leading to decreasing rates of deposition. Taylor suggested that there was a a trend with the number of benzylic hydrogen available, and the inhibition in the rate of deposition, with separate trends of the mono-aromatic and bi-aromatic species. Wong and Bittker investigated the deposition of four hydrocarbons over a temperature range of 150-450 °C.[141] In this study it was found that benzene was a pecu-

liar molecule, as it has no labile C-H bonds to abstracted easily, and different results would be expected for alkyl substituted benzene molecules. As such it is not particularly representative of the fuel.
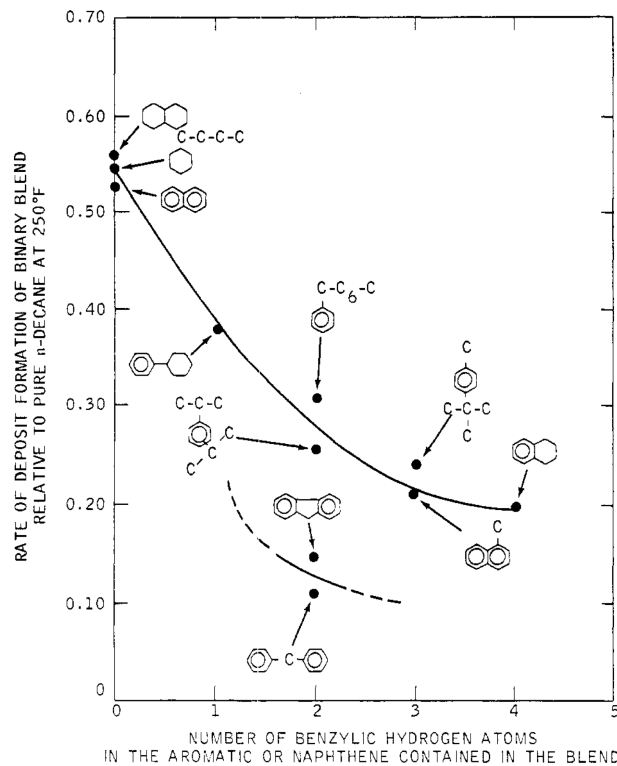
Fig. 3.3: Effect of aromatic structure on deposition rate seen by Taylor in 1969 (taken from [134])

Research has been carried out recently by groups at the University of Dayton and French Institute of Petroleum and Energy (IFPEN) investigating the effect that hydrocarbon structure has on the induction period and total deposition.[138, 140, 144–146] It has been found that despite increasing the induction period of oxidation in aviation fuels, aromatic hydrocarbons increase the total amount of deposit formed during the oxidation process. Increasing the size of the aromatic species added to a test fuel has shown an increase in the amount of deposit, with 1-MN leading to a dramatic increase in deposit over single ringed aromatics. This leads to a picture where aromatics are slower to oxidise, and slow the rate of deposition, but form more deposits eventually. This is highlighted by Heneghan *et al* where the the addition of antioxidant to a fuel leads to slow deposition but more deposit over all.[147] This would suggest that the product forming reactions for the AO_2 recombination are much slower than that for RO_2 recombination, but the products

must at least be much more polar compared to the bulk fuel, if not more thermodynamically stable, to form increased amounts of deposit.

The group based in IFPEN have investigated the role that aromatic hydro-carbons and chain length have on thermal stability. Their work showed that aromatics increased the induction period slowing the deposition rate. In the case of 1-methyl-naphthalene (1-MN) the increase in induction period was dramatic, with the addition of 10% 1-MN resulting in a 25 fold increase. This supports the finds of Igarashi *et al* previously. However the inclusion of 1-MN lead to greater total deposition, indicating that they are susceptible to oxidation. It's proposed that the aryl C-H bonds are weaker than alkyl C-H, and act as antioxidants in the fuel. It is also suspected that they are prefer-entially oxidised, forming phenols which also act as antioxidants, increasing the induction period. This explains how the addition of aromatics increase total deposition as was found by the group in Sheffield.[148] The mechanism proposed by Igarashi is presented below.[142, 143]

The Zabarnick group at the University of Dayton demonstrated that increasing aromatic species size leads to increased deposit formation.[145, 146] It is suggested that because of their size, it requires fewer monomer units to form the insoluble gums. This coupled with the work from IFPEN suggests that larger aromatic species are easier to oxidise, the likely cause being that oxidising one of the rings maintains aromaticity in the other ring, with the aromaticity stabilising the radicals through conjugation. This would also account for these species demonstrating antioxidant effects on the fuel.

Jones and Balster added an aromatic hydrocarbon solvent to a hydrotreated fuel already doped with antioxidants, which had already shown to have good thermal stability, to investigate the role that the alkyl aromatics on a fuel thermal stability.[149] It was found that the addition of 12% by volume of aromatics to the fuel reduced the thermal stability, with the fuel having its time to reach a 50% oxygen depletion in the static bomb test decreased by 3 hours, from 13 hours to 9 hours. This can be seen in figure 3.4. The authors state that this reduction in thermal stability was caused by the labile C-H bond on the alkyl aromatics and thus they are preferentially oxidised at a much quicker rate.
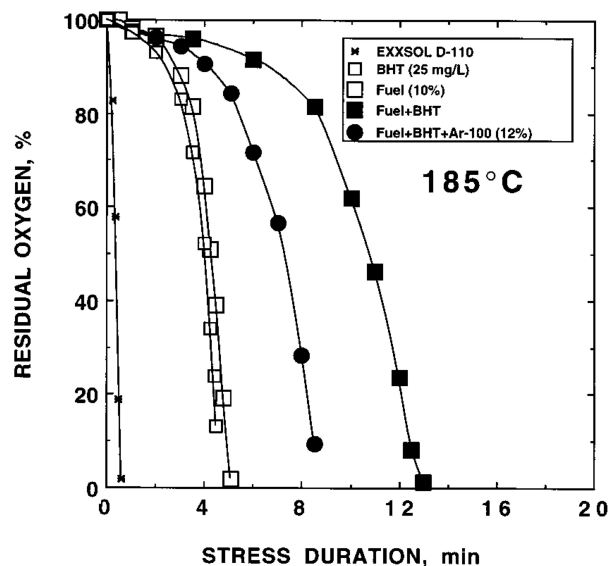
Fig. 3.4: The affect of the addition of alkyl aromatics to a hydrotreated fuel on its oxygen consumption in a static fuel tester, reprinted with permission from [149].

3.1.2 Minor components, additives and impurities

The hydrocarbon component of the fuel controls its bulk properties but the majority of the work investigating the thermal stability of a fuel has focused on the minor components. This is because the heteroatomic impurities and additives are generally thought to control the thermal stability and deposition behaviour of the fuel. These minor components in the fuel include polar oxygenated species, which either occur naturally or are added to the fuel as additives, sulfur and nitrogen containing compounds and metal impurities. This section will give an overview of the affect that these species have on thermal stability.

Fuel additives

A number of additives are added to the fuel to alter its properties and deal with specific issues in the fuel. The most important of these additives for thermal stability is antioxidant. The commonly used antioxidant is butylated hydroxytoluene (BHT), which is a highly sterically hindered phenol, but other hindered phenols are approved for use.[7, 20] Static dissipators (SDA) are used to improve the conductivity of the fuel and stop accidental sparking and

ignition of the fuel. Fuel system icing inhibitors (FSII) are added to stop the formation of water ice during high altitude flights. If fuels have poor lubricity, lubricity improvers can be added, to ensure that excessive wear does not occur. They also have the benefit of improving the resistance of the air-frame to corrosion so can also be called corrosion inhibitors (CI). Metal deactivators (MDA) are a subset of antioxidants, and are used in the fuel to chelate copper and stop it from reacting with the fuel, but can also act as a hydrogen donating antioxidant. Some of these additives can be seen in figure 3.5. Other additives can be used to counter specific problems encountered during service. Biocide can be used to deal with the microbial growth in the fuel tanks and leak detection additives during fuel tank filling. Significant study has focused on the affect of doping fuels with antioxidants and MDA. This will be the main focus of this section, with limited consideration of the other additives.
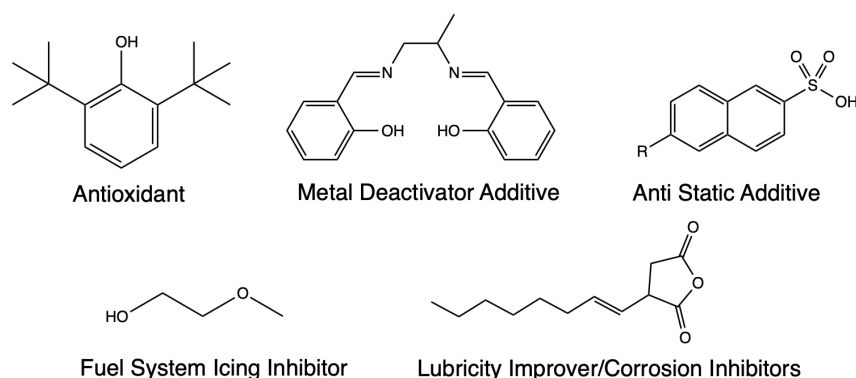
Fig. 3.5: Additives approved for use in aviation fuel.

A number of studies have been carried out investigating the affect of doping fuels with approved additives, and unapproved derivatives and alternatives, on the fuels thermal stability. It was reported that the addition of additives to shale derived fuels had limited effect on the level of deposition, but antioxidant did improve the storage stability.[150] Nitrogen based antioxidants were shown to have a complex relationship in the fuel, with them neutralising acids formed during oxidation, but generally agreed to reduce the thermal stability.[151]

A study by Abdallah tested the affect that different additives packages had on the breakpoint of a fuel and the deposit of the fuel in the JFTOT.[152] Antioxidants (AO) were added to a base fuel with a high concentration of polar species, the author reported 181 ppm of phenols, with no affect observed on the break point of the fuel. Antioxidants were also added at a higher concentration of 400 ppm without the breakpoint being affected. The author speculates that this lack of response to antioxidants could be caused by the

fuel already having a high concentration of naturally occurring phenols in the fuel fulfilling the role of antioxidants in the fuel. The author was also able to show that icing inhibitors (+10°C) and metal deactivators increased the breakpoint of the fuel, with metal deactivators improving the breakpoint by at least 45°C, with the breakpoint of the fuel extending beyond the range of the test. Static dissipators (SDA) and corrosion inhibitors (CI) lowered the break point of the fuel by -5°C and -10°C respectively. Abdallah combined additive packages and doped them in the fuel. FSII when used in combination with CI, AO and SDA, it was found that its positive effects on breakpoint were nullified, although the overall deposit formed above the breakpoint was reduced.

Abdallah also investigated the affect that doping had on the amount of deposition in the JFTOT.[152] It was found that AO, SDA and CI all increased the amount of deposit compared to the reference fuel when heated above the breakpoint. The same increase in deposit was observed when the fuel was doped with AO, CI, SDA, and FSII. The author highlighted the interesting antagonist behaviour that all these additives had on the deposit. As AO did not affect breakpoint of the test, but increased the level of deposit, it is clear that the heteroatomic aromatics such as AOs can react to form deposits without being involved in the oxidation reactions.

Rawson *et al* demonstrated that the addition of synthetic antioxidants to thermal stressed MEROX treated and hydroprocessed fuels, results in all fuels demonstrating an improvement in induction period during testing in the PetroOxy static bomb reactor.[153] However, it was also found that the addition of antioxidants to aged fuels had little effect on the level of peroxides formed in the fuels. As such, it can be concluded that antioxidants have a limited role in the breakdown of peroxides in the fuel. Therefore, it would be expected that at longer test times greater levels of deposition should be seen. The hydroprocessed fuel had slower antioxidant consumption during storage than the MEROX treated fuel The authors stated indicated that the synthetic antioxidants added to the MEROX fuel were preferentially consumed over the naturally occurring phenols. This would suggest that hydroprocessed fuels are naturally more stable to storage than MEROX fuels, but that they oxidise quicker under thermal stressing due to the lower concentration of natural antioxidants in the fuels, as seen by the shorter induction period times for these fuels in the PetroOxy tests.

Morris *et al* also found that the addition of antioxidants to fuels had limited impact on the level of peroxides formed in a fuel during storage.[154] However, It was found that the addition of antioxidants to a hydroprocessed fuel prior to testing stopped the formation of peroxides during thermal stressing in the low pressure reactor at 90 °C in an oxygen rich environment. Without antioxidants, the hydroprocessed fuel would produce 2400 ppm of active oxygen in 64 hours of testing, compared to 8 ppm when 24 mg/L of antioxidant was added to the fuel. Dinkov *et al* investigated the affect of that adding antioxidants to bio-fuel blends on their properties by measuring the Total Acid Number (TAN), density and viscosity, total solubles formed during oxidation and the concentration of peroxides.[155] It was found that the addition of 250 ppm of antioxidants had no impact on the physical properties of the bio-fuel blend. Moreover, it reduced the TAN and concentration of unsaturated hydrocarbons in the blends. The antioxidants reduced the amount of insoluble material formed during oxidation for all blending ratios. For blends with <10% bio-fuel content, it stopped the formation of peroxides during heating at 93 °C for 16 hours. At higher bio-fuel percentage blend concentrations, this reduction was not observed. As the antioxidants had no effect on the concentration of peroxides at 30% blending ratio, but did reduce the amount of insoluble material, the relationship is more complex than that as reduction in peroxides leads to less insoluble material formed. The reason for the observation could be that increasing bio-fuel blend ratio increases the solubility of the fuel, as the authors note. However, an iso-octane wash was used to separate the insolubles. Thus, it cannot account for all of the observations.

Jones and Balster investigated the interaction of synthetic antioxidants with those naturally occurring in the fuel and the affect of blending of straight-run fuel with solvent.[149] These experiments, fuels and industrial hydrocarbon solvents were doped with antioxidants and thermally stressed in a static bomb reactor, measuring the oxygen depletion. The authors reported that as the concentration of naturally occurring and synthetic antioxidants in the fuel increased, so did the time needed to induce rapid oxidation, indicating that both classes of antioxidants participated in chain-breaking mechanisms. It was also found that a synergistic effect was observed, when 5% of the fuel with natural antioxidants was added to the paraffinic solvent, and the synthetic antioxidant was in concentrations over 10 mg/L. These results can be seen in figure 3.6. However, deposition studies were not carried out so it is unclear if this high concentration of polar species lead to greater deposition in longer tests. Moreover, the authors state that because of the level of dilution of the

fuel in the blends tested, to achieve similar results in straight-run fuel a high concentration of >100 mg/L would need to be used.
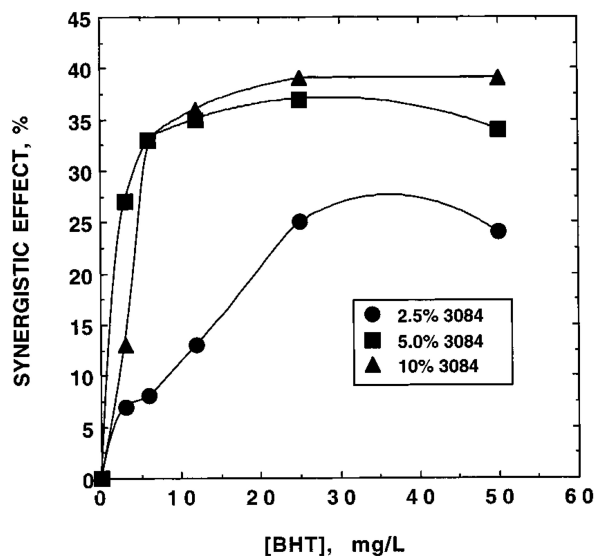
Fig. 3.6: The calculated synergistic effect for an industrial solvent, blended with increasing concentration of a fuel with naturally occurring antioxidants, and doped with increasing concentrations of the synthetic antioxidant BHT. Reprinted with permission from [156].

Kerkering *et al* studied the effect of different phenol antioxidants on the oxidation induction period and nature of sedimentation.[157, 158] In the first study, a middle-distillate model fuel was doped with 0.1 mol/L polar species, including phenols. The samples were heated at 120 °C for 24 hours in an autoclave. 2,6-dimethylphenol reduced the amount of sediment formed, from 164 mg to 148 mg over 24 hours, and 2-naphthol reduced sedimentation by 1 mg. Both phenols tested reduced the percentage of oxygen in the sediment and increased the percentage of carbon in the deposit, but had no effect on the percentage of hydrogen. This indicates that the deposit is formed from aromatic rings, and with the 2-naphthol having a higher carbon percentage and a lower oxygen percentage compared to 2,6-dimethylphenol, that the phenols are forming a major constituent of the deposit. The authors proposed possible products from the electron-spray mass-spectrometry carried out which can be seen below in figure 3.7. It was conclude that the phenols were preferentially oxidised and formed polymeric insoluble products up to 6 units long during sedimentation. In a follow up study, model fuels were doped with different naturally occurring and synthetic phenols, and heated in the PetroOxy static fuel tester at 140 °C. All phenolic antioxidants tested improved the induction period of the fuels. However, the stability increase by

the individual phenols was dependent on the model fuel being tested, but the general trend of phenols with multiple aromatic rings and substitutions on the ortho and para position being the most effective held true for all fuel. It was suggested that the increase in the oxidative stability was due to the reduced bond strength of the O-H bond and the stabilisation of the radical species formed by the substitutions on the ring in those positions. This study did not investigate the affect that the antioxidants had on the total deposition or on the nature of the products formed.
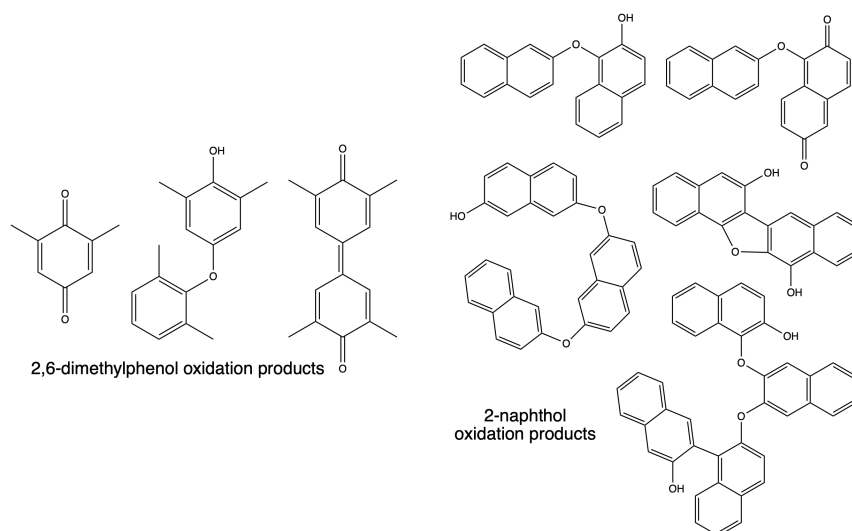
Fig. 3.7: Possible oxidation products found in the sediment for 2,6-dimethylphenol and 2-naphthol proposed by [158].

Heneghan *et al* investigated the effect of number of additive packages including antioxidants.[159] It was found that when antioxidant was added to a straight run Jet-A fuel, little affect was observed on the temperature at which oxidation occurred in a single-pass heat-exchanger test rig, and had a negative effect on the level of deposition. Improvements were observed when antioxidants were used in combination with MDA. Jones *et al* observed that the doping of fuels with antioxidants slowed the rate of oxidation.[160, 161] However, when not used in combination with MDA and dispersants, the antioxidant had little impact on the level of deposit. A number of synthetic antioxidants were added to bio-fuels by Karavalakis *et al* and Focke *et al*, the structure of which can be seen in figure 3.8.[162, 163] Focke *et al* demonstrated that tert-butylhydroquinone (TBHQ) improved the stability of bio-fuels in the Rancimat test and at doping levels of 0.5% wt and above the bio-fuels had induction times exceeding the European minimum of 6 hours. Karavalakis *et al* found that TBHQ, propyl gallate (PG), and pyrogallol (PA) improved the induction period in the Rancimat test by 19, 15 and 14 hours respectively.[162]

Butylated hydroxytoluene (BHT) and butylated hydroxyanisol (BHA) were less effective, only improving the induction period by 2 and 45 hours respectively. The authors suggested that the greater stability demonstrated by TBHQ, PG and PA could be attributed to them having more than one phenol group, and them being in the ortho or para position supporting the findings by Kerkering *et al.*[164]
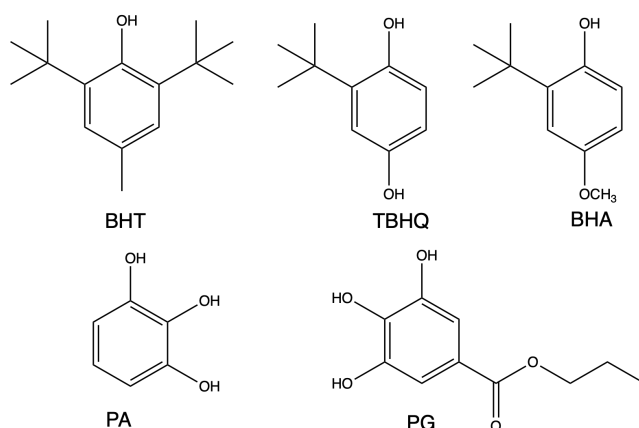
Fig. 3.8: Phenolic antioxidants used in the study by [162, 163]. Butylated hydroxytoluene (BHT), tert butylhydroquinone (TBHQ), butylated hydroxyanisol (BHA), propyl gallate (PG), and pyrogallol (PA)

A number of papers have looked at the development of future antioxidants for using in petroleum products.[165–171] This review will briefly summarise the findings and proposals from these papers. Most of the literature in this field suggests novel antioxidants based on a heteroatomic aromatic backbone with nitrogen and oxygen groups present. A paper by Wijtmans *et al* found that 6-Substituted-2,4-dimethyl-3-pyridinols compounds were very effective antioxidants for slowing the autoxidation of sytrene, with the most electron rich pyridinols performing the best.[165] Valgimigli and Pratt proposed antioxidants which had multi-ring sytems and both oxygen and nitrogen present, as well as N,N-diarylalkoxyamines, as a next genration of antioxidants.[166] N,N-diarylalkoxyamines was found to react rapidly with peroxides independent of temperature, which the authors attributed to the lack of a reaction barrier. A study by Haidasz *et al* studied the mechanism of oxidation inhibition of N,N-diarylalkoxyamines and N-phenyl-β-naphthylamines though kinetic isotope studies.[167] The two classes of antioxidants demonstrated different mechanisms for reacting with radicals. These can be seen in figure 3.9. The N,N-diarylalkoxyamines decompose though N-O homolytic fission and disproportionation. The N-phenyl-β-naphthylamine instead decompose though a retro-carbon-yl-ene reaction. The authors comment that this make N-phenyl-

β-naphthylamines more suitable for use as antioxidants as deleterious side reactions are limited.
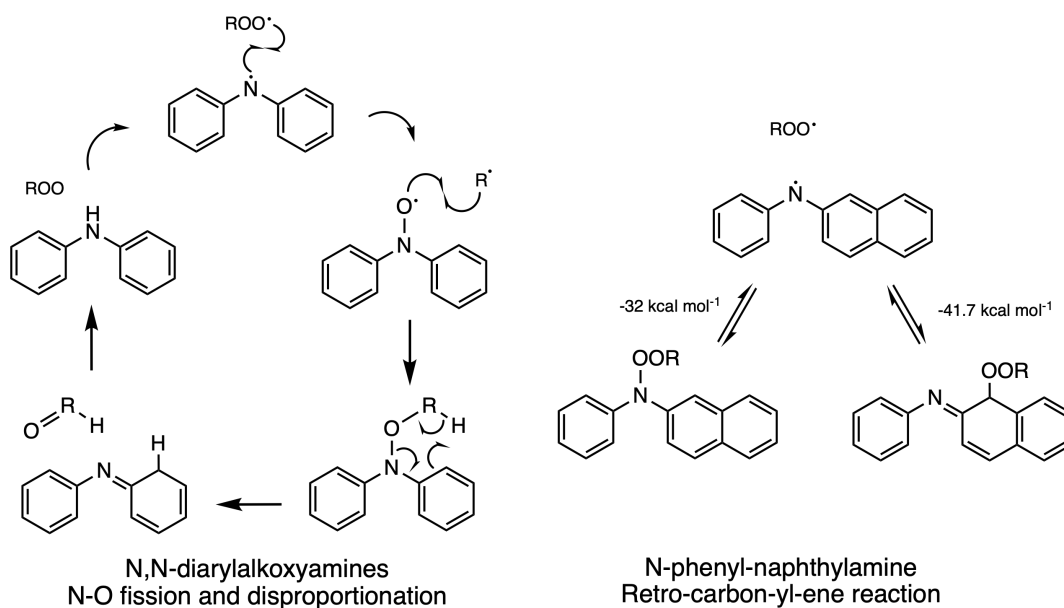
Fig. 3.9: Mechanism for radical decomposition by proposed antioxidants, from [166, 167].

These findings are supported by the work of Bendary *et al*, who investigated the effectiveness of phenols and anilines as antioxidants, through chain breaking mechanism.[172] In that study the authors found that anilines reacted more readily with hydrogen peroxide in scavenging reactions and thus slowed the rate of oxidation more than phenols. This was attributed to the anilines having lower ionisation potential with the authors stating that the peroxide scavenging reactions being controlled by the rate of electron transfer. However, the nitrogen containing aromatics reactivity was far more sensitive to the structural position of the amino group and they were less reactive to free radicals in the experiment. This would suggest that nitrogen containing antioxidants have a duel mechanism to slow oxidation. The first by reacting with peroxides, similar to the suspected role of sulfur, and the second by donating hydrogen to radicals formed in the fuel. Interestingly, the number of functional groups and position of the functional groups effected the reactivity of both types of antioxidants to hydrogen transfer reactions with radicals. Antioxidants with another functional group in the meta position had much lower reactivity.

Work by Beaver *et al* investigated the use of potential future antioxidants for use in high temperature fuels.[168–171] In the first study they investigated

dicyclohexylphenyl phosphine (DCP) reaction with molecular oxygen in the fuel.[169] The authors found that phospha dioxirane was formed during the oxidation of dodecane and that this similar reactivity was seen in other phosphine species. The formation of phospha dioxirane occurred through a low energy reaction, with an activation energy of 21 kcal mol^{-1}, at 160 °C. The DCP was also found to reduce the level of deposit formed in the tube reactor below that of the neat fuel in both the oxidative and pyrolytic regions. A concern for this additive would be that it could stimulate microbial growth as fuel lacks a natural source of phosphorus in the fuel naturally. As such, in the 2nd and 3rd paper oxygen based antioxidants were investigated.[170, 171] In these studies the authors proposed tetralin, α-tetralol and α-tetralone, which can be seen in figure 3.10. Tetralin and α-tetralone lead to a reduction in the level of deposition in a tube reactor, with the effect being dramatic when both were doped into the fuel, α-tetralol lead to a negligible drop in deposition. At longer tests in dodcane the α-tetralone lead to an increase in deposit formed when compared to the base dodecane, particularly at higher temperatures. The authors speculated that the antioxidants improved the thermal stability of fuel though two methods, one as a preferential hydrogen donor in the fuel, inhibiting aromatic oxidation. Interestly, the other was that the dopants changed the solubility of the fuel, and thus made it a better solvent for the polar oxidation products and limited agglomeration.

OH   O

Tetralin   Tetralol   Tetralone
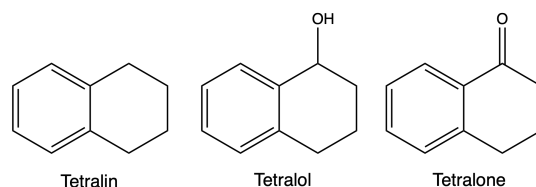
Fig. 3.10: Tetralin, α-tetralol and α-tetralone antioxidants proposed by [170, 171].

Waynick reviewed the development of metal deactivators and how they affect the thermal stability of aviation fuels.[173] The author presented evidence for MDA's improving the thermal stability of fuels, in the JFTOT test, without the presence of metal impurities in the fuel. However, the rate of oxygen was more complex as at two different copper concentrations, 1 and 4 ppb, the rate was slow significantly for the fuel with 1 ppb of copper but the MDA had a smaller effect on the higher concentration. A number of reasons for this were postulated for this, that the MDA is passivating the surface of the JFTOT and thus stopping heterogeneous catalysis, and at the higher concentration the MDA was chelating with the copper and could not bind to the surface. Another reason could be at that copper concentration, more of the MDA is chelating

with the metal, and thus cannot fulfil its duel role as an antioxidant in the fuel as effectively. In a further test, where MDA was added to fuel in different stages of the JFTOT test, it was found that the MDA again reduced depositon in the test even after deposit had already formed on the surface in the earlier testing. The author stated that this was evidence that surface passivation could not be the reason for reduced deposit formation in the JFTOT test. During longer testing after initial deposition, the level of deposit was worse for a fuel doped with MDA than for a fuel without the MDA. This indicates that while the MDA reduces the rate of oxidation and thus deposition it can eventually lead to greater deposition.

Pande and Hardy carried out longer JFTOT tests to understand the behaviour of MDA doped fuels under extended thermal stressing.[174] It was found that when MDA added to fuel at concentrations of 35 ppm it improved the gravimetric rating of the JFTOT test, because of the reduction in filterable insoluble material, whereas when antioxidant was added by it self no improvement was observed. The author postulated that due to the test length of 120 hours the effect of surface passivation of the steel metal strip used to stimulate heterogeneous catalysis was not important. The authors also concluded that MDA cannot be improving the thermal stability of a fuel though antioxidant behaviour alone, as the BHT didn't improve the thermal stability in these tests, although Waynick pointed out that BHT is less effective at improving thermal stability at the temperature and duration of testing used in the study.[173] Waynick suggests that the improvement by MDA could be due to acting as a Brønsted base which can neutralise the acidic oxidised products that can react further to form insoluble species and deposits with the author stating that there is evidence for the amount of deposit being linked to acidity and that more work is required to investigate this observation in relation to MDA.

The study by Pande and Hardy also investigated how doping a fuel with MDA and BHT during storage effected its thermal stability.[174] It was found that when 35 ppm of MDA and 24 mg/L of BHT was added to the fuel its was less effective at reducing insoluble material than just the MDA at this concentration. Interestingly, when 15 ppm of MDA was used with the same concentration of BHT, the reduction in insoluble material was the same as when MDA was used by itself. This indicates that the two additives when used together have a deleterious synergistic effect. However, the doped fuel still performed better than the neat fuel in the gravimetric JFTOT. A similar reduction in deposit was observed by Abdallah when a fuel was doped with

MDA, the author also noted that the character of the deposit formed in the JFTOT tests was changed by the addition of MDA, and that while increasing temperature increased deposit it didn't produce the same linear response with the deposit build up moving to closer to the pipe inlet.[152] Heneghan *et al* also observed that MDA was the most effective additive at reducing the formation of insoluble material.[159] However, it was observed in that study that the pressure dropped in the filter with the addition of MDA, indicating that deposit was formed. With the material not being collected because it was soluble in the haxane wash used. In a similar study by Zabarnick and Grinstead in the QCM static bomb reactor fuels were doped with MDA, BHT and a dispersant.[175] In this study, 5 of the fuels demonstrated an increase in the amount of deposit formed during test, 2 decreased and 1 was unaffected. The authors stated that all fuels demonstrated improved thermal stability with MDA doping at higher temperatures.

This was supported by the findings of Jones *et al* in a study of 6 fuels with MDA, BHT and dispersants added, with the oxygen consumption and total deposit formed measured.[160] The rate of oxygen consumption was reduced for the 3 fuels with metals present and delayed deposition for 3 of these fuels. The MDA had little effect on the 3 fuels with no metals present. This study also found the complex behaviour of the additives when used in combination with each other, with the resulting thermal stability also effected by the fuels base chemical composition. This study highlighted that the dispersant was particularly effective at slowing oxidation and deposition, which the authors attributed to it stopping agglomeration of polar oxidised products.

Another study by Zabarnick and Whitacre doping a fuel with varying levels of MDA in the QCM at 140 °C demonstrated that increasing the concentration of MDA increased the induction period and that this occurred above the concentration need to chelate the copper present in the fuel.[176] The authors proposed that this observation was caused by either the MDA acting as an antioxidant or by complexing with acids in the fuel. They expanded on the mechanism already postulated, by stating that as the fuel oxidised the MDA would be protonated and thus bind less strongly with copper. This would explain the increasing time of the induction period, as once all the MDA had been protonated the released copper would greatly increase the rate of oxidation. Thus, as the oxidation mechanism progresses it would be expected to increasing concentration of protonated MDA. However, GC-MS studies were inconclusive.

As would be expected fuel additive packages have a significant impact on their thermal stability. Antioxidants and Metal deactivators improve the storage stability and resistance to oxidation of fuel when used to deal with specific problems in the fuel. However, it is clear that misuse and over use can lead to great deposition under extended periods of heating. An interesting area of future study would be the investigation of the affect of using multiple additive packages in combination with each other. The literature indicates that some combinations demonstrate a synergistic improvement, while other have a negative effect when used together.

Heteroatomic species

The additive packages used in aviation fuel are a subset of the heteroatomic minor compounds found in the fuel. The concentration of these heteroatomic species is significantly altered by the origin of the feedstock and the post-distillation processing that the fuel undergoes. The heteroatomic minor species found in the fuel can be oxygenated species, as well as nitrogen and sulfur contain compounds, with these species being both aromatic and aliphatic in nature.[177–179] This section focusing on the naturally occurring oxygen and nitrogen species in the fuel, as they have been suggested to have negative effects on the fuel thermal stability, particularly the heteroaromatic species as they are thought to react with the radical product of oxidation to form insoluble material. The role of sulfur species will be treated separately in a subsequent section. The chemical structure of some of the heteroatomic species found in the fuel can be seen in figure 3.11.

Phenols are the most abundant heteroatomic species found in the fuel, with them occurring naturally in the fuel, and being added in the form of additive packages discussed previously to improve their storage stability. As discussed in the previous section, antioxidant additives are thought to slow the rate of oxidation through radical chain breaking reactions by hydrogen abstraction reactions, and stabilising the radical with the steric large side groups hindering further reaction. However, naturally occurring phenols have demonstrated a more complex relationship in the fuel. In a review of thermal stability of diesel oils by Batts and Zuhdan Fathoni, there were conflicting reports of phenols either had a no effect of sedimentation, or of them causing a decrease in stability.[150] However it was highlighted that Naphthol was particularly deleterious to thermal stability. It was suggested that this could be due to it
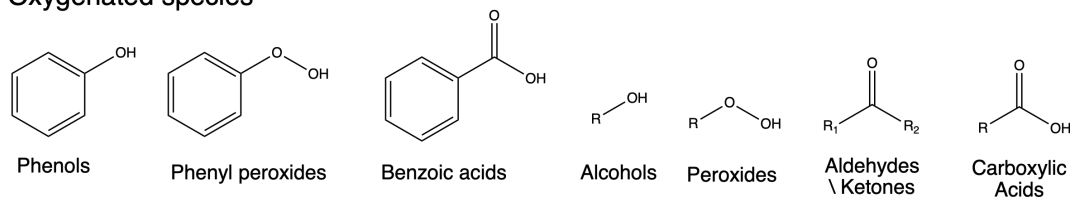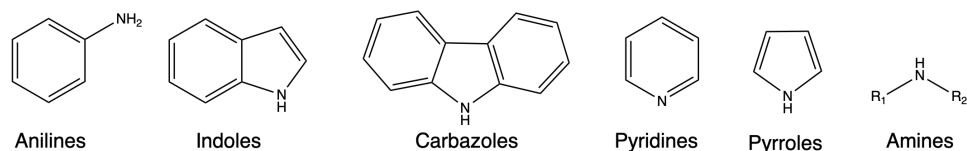
Fig. 3.11: A non-exhaustive list of some of the naturally occurring heteroatomic species found in aviation fuel, with the exact composition dependant of the fuels origin and post-distillation processing.[177–179]

being susceptible to oxidative coupling and forming larger polar species.[180, 181]

The mechanism for this oxidative coupling has been studied in great depth by the groups of Hardy and Beaver.[15, 180–185] Hardy and Wechter proposed the importance of Soluble Macromolecular Oxidatively Reactive Species (SMORS) in the formation of insoluble materials in middle distillate fuels in 1990.[180] The authors found that when methanol soluble species were extracted from pre-aged and thermally stressed fuel, this resulted in an improvement in the thermal stability of the fuel, and that a correlation existed between the concentration of methanol soluble species extracted and the overall sediment formed post oxidation. This relationship between the amount of insoluble material extracted pre-stressing, termed SMORS, and the total amount of insoluble gums formed post-stressing can be seen in figure 3.12.

Hardy and Wechter analysed the SMORS material, they concluded that it was soluble in middle distillate fuel, and had higher molecular weights than single molecules found in the fuel. From the correlation of SMORS material with the total insoluble sedimentation the author proposed that SMORS were required to form the sediment in fuels. However, it was pointed out that it was not the only thing that determined the amount of sediment formed, with acidity of fuels during testing also being of particular importance in their testing. The authors suggested that the SMORS and other fuel species react with dissolved oxygen to form acid which then react ionically with basis SMORS species to
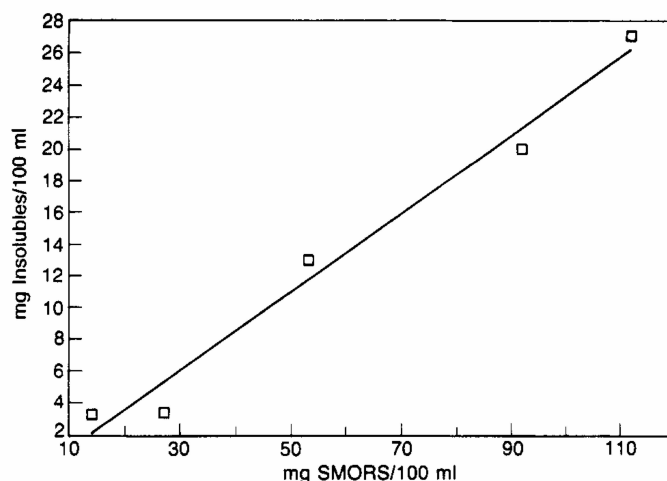
Fig. 3.12: The amount of SMORS material extracted pre-stressing correlated to the total amount of insoluble gums formed post-stressing. Reprinted with permission from [180].

precipitate out. Although, this seems unlikely that ions would form in the fuel, as the enthalpic penalty would be particularly high. Evidence was provided for this mechanism, with the molecular weight of the SMORS products being in the range of 650-1000 Da, but the coupling could be caused by other mechanism.[181] These species had high oxygen and nitrogen content in them, with oxygen making up between 9.7-13.7% of the molecular weight, and nitrogen being on average 4%. Dihydroquinolines, indoles, carbazoles and multi-ring nitrogen containing aromatics were suggested as chemical structures for the nitrogen containing species.

Beaver *et al* developed the oxidative coupling mechanism further and suggested that they progressed through a mix of radical reaction mechanisms and electrophilic aromatic substitution reactions with the aromatic oxidation products and heteroatomic species present in the fuel.[15, 182–185] In a paper from 2005, Beaver *et al* proposed that the formation of deposits and sediments in storage and thermally stressed conditions proceeded though the same bulk mechanisms. In the mechanism, seen in figure 3.13, the phenols present naturally in the fuel could be oxidised to a quinone. The quinone is more electrophillic than the phenol, and as such could react with other electron rich heteroaromatic species present, through coupling reactions to form extended oxidised aromatic systems. The quinone species were expected to react with the more electron rich nitrogen containing aromatics such as indoles and carbazoles, rather than oxygen and sulfur containing aromatics. The resulting products formed in the mechanism had molecular weights and chem-

ical formulas similar to those found by Hardy and Wechter.[181] The coupling reactions were proposed to occur through electrophilic aromatic substitution. Evidence for these mechanism were provided by the rate enhancement behaviour seen in the literature of acids and copper present in the fuel. The authors linked the acids to enhancing the rate of electrophilic aromatic substitution, as it can act as a proton shuttle during a number of steps. The copper was expected to increase the rate of reaction of the peroxyl radicals in step 3 and 4. However, it could also increase the rate or the electrophilic aromatic substitution reactions through the Ullmann reaction. Experimental tests were carried out to validate this mechanism, with them proving inconclusive, with no deposit formed during autoxidation when oxygen was sparged from the flow reactor with Silicosteel treatment. However, when oxygen was present in the fuel, insoluble deposit was formed in the autoxidation region. The authors speculate that the electrophilic aromatic substitution reactions in the SMORS mechanism can occur without the presence of oxygen, but as deposition only occurred in the pyrolytic region in the sparged system, this seems unlikely.

In a series of three papers, Beaver *et al* investigated the SMORS mechanism they proposed further, and the role of specific species in this mechanism.[182–184] In the first paper in the series by Sobkowiak *et al*, the role of phenols, indoles, and carbazoles was investigated.[182] In this study, 4 fuels with varying polar concentrations were investigated, and different compositions of the polars. The fuels were selected to validate the mechanism presented in figure 3.13, which indicated that both phenols, as well as nitrogen species such as indoles and carbazoles are important for deposition. It was found that increasing the total polar concentration lead to an increase in the total deposit formed, both when thermally stressed when neat, and when blended in a 1:1 ratio with a Fischer-Tropsch fuel. However, hydrocracked fuel 3658 was an outlier, with it having high indole and carbazole concentrations but was an intermediate depositor. This was also found in previous testing in the QCM static thermal stability tester and is contrary to the expected result from the SMORS mechanism. The 4 fuels selected were tester in flow reactor. Better correlation was found for the concentration of phenols present in the fuel and the total amount of deposit formed. However, the neat fuel 3658 was still an outlier. The authors proposed that this could be caused by the increased indole/carbazole concentration changing the nature of the deposit pre-cursors by preferentially reacting with peroxyl radicals or by changing the solvent properties of the fuel. The two plots of total carbon deposit verses total polar and phenol concentration can be seen in figure 3.14 It was found that at indole
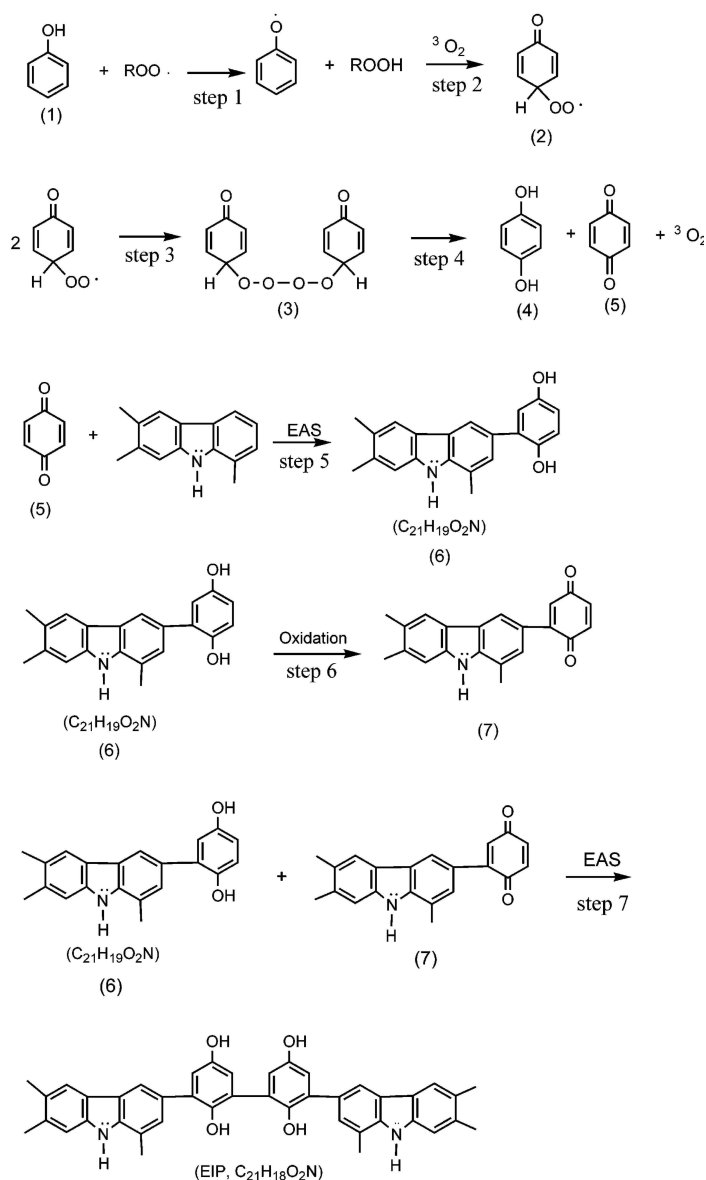
Fig. 3.13: The SMORS mechanism proposed by Beaver *et al* for the formation of insoluble sediment and deposits in storage and thermally stressed conditions conditions. Reprinted with permission from [185]

and carbazole concentrations higher than 85 ppm a change of mechanism occurs and the trend of total polar concentration verses deposition breaks down. The results lead to the conclusion that step 1 in figure 3.13 was the rate determining step and that increasing indole and carbazole concentrations can alter this rate by reacting with the peroxyl radicals.

In the second paper in the series, Aksoy *et al* investigated the link between the SMORS species formed and the total deposit formed, and that these species
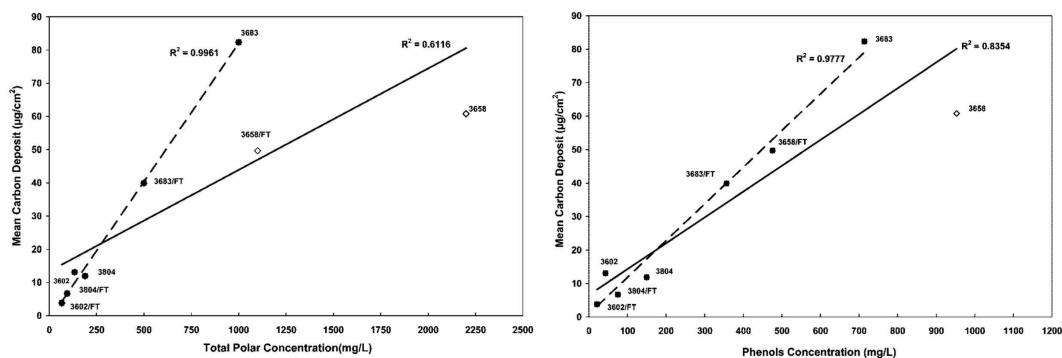
Fig. 3.14: Carbon deposit as a function of total polar concentration and phenol concentration in the fuels tested in the study by Sobkowiak *et al*. Reprinted with permission from [182]

are also responsible for changing the smoke point.[183] It was found that the smoke point decreased as the level of thermal stressing increased and that this was caused by an increase in the concentration of SMORS species during thermal stressing. One reason for this could be that increasing the concentration of SMORS species leads to an increase the aromatic content of the fuel and that this will decrease the smoke point. This is supported by the finding by the authors that blending with Fischer-Tropsh fuels increased the smoke point by diluting the SMORS species. The 4 fuels investigated in this study demonstrated good storage thermal stability, with all of them demonstrating low levels of deposit formed over storage, with this being suggested as being due to the low concentration of aromatic species in the fuel by the authors. This was particularly true for fuel 2827, which had been stored for 14 years, but formed not extractable precipitate in the intervening time. Thermally stressing all fuel increased the total amount of deposit formed in all fuels and increased the concentration of SMORS species in the new fuels. However, it the concentration of SMORS species decreased for the old fuel, and no trend was observed for the concentration of SMORS species and total precipitate formed. When phenols, indoles and carbazoles were doped in the the fuels, it was found that the total deposit formed increased as the polar concentration increased, indicating that these pre-cursors are important in the mechanism. This finding also supports the previous papers proposition that step 1 in figure 3.13 is the rate determining step. However, the linear relationship between added polar concentration and total deposit plateaued above 100 ppm, but this could be due to the additive package having indoles and carbazoles present in them. It was also suggested by the authors that another caused of this observation could be due to the indigenous polar

species in the fuel aid in the production of peroxyl radicals which can react together through alternative mechanism.

In the third paper in the series, by Gül *et al*, investigated the role that peroxyl radicals have on the SMORS mechanism and affect that chain reaction inhibitor have on them.[184] The previous 2 papers in the series had proposed that step 1 in figure 3.13 is the rate determining step. In this paper, flow reactor tests were carried out with fuels doped with 1,4-dihydrobenzene (DHB), to block this step in the SMORS mechanism by preferentially reacting with the peroxyl radicals. As the concentration of DHB was increased, the total amount of deposit dropped dramatically in fuel POSF-3804 under thermal stressing, with 5647 ppm DHB leading to a drop in total deposition of 88%. The mechanism for this is shown in figure 3.15. As can be seen, the overall result of this mechanism is the production of oxygen, hydrogen peroxides and benzene, while inhibiting the peroxyl radicals by hydrogen donation. The authors noted that when the DHB was at lower concentrations, it would increase the rate of oxidation, as it could initiate the mechanism by reacting directly with oxygen in the fuel and producing hydroperoxyl radicals. At high concentrations it was suggested the negative effect of these reactions was out stripped by the positive effect of the DHB reacting with the peroxyl radicals generated during oxidation. Similar results were observed with other fuels tested, but to a lesser extent, with this being suggest to be caused by a change in polar concentrations in the fuels.
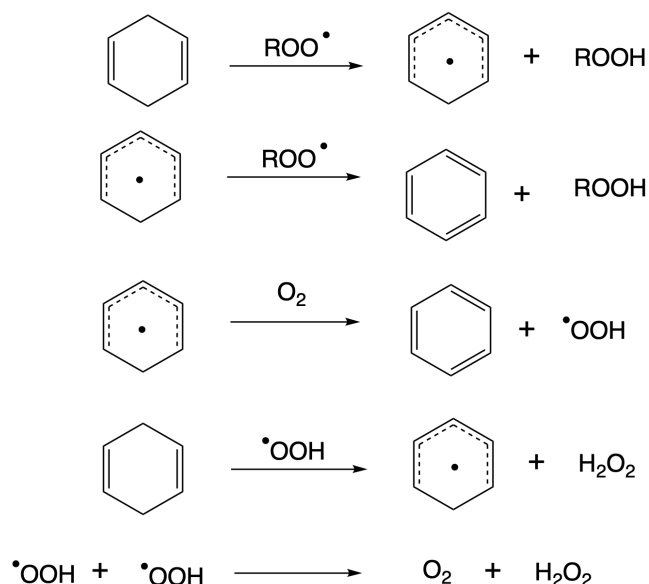
Fig. 3.15: Mechanism for the inhibition of peroxyl radical in the SMORS mechanism proposed by Gül *et al*. Reprinted with permission from [184]

A further study investigating the SMORS mechanism was carried out by Kabana *et al.*[15] In this study, flask oxidation studies were carried out on fuels doped with pre-cursors for the SMORS mechanism, namely 2-methylindole and 1,4-benzoquinone. It was found that the addition of these species increased the total amount of deposit formed during thermal testing. The mechanism was further investigated by the addition of 2-methylindole and benzoquinone oligomers to the test fuel, upon which rapid and significant deposition occurred. The authors suggested that this was further evidence that step 1 in the mechanism presented in figure 3.13 is the rate determining step. As such, the authors suggested that inhibiting this step could reduce deposition, but that naturally occurring species such as pyyroles and alkenes could react directly with oxygen in the fuel to initiate the reaction or the fuel species cumene could be naturally converted into benzoquinone in the autoxidation regime. Thus, limiting the concentration of heteroatomic would not necessarily stop deposit formation during storage or under thermal stressing. In support of the previous studies, it was also found that thermal stressing increased the aromatic/aliphatic ratio, and this ratio was higher in the SMORS products and thermal deposit. The principle conclusion from the studies by Beaver *et al* is that increasing the concentration of phenols in an aviation fuel increases its propensity for forming deposits and that peroxyl radicals critical species to control in the autoxidation mechanism. The production of these peroxyl radicals and phenols can be altered by the chemical composition of the fuel, with increasing aromatic content, and reactive electrophilic polar concentration leading to rate enhancement of the production steps.

In two reviews by Batts and Zuhdan Fathoni, the authors stated that peroxides and phenols were generally found to have the most negative impact of the thermal stability.[150, 151] The peroxides species in particular have been found to have significant negative impacts of the thermal stability. In a study by Taylor and Frankenfeld, peroxide species were shown to cause significant sedimentation, all chemical structures having this effect. The most deleterious peroxide species was found to be tert-butyl peroxide.[186] This is likely caused by the bulky tert-butyl group being able to stabilise the radical formed and thus able to promote the fission of the oxygen-oxygen bond. In the same review by Batts and Zuhdan Fathoni, ketones, acids and esters were found to be deleterious to the thermal stability of the fuel, and ethers had no effect of the amount of deposit formed. It was also reported that the removal of oxygen during storage minimised the formation of sediment. Interestingly, Taylor and Frankenfeld demonstrated that deoxygenated fuels were resistant

to the deleterious effects of carboxylic acids in general.[186] This could be a result of deoxygenated fuels being stored in the absence of light leading to a total reduction in sedimentation by over 95% over 15 to 30 day period and by 87% over a 60 day period.[187]

Taylor and Frankenfeld in the same study were able to demonstrate that aromatic ester, such as methyl benzoate, were mildly delirious. Non-aromatic esters demonstrated differing behaviour, as cyclohexyl formate had no affect, but pentyl formate had intermediate negative effects. The same observation was seen in ketones, with the straight hydrocarbon chained 5-nonanone being a mild depositor, and 4-methylcyclohexanone having no impact. The reason for this could be caused by the cyclic structure fixing the oxygenated species in this form and placing significant steric barriers on further reaction. The two compounds showing the greatest tendency to interact were 2,5-dimethylpyrrole and n-decanoic acid as it was found carboxylic acids accelerated sedimentation with 2,5-dimethylpyrrole. This supports the findings of Hardy and Beaver, that nitrogen compound negatively effect the thermal stability of fuels. In contrast, it was found that when oxygenated species were added in combination with each other, they result in synergistic stabilisation and a reduction in deposition. This could be a result of the change in solvent properties of the fuel samples with the oxygenated species in them which leads to oxidised products being stabilised in an partially polar solvent matrix.

Hazlett also carried out a review of the affect that oxygenated species on the thermal stability of fuel.[188] In this review Hazlett highlighted a study by Mayo *et al* re-added polar material from previously oxidised fuels to an unoxidised fuel, with monomeric and polymeric polar material being added separately. The monomeric polar species had minimal effect on the breakpoint of the fuel in the JFTOT test. However, the polymeric polar species caused a 20 fold increase in the dielectric measurement of the JFTOT test compared to the base fuel. This would provide some supportive evidence for the SMORS mechanism proposed byt Hardy and Beaver. However, it is not clear what chemical species are being doped into the unoxidised fuel, as it would be expected that specific monomeric species would take part in this mechanism. Work by Turner *et al* presented in this review also highlights the affect of pre-heating a fuel has on its thermal stability in the JFTOT test and how this is linked to polar species already present in the fuel. Turner *et al* were able to show that two fuels at 60 °C resulted in an increase in the concentration

of peroxides, acids and insoluble material present in the fuel. When the fuels were subsequently tested in the JFTOT, no correlation was observed between the acid number and the breakpoint of the fuel, or the amount of deposit formed during testing. However, another study by Kendell *et al*, demonstrated that strong acids were the most deleterious species by weight. This inconstancy could be caused by the nature of the acids being studied by Turner *et al* not being known, with Kendell *et al* in their study finding that weak acids had no effect on thermal stability, and that the chemical structure of the acid was important for determining its affect.

Nitrogen containing impurities can also be found in the fuel. However, much less study has been carried out investigating their affects on thermal stability. The main reason for this is historical, with the level of nitrogen species found in fuels from conventionally derived fuels generally being very low, but with greater utilisation of shale and other alternative sources this is changing. Nitrogen species present in the fuel at detectable limits are; amines, amides, analines, indoles, pyridines, pyrroles, carbazoles, and quinolines. There is agreement in the literature that the aromatic nitrogen species, indole, carbazoles, quinolines pyridines and pyrroles, are deleterious to the thermal stability of a fuel.[150, 151, 189] As discussed above, they are linked to be involved in the SMORS mechanism developed by Beaver *et al*.[15, 182–185] However, it has been proposed that the aliphatic nitrogen species have no effect on the fuels thermal stability properties.

Even among the aromatic nitrogen heterocycles there is variation in the reactivity of the species. Pyrroles and indoles have been shown to have the biggest negative impact with pyridines having a smaller effect on the thermal stability.[187, 190, 191] Pyrroles have been demonstrated to being particularly reactive, with it being reported that doping levels 0.01-01.1% resulted in a drop in the breakpoint of a reference fuel by 40 °C.[2] Indoles had a less significant effect but still lead to a reduction in the breakpoint by 20 °C. The likely reason for this is the difference in the chemical structure, with the pyrroles and indoles having easily abstractable hydrogens bonded to the nitrogen, which can help to facilitate radical reactions in the fuel. A number of studies have invesitgated the reactivity of 2,5-dimethylpyrrole, with Loefler and Li finding that it was particularly deleterious to the thermal stability of the fuel.[192] This was also found by Beaver and Hardy. Loefler and Li compared its N-methylpyrrole, where the hydrogen atom attached to the nitrogen has been replaced with a methyl group, and dimethylquinoline. 2,5-dimethylpyrrole was found to result

in the biggest drop in thermal stability and when the fuel was stored in the presence of light the concentration of 2,5-dimethylpyrrole dropped from 500 ppm to 10 ppm over the two day period. The cause of this is most likely the easily fissionable N-H bond, which can be fissured by the ultraviolet light, with the symmetry of the molecule potentially promoting reactivity.

| Very deleterious | Mildly deleterious | Inert |

RNH$_2$, PhNH, RCONH$_2$
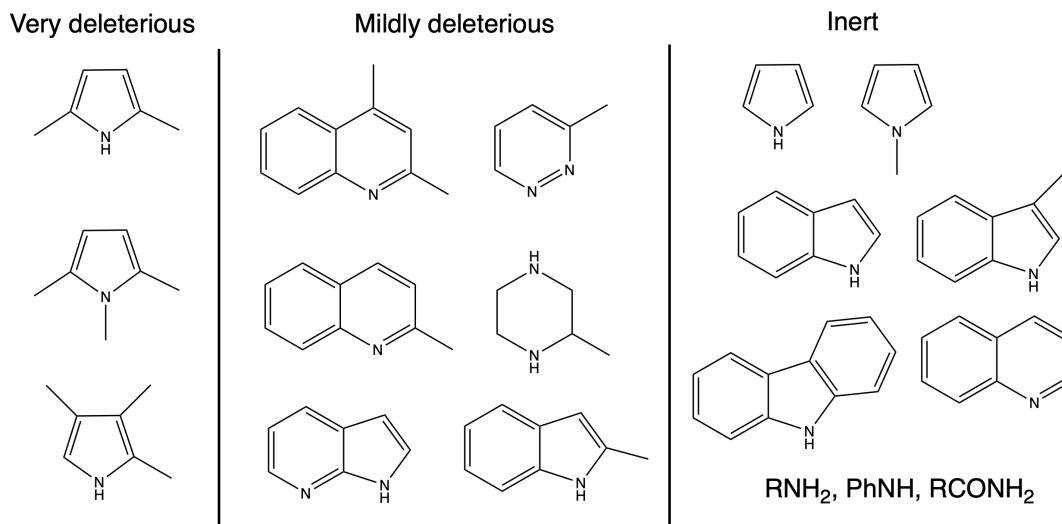
Fig. 3.16: Nitrogen species studied by Loefler and Li and Frankenfeld *et al*.[187, 190–192]

Frankenfeld *et al* extended this study by investigating a wider range of nitrogen compounds, which can be seen in figure 3.16, and their affects on sedimentation in the fuel. The authors found that the reactivity was linked to the basicity, with nonbasic nitrogen being more deleterious, and that substitution of the aromatic rings could also have an affect. This alkyl substitution on the carbon adjacent to the nitrogen group was particularly effective at promoting instability of the fuel when the nitrogen species was doped into it. However, alkylation at other positions seemed to reduce the affect of the nitrogen to induce stability issues.

Frankenfeld *et al* were able to show the reactivity series as substitution occurred for the pyrrole, indole and quinoline family of heterocycles. The 2 and 5 substituted analogues were found to be the most deleterious for each family. The results were more complex when the nitrogen species were added in combination with each other, with most reducing that stability, but with 2,5-dimethylpyrrole added with 2-methylindole leading to an increase in the thermal stability. These findings, in conjunction with other studies, resulted in the conclusion that the total nitrogen concentration could not be used to predict the thermal stability of a fuel.[150, 151]

Nitrogen containing species have also been shown to act as antioxidants in the fuel. Siddiquee and Wijtmans demonstrated that different nitrogen containing antioxidants had different reactivities as antioxidants. However, that when used together they can results in an increase in the total amount of deposit formed.[165, 193] This suggests that the radical products of the nitrogen antioxidants react with phenols and peroxides in teh fuel, yielding polymeric oxidation products. This supports the SMORS mechanism proposed by Hardy and Beaver.[15, 180–185]

Substituted pyridines and quinolines when added in combination with tert-butylhydroperoxide was found have mildly deleterious effects on the amount of deposit formed. However, when added in combination with sulfonic acid, the results was a large increase in the levels of sedimentation. This would suggest that some kind of acid-base reaction is occurring, and that the picture of nitrogen's reactivity in the fuel is more complex than that presented by Frankenfeld *et al.*[187, 190, 191] Carbozoles demonstrated the opposite behaviour, with the addition of acid in combination reducing the sedimentation, while peroxides resulting in an increase in insoluble material being formed. The authors speculated this was due to the peroxides acting as initiator in the oxidation rather than reacting with the nitrogen species directly.[150, 151] Similar results were reported by Hazlett, with high sulfur and high nitrogen doping in a fuel reducing a reference fuels breakpoint in the JFTOT test by as much as 60 °C.[2] However, it was noted by the author that this interaction depended on the chemical structure of the sulfur species, with benzothiophenes not having an affect on the deposition. The literature is more conclusive on the interactions between acids and nitrogen species, with similar results seen for the sulfonic acid as with carboxylic acids. Indoles and pyrroles were found to reduce the breakpoint of a fuel when doped with hexanoic acid, quinolines and pyridines having a smaller effect.[2]

A recent study by Zabarnick *et al* investigated the affect of doping an industrial solvent with indole and other heteroatomic species in combination.[179] Doping with indole at 100 mg/L resulted in an increase in the amount of insoluble material formed from 0.5 to 0.8 μg/cm^2 when compared the the nitrogen sparged industrial solvent reference. 17% of the indole was consumed during this set of testing. The addition of 100 mg/L of 2-ethylphenol to the indole resulted in a negligible increase in the level of deposition formed during testing in a static bomb reactor. However, the addition of 100 mg/L hexylsulfide and indole to the industrial solvent resulted in a jump in deposition to 3.3

µg/cm², with only 12% of the sulfide and 39% of the indole remaining. When all three species were doped at levels of 100 mg/L in the same sample, the amount of deposit formed increased to 7.4 µg/cm² and approximately 5% of the nitrogen and sulfur was left unconsumed. The oxygen depletion plots from this study demonstrated that this final system oxidised slowest, so clearly the heteroatomic species act as antioxidants in the fuel, but produced the greatest amount of deposit. The results from this study would support the SMORS mechanism proposed by Beaver *et al* as the nitrogen and phenolic species would react together through oxidative coupling reactions proposed in figure 3.13. However, this reaction does not include the involvement of sulfur species, and clearly from this study they are important. The authors suggested a mechanism that could account for the observation, with the formation of sulfenamides, sulfonamides and sulfonate salts from a range of acid sulfur species found in the fuel during the oxidation process. However, it is not clear what role the phenols have in this mechanism, with them likley to act as retardants for the mechanisms suggested. These schemes can be seen in figure 3.17
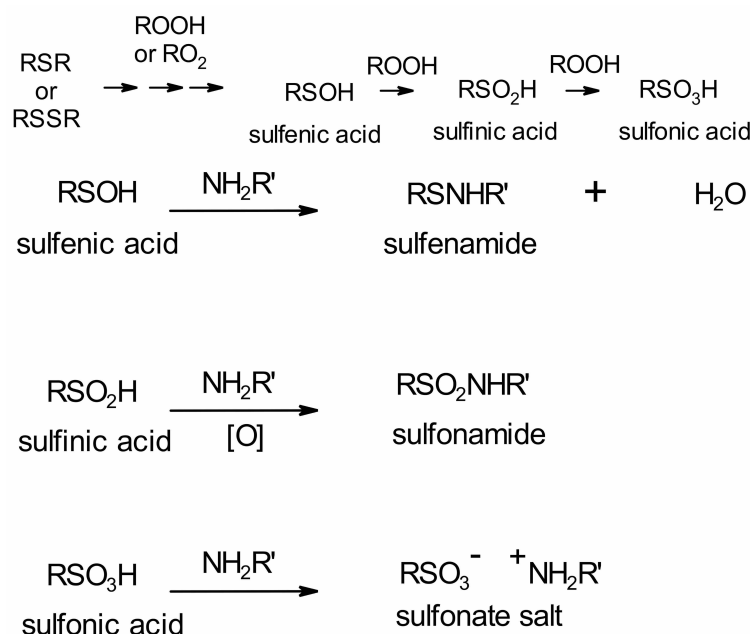
Fig. 3.17: Mechanism for the formation of sulfenamides, sulfonamides and sulfonate salts proposed by Zabarnick *et al*. Reprinted with permission from [179]

Effect of sulfur

The role that sulfur plays in the oxidation process is open to debate, with this being reflected by the literature.[192, 194–198] Sulfur species are known to improve the lubricity of the by binding to the metal surfaces. Sulfurs use in aviation fuel is not controlled, due to this improvement in lubricity, as it stops excessive wear of the aircraft systems.[199]. Sulfur has also been shown to improve the thermal stability of aviation fuel by reacting with peroxides in the fuel. While also linked to reducing the thermal stability of the fuel by increasing deposition.

A number of sulfur species can be present in the fuel, as can be seen in figure 3.18. These include, sulfides, disulfides, aliphatic thiols (also known as mercaptans), aromatic thiols (also known as thiophenols), aryl sulfides and disulfides, thiophenes, benzothiophenes and dibenzothiophenes, as well as substituted variants of these species.[200] Oxidised sulfur species such as, sulfoxides, sulfones and sulfonic acid can also be found in the fuel. In a study by Lobodin *et al* these sulfur species were classified into three classes.[201] Non-reactive sulfurs such as thiophenes and diaryl sulfides, reactive sulfurs such as sulfides and disulfides, and thiols which were so reactive to the silver used in the extraction technique used that they could not be separated. Link *et al* were able to further separate the sulfur species by reactivity, polarity and aromaticity.[202] In that study it was found that thiols, sulfides, and disulfides were the most reactive, while thiophenes, benzothiophenes, and dibenzothiophenes were the least reactive. However, the literature indicates that the reactivity of sulfur is more complex. In 1976, Taylor found that thiophenes contributed the most to deposition, which the author attributed to weakness of the aryl S-H bond.[195] However, the author agreed that disulfide compounds were particularly deleterious to the thermal stability of fuel and that diphenyl sulfide and dibenzothiophene had little effect.[196]

Two reviews by Batts and Zuhdan Fathoni demonstrate the divide in the literature on the role of sulfur in the autoxidation of aviation fuel.[150, 151] These papers were focused on the use of diesel and shale fuels but most of the material covered was applicable to the aviation field. In the first paper, in which they focused on diesel fuels, it was reported that a number of previous workers had highlighted that thiophenols and thiophenes were the most deleterious to the fuel. Loefler *et al* supported the finding that thiophenols had the biggest negative effect on the thermal stability.[192] However they
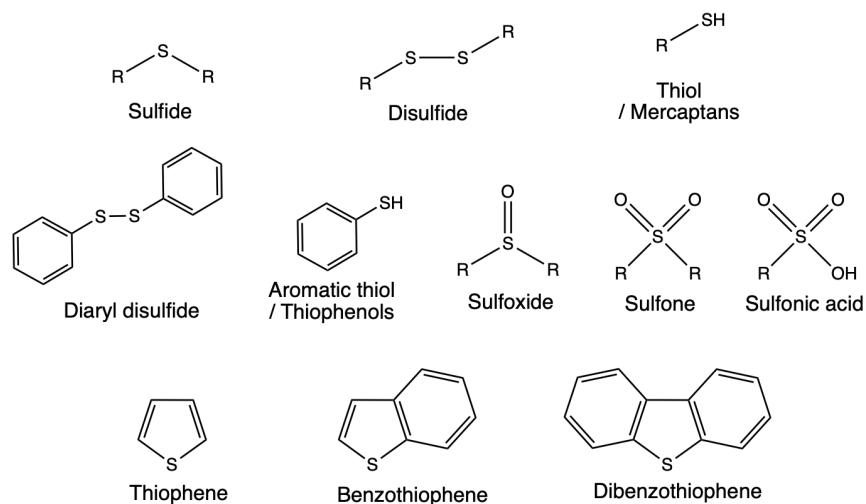
Fig. 3.18: Sulfur species found in the fuel.

found that tetrahydrothiophene was more reactive to oxidation that thiophenes, followed by polysulfides and mercaptans. The review by Batts and Zuhdan Fathoni also supported this finding, by quoting technical reports which found similar findings, and linked this to the catalysis of the reaction of hydrocarbons with oxygen to form peroxides.[150] This cannot be true catalysis, as sulfur is found in the deposit at high concentrations than in the fuel, so is likely reacting with the fuel during autoxidation and contributing to the insoluble products. Part of this increased reactivity for thiophenols could be caused by the findings of another study they highlight, where thiophenols react with brass, to form mercaptan gels. As copper has been heavily linked to reducing the thermal stability of aviation fuels, it is likely that the thiophenols are reacting with the copper in the brass, forming complex which could react with the fuel. Two studies investigated by Hiley *et al* and Offenhauer *et al* found that thiophenols also increased sedimentation and gum formation.[203, 204] They also saw that sulfonic acid is very reactive, but that mercaptans and diaryl disulfides were less reactive. This is an interesting point, as sulfonic acid is a product of sulfur oxidation, so the thermal stability of aviation fuel with high sulfur concentrations is likely to change as a function of time stored and heated, as sulfonic acid is formed. This may be reasoning for the findings of Frankenfeld and Taylor, that longer storage and presence of light caused increased gum formation.[187]

In the second paper Batts and Zuhdan Fathoni focused on shale derived fuels. However, due to lack of data on the effect on shale most of the literature was on the petroleum field.[151] Early work showed that sulfur species act as

antioxidants by reacting with peroxides present in the fuel. Thompson *et al* stated that stated that disulfides and polysulfides promoted instability, while mercaptans and aliphatic sulfides had mildly stabilising effects.[205, 206] As stated previously, later research demonstrated that thiophenol, thiophenes, polysulfides and mercaptans were deleterious to the fuel.[192] This is further supported by the findings of Mushrush *et al* who showed that thiophenes and thiophenols were the most reactive, followed by aliphatic thiols and sulfides.[197, 207] However the differences seen could be due to the nature of the experiments, as Mushrush *et al* and Batts and Zuhdan Fathoni both demonstrated that benzo and dibenzothiphenes were nonreactive to the peroxide t-BHP and the sulfide and disulfides were the most reactive.[151] Similar findings were seen by Daniel and Heneman when they doped jet fuel with 10-1000 μg of S mL^{-1}, with thiols and thiophenes decreasing stability and sulfide and disulfides increasing stability.[208] This leads to the conclusion that the different sulfur compounds react in different ways and that sulfur has a duel role in the oxidation mechanism, with some increasing stability by reacting with peroxides, and other reacting with oxygen or polar species to reduce stability by forming insoluble gums. This is reflected by the confused picture presented in table 2 of the second paper of Batts and Zuhdan Fathoni, which shows that the same sulfur species can stabilise and destabilise the fuel.

The findings of numerous authors, including Mushrush, Heneman and Batts *et al* was supported by work carried out by Bauldreay *et al*.[151, 197, 207, 208] In their study they found that sulfides and disulfides were the most reactive species to peroxide, with aromatic sulfur species being less reactive to peroxides.[199] This was similarly found by Naegeli in a study of sulfur species in fuel and dodecane.[209] In that study it was found that sulfur in fuel lead to the formation of antioxidants during oxidation, but that these can then form a part of the deposits. Naegeli also found that the antioxidants formed were acidic in nature, due to the fact that the addition of organic base increased the oxidation rate, so must be neutralising the antioxidants. Disulfide and alkyl thiols were the most reactive to peroxides, slowing the rate of oxidation in a dodecane-cumene peroxide mixture. This was not seen when sulfur was added to a pure dodecane solution. Aromatic sulfur species were less reactive to the peroxides. The addition of SO_2 to the dodecane-cumene mixture increased the rate of oxidation dramatically, however it in not clear is this was SO_2 or sulfones. Naegeli proposed that SO_2 increased the rate of oxidation as it is a reactive intermediate towards insoluble product formation. They postulated that as

disulfides play a role in the formation of insoluble deposits and that they are the cause of sweetened fuels, a process which increases the concentration of disulfides in the fuel, to have poor thermal stability. This also supports the findings by Rawson *et al* and Kendall *et al* who found that sweetened fuels increased the rate of deposition when compared to hydrotreated fuels.[210, 211] This can be seen in figure 3.19. Howard and Korcek demonstrated that sulfides are less reactive than the corresponding esters to peroxides, but they also found that the radical sulfur species are 3-5 times more reactive in hydrogen abstraction reactions.[133] This has also been shown by Chauvin *et al*, in their study of sulfur radical species, with hydropersulfides being very reactive to hydrogen transfer reactions.[212] Kauffman investigated the role of sulfur species in the oxidation and deposition mechanism, and found the oxidisable sulfur species, highlighted as mercaptans, sulfides, and disulfides, reduced peroxide formation but increased phenol formation.[194] The phenols increase the bulk oxidation and the formation of insoluble deposits. However, in disagreement with other studies, it was found that sulfoxides and sulfones had little effect on the deposition. It was proposed that this is due to the oxidised sulfur species are acid, and they react with basic nitrogen species in the fuel to initiate deposition, demonstrated by a acid-neutralisation study.

In another study, Rawson *et al* researched the effect of doping model fuels with different sulfur species in a small scale reactor device.[213] They found that benzyl sulfonic acid and diphenyl disulfide, as well as elemental sulfur, increased the sedimentation the most. While the aliphatic cyclic sulfur species and the least effect on deposit growth. However, these findings were not seen jet fuels with known sulfur species present, indicating that the process is more complex. In a study of the oxidation of middle distillate marine fuels Bhan *et al* showed that neutral sulfur species, as well as aromatic polar species, were the fastest to oxidise in the fuel.[214] However, the study failed to identify the oxidised products formed. Aromatic sulfur was also shown to be the least reactive aromatic heterocyclic species in a study by Siddiquee and de Klerk, as benzothiophene showed no oxidation when heated to 130 °C for six hours.[193] In that study the authors state that their previous work has shown that dibenzothiophene can be oxidised to sulfones, and that the sulfones can go on to form addition products of the sulfones, which can be found in the deposit.

Sulfur species have been linked to co-oxidise and react with a number of other heteroatomic and cyclic species present in the fuel. In one study, Bergeron *et*
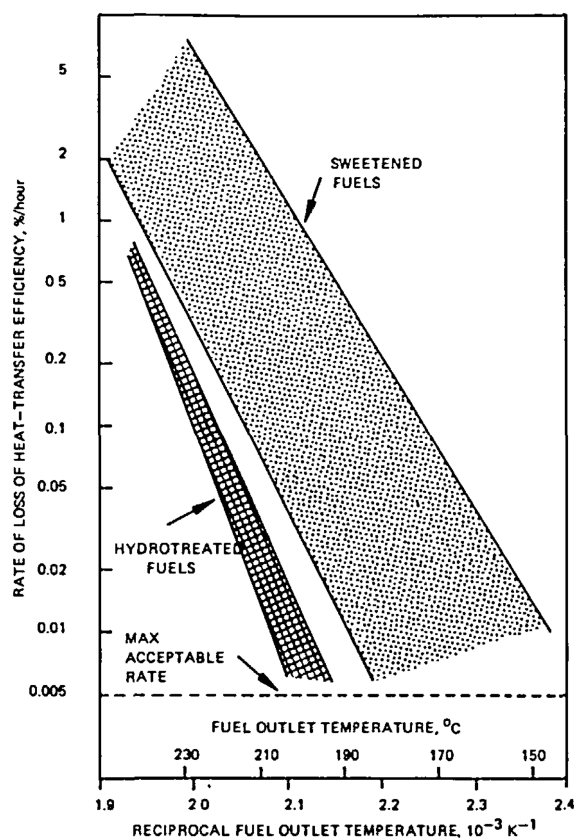
Fig. 3.19: Effect of the sweetening and hydrotreating process on the deposition rate of fuel (taken from [210]).

al attributed the colour change during oxidation of hydro-cracked diesel to the sulfur and nitrogen concentration, as well as the aromatic content.[215] Morris and Mushrush demonstrated that heating indene in the presence of thiols increased the rate of oxidation, and that alcohols, ketones, sulfoxides and sulfones were present in the products.[216] However, this was not observed in the oxygen limiting conditions of the JFTOT test. As such oxygen from the atmosphere is clearly being introduced into the fuel oxidation products. Frankenfeld *et al* investigate the interactions between nitrogen and sulfur compounds, over a 100 day period to measure sedimentation, in which they found that aromatic thiols were particularly susceptible to reacting with the nitrogen species pyrroles.[191] However, they found that sulfur was not found in the deposit in the testing they were carrying out, with nitrogen species being the major depositor, and sulfur and oxygen species only increased the rate of deposition.

Sulfur has been shown to be found in the deposits in high concentrations by a number of studies. Hazlett *et al* showed through elemental analysis

that sulfur was found in the deposit 54 times great than the concentration found in the fuel by mass.[188] This was similarly found by Sharma *et al* who found that the H/C atomic ratio of 1.36 in the sediment compared to 1.63 in the fuel indicates that aromatic sulfur species are responsible for the deposit.[217] Wechter and Hardy went further and pinpointed that the deposits originate from sulfonic acids formed during oxidation of the aromatic sulfur species.[218] They confirmed this by doping fuel with sulfonic acids, resulting in rapid sedimentation, however it is not clear if all sulfur species oxidise to sulfonic acids. Mushrush *et al* found that in fact sulfones are the primary product of tetrahydrothiophene, and that benzothiophene remain mostly un-oxidised in mild storage conditions.[207, 219, 220]

However, in another study the authors showed that sulfonic acids are the primary product of the oxidation of sulfides and disulfides.[197] In these studies sulfoxides would react readily with peroxides, to form sulfones which reacted more slowly, however it was noted that the sulfonic acid formed in this process even in small concentrations was particularly deleterious for deposition.[219] Zabarnick investigated the thermal stability of a number of jet fuels in a small scale reactor device.[221] In this study it was found that phenolic and sulfur species inhibited oxidation, but that these species were more likely to be found in the deposit. From XPS and Auger spectroscopy data, it was also shown that the sulfur was found to oxygen and carbon in the deposit, indicating that sulfoxides, sulfones and sulfonic acid form part of the deposit. This was supported by work by Epping *et al* who also showed that sulfur was in higher concentration in the deposit, and that it was in the oxidised state of sulfoxides and sulfones.[158]

The role of thiols, sulfides and disulfides is still unclear, as depending on the design test used, they can appear to increase or decrease the rate of oxidation. This is likely to be due to them acting as antioxidants, so increase the induction period of the fuel, but also increase the amount of deposit forming sulfoxides, sulfones and sulfonic acids, which can then go on to react with oxygenated products and nitrogen impurities. Disulfides are the most reactive to peroxides in the fuel, with sulfoxides being formed int he resulting reaction. The sulfoxides can then react further with peroxides to form sulfones and sulfonic acid. However, the literature indicates that these reactions are slower, indicating that the barrier to reaction is higher. This can be seen in figure 3.20. There is some modelling evidence to support this statement in the literature, in work carried out by Zabarnick *et al*.[14, 222] In a DFT study, they

showed that diethyl sulfide and diethyl disulfide can react with a peroxide to form sulfoxide and alcohol species.[222] They also demonstrated in this study that triphenylphosphine can also react in a similar way, with a lower barrier, indicating that increased phosphorus in the fuel in future would potentially be an issue. The studies are not clear whether the aromatic or aliphatic sulfur species are more reactive, with separate studies finding different reactivities, however the majority of the literature points to sulfur decreasing the thermal stability of the fuel.
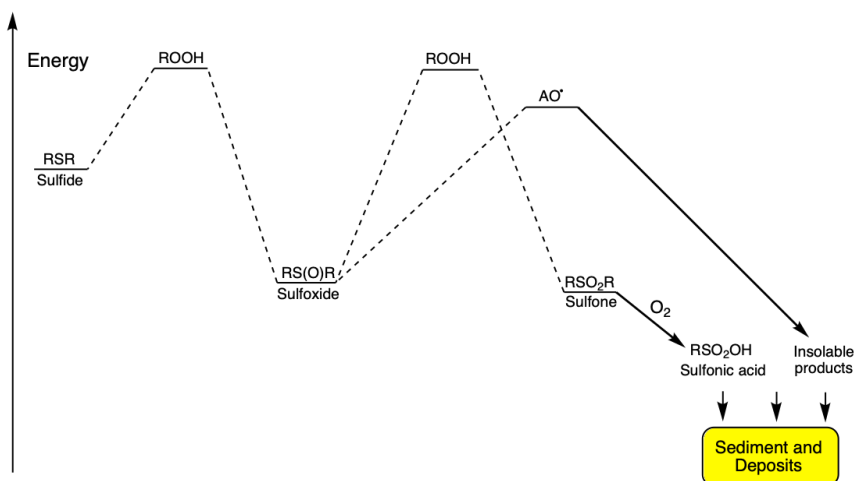
Fig. 3.20: Possible routes for the oxidation and deposition of sulfur from the literature.

Dissolved metals and metal surfaces in fuel

Metal contaminants, especially copper, have a negative affect on the fuels thermal stability and cleanliness. In general this is thought be because they facilitate the fission of peroxides, either through catalysis or by reacting with the peroxides in a one electron reaction. Metal surfaces are also implicated in activating oxygen present in the fuel, initiating oxidation. This section will review previous studies into the role of metals into the autoxidation of aviation fuel and hydrocarbons. This will focus on how dissolved metals are involved in the oxidation mechanism and the affect that changing metal surfaces has on the thermal stability.

The role that metals play in the oxidation of hydrocarbons is a research question that crosses a number of disciplines, including enzyme catalyse reactions, and in chemical industry.[223–225] This is because metals are

capable of cycling through oxidation states and being stable in open shell electronic states. This allows them to react with the dissolved oxygen in the fuel and with the hydrocarbons directly.

The most famous of these reactions is the Fenton reaction for iron, with the original discovery of the increased rate of oxidation in the presence of iron species dating from 1894.[226, 227] During the Fenton reaction ferrous ions can react twice with peroxide species, to form two radical peroxide species through electron transfer reactions, and regenerates the iron catalyst. The reaction scheme can be seen below in figure 3.21. Significant work has been previously carried out investigating this reaction in the field of polymer science and bio-inorganic chemistry. The most pertinent work to this thesis investigating the role of iron in the oxidation of hydrocarbons and the mechanisms involved will be discussed.

$$Fe^{2+} + H_2O_2 \longrightarrow Fe^{3+} + HO^{\bullet} + {}^{-}OH$$

$$Fe^{3+} + H_2O_2 \longrightarrow Fe^{2+} + HOO^{\bullet} + H^{+}$$

$$2H_2O_2 \xrightarrow{Fe^{2+/3+}} HOO^{\bullet} + HO^{\bullet} + H_2O$$
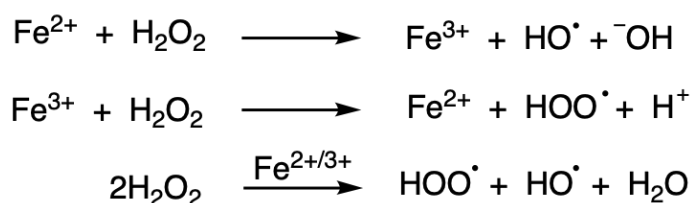
Fig. 3.21: Fenton reaction, with Fe^{+2} and Fe^{+3} reacting with peroxide species to form 2 radical species and water overall.

Frizen *et al* investigated the decomposition of benzoyl peroxides by ferrocene using DFT. [224] They were investigating the initiation of the polymerisation of styrene to understand to nature of the reactive species. The ferrocene reacted with the peroxide forming a structure where one of the cyclopentadienyl ligands had underwent ring slippage. The peroxide oxygen-oxygen bond had been broken, and the spin and charge density on the iron centre demonstrated that the reaction involved the transfer of electron density into the peroxide. This study indicated that it was shared evenly by the fragments, in conflict with the excepted mechanism, but they say supported by previous experimental evidence of paramagnetism. They demonstrated that forming the complex was energetically favourable, by -21.7 kcal mol^{-1}, however removing one of the peroxyl radicals had an energetic barrier of +31 kcal mol^{-1}. They suggested that this wasn't likely, and instead offered an alternative route to radical initiation, seen in figure 3.22, and say that it initiates the polymerisation of styrene, with only a barrier of +5 kcal mol^{-1}. When the iron species formed in this reaction reacts with another monomer, it was shown to react rapidly,

with a barrier of +21 kcal mol^{-1}. The study by Frizen *et al* indicates that the metal acts as an rate enhancement agent, rather than a true catalyst, as it is not reformed in the reaction.

$$Cp_2Fe^{\delta+}(PhCOO^{\delta-})_2 + H_2C=CHPh \longrightarrow Cp_2Fe\text{-}PhCOO^\bullet + PhOO\text{-}H_2\overset{\bullet}{C}HPh$$
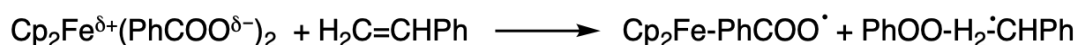
Fig. 3.22: Proposed reaction for the initiation of styrene polymerisation by ferrocene by Frizen *et al*.[224]

Three studies by Buda *et al* also investigated the Fenton reaction using DFT and molecular dynamics.[228–230] They were investigating the Fenton reactions in aqueous environments so some of the conclusion drawn are not applicable to fuel autoxidation. The first study suggest that Fe^{2+} can react with peroxides to break the oxygen-oxygen bond, with a barrier of +6 kcal mol^{-1}.[229] The resulting product was an iron species with 2 OH radicals as ligands, due to hydrogen transfer from a water ligand. This can only happen in aqueous solutions, and as such has limited application in the study of fuel oxidation, however acids are known to increase the rate of oxidation when they act as co-catalysts with metal contaminants.[231] This could be due to their ability to intramolecular hydrogen transfer. In the second study they investigated the Fe^{3+} active species and the formation of the OOH radical.[228] The formation for the $Fe\text{-}OOH_{(aq)}$ complex was -146 kcal mol^{-1}, however the authors speculate that this is high due to the lack of solvent effects being taken into account. Findings in the first 2 studies lead to the authors investigating the $Fe^{4+}=O$ species in there final paper in the series.[230] This species was found to be very reactive, and could convert methane into methanol in aqueous solutions, with a barrier of +22.8 kcal mol^{-1}. They suggest that findings from this study, with those from their previous work, show that the reactive ferryl species is of importance in the oxidation process of hydrocarbons.

Copper is the most active metal contaminant found in aviation fuel and significant study has been carried out looking at its role in fuel oxidation.[231–235] It has been shown to cause thermal stability problems at levels of 10 ppb, with Taylor and West demonstrating that is it causes particular problems for thermal stability when compared to other metals.[231–233] Mills *et al* investigated the affect of doping fuel with copper on the rate of heat transfer coefficient change.[234] This can be used as a sign of deposit growth on the surface of metal in contact with the fuel. Mills showed that increasing the concentration of copper increased in the deterioration of the heat transfer coefficient, with the base fuel having a deterioration of 0.26% per hour, and the addition of 30

μg/L of copper increasing the deterioration to 5.9% per hour. The increase in deterioration rate of the heat transfer coefficient had a linear relationship with the concentration of copper in the fuel. This was also seen by Colbert *et al*, where they doped fuels with a range of copper concentrations, between 50-800 ppb.[235] This work showed a strong linear correlation between the deposition rate and the copper concentration. Pereira and Pradella also found a linear relationship between the amount of gums formed during storage in ethanol derived Brazilian gasoline and the concentration of dissolved copper, but only above 0.1 mg/kg.[236, 237]

One of the reasons is that have been suggested copper being so reactive, is it can easily cycle through the +1 and +2 oxidation states, allowing it to follow a Fenton reaction scheme.[11] A previous study looked at the reaction of copper with a peroxide using DFT to investigated the mechanism.[222] They looked at two possible reaction routes, an ionic and covalent routes. The ionic route focused on the redox potential of the ions, leading to a high energy pathway which is not possible, with and energy penalty of +430 kcal mol^{-1}. The covalent pathway went *via* the formation of a metal oxygen bond. The metal transfers electron density into the bound oxygen, breaking the peroxide bond. However as the reaction pathway in figure 3.23 indicates, this mechanism has a large energy barrier to the formation of a radical, with +222 kcal mol^{-1} of energy required to form the RO + CuOH^{2+} species from the low energy ROOH-Cu^{2+} structure. It also appears to not truly catalytic as the free metal is not reformed without the input of energy, and the copper does not cycle through oxidation states. This is supported by experimental studies that indicate copper is extracted from the fuel end up forming part of the deposit.[238]

One of the reasons that the study could show such a sizeable barrier required to expelling a radical is that calculations were carried out without the use of ligands on the copper. This had a big effect, with the copper-peroxide complex forming exothermically, and trapping the reaction in a low energy well. This ligand effect has been used to limit the reactivity of copper in the fuel by the use of MDA.[239] The Fenton mechanism requires the free movement of the ligand environment around the metal to stabilise the changing oxidation states. The MDA forms a chelated complex with the copper holding it in single geometry. This deactivates the copper and thus improves the thermal stability of the fuel. From this finding it would be expected that the affect of adding more MDA to a fuel would plateau off as all copper is chelated.
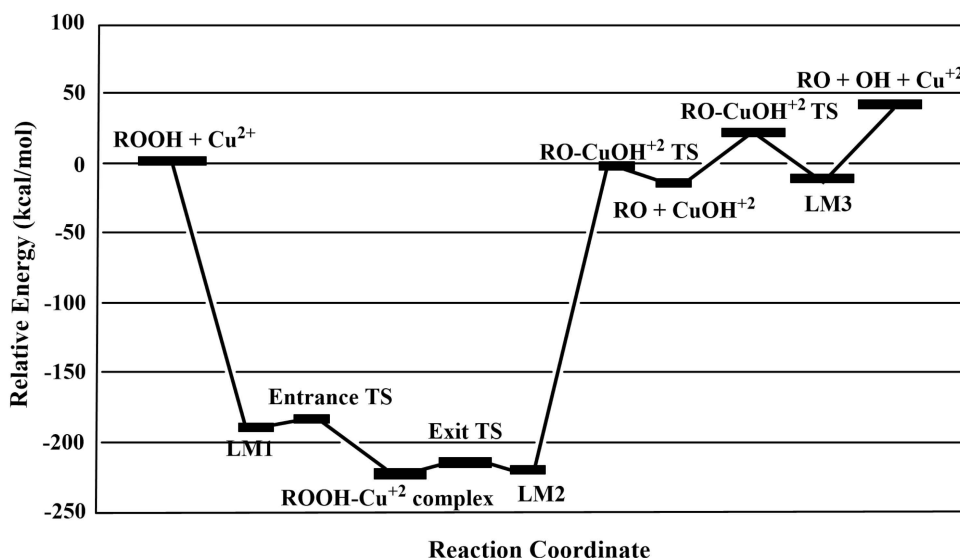
Fig. 3.23: Proposed reaction by Phelps *et al* for copper^{2+} with 1-phenylethyl hydroperoxide (ROOH) (adapted from [222])

This is however not observed, with surface passivity and antioxidant effects attributed as the cause.[173] Because of this specific activity towards copper, MDA is less effective at reducing the affect that other metals have on the oxidation rate.[231] This has not caused issues due to copper causing the biggest inservice issues.

Another mechanism has been suggested, by Waywick and Pereira *et al*, where the dissolved copper reacted with oxygen directly.[173, 237] In this mechanism, it is proposed that the copper reacts with triplet oxygen, forming a complex with a radical oxygen in the doublet form. This allows for it to react with the fuel directly and abstract a hydrogen from the hydrocarbons. This mechanism can be seen in figure 3.24 Is offers a possible route to the initiation of the oxidation process. It supports the findings of Nery and Pereira, who showed that when copper contamination is added to fuels in storage, they demonstrate a 20 fold increase in gum formation.[236, 237] It was even demonstrated in these studies that without copper contamination, negligible gums were formed in a fuel after 47 days, indicating that metals are important for initiating the autoxidation process.

Interestingly Morris *et al* found that copper rich fuel sediments had limited impact on the oxidation rate of a fuel when it was heated under limited oxygen conditions.[240] This supports the mechanism and findings proposed by

$$Cu^{n+} + O_2 \longrightarrow \left[Cu^{n+}\text{-O-O}^{\bullet} \right]$$

$$\left[Cu^{n+}\text{-O-O}^{\bullet} \right] + RH \longrightarrow Cu^{n+} + HOO^{\bullet} + R^{\bullet}$$
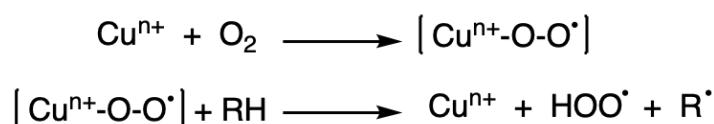
Fig. 3.24: Proposed mechanism of the reaction of copper and oxygen in the fuel.[173, 237]

Waynick and Pereira, as without oxygen present the oxidation can not be initiated. Morris proposed that this behaviour could also be caused by the copper being sterically hindered, or electronically not available for reaction. In this study, the affect of dissolved copper on the oxidation rate was also investigated, with it found that as the copper concentration increased the rate of oxygen consumption also increased. It was also found that as the oxygen was consumed, hydroperoxides were formed in the fuel, again supporting the mechanism by Waynick and Pereira. Although it should be noted that the hydroperoxides could be formed as part of a more complex mechanism.

Other metals have been shown to affect the thermal stability of aviation fuel.[231–233] Work carried out for the Coordinating Research Council (CRC) in 1979 showed that 200 *ppb* of lead, 100-200 *ppb* of zinc and 25-100 *ppb* of iron can significantly reduce the thermal stability of fuel. West *et al* demonstrated that manganese can have as negative an effect as copper in aviation fuel.[231] Manganese had a more detrimental affect than copper when naphthenates were added to the sample. West found that iron and zinc had similar impacts on the fuels thermal stability supporting the findings of Taylor.[233] In that study a fuel was doped with 50 *ppm* of copper, cobalt, iron and nickel acetylacetonates, with the effect on the deposition rate measured. As can be seen in figure 3.25, iron, cobalt and nickel impacted the fuel to a similar extent, with the deposition rate being a factor of 40 times higher than the undoped fuel. Copper was more demonstrated to be more reactive supporting findings from previous studies. In that study, it was also shown that high vanadium content alloys had a negative effect on thermal stability, with higher the vanadium concentration on the allow the worse the thermal stability of the fuel.

A literature review by Pradelle *et al* highlighted the affect of metal contamination in the Brazilian gasoline industry.[236] In these studies it was demonstrated that copper was the most deleterious contaminate, but that iron in high concentration could also caused a build up of gums in storage over 7 days.
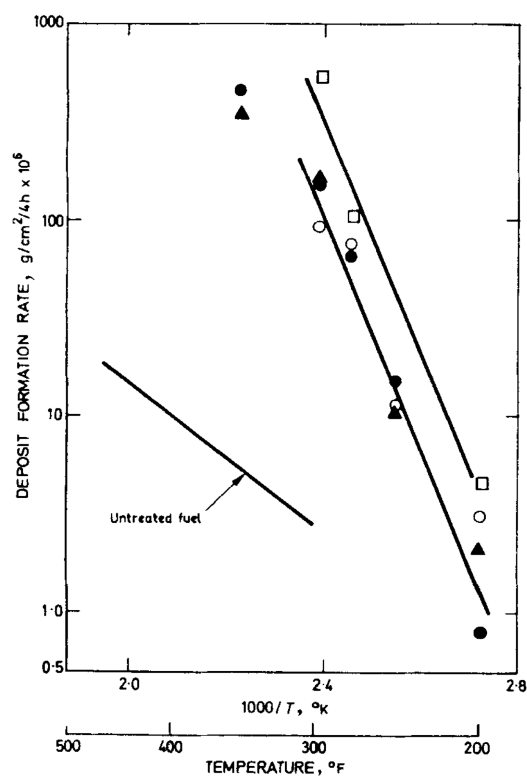
Fig. 3. *Arrhenius plot of rate of deposit formation of fuels containing 50 ppm added metal*

● $Fe^{III}(AcAc)_3$; ○ $Ni^{II}(AcAc)_2$; □ $Cu^{II}(AcAc)_2$; ▲ $Co^{II}(AcAc)_2$

Fig. 3.25: Effect of metal doping on deposition rate seen by Taylor in 1968 (taken from [233])

Nickel and zinc were less effective, but had a negative effect, while lead had no affect.[241] Copper and iron were also shown to affect the amount of gums formed as the storage length was increased, even at low concentration, while at the concentration tested the other metals had little effect. The same affects were seen by A'reff when investigating copper and iron contamination in oil form the Baiji Refinery.[242] Copper was found to have a bigger impact on the formation of gums that iron, however iron had significant effects, and the increase in gum formation effected the viscosity of the samples.

Jain *et al* found that while copper increased the rate of oxidation in bio-fuels the most, cobalt, manganese nickel and iron also had an effect.[243] They suggested that the metals had a catalytic role in the oxidation process, as even 2 mg/L the induction period was reduced, and increased linearly as the concentration increased. Because of this linear response it was also suggested that the amount of antioxidant needed to maintain an induction period of 6 hours could be predicted.

A number of studies have investigated the affect of chelating the metal centres using ligand has on the rate of oxidation.[152, 231, 244] Adjimani *et al* studied the affect of adding chelating antioxidants in ferric systems in biological conditions.[244] An interesting result was that benzohydroxamic acid (BHA) and desferroxamine B (FOB) had a high iron binding ability, whereas 2,3- dihydroxybenzoic acid (DHBA) did not chelate as well. As they are similar strucutres, seen in figure 3.26, some of this must be due to electronic factors. However all the chelaters tested reduce the oxidation, as they demonstrated antioxidant and peroxide scavenging activity. When applied to fuel, this would suggest that metal chelators could be used selectively in fuel, to bind particular metals known to be present. They would also demonstrate antioxidant behaviour, thus allowing for a single additive being used to solve multiple problems.
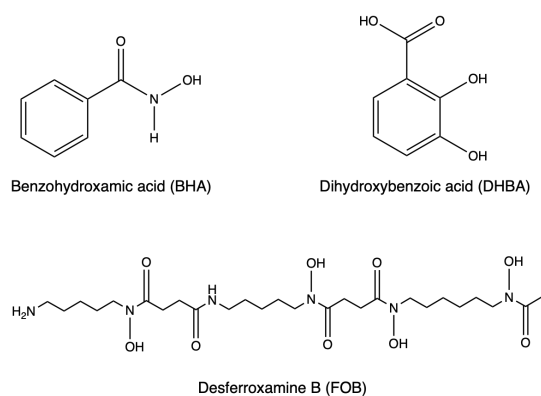
Fig. 3.26: Chelating antioxidants used by Adjimani *et al* in their study.[244]

As discussed previously Abdallah *et al* investigated how additives alter a fuels thermal stability. One of the additives that was investigated was metal deactivators (MDA). This work was carried out on a single hydroprocessed fuel, as such the metal content in the fuel would be expected to be low, however no more information was given about the fuel. Despite this, MDA was seen to improve the thermal stability of the fuel the most out of the additives investigated. This is likely to be due to it chelating copper in the fuel, but also due to its antioxidant propeties, supporting the findings of Adjimani *et al*.[244] Mills *et al* also found that when MDA was added to a fuel, it reduce the rate of oxidation, however the chelated species still had some residual negative effects on the fuel.[234]

West *et al* investigated the rate of hydrogen peroxide decomposition with dissolved copper, iron, manganese and zinc in the presence of naphthenates and 2,2,6,6-tetramethyl-3,5-heptanedioates as ligands and co-catalysts. They

showed that when naphthenates were added with metals that copper and manganese had the most deleterious impact on the fuel, with iron and zinc naphthenates being less reactive. Copper 2,2,6,6-tetramethyl-3,5-heptanedioates was less reactive than the copper naphthenate at temperatures 105-165 °C. However, at temperature 165-205 °C the opposite was seen. potentially due to the naphthenate complex breaking down at this temperature. Although this observation was not seen for manganese naphthenate, and in fact the rate was too high to measure at 165 °C. Only copper was investigated with metal deactivators, with the addition of MDA greatly reducing the rate of peroxide decomposition caused by the copper naphthenate, and when extra naphthenate was added as a co-catalyst. However, it would be of interest to investigate the effect that MDA has on other metals. They would have different oxidation states and geometries available, and as such, you would not expect this observation to necessarily hold true for all metals.

A lot of understanding on the role of metals in autoxidation can be inferred from the study of the affect that changing the metal surface has on the rate of fuel oxidation and deposition. Smith found that copper and nickel alloys had a negative effect on the tube deposit rating and filter pressure drop, when compared to aluminium standards, while steel alloys and titanium showed no affect.[245] The importance of these test on the liquid phase autoxidation was highlighted by the fact that copper was picked up from the copper alloys, even in storage conditions, and thus would effect the fuels thermal stability. Jones *et al* demonstrated that the autoxidation could be inhibited further by coating of the metal surface with silica, or by additives and natural antioxidants in the fuels being tested binding to the reactive surface.[246] Ervin found similar findings for the use of silica coatings on the metal surface and passivisation of the metal surfaces with additives.[247] This study also found that when proportion of the tube was coated in the silica, the deposition happened down stream on the steel surface, further reinforcing the evidence that the metal surface help facilitate the autoxidation.

Eser *et al* showed that Inconel 600, SS 304 and iron were the 3 most reactive surfaces in their study.[248] This is in agreement with previous studies, which found that the metals nickel, manganese, chromium and cobalt had significant negative effects on the thermal stability of a fuel, with these being significant components of the Inconel 600 and SS 304 alloys. Hazlett *et al* found similar results for the reaction of dodecane over metal srufaces.[249] SS 304 had the biggest affect, increasing the amount of alkenes, with SS 316 being more

reactive than aluminium. Wong found that SS 316 was also more reactive that aluminium, with it having a breakpoint in the JFTOT 30 °C lower.[141] Another study by Stavinoha *et al* looked at deposition on SS 316 and 304, Al, Mg, Au and Cu surfaces.[250] They measured the deposit thickness using 2 methods, Auger ion milling and the dielectric breakdown method, with discrepancies between the results. These discrepancies are thought be due to some of the metals being stripped from the surface and becoming part of the deposit, thus changing its conductivity. The Auger ion method showed that copper had thickest deposit, followed by Mg, SS 316, Au and Al, with the method not carried out on SS 304. The dielectric method has SS 316 and SS 304 having the thickest deposit, followed by Au, Mg, Al and Cu. The differences suggests that copper and magnesium are stripped from the surface and can be found dissolved in the fuel and thus forming part of the deposit. This is interesting as it supports the findings of Phelps and West *et al* who suggest that copper forms part of the oxidation process but is not a catalyst.[222, 231]

3.2 Previous models for thermal stability

Significant research has focused on developing modelling approaches for understanding the thermal stability of aviation fuel. This is for a number of reasons. The first is practical, being able to predict how a fuel behaves under heating in the fuel systems allows for engineers to develop new air frame components, without the need to carry out expensive testing. The second reasoning for the development of these models is that they allow for greater fundamental understanding of the autoxidation process and aid in the development of future synthetic fuels. The modelling of the thermal stability process has taken a number of different approaches. These include the simulations of the physical characteristics of the flow, and its effects on heat transfer and deposition, as well as modelling of the detailed chemical mechanism that govern liquid phase autoxidation.

Early modelling approaches focused on predicting the formation of deposits on the metal surfaces in experimental devices. Szetela *et al* proposed a 2-step mechanism, where fuel reacted with oxygen to form products, and these products react with the fuel to form deposits.[251, 252] This implies that there is a liquid phase step in the deposition mechanism, where initial oxidation products are formed, and then these react to form the deposit. However, this model is limited as it does not take into account the chemical composition of

the fuel and treats the whole autoxidation process as obeying an Arrhenius relationship.

$$Fuel + O_2 \rightarrow Fuel + P$$
$$Fuel + P \rightarrow Fuel + D$$
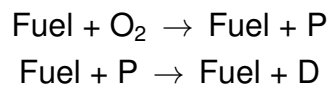
Improvements to the modelling were made by the introduction of a 3-step mechanism to incorporate the production of CO_2 observed in testing.[253] This led to marginal improvements in agreement with experiments, as the mass transfer and oxygen consumption were better described with this model, as now not all oxidation products lead to the formation of deposit. This means the yield of the reaction was no longer an unphysical 100%. This model was successfully implemented into 2-dimensional Computational Fluid Dynamics (CFD) code.[254] In that study Krazinski *et al* the precursors were modelled at being formed in the bulk liquid and being transported to the wall. At the wall they would bind to form the deposit. It gave good prediction for a number of flow and temperature conditions. However, it is clear from this model that more complex mechanisms are involved, with not all oxidised hydrocarbon leading to deposition, and that it is a multi-step and multi-product process.

$$Fuel + O_2 \rightarrow Fuel + P$$
$$Fuel + P \rightarrow Fuel + D$$
$$Fuel + P \rightarrow Fuel + CO_2$$
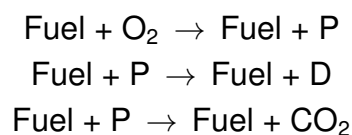
Katta *et al* investigated the deposition using computational fluid dynamics coupled to chemical kinetics.[255, 256] In this work the author improved on the 3-step model that they used to compare against. In the first paper, deposition on a fuel injector feed arm was simulated using the 3-step mechanism for the global mechanism, coupled to a deposit forming step meant to simulate the transport and binding to the metal surface.[255] It was found that this extra transport and deposit forming step was important for modelling the induction period found in the experiments for deposit growth and that without it the model was ineffective. This model was then able to predict the effects of lowering the flow rate in the test on deposition growth. However, the authors note that the model was not able to be applied to other experimental rig, and the chemistry of the global autoxidaiton mechanism required optimisation for each fuel and testing condition.

In the second paper, Katta *et al* tried to improve further, by taking into account that experimental work had demonstrated that the rate of autoxidation was independent of oxygen concentration.[256] This 9-step model was based on static flask and flowing tube experiments incorporating the liquid phase and wall reactions. It importantly included reactions involving peroxides, which have been heavily linked to increase the rate of autoxidation. It also included an agglomeration step, taking into account the role of solubility and physical mixing processes in the deposition mechanism. The authors noted that the mechanism had no initiation step, and thus to compensate, the first bulk reaction was made zeroth-order in relation to the concentration of oxygen in the fuel. The reactions on the wall interestingly did involve a reaction that could be considered an initiation step, with oxygen binding to the wall, and thus would be activated to react with the fuel. The model gave some good comparisons to experimental deposition data. However, it failed to predict the concentration of deposit precursors and peroxides in the thermally stressed fuel.

$$\text{Fuel} + \text{O}_2 \rightarrow \text{ROOH}$$
$$\text{Fuel} + \text{ROOH} \rightarrow \text{Solubles}$$
$$\text{F}_s + \text{ROOH} \rightarrow \text{P}$$
$$\text{Fuel} + \text{P} \rightarrow \text{Solubles}$$
$$\text{Fuel} + \text{ROOH} \rightarrow \text{D}_{\text{bulk}}$$
$$\text{Fuel} + \text{D}_{\text{bulk}} \rightarrow 2\text{D}_{\text{bulk}}$$
$$\text{O}_2|_{\text{wall}} \rightarrow \text{D}$$
$$\text{P}|_{\text{wall}} \rightarrow \text{D}$$
$$\text{D}_{\text{bulk}}|_{\text{wall}} \rightarrow \text{D}$$
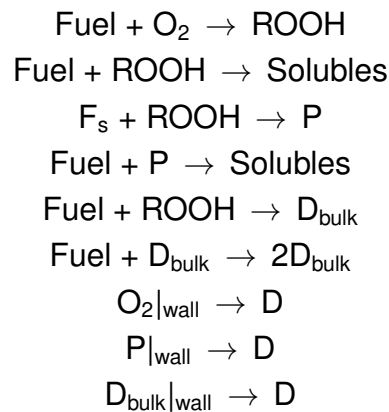
Katta *et al* discussed improvements to the 9-step mechanism as the description of the ROOH term in the mechanism, which denotes peroxides and peroxyl radicals, is not well described. The mechanism also fails to take into account the role of sulfur and metals in the autoxidation mechanism. To simulate these processes, the 9-step mechanism included a species F_s, supposed to represent the impurities in the fuel. To improve the description of different fuel blends, Katta *et al* altered the mechanism so that F_s had an influence on all of the steps in the bulk. giving the following 6 rate expressions,

$$k_a = \frac{1}{F_s}^{0.4} A_a e^{\frac{-E_a}{RT}}, \tag{3.1}$$

$$k_b = [F_s]^{0.4}[ROOH]A_b e^{\frac{-E_b}{RT}},$$
(3.2)

$$k_c = [F_s][ROOH]A_c e^{\frac{-E_c}{RT}},$$
(3.3)

$$k_d = \left[\frac{[O_2]_{in} - [O_2]}{[O_2]_{in}}\right]^3 [P][F_s]^{-1}A_d e^{\frac{-E_d}{RT}},$$
(3.4)

$$k_e = [F_s][ROOH]A_e e^{\frac{-E_e}{RT}},$$
(3.5)

$$k_f = [D_{bulk}]^{0.4}A_f e^{\frac{-E_f}{RT}}.$$
(3.6)

These expressions allow for the fuels chemical composition to affect the modelled rate of autoxidation. F_s is the sulfur and antioxidant concentration. As the concentration of this chemical species increases the oxygen consumption in the model decreases. As the concentration of the F_s species effects the production of solubles, it also has an impact on the concentration of ROOH and D_{bulk} species formed. Thus, by linking these findings, Katta *et al* were able to demonstrate that the consumption of oxygen is linked to the concentration of ROOH. Through this mechanism the affect of changing a fuels chemical composition on its thermal stability was able to be simply modelled.

Katta *et al* also offered an expression for the rate of surface deposition, which depends on the concentration of oxygen, P and D,

$$\frac{d[D]}{dt} = [O_2]_{wall}A_g e^{\frac{-E_g}{RT}} + [P]_{wall}A_h e^{\frac{-E_h}{RT}} + [D_{bulk}]_{wall}A_i e^{\frac{-E_i}{RT}}.$$
(3.7)

This modified 9-step mechanism was used to model the decomposition and oxygen consumption at a number of flow rates and temperatures successfully. The authors stated that the improvements were based on the improvement of the description of the impurities in the fuel, though the influence of F_s, and by coupling this species to the concentration of oxygen and peroxides in the

fuel. This means that the chemical composition of an aviation fuels effects its thermal stability and that this can be effectively modelled though the alteration of rate coefficients for the fuel being investigated.

However, this model does not help us to gain knowledge of the detailed mechanism involved. Peroxides, sulfur and antioxidant concentrations were coupled together in this mechanism as experimental evidence demonstrated that they are important, but demystifying the role they play in mechanism is not achieved using the 9-step mechanism. The modified 9-step mechanism also fails to model that a number of experiments have shown that heteroatomic species are found in great quantity in the deposit and that they can deposit without oxygen being present in the fuel. A more detailed modelling approach would be required to go beyond repeating experimental observations to understanding.

Significant work in this area has been carried out by a group at the University of Dayton. In 2 papers in 1998, Zabarnick developed and applied a 17-step Pseudo-Detailed reaction mechanism, seen in the first 17 reactions in table 3.1, to static and flowing systems.[156, 257] In the first paper, published in by Ervin and Zabarnick, the 17-step Pseudo-Detailed reaction mechanism was used investigate to isothermal and nonisothermal conditions in the near-isothermal flowing test rig (NIFTR).[156] In a case where a hydrotreated fuel was tested and modelled, the authors were able to accurately predict the oxygen concentration in the fuel, showing that at 170 °C the oxygen started to deplete and was all used up at the temperature reached 210 °C. However, the model was less accurate at predicting the exact concentration of peroxides in the fuel, with the general features being well simulated but the concentration being above the measured concentrations. The model was able to predict that as the oxygen was depleted the peroxide concentration increased. This suggests that the 2 species are correctly being linked in the model, but that steps are missing, with the there being other fates for the oxygen and peroxides in the fuel. The authors suggest that the discrepancies could be caused by the heteroatomic concentration in the fuels being low due to it being hydrotreated.

The model was used to predict the response of a straight run fuel to residence time and temperature, with the results being compared to experimental results in a modified NIFTR. The 17-step Pseudo-Detailed mechanism was able to accurately predict the oxygen concentrations at a number of wall temperatures

Tab. 3.1: Pseudo-Detailed reaction mechanism proposed by Kuprowicz *et al.*[14, 257]

N	Reaction	A (mol,L,s)	E_a (kcal mol^{-1})
1	$I \rightarrow R\cdot$	1×10^{-3}	0
2	$R\cdot + O_2 \rightarrow ROO\cdot$	3×10^9	0
3	$ROO\cdot + RH \rightarrow RO_2H + R\cdot$	3×10^9	12
4	$ROO\cdot + ROO\cdot \rightarrow$ termination	3×10^9	0
5	$ROO\cdot + AH \rightarrow RO_2H + A\cdot$	3×10^9	5
6	$A\cdot + RH \rightarrow AH + R\cdot$	1×10^5	12
7	$A\cdot + ROO\cdot \rightarrow$ Products$_{AH}$	3×10^9	0
8	$R\cdot + R\cdot \rightarrow R_2$	3×10^9	0
9	$RO_2H \rightarrow RO\cdot + \cdot OH$	1×10^{15}	39
10	$RO\cdot + RH \rightarrow ROH + R\cdot$	3×10^9	10
11	$RO\cdot \rightarrow R_{prime}\cdot +$ carbonyl	1×10^{16}	15
12	$RH + \cdot OH \rightarrow H_2O + RO\cdot$	3×10^9	10
13	$RO\cdot + RO\cdot \rightarrow RO_{term}\cdot$	3×10^9	0
14	$R_{prime}\cdot + RH \rightarrow$ alkane $+ R\cdot$	3×10^9	10
15	$RO_2H + SH \rightarrow$ Products$_{SH}$	3×10^9	18
16	$ROO\cdot \rightarrow R\cdot + O_2$	1×10^{16}	19
17	$ROO\cdot + R\cdot \rightarrow$ termination	3×10^9	0
18	$RO_2H + M \rightarrow RO\cdot + \cdot OH + M$	3×10^{10}	15

and residence times. As both increased the depletion of oxygen increased, with the experimental and modelling data at 185 °C used to adjust the sulfur and antioxidant concentrations used in the model. The model was less accurate in predicting the oxygen depletion for the straight run fuel when compared to the hydrotreated fuel used in the the first test, the results for both of these fuels can be seen in figure 3.27. The oxygen started to deplete at 240 °C, whereas in the in experiment this occurred at 170 °C again, with consumption being slower than in the hydrotreated case which wasn't seen in the model. The peroxide concentration were at the detection limit in the experiments with the model also showing a very low concentration of peroxides. These differences were suggested by the authors to be caused by the increase in sulfur and antioxidant concentrations in the straight run fuel compared to the hydrotreated fuel, which caused inconsistencies in the case for hydrotreated fuel, and were shown in this study to be linked to the formation and consumption of peroxides in the fuel. This affect is particularly sensitive to temperature, with the reactions peroxide forming and consuming reactions, becoming more important at temperatures above 175 °C.
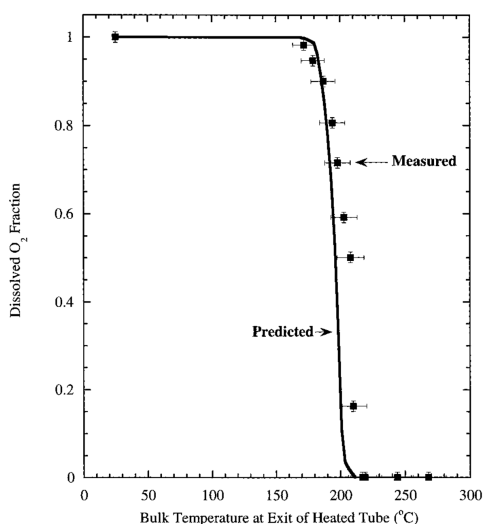
Figure 2. Dissolved O$_2$ concentration at heated tube exit (16 mL/min and F2747 fuel).
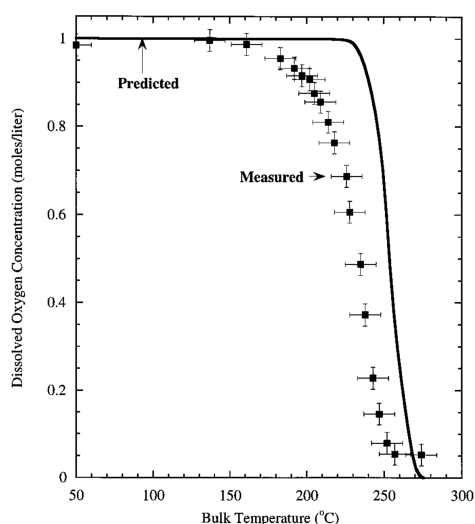
Figure 5. Predicted and measured dissolved O$_2$ concentration at heated tube exit (16 mL/min and F2827 fuel).

Fig. 3.27: Predicted oxygen consumption, hydrotreated F2747 on the left and straight run F2827 on the right, compared to experimental measurements, reprinted with permission from [156].

In the second paper, Zabarnick used the 17-step Pseudo-Detailed mechanism to study the role of antioxidants in the autoxidation process, by modelling a static fuel system.[257] The study was able to accurately predict the rate of oxygen consumption in the static test at 140 °C, and was able to show that antioxidants are required to react with peroxyl radicals in the fuel to remove them, and slow the oxidation rate. The calculated oxygen concentrations was linked to the concentration of antioxidant. Once the antioxidant has been used up, the oxygen depleted rapidly. This was done with sulfur concentration set to 0 in order to eliminate its effect on the mechanism. This allowed the authors to demonstrate that the concentration of peroxides in the fuel can be effected by the antioxidants alone. The oxygen consumption had good agreement with experimental data, with the trend being matched exactly, but the rate of oxidation being slightly higher in the model. The author attributes this difference to heating up time in the experimental device. At higher temperatures the rate of oxygen consumption increased. It was also observed that at this temperature, as the concentration of antioxidants in the fuel was increased, the oxidation rate was initially higher and the oxygen consumption profile was shaped differently. This was in agreement with previous experimental findings, and the author suggested that there was an optimal limit for antioxidants. The likely cause of this observation were the reactions in the 17-step Pseudo-Detailed mechanism involving antioxidants or antioxidant radicals, which became more important at higher initial antioxidants concentration. This increased antioxi-

dant concentration could also affect the solubility and viscosity properties of the fuel being tested, not detected in the chemical modelling.

In the paper the author was also able to show that the concentration of antioxidants, which react with the peroxyl radicals, had a logarithmic relationship to oxygen consumption. Whereas, sulfur which reacts with peroxides, had a linear relationship. This allowed the model to clarify the importance of antioxidants in the fuel compared to sulfurs in inhibiting autoxidation. However, it was not able to completely understand experimental results of thermally stressing blends of two fuels. Interestingly the 17-step Pseudo-Detailed mechanism was able to demonstrate synergistic effects of having sulfur and antioxidant species in the fuel, for both the flowing and static fuel case, with the inclusion of both greatly slowing the rate of oxidation.

The 17-step Pseudo-Detailed mechanism was used in a paper by Kuprowicz *et al* where the initial oxygen concentration was altered over a range of temperatures.[258] The mechanism under predicted the oxygen consumption with it becoming ore dramatic at higher initial oxygen concentrations. The authors attempted a number of alterations and addition to the mechanism to better simulated the oxygen depletion and get better agreement with experimental data. Reducing the activation energy of the homolytic fission of by 0.5 kcal mol^{-1} had limited effect, with the oxygen consumption still being slower than the experimentally observed rate. In the study, the unimolecular isomerisation of alkyl peroxyl radicals, where the oxygen radical moves along the hydrocarbon chain, was also shown to have little affect on the rate of oxygen consumption. However it was found that the inclusion of peroxyl radical decomposition and termination steps improved the agreement with experiments, a summery of these results can be seen in figure 3.28. Another interesting finding of this study was that the hydrocarbon composition of an aviation fuel, modelled though the alteration of the reaction parameters, can have a big effect on the autoxidation rate. The authors proposed that even at low concentration aromatic hydrocarbons can have a big effects on a fuels thermal stability.

A separate study carried ot at the University of Dayton by Doungthip *et al* investigated the effects of metal surface catalysis on autoxidation.[259] This was done though the inclusion of a reaction step to the 17-step Pseudo-Detailed mechanism on the wall surface, with simulated the homolytic fission of peroxides. The affect of this was investigated in CFD simulations of isothermal
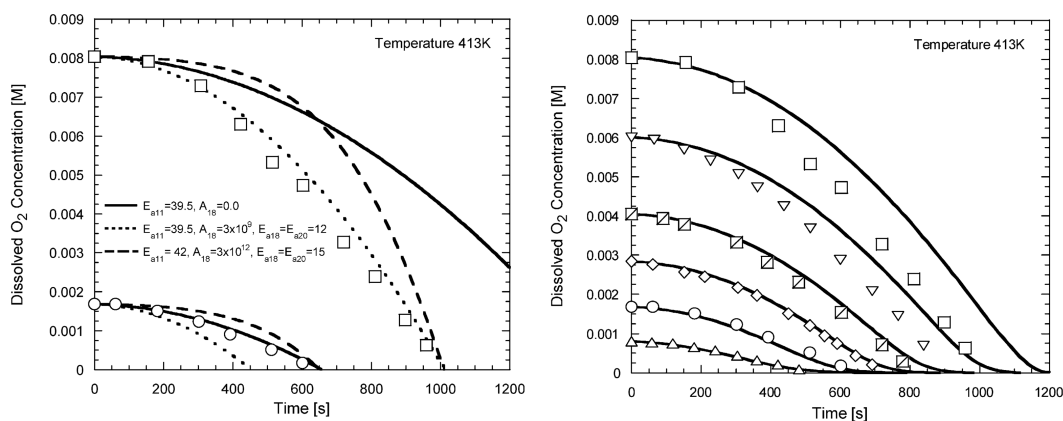
Fig. 3.28: Predicted oxygen consumption with different modifications to the Pseudo-Detailed mechanism. On the left the influence of peroxide homolytic fission and alkyl-peroxyl radical isomerisation is investigated. E_{a11} is the activation energy of peroxide fission with E_{a18} and E_{a20} being activation energies for alkyl-peroxyl isomerisation reactions. In the figure on the right the effect of peroxyl radical decomposition and termination is modelled with the results in both figures being compared to experimental measurements. Reprinted with permission from [258].

and nonisothermal tube reactor and compared to experimental results. The inclusion of this step improved the modelling of the oxygen consumption, and through the alteration of the activation energy, was even able to predict the effects of surface passivation. Treatment of the metal surface in the experiments slowed to rate of autoxidation something which could be seen in the CFD model. However, the authors acknowledged that the new term was not a detailed chemical step, and rather was a global term for surface effects. This could be the reason for the poor agreement with experimental peroxide concentrations, which had a much more server drop in concentration than in the model. This could be due to the surface activating the oxygen or hydorcarbons, help initiating the oxidation process, or binding the peroxide so it is not present in the fuels. The authors also note that the peroxide concentrations in the experiments were at their detection limits and this could be the cause of the discrepancy. The implication of the study is that a lot of the autoxidation mechanism happens at the surface and its affects should be modelled thoroughly.

The 17-step Pseudo-Detailed mechanism used in these papers was able to successfully model the deposition and oxygen consumption. However, it fails to give a complete picture of the mechanisms which govern the autoxidation process. The limit of this model is also that it relied on the rate parameters

being optimised to fit the experimental data. The reactions are represented as single step reactions which have Arrhenius behaviour, but they could be more complex multi-step processes, and the steps in the model are in-fact a global mechanism for each species class. From these findings two assumptions can be made. The first is that using these more fundamental modelling approaches the behaviour of a fuel under thermal stressing can be predicted. The second is that as the model requires optimising against experimental data and over estimates the oxidation rate, more chemical detail is required to fully predict how a fuel with known chemical composition would behave under thermal stressing. One clear area where the 17-step Pseudo-Detailed mechanism failed to describe the fundamental chemistry of autoxidaiton is in its description of peroxides.

Further improvements to the model were made by group at the University of Dayton, through the inclusion of metal catalysed fission of peroxides in a paper by Kuprowicz *et al*, as metals have been shown to be an important impurity.[14] The mechanism also improve the description of phenols, sulfurs and peroxides species. The mechanism was used to accurately predict the autoxidation of 7 fuels, with the rate parameters of the mechanism kept the same for all fuels, with only the concentrations of species in the mechanism altered to match those found in the fuel. The rate parameters for the reactions in the mechanism in table 4.5 were calculated by using known parameters for specific chemicals in a species class, such as BHT for phenols. As such the authors state that these parameters are unlikely to be very representative of the reaction rate for all species in those classes. Thus, the model used species concentrations that were lower than those measured within the fuel. The new modified 18-step Pseudo-Detailed mechanism was able to qualitatively describe the oxidation rates, and gave reasonably good agreement with experimental data, with only the fuel F3084 being noticeably divergent. These results can be seen in figure 3.29 As the authors kept the rate parameters constant throughout the investigation, the mechanism offers fundamental understanding of how the autoxidation mechanism unfolds, and not how a fuels chemistry affects its thermal stability.

The deposition of the 7 different fuels was also investigated in the paper, with the inclusion of wall reactions and bulk agglomeration steps allowing the model to accurately predict the location of deposition in the NIFTR testing. Three different sub-mechanisms were employed to investigate the deposition on the wall, with those involving the antioxidant and phenol being in the deposit,
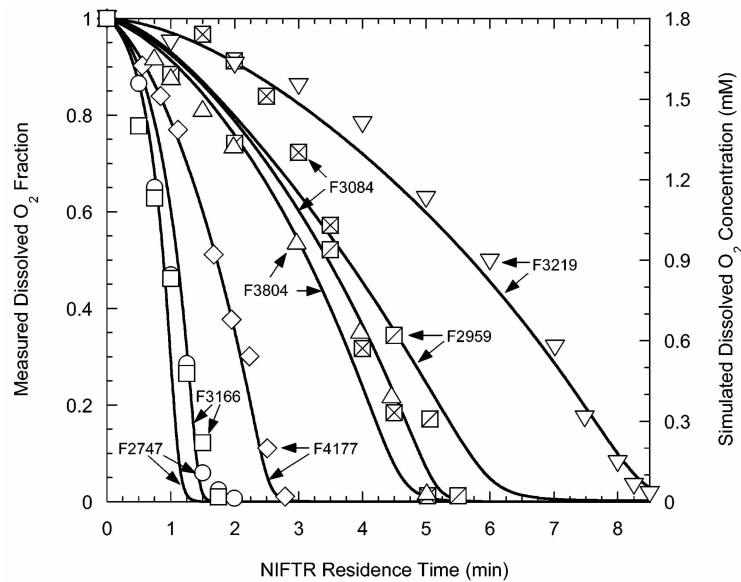
Fig. 3.29: Predicted oxygen consumption for 7 different fuels using the 18-step Pseudo-Detailed mechanism, with the results compared to experimental measurements. Reprinted with permission from [14].

found to improve the estimation of the depth and location of the deposits. sub-mechanism c, which was a 3-step mechanism which included bulk and wall reactions, performed the best for all fuels except again F3084. This inaccuracy could be caused up-steam in the bulk 18-step Pseudo-Detailed mechanism as it was shown to under predict the rate of oxidation in the bulk. However, sulfur was not included in the deposition sub-mechanism, as the authors state that sulfur had been shown to take no part in deposition. This is contrary to significant experimental evidence that demonstrates that sulfur is found in the deposit in high concentrations, and is often in an oxidised form. As the literature indicates that the exact chemical composition of the impurities, particularly for sulfur, also affect the thermal stability of a fuel. If the fuel F3084 has particularly reactive sulfur or polar impurities, it could also be that the mechanism is under representing their reactivity in the fuel, by lumping the rate together.

Sander *et al* used the a trimmed back 16-step Pseudo-Detailed mechanism coupled to the 3-step deposition sub-mechanism to investigated the affect of fluid dynamics and heat transfer in the Jet Fuel Thermal Oxidation Tester (JFTOT).[260] The authors used the measured outlet temperature to validate the fluid dynamics model used and were able to demonstrate 20% of the dissolved oxygen was needed to be consumed for deposition to occur, and the location of deposition. However, the absolute depositon depths could not

be compared to experiments, but the estimate could be used to determine if a fuel would pass the ASTM D1655 fuel specification test. The 16-step Pseudo-Detailed mechanism was used as the previous model under predicted the oxygen consumption. The peroxyl fission activation energy was lowered to be representative of the benzylic hydrocarbons being the main source of R groups involved in autoxidation. It was also found that the artificial initiation reaction was not needed. The 3-step deposition sub-mechanism had rate parameters altered to better describe the JFTOT. The CFD model was able to accurately predict the oxygen consumption profile, seen in figure 3.30. The experimental observation that oxygen consumption begins at 220 °C, equivalent to 160 °C bulk temperature, and has all occurred by 300 °C slightly under-predicts the oxygen consumption seen in the experiments but is within the range seen for conventional fuels.
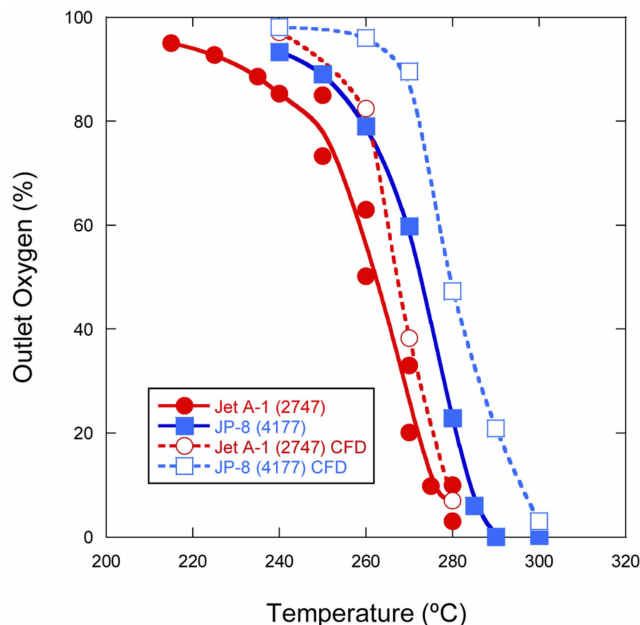
Fig. 3.30: Predicted oxygen consumption for 2 fuels using the 16-step Pseudo-Detailed mechanism and 3-step deposition sub-mechanism, with the results compared to experimental measurements. Reprinted with permission from [260]

It is important note that the mechanisms developed were only valid for the experimental device they were used to be compared against. The reason for this is that many of the steps present in the pseudo-detailed mechanisms represent global reaction steps, rather than single step in a chemical reaction, and thus require optimisation.

A more fundamental modelling approach can be taken, with the intricacies of the mechanism investigated, this allows greater understand of the role that each chemical component of the fuel has on autoxidation. One such investigations has been carried out by Phelps and Zabarnick.[222] In this study, DFT was used to theoretically model a number of chemical reactions of importance to the autoxidation of jet fuel, including the hydrogen abstraction by 2-butylperoxy radical, the reaction of sulfur species with peroxides and the catalytic fission of peroxides by copper. The reactions involving sulfur and copper with peroxide have been discussed in previous sections, so this section will focus on the hydrogen abstraction reactions and the effectiveness of this modelling approach.

In the study of the hydrogen abstraction reactions by peroxyl radicals it was found that the chemical structure of the peroxyl had no effect. However, this is contrary to some experimental evidence, which stated that the steric hindrance of the peroxyl affected the rate. The authors were able to show the importance of heteroatomic impurities in the fuels as they had hydrogen abstraction activation energies over 10 kcal mol^{-1} lower than those found for hydrocarbons. At 170 °C the Boltzmann distribution means that 99% of the reactions will occur though the heteroatomic route. Phenolic species were also found to be better antioxidants than nitrogen and sulfur containing aromatics with this being attributed to the X-H bond strengths being weaker. Aromatic hydrocarbon also demonstrated the same behaviour as the benzylic hydrogens had low activation energies.

The authors state that DFT studies allow for fundamental understanding of the autoxidation mechanism, allowing for chemical kinetic mechanisms to be built up from first principles. This is important as not only can accurate rate parameters for the reactions be predicted, but also the intricacies of the mechanism allows for future study to be directed. The authors also make a point that understanding the role of a fuels solvation and transport properties is important to understand in future studies, as the solvent molecules could interact with the transition states and intermediates in the reactions, offering intermolecular bonding which lowering the energy and facilitating reactions. Linked to this is the authors discussion of errors associated with the basis set superposition when the reactants and products are not optimised in the same calculation. This also introduces chemical errors in the calculated rates as the intermolecular bonding of fuel species can facilitate vibration along the reaction coordinate of interest.

Interestingly, the nature of the hydrocarbon composition is not dealt with in the 18-step Pseudo-Detailed mechanism proposed by the University of Dayton, not has it been discussed in models up to this point. As the experimental evidence available in the literature clearly shows that this is an important to understand more, it is worth dedicating some time to discussing literature that has tried to address this using modelling approaches.

Detailed models for the autoxidation of hydrocarbons using Reaction Mechanism Generator (RMG) has been carried out by a group at IFPEN. In the first paper Ben Amara *et al* investigated the affect of changing the concentration of methyl oleate, a FAME derived product, in n-dodecane to simulate increasing FAME use in aviation fuel.[261] Ben Amara *et al* used RMG to develop a detailed chemical kinetics mechanism to predict the autoxidation rate. This mechanism had 174 species and 3275 reactions in it so is substantially larger than the previous models discussed. However, interestingly only 15 reactions were found to have significant impact on predicting the rate of oxidation, with these improving reactions with dissolved oxygen and the reaction of peroxyl and peroxide species. The model developed was able to qualitatively predict the affect of increasing the % of methyl oleate in n-dodecane, with this increase causing the length of the induction period to decrease. However, numerically the predictions were most accurate at low concentrations and high concentrations, but the validity of the model was not effected by changes in temperature. Improvements were made to the accuracy of the model by deriving an analytical expression for the induction period form the kinetic mechanism, the results of this can be seen in figure 3.31 and the expression can be seen in equation 3.8.

$$IP = \frac{b + \sqrt{b^2 - 4ac}}{2a},\tag{3.8}$$

where

$$a = \frac{1}{2}([R_1H]_0(\beta^2 - 2\gamma) + (\delta^2 - 2\epsilon)[R_2H]_0),\tag{3.9}$$

$$b = \beta[R_1H]_0 + \delta[R_2H]_0,\tag{3.10}$$
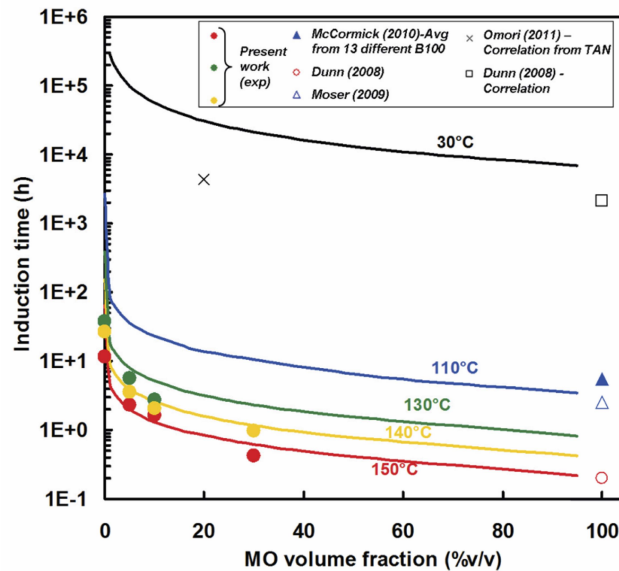
Fig. 3.31: The results of the analytical derived IP with experimental data from the same study (n-dodecane/methyl oleate blends) and literature for pure compounds, middle-distillate/FAME blends. Reprinted with permission from [261]

$$c = 0.05([R_1H]_0 + [R_2H]_0). \tag{3.11}$$

As such, the analytical rate is related to the concentration of the initial n-dodecane ($[R_1H]_0$) and the initial methyl oleate ($[R_2H]_0$). It also has a set of coefficients, denoted by the greek symbols, which relate to the rate of reaction for some important reactions in the model, but interestingly not all 3275 of them. A number of conclusion can be drawn from this approach, the first being that not all chemical reactions are of importance to accurately model the autoxidation of an aviation fuel. This means that despite an aviation fuel having potentially thousands of chemical species present in it, and thus the oxidation mechanism also having thousands, it is not necessary to model each of these chemical reactions to understand an predict a fuels behaviour under thermal stressing. The second conclusion from this paper, is that though the use of RMG and other similar tools, future development of bespoke oxidation mechanism for designer fuels is possible. However, if not all reactions are important, would it be possible to develop a Pseudo-detailed mechanism that would be able to model any given fuel, with a limited number of chemical reactions.

A second paper investigated the affect of changing chain length of n-alkanes on the autoxidation using RMG.[138] The RMG oxidation mechanism were able to show that the products formed were not dependant on the chain length of the alkane with them all forming alkene, aldyhydes, ketones, carboxylic acids and alcohols. The mechanism was able to model the production and consumption of peroxides well with their importance in the autoxidation being highlighted as important. The RMG models were also able to predict the observation that as chain length increases so does the induction period, with the time taken eventually reaching a plateau at C_{12}. The agreement with experiment was decreased at lower temperatures but was still a factor of 2 or 3 different from the experimental times. Improvements could be made by reducing the initial concentration of oxygen in the experiments with this likely caused by the model under predicting oxidation rate.

The authors noted that the computational memory and processor requirements limited the size of the model and the chain length of alkanes to C_{14} as at this point the RMG kinetic model had 440 species and 26669 chemical reactions in it. As the previous paper noted, not all of the chemical reactions are important, and increasing the size of the mechanism doesn't improve its accuracy or give greater understanding of the autoxidaiton process. With the finding that the alkanes produced similar products during oxidation, and after C_{12} reacted at the same rate, it may not be necessary to model all of the alkanes present in a fuel individually.

A paper by Mielczarek *et al* developed a kinetic model for the oxidation of toluene using RMG with quantum chemistry derived thermodynamic parameters being calculated for important species.[144] The kinetic mechanism consisted of 173 chemical species and 2309 reactions, which included key termination reactions present in the literature generated in a separate RMG model. The authors found that the inclusion of the termination steps and improvement of the thermodynamic data for important species, lead to greater agreement with experiments, seen in figure 3.32. However, similar to previous studies the agreement was poorer at lower temperature. The authors state that the inclusion of the termination steps is important, as they provide a sink for the radicals in the autoxidation process, and without them the mechanism over predicts the oxidation rate. The mechanism offered some incite into the dominant reaction routes in the autoxidation of toluene, with peroxyl and peroxide species again being of importance, and benzyl alcohol, benzaldehyde and benzoic acid being the main products.
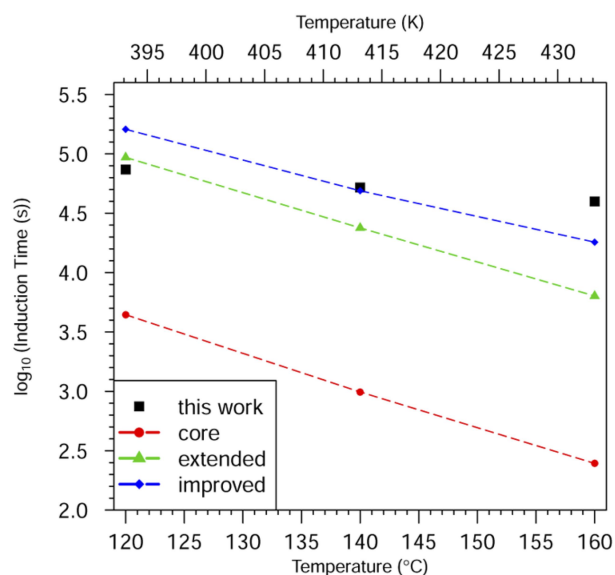
Fig. 3.32: Logarithm of the induction time for the core mechanism, extended mechanism with added termination reactions and the improved mechanism with thermodynamic data for specific species using quantum chemistry calculations, compared against experimental data. Reprinted with permission from [144]

The improvements to the thermodynamic data of specific species using quantum chemistry in the mechanism lead to benzoic acid not forming in the model. Instead the decomposition products of carbon dioxide and benzene radical. Some of this reaction would be expected, but at such high pressure in the experiment, it would be expected that some benzoic acid is formed. DFT calculations were performed to understand the process more, but as the authors note, due to the complex electronic structure of the problem multi-reference calculations would need to be performed. The author notes that using RMG and other modelling approaches, can overlook the effect of diffusion across the vapour-liquid barrier, and transport and deposition to the metal surface. They stated that it appears to have no effect in predicting the rate of oxidation in the PetroOxy static fuel tester used in the paper, but that the mechanisms developed are specifically built to predict the liquid phase autoxidation.

In the most recent paper in this series, Chatelain *et al* investigated the affect of branching of alkanes on their thermal stability, using RMG and experimental validation.[139] In this study the authors investigate four C_8 isomer, n-octane (C8), 2-methylheptane (MH), 2,5-dimethylhexane (DMH), and 2,2,4-trimethylpentane (TMP). The results showed that increasing the branching of alkanes decreased the induction period, except for the special case TMP.

The models had good agreement with the temperature dependence of the induction period, and gave the general trend of the effect of branch, but could not distinguish between MH and DMH. The modelling study was able to clarify the reason for some of the observation in the literature, with the authors stating that the effect of branching on the reactivity of alkanes can be attributed to the rate of hydrogen abstraction from the C-H most reactive. It was also clear that the reaction of peroxides and peroxyl radical species and derivatives was important. Particular the quaternary peroxyl species with multiple peroxyl groups present on the same alkane chain.
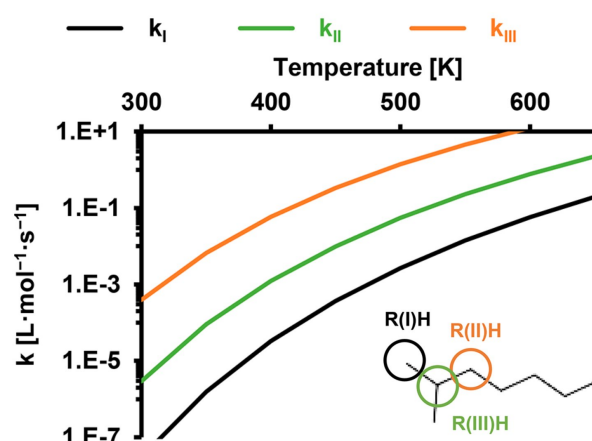
Fig. 3.33: The rate constants for the hydrogen abstraction from the three different sites possible on an alkane. Reprinted with permission from [139]

3.3 Physical considerations

Despite this thesis focusing on affect of an aviation fuels chemical composition has on its thermal stability it is also important to briefly cover the literature on the effects of some physical phenomena on thermal stability.

Time and storage

A number of studies have looked at the effect of storage and heating time. As was seen by Frankenfeld and Taylor, the longer that a fuel was stored, particularly in the presence of light, the greater the level of deposition in testing.[187] The fuels stored in the presence of sun light or UV radiation had logarithmic growth in sediment as a function of the time stored in days,

whereas the growth in sediment of the fuels stored in the dark was linear. The reactivity of chemical species when exposure to light also changed in this study, with alkyl indoles being more susceptible to the UV catalysed reaction than alkyl pyyroles. The presence of light has also been linked to the UV catalysed homolytic breakdown of peroxide, with this initiating oxidation at ambient temperature.[11, 262]

The Frankenfeld and Taylor study also demonstrates that a fuels chemical composition has an affect on its sensitivity to storage conditions. Increasing concentration of heteroatomic species, in the presence of light, increased the sedimentation in storage. This is likely due to X-H or X-C-H bonds being weaker than alkane C-H bonds and thus are more susceptible to homolytic fission. This could also be true of aromatic C-H bonds, and as such low aromatic synthetic fuels would be expected to perform better under these storage conditions. This finding was supported by Karavalakis *et al*, who carried out a storage study of bio-diesels with different synthetic antioxidants, with multi phenolic groups leading to greater stability.[162] They found that after 4-6 weeks of the 10 week study, the fuels induction period dropped below the 20 hours standard. It was also observed that all of the fuels had higher acidity and viscosity after storage due to the formation of oxidation products. Rawson *et al* investigated the affect of adding antioxidants to a range of aged MEROX and hydrotreated fuels.[153] It was found that this improved the thermal stability by increasing the induction time, but had little effect on the formation of peroxides. This would suggest that antioxidants have little effect in the storage stability, not stopping the formation of peroxides, but can be added to fuels just before used to improve stability during use.

Bhan *et al* aged a series of marine fuels, at 65°C, in which they found that the neutral compound in the fuel were oxidised. This resulted in an increase in acidity or basicity of the fuels during the length of the study.[214] It was also observed that sediment would form during storage, and that this was particularly bad for fuels with heteroatomic species and high aromatic concentrations, similar to the findings of Frankenfeld *et al* and Karavalakis *et al*.[162, 187]. However, they did note that this was not necessary for sediment formation. Grishina *et al* proposed an kinetic equation for the formation of insoluble gum in diesel during storage.[263] This relationship can be seen in equation 3.12, and was valid for long term storage beyond 5 years, with the rate constant k being found to have a value of 0.000210. The process was

slow and linked to temperature indicating that the underlying chemistry for storage and thermal instability are the same.

$$log\tau = (n+1)logc_{gum} - logk(n+1). \tag{3.12}$$

Mushrush *et al* showed that nitrogen species found in the fuel are particularly bad for storage.[189, 264] However, they did not show that any specific species was particularly deleterious, but did find that pyridines, indoles and quinolines made up the majority of the nitrogen species in the fuels studied. They did find a relationship between the basicity of the fuel and its storage stability, with stable fuels having a much lower level of basic nitrogen species. supporting the findings of Bhan *et al*.[214]

The literature indicates that length of time that a sample of hydrocarbon or fuel is heated for during testing also has an effect on the thermal stability and deposition. Marteney and Spadaccini carried out a study where a fuel was tested for 8, 16, and 32 hours in a tube reactor.[265] It was demonstrated that increase length of testing lead to progressively more deposition and that in longer tests the deposition occurred at location to close to the fuel inlet and less deposit formed near the tube outlet. Three phases of oxidation and deposition can be seen in a number of tests. Clark and Stevenson carried out testing in a Mini injector feed arm rig (MIFAR) to measure the rate of deposition.[266] They found that the deposition had three phases associated with it. The first was an induction period, between 0-5 hours, in which little deposition occurred. This was suggested to be caused by the difference in the heat transfer of the clean metal surface in the initial testing and the later surface with deposit growth and increased roughness. However, Mills *et al* showed that increased deposition had a negative effect on the heat transfer coefficient.[234] Between 5-15 hours, Clark and Stevenson observed rapid constant deposition occurred, after which there was a drop in the rate of deposition until the end of the test at 20 hours. They also supported the findings of Mills *et al* by finding that the insulating effects of the increasing deposit thickness was the cause of the drop in deposition rate. This was also found by Smith with the heat transfer coefficient being sensitive to the thickness of the deposit formed.[267] However, Smith found that it didn't always drop immediately, sometime rising before dropping. They stated that the drop in the heat transfer coefficient could not be guaranteed until the deposit had grown in thickness enough to break through the laminar sub-

layer. It was also demonstrated in the Clark and Stevenson study that the the lengths of induction period was linked to rate of deposition, with fuels with short induction periods having higher deposition rates. However, they did not comment on the affect of induction period on the total amount of deposit formed.

The findings of the work by Clark and Stevenson suggest that it is not just physical phenomena involved, but that an aviation fuels chemistry contributes to the observed effects. Sicard *et al* found something similar when studying the autoxidation of model hydrocarbons.[268] They did not look at the deposition, but the depletion of oxygen in a static reactor vessel called a PetroOxy heated to 150 °C and over pressured with oxygen. They stated that there is an initial induction period, where peroxides and mildly oxidised species are formed, this stage of the mechanism was coupled with a rapid drop in oxygen pressure in the PetroOxy. They then observed an increase in the pressure, which they attributed to a second stage in the oxidation, where small volatile products are formed. This coincided in lower molecular weight hydrocarbons forming. The third stage of oxidation had a slow pressure drop associated with it, and involved the consumption of the polar oxidised species, forming heavier oxidised additions products. These were characterised as lactones and esters. This was also the point that deposits formed in the PetroOxy tests. At the end of an 80% drop test, when the reactor was cooled, the residual pressure was 20 kPa. Thus it was assumed that all of the oxygen has been reacted and incorporated into the oxidised products at this point, and this third slow oxidation stage is in a deoxygenated environment.

Temperature

The role of temperature is obviously important in the autoxidation process. It was found that increasing the Mach number, thus increasing the temperature, during test flight simulations lead to a dramatic increase in the pressure drop in the inlet nozzle due to deposition.[2] The increase in Mach number resulted in a peak temperature increase from 205 °C to 260 °C, with the lower temperature demonstrating limited pressure drop, thus between 205 and 260 °C significant autoxidation rate increase occur.

Spadaccini *et al* stated that the fuel temperature was the most important factor effecting the autoxidation rate in their study on the formation of deposit

in multiple tube coking rig.[10] Autoxidative deposition was found to peak at 315 °C, above which there is a drop in deposition, which was stated to be due to the oxygen having been consumed. Above 426 °C pyrolytic deposition occurred and increased until the stop point of the test at 800 °C. Smith found similar results in a study of the thermal stability of 8 fuels over a temperature range of 150-208 °C, with deposition being found to increase with temperature, observed though a decrease in the heat transfer coefficient in the single tube heat transfer rig.[267] Similarly in their study of pure hydrocarbons Wong and Bittker found that depositon peaked at 350 °C.[141] Sander *et al* using the JFTOT were able to demonstrate the all of the bulk liquid phase oxygen consumption occurs in a range of 80 °C, between 160-240 °C, corresponding to wall temperatures of 220-325 °C.[260] However, this was effected by the chemical composition of fuels, with some fuels tested demonstrated much quicker autoxidation.

Siouris *et al* showed that the increase in wall temperature lead to a proportional increase in the amount of deposit formed, in the Aviation Fuel Thermal Stability Test Unit (AFTSTU), at flow rates of 23 l/hr. As the wall temperature was increased from 310 °C to 330 °C this resulted in an increase in deposit of 10 μl. However, they found that increasing the temperature of the fuel inlet from 150 °C to 165 °C resulted in an increase of <1 μl. The authors state that the temperature of the metal surfaces was far more important in determining the growth of deposit. The increase of only 20 °C causing such dramatic changes in deposition suggests that at this temperature, the initial chemical binding to the bare wall can occur rapidly for the single fuel tested. If this is dependant on the chemical composition of the fuel is unknown, as it would be expect that for fuels with high concentrations of polar species that can more easily chemically bond to the walls, would demonstrate this transition at lower temperatures. Marteney and Spadaccini carried out a study of the deposition rate of a number of fuels over a temperature range of 150-600 °C.[265] This study also showed that the wall temperature was more important at predicting the rate of deposition than the temperature of the bulk fuels, with the greatest rate of deposition occurring between 270-330 °C.

Taylor carried out studies investigating the deposition of pure hydrocarbons and mixtures over a temperate range of 93-260 °C.[134] This study found that the single component samples behaved according to Arrhenius rate theory, over the temperature range within the glass tube reactor test rig, with increasing temperature lead to greater deposition. However, Taylor did note

that the chemical structure of the hydrocarbon effected the rate of deposition and that the addition of aromatics slowed the start of deposition. A number of studies demonstrated that this linear Arrhenius behaviour no longer hold true when the wall temperature gets above 370°C.[10, 234, 269] This is has been speculated to be due to a change in mechanism initiated by the depletion of the oxygen dissolved in the fuel.

Beaver *et al* have suggested that thermal stability an storage stability are governed by the same chemical mechanism, and that the temperature of test merely affects the rate of these phenomena.[180, 181, 185] They suggest that the differences are related to physical processes which include the chemical bonding to the metal surfaces of the deposit. They proposed that the polar species agglomerate together and insoluble sediments at storage temperatures. At increased operating temperatures, these reaction not only proceed at a much higher rate, but also causes the products to bind to the surface. Thus, forming insoluble deposits on the fuel system working parts. This suggest that binding to the surface is not barrier-less and requires energy to be put into the system to form the chemical bond to the surface. Experimental evidence for the link between storage and thermal stability can be seen in a study by McCormick and Westbrook, which showed that an induction periods of 3 hours or in the EN14112 and D2274 tests was sufficient for the fuels to be stable in storage for 12 months at 21°C.[270] Both these sets of authors however state that this may not be true going forward, with a change in the fuel chemical composition, and additive packages used.

Pressure, flow rate and Reynolds number

Hamadache *et al* found that decrease in flow rate lead to an commensurate increase in deposition.[271] This as due to the increased residence times leading to greater total heat being imparted into the fuel. Areas of low flow rate were also found to have drops in heat transfer coefficients, indicating that areas of low flow, or stagnant conditions, would be areas of concern in fuel systems. Smith found that in fixed temperature conditions, the higher the flow rate the higher the observed loss in heat transfer.[267] However, it was found that when the flow rate reached the turbulent regime, 600 kg/hr, the result were more complex. The heat transfer coefficient sometimes not being affected until the deposit had broken though the laminar sub-layer, and in other fuels tested the increase in flow rate above this point lead to a drop in

the deposition. Smith suggested that the reasoning for these observations could be due to a number of factors. These included, residence time, amount of deposit precursors in the fuel, turbulence, surface temperate, laminar sub-layer thickness and the roughness of the deposit. Residence time was discounted, as it did not support the findings at lower flow rates below 600 kg/hr, and was in conflict with others. It was suggested that the observation was due to increased mixing and higher wall temperature due to the higher flow rate being the cause of increased deposition below 600 kg/hr, and that when the sub-layer was broken in the turbulent regime this was also observed. This lead to Smith to propose a relationship dependent on the Reynolds number, seen in equation 3.13

$$Nu = 0.0204Re^{0.925}. \tag{3.13}$$

A similar expression was found by Chin and Lefebvre for the rate of deposition for two fuels.[272]

$$k = C_1 Re^{0.65}, \tag{3.14}$$

with further testing allow for the authors to expand C_1 was able to,

$$C_1 = C_2 exp^{\frac{C_3}{T_F - 273}} exp^{\frac{T_W - T_F}{166}}, \tag{3.15}$$

where T_F is the fuel temperature and T_W is the wall temperature. C_2 and C_3 were constants that were dependent on the fuel being tested. They similarly postulated that at increasing flow rate and Reynolds number, the heat transfer between the wall and the fuel is increased, leading to greater mixing of deposit precursors.

Spadaccini *et al* investigated the affect of flow rate on thermal stability, and stated that increasing the flow rate lead to increased deposition, this was in disagreement with other studies. It was postulated that the reason was the increased flow rate lead to great turbulence, and thus lead to greater heat transfer into the liquid. This increased turbulence could also lead to longer residence times close to the wall, contributing to the greater deposition. In

another study Marteney and Spadaccini also investigated the deposition rate of a number of fuels at different flow rates.[265] They found that increasing the flow rate into the turbulent region reduced the temperature where the maximum deposition occurred by 25 °C, whereas laminar and transitional flow regimes had little effect, other than at very low flow rates where deposition occurred at much lower temperatures. This was speculated to be due to the chemical reactions being mixing limited at very high temperatures.

Spadaccini *et al* researched a number of factors in there study on autoxidation and pyrolysis coking.[10] They stated that increasing pressure had little impact on the deposition. Taylor also investigated the affect of pressure, between 1800-69000 kpa, on thermal stability.[135] It was found that increasing pressure had no effect on one fuel tested. However, the increase in pressure caused a decrease in the deposition of the other fuel tests. This was speculated to be caused by a change in the solubility of the fuel at increased pressures.

Moses acknowledged the confusing picture of flow rates effect on the thermal stability of fuels, and carried out investigations into the affect of Reynolds number in two pipe geometries to attempt to clarify the phenomena.[273] In this study it was found that increasing Reynolds number, so increasing flow rate, lead to deceasing deposition rates. The reasoning given for this was that most of the autoxidation reactions and deposition happens in the laminar sub-layer where the temperature is highest in the fuel. Thus, increasing the flow rate leads to a reduction in the thickness of the sub-layer.

Moses stated that in studies were increasing flow rate lead to increasing deposition, this was a result of the fuel undergoing pre-heating before testing, and thus deposit precursors are already formed in the fuel and increased turbulence just improves mixing. This would mean that in high Reynolds number areas in the fuel system, where the fuel has already undergone pre-heating, you would expect a build up in deposit. How the fuel has previously been stored would also likely impact the behaviour in these conditions.

3.4 Summary

This review of the literature indicates that there is still a number of unanswered questions about the autoxidation mechanisms of aviation fuel. The affects of

physical phenomena on the thermal stability have been well studied, with the recent paper by Moses demystify the contradictory picture that had been seen in some previous studies.[273] As the literature indicates, there is a linear response to temperature increases in testing, and has often been shown to follow an Arrhenius relationship. However, as the jet engine and air-frame are developed, increased study is required to investigate the response of the fuel at higher standard operating temperatures. The more extreme operating conditions also means that the effect of variables not considered in great depth up to this point also need to be studied, with the effect of surface roughness at high Reynolds numbers gain greater attention recently, due to the increased usage of additive manufacturing in the aviation sector.[274]

Significant study in the literature has been applied to investigating the role that an aviation fuels chemical composition has on its thermal stability and autoxidation. The majority of these studies have been focused on the affect of the minor components have on the these properties. The minor components in the fuel include the oxygenated polar species, sulfurs, metal impurities, additives and increasingly nitrogen polar species as well. The picture of the affect that some of these species is fairly clear, but their exact roles in the autoxidation mechanisms is still inconclusive, with the role of sulfur being particular unclear. Detailed mechanistic studies are required to validate the hypothesised reaction mechanism presented in the literature and apply them to the wider autoxidation mechanism. It is also not well understood how these minor species act in combination with each other, with more study required to be able to predict this behaviour.

The literature indicates that a number of possible products can be formed, with their chemical and physical nature, dependent on the temperature and flow regimes. Standard oxidation products have been shown to be formed in the oxidation process, with alcohols, aldehydes, ketones, acids and ethers been seen in detectable concentrations in the thermally stressed fuel. These species are more polar than the hydrocarbon component of the fuel, and as such will agglomerate together to minimise the negative enthalpic interactions with the apolar hydrocarbons. The SMORS mechanism proposed by Hardy *et al* and developed by Beaver *et al* has suggested that these primary oxidised products can then react together through oxidative coupling and electrophilic substitution reaction, and with naturally occurring polar species found in the fuel, to form the insoluble material that results in sedimentation and deposit. This original mechanism was developed for the reaction of oxidised products

with phenolic and nitrogen species in the fuel, with recent work by Zabarnick *et al* focused on the inclusion of sulfur species in this mechanism.

The nature of the insoluble material is dependent on the temperature and flow conditions. As Moses demonstrated, an increase in Reynolds number results in the reduction of the laminar sub-layer, and thus limited the extent of reaction. However, it has been acknowledged that pre-heating of the fuel and increases in surface roughness can result in an increase in deposition. Interestingly, the initial deposit on the surface has a high concentration of sulfur and oxygen. This would suggest that at high temperatures, the heteroatoms in the insoluble sediments is able to chemisorbed to the surface, and form strong covalent bonds. The initial deposit would then be able to react through the same SMORS mechanism as in the liquid phase, increasing the weight of deposit over time. All of these processes leads to an improved picture of a global oxidation mechanism which can describe the formation of sediment at storage temperatures and the deposits found at higher temperature synonymous with thermal stability issues.

A number of modelling approaches have been carried out in the literature, in an attempt to gain greater understanding of the autoxidation mechanism, and predict the deposition of fuels. This work start with models that were constructed of a minimal number of global steps to predict the formation of deposits in simple systems. These mechanisms have slowly been developed to include better descriptions of the chemistry and the global transport mechanisms that form the deposits. The most developed model for this study of the global transport and deposition of the oxidised products has been presented by Katta *et al*. However, this approach does not include detailed description of the chemistry that happens in the bulk, and thus fails to predict the concentration of the oxidised species talking part in the transport and deposition mechanisms.

Significant work has been carried out by the group at the University of Dayton to develop models for predicting the autoxidaiton of fuels in the bulk, and to plug these models into ancillary models for transport an deposition. These models have developed to the point to where they include some chemical information about the minor components of the fuel and how they react with each other. However, the different chemical species in a class are not differentiated from each other, and the second stage involving the coupling reactions is left underdeveloped. The mechanism is able to be adapted

to the concentration of different minor components in the fuels, but does not differentiate the results of changing the hydrocarbon component has on the thermal stability of a fuel. The mechanism developed up to this point have treated the fuel hydrocarbon component as having the same chemical composition and response to thermal stressing in the same way. During this review, it have been seen that different hydrocarbon in the aviation fuels act differently in autoxidaiton conditions.

All mechanisms and models developed up to this point have treated the fuel as being composed of a generic hydrocarbon species, represented as RH, which undergo the same oxidation reactions at the same rate. However, Experimental evidence clearly indicates that this is not true, with the hydrocarbon species present in the fuel reacting in chemically different ways, and undergoing oxidation at different rates. As such, it would make sense to develop a more tailored mechanism to appreciate these nuances. This would allow the prediction of the concentration of polar oxidised species to be more accurate, which can result in improved implementation into further studies of transport and deposition studies. The purpose of this work is to demonstrate the effect that changing hydrocarbon composition has on the mechanism and kinetics of oxidation.

3.5 Thesis objectives

This literature review has highlighted a number of objectives that the rest of this thesis will study.

1. Study the role that hydrocarbon chemical composition has on autoxidation, thereby demonstrating that it has a significant impact on thermal stability of a fuel.

2. Provide greater clarity on the mechanism which govern the autoxidation of hydrocarbons, through experimental and modelling studies, developing a mechanism that combines the multiple facets of oxidation seen in the literature and can be used to predict the thermal stability behaviour of synthetic aviation fuels in order to aid in their development.

3. Develop and expand the current pseudo-detailed mechanisms to included the effects of changing the hydrocarbon composition of the fuel

to help achieve the previous aim. Thus, build a base mechanism that can be extended with other chemistry and applied to larger scale modelling.

4. Carry out spin unrestricted and multi-reference quantum chemistry calculations to investigate the complex electronic structure problem of the bi-radical systems involved in autoxidation.

Investigations Into Hydrocarbon Autoxidation

4

As is clear from the review of the literature presented in chapter 3, greater understanding of the role that a fuels hydrocarbon composition has on its thermal stability is needed. As such it is an active research interest in the thermal stability field.[138, 140, 145, 261, 275, 276] It is important to investigate the underlying chemical mechanisms which govern the oxidation of the hydrocarbons in the aviation fuel and how mixtures of them interact. This work will be the main focus of this thesis and it will use experimental and modelling techniques to investigate the problem.

4.1 Experimental methodology

For the experimental investigations carried out in this thesis, the PetroOxy thermal stability tester device is suitable, as it allows for the testing of the rate of oxidation of samples in a small scale static reactor. The PetroOxy device, or similar small scale static testers, have been used to investigate the autoxidation and deposition of fuel by other research groups in the field.[138, 140, 145, 146, 213, 257, 261, 276] A schematic and image of the PetroOxy device can be seen in figure 4.1. The device has a 25 mL aluminium reactor which has a gold foil surface layer. The reactor is sealed by a screw top lid with disposable PTFE seals, and a latch locked insulated safety lid. Oxygen is pumped into the reaction chamber through an inlet, and the atmosphere and vapours in the chamber can be pumped out through an outlet. This allows the chamber and sample to be purged before testing. The sample is sealed in the reactor which is subsequently filled with oxygen, before it is purged and refilled prior to heating, this ensures that the dissolved oxygen in the sample has reached equilibrium prior to testing. The sample is then heated to the testing temperature. The pressure and the temperature are recorded throughout the test, with the data exported to a connected computer using the OxyLogger software, it can also be stored and printed directly from the PetroOxy device.

143
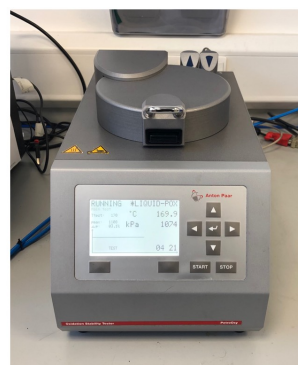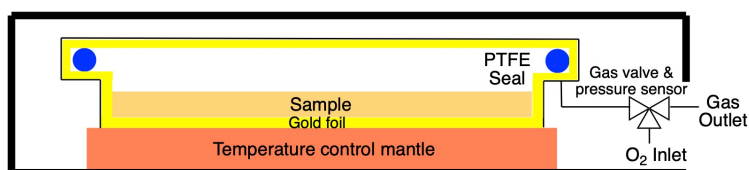
Fig. 4.1: Schematic and image of the PetroOxy thermal stability tester device.

The PetroOxy investigates the rate of oxidation by filling the reactor chamber with oxygen and measuring the pressure drop as the sample is heated. As the sample reacts, the dissolved oxygen concentration in the fuel drops, leading to the oxygen in the vapour phase above the sample moving across the phase barrier into the liquid. From this the rate of oxidation can be obtained. In the experiments in this thesis, 5 mL of sample was used, with the oxygen pressure in the chamber being 700 kPa. The sample is then heated to 170 °C, resulting in an increase in the pressure of the system, due to the oxygen having greater kinetic energy and some of the sample vaporising. The experimental conditions used in this thesis, the static sample and oxygen rich environment, do not reflect those found in the fuel systems. However, they represent accelerated autoxidation conditions. This allows for the fundamental oxidation mechanism of hydrocarbons to be studied and for a greater understanding of the role that its chemistry has its autoxidation.

To validate the use of the PetroOxy in this study, initial investigations were carried out, to determine the repeatability of the device. The PetroOxy has been approved for use in testing the thermal stability of middle distillate fuels by ASTM international.[277] In the test method specified in D7545-14, the hydrocarbon sample is heated to 140 °C at 700 kPa, with the time taken to reach a 10% drop for the maximum testing pressure recorded as the breakpoint, also called the induction period. The repeatability quoted in the standard for this test procedure can be seen in equation 4.1

$$r = 0.0288X + 0.4965, \tag{4.1}$$

where X is the the mean of two test results expressed in minutes, rounded to the nearest 0.01 minute. A group working at IFPEN have also used the PetroOxy device to study the oxidation of middle distillate fuels, using the same test method, and found a similar repeatability relationship,

$$r = 0.014X + 1.229, \tag{4.2}$$

with X being the mean of 2 or 3 tests runs expressed in minutes.[140] In this thesis higher temperatures and pressure drops are used in order to investigate a greater extent of the autoxidation mechanism. As such, method validation and repeatability studies at test conditions more representative of those used in this thesis were carried out. This was done to ensure that there was good repeatability for the time taken to reach the higher % drop at the higher temperatures. For this repeatability study, 5 mL dodecane samples were heated to 160 °C at a starting pressure of 700 kPa, and the time taken to reach a 40 % pressure drop for the maximum pressure was measured. The reason for the 10 °C lower test temperature in the repeatability study than those used in the rest of the thesis was from advice from Anton Paar, the manufacturers of the PetroOxy device, who recommended a test time of approximately 1 hour for such repeatability tests. Two PetroOxy devices were used in this thesis and repeatability testing was carried out on both with the data being presented separately. The two PetroOxy devices had the same specifications and the same testing parameters were set for both devices. The two devices will be referred to as PetroOxy1 and PetroOxy2 in the repeatability study. Twelve identical test runs were carried out on each PetroOxy, with the data for both are presented in table 4.1.

The results of the repeatability tests indicate that the two PetroOxy devices are able to produce the same spread of data but have individual internal calibration biases which means that they have different mean values. However, within the data sets for the individual PetroOxy devices good repeatability was achieved. For PetroOxy1, the repeatability was 1.86 minutes in the ASTM standard, 1.94 minutes from the IFPEN study and the standard deviation was 1.87 minutes. Similarly for PetroOxy2 the repeatability in minutes was 1.98, 2.00 and 1.86 respectively for the three measures.

Tab. 4.1: Time taken in minutes for dodecane to reach a 40% drop at 160 °C in PetroOxy.

PetroOxy1												
Test	1	2	3	4	5	6	7	8	9	10	11	12	Mean
Time / mins	49.26	51.13	50.05	46.08	46.51	46.7	44.76	45.16	46.45	46.51	48.1	47.95	47.38
PetroOxy2												
Test	1	2	3	4	5	6	7	8	9	10	11	12	Mean
Time / mins	55.6	53.51	52.71	50.78	50.63	50.16	49.11	49.66	51.56	51.05	53.91	50.38	51.58

Tab. 4.2: Uncertainty analysis of dodecane verification tests in table 4.1

PetroOxy1		
	Formula	Uncertainty in minutes
ASTM	$r = 0.0288X + 0.4965$	1.86
IFPEN	$r = 0.014X + 1.229$	1.94
Standard deviation	$r = \sqrt{\frac{\sum(x_i - \bar{x})}{n}}$	1.87
PetroOxy2		
	Formula	Uncertainty in minutes
ASTM	$r = 0.0288X + 0.4965$	1.98
IFPEN	$r = 0.014X + 1.229$	2.00
Standard deviation	$r = \sqrt{\frac{\sum(x_i - \bar{x})}{n}}$	1.86

For PetroOxy1, 3 out of 12 tests were outside the ASTM and IFPEN repeatability measure and for PetroOxy2, 2 out of 12 tests were outside the repeatability range. However, as the tests were carried out at higher temperature, and to greater pressure drops, this decrease in the repeatability is to be expected. Due to the internal calibration biases of the devices the repeatability of the individual devices cannot be applied to the other device. However, the ASTM D7545-14 standard also has reproducibility measure which give the difference between 2 device operated in different labs and by different operators. The expression for this is give by,

$$R = 0.0863X + 1.3772, \qquad (4.3)$$

where X is the mean of two tests in minutes to the nearest 0.01 minute. When this analysis is carried out, using all 24 test runs over the 2 devices, the uncertainty of the reproducibility is 5.65 minutes. Only 1 test in 24 was outside this range. As stated previously, these tests we carried out at higher temperatures and to greater pressure drops, and as such this reproducibility is particularly good.

In support of the validation study carried out using dodecane above, further tests were carried out using verification fluid purchased from Anton Paar, using the test protocol suggested [278]. This test procedure uses a 5 mL sample of the reference diesel fuel, heated to 140 °C at 700 kPa, and the time to reach a 10% drop from the maximum pressure is recorded. The test protocol has an expected time to reach a 10% pressure drop of 93 minutes with an allowed deviation of ± 9 minutes.[278] 3 repeats were carried out on each PetroOxy device

Tab. 4.3: Time taken for verification fluid in minutes to reach a 10% drop at 140 °C in both PetroOxy devices

Test	1	2	3
PetroOxy1	87.33	88.75	91.53
PetroOxy2	94.26	94.65	94.96
expected value 93 ± 9 minutes			

The uncertainty stated for the verification fluid tests is 10%. When this uncertainty is applied to the dodecane study, all test runs fall within the

repeatability. As such, the results of both of these studies indicate that the PetroOxy has good repeatability and reproducibility at the higher temperature and pressure drops being used in this thesis, and it is valid to proceed using this method. Repeat measurements will be carried out for tests unless stated otherwise for constraints of time. The PetroOxy pressure drop traces presented will originate from PetroOxy2 unless stated otherwise, as the verification fluid study showed that it had a lower deviation from the expected value, but the data from both will be used in the analysis of data trend and will be presented in the appendix.

The products formed during the oxidation of aviation fuel and hydrocarbon samples are characterised using Fourier-transform infrared spectroscopy (FTIR) and Gas chromatography mass spectrometry (GC-MS). This was used to determine the chemical functional groups present in the stressed samples and the molecular weight of the stressed samples. For the pure hydrocarbons this analysis was carried out at different stages of oxidation to analyse the progression of product formation during the mechanism. The FTIR studies were carried out using a Bruker Alpha ATR spectrometer, with the spectrometer set to absorbance mode and scans between 500-4000 cm^{-1} with a resolution of 1 cm^{-1}. The light source was a silicon nitride Mid-IR emmiter with a KBr beam splitter. The GC-MS studies were carried out at the University of Sheffield faculty of science mass spectrometry service. The Agilent 7200 Accurate Mass GC-MS Qaudrupole time of flight spectrometer with electron ionisation was used. The results were analysed using the MassHunter software to compare the molecular mass match to the NIST database. However, for both FTIR and GC-MS, due to the oxidised samples being complex mixture this analysis is only qualitative in most cases. GCxGC analysis of the fuel from the JETSCREEN project were carried out by collaborator at IFPEN.

4.2 Autoxidation of JETSCREEN fuels in the PetroOxy

It is important that the autoxidation behaviour of aviation fuel in the accelerated oxidation condition in the PetroOxy device is investigated. From these studies we will be able to study the role that an aviation fuels chemical composition has on its thermal stability and its response to the PetroOxy test.

A series of fuel blends with known chemical composition, developed as part of the Horizon 2020 JETSCREEN program (grant number 723525), were selected as a starting point for this study. The test matrix constituted 11 fuels of varying chemical composition. A group based on a Jet A1 standard fuel was provided with increasing levels of hydrotreatment to remove aromatics from the fuel in stages. Group B consists of fuels which are sythetically derived from a number of different sources with no antioxidants added post-production. These include B1, an Alcohol-to-Jet (AtJ) fuel and a hydroprocessed esters and fatty acids (HEFA) fuel, both of which have no sulfur or aromatics. The final fuel in this series was a catalytic hydrothermal conversion jet fuel (CHCJ), high in cycloalkanes, with no sulfur and an aromatic concentration of 14.6m/m%. A series of fuels with varying sulfur concentration were developed from a base fuel with an intermediate aromatics concentration, these are denoted by the prefix D. These blends were developed by IFPEN with different blended levels of mercaptans and di-tert-butyl disulfide. The test matrix can be seen in table 4.4.

Tab. 4.4: JETSCREEN fuels matrix.

JETSCREEN Fuels	
Code	Chemical description
A1	Jet A1 reference fuel, 17.2m/m% Aromatics, 300ppm Sulfur
A1.1	16.5m/m% Aromatics, <1% Naphthalenes, 100ppm Sulfur
A1.2	14.5m/m% Aromatics, <0.1% Naphthalenes, 10ppm Sulfur
A1.3	8.04m/m% Aromatics, <0.1% Naphthalenes, 10ppm Sulfur
B1	ATJ synthetic fuel, 0m/m% Aromatics, 0ppm Sulfur
B2	HEFA synthetic fuel, 0m/m% Aromatics, 0ppm Sulfur
B3	CHCJ synthetic fuel, 14.6m/m% Aromatics, 0ppm Sulfur
D1	10 ppm Sulfur, 13.3m/m% Aromatics
D2	100ppm Sulfur, 13.3m/m% Aromatics
D3	300ppm Sulfur, 13.3m/m% Aromatics
D4	100ppm Sulfur, 8m/m% Aromatics

More detail on the hydrocarbon chemical composition of the fuels is available in the GCxGC data give in figure 4.2. The di-aromatics in A1, such as Diphenylmethane, have mostly been removed to produce A1.1 though mild hydrotreatment. The di-aromatic concentration is 1.7% in A1 dropping to 1.08% in A1.1, while the mono-aromatic concentration has only dropped from 15.5% to 15.4%. More severe hydrotreatment in A1.2 has removed almost all of the di-aromatics and multi-ringed Naphthalenes, with the concentrations dropping to 0.055% and <0.1% respectively. The increased post-distillation

processing has also increased the amount of iso and cylcoalkanes present in the fuel. In the most severe hydrotreated fuel A1.3, the mono-aromatic concentration of the fuel has been dropped to 8.0% and the iso and cylco alkanes concentration has increased again, as the aromatics are being hydrogenated into alkanes. The B1-AtJ and B2-HEFA fuels have similar hydrocarbon composition, with B1-AtJ being formed of 99% iso-alkanes and the B2-HEFA having 82.3% iso-alkanes, 15.3% n-alkanes and 2.2% cycloalkanes. As such, the majority of both these fuels is iso-alkanes or n-alkanes, and should have similar responses to thermal stressing. Whereas, the B3-CHCJ is 58.5% cycloalkanes, 14.4% mono-aromatics, 17.5% n-alkanes and 9.4% iso-alkanes. This means that is has quite different chemical composition to the other two B group of fuels, and the effect this has on the rate of autoxidation is interesting to study. The D group blends, based on a blend based off a synthetic fuel, have the same hydrocarbon composition with only the sulfur concentration changing. They have 12% n-alkanes, 17.7% iso-alkanes, 56.4% cycloalkanes, as well as 13.3% aromatic concentration, of with 2.3% is mono-aromatics and 11% is di-aromatic. The D and A group of fuels have very different hydrocarbon composition, making them interesting to study, particularly with the D group of fuels having such high cycloalkane concentrations. A bar chart of the breakdown of the GCxGC data of these fuels can be seen in figure 4.2.
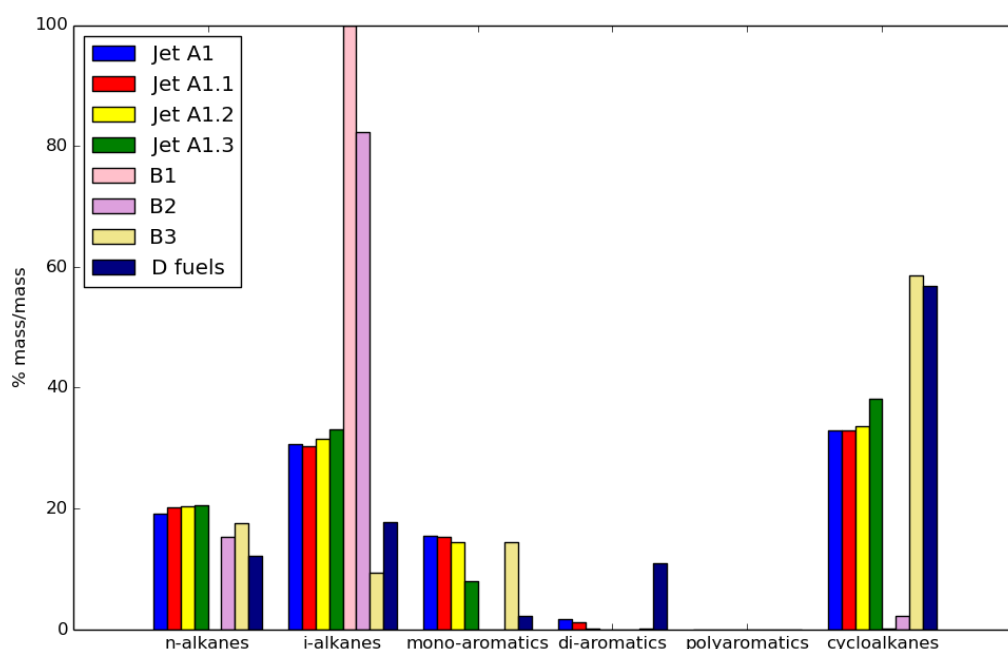
Fig. 4.2: Hydrocarbon composition breakdown from the GCxGC data for the JETSCREEN fuels.

The 11 fuels were thermally stressed in the PetroOxy, until the pressure had dropped by 90%. This pressure drop was attributed to a loss of oxygen from the head-space and it being incorporated in the oxidised fuel. The results of these tests can be seen in figure 4.3. From these tests it is obvious that a fuels chemical composition has a dramatic and complex affect on its oxidative stability.
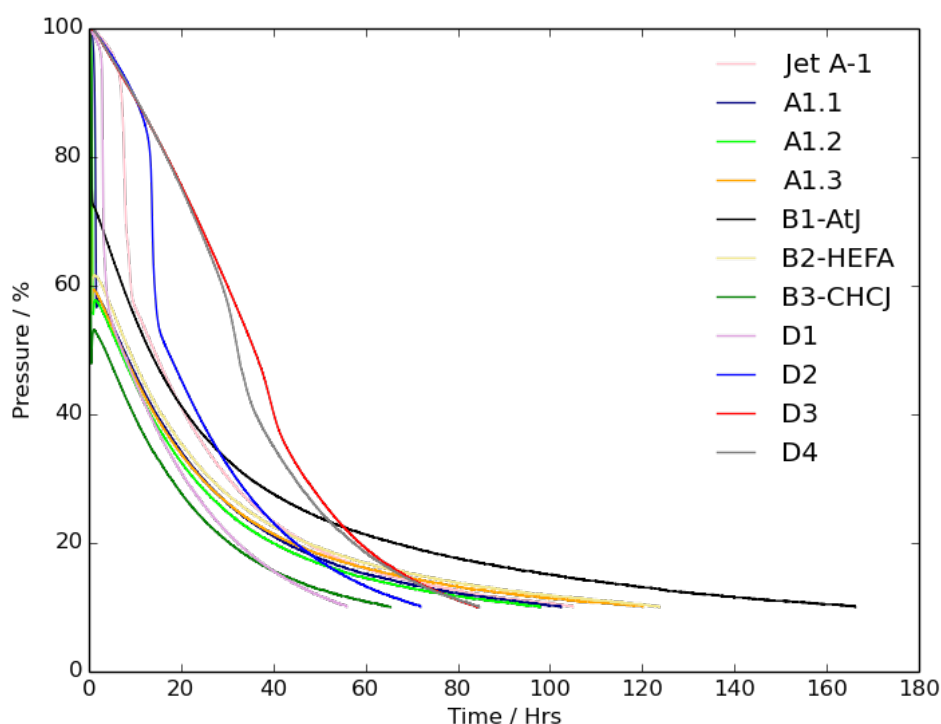
Fig. 4.3: Time taken for 90% pressure drop for all the JETSCREEN fuels at 170 °C.

In the A group of fuels, the order of the time taken to reach 90% drop was A1.3 > A1 > A1.1 > A1.2. For fuels A1-A1.2 this trend follows the concentration of aromatics in the fuels and they have been linked in slowing the rate of oxidation. However, it is clearly more complex than just increasing aromatic concentration reducing the rate of oxidation, as A1.3 which has the lowest aromatic content takes the longest time to reach a 90% drop. IFPEN reported that the induction period (time taken to reach a 10% drop) increases as the concentration of aromatics increases. This can also be seen in the data presented in 4.3 and can be seen more clearly in 4.4. The ranking of the time taken for the induction period (IP) in the A group of fuels is A1 > A1.1 > A1.2 > A1.3. This supports findings seen in the literature and suggests that different hydrocarbons behave differently in the different stage of the

oxidation mechanism. After the IP, all of the fuels undergo a rapid oxidation, with the gradient being almost vertical. This suggests that in the initial stages of oxidation reactive radical species are being formed, with the aromatics present in the fuel donating a hydrogen to radical alkanes in the fuel, thus producing a stable radical species. This is analogous to the how antioxidants work, both natural and additive packages, and is very likely to be the same hydrogen transfer reaction. When the concentration of un-reacted aromatics in the fuel has been depleted the reactive radicals formed in the fuel can then undergo propagation and chain breaking reactions leading to a rapid increase in reaction rate. Peroxides have been linked to being the cause of these chain breaking and propagation steps, with this being covered in more detail in chapter 5. Due to Jet A1 having a disproportional longer time for the induction period than A1.1 clearly the chemical structure of the aromatics in the fuel matters as well. The difference between the aromatic composition of the two fuels is the di-aromatic concentration which is 1.7% in A1 and 1.08% in A1.1. Di-aromatics have been linked to greatly reduce the rate of oxidation and deposition and as such some of the increase in induction period could be accounted for by aromatic composition.[134] The difference in sulfur concentration is also likely to have a significant affect on the rate of oxidation because, as discussed in chapter 3, they have been shown to react with peroxides.

Following the rapid oxidation step, the PetroOxy data shows a discontinuity, indicative of a change in reaction rate, usually seen when the chemical mechanism changes. This is partly caused by a lack of oxygen in the atmosphere of the PetroOxy device. Thus, there is a change in environmental conditions. However, it was observed that it is also at this point that there is a change in colour and deposition occurred for the thermally stressed fuels and hydrocarbon samples. As such, this stage of the global oxidation mechanism is likely to be caused by the oxidised products formed during the IP and rapid oxidation stages agglomerating together, due to their change in polarity, and reacting to form insoluble material. At the end of the testing deposition was observed on the surface of the PetroOxy reactor chamber. This deposit was darker and more difficult to remove for the fuels with the higher aromatic content. This supports findings in the literature that indicate that the carbonaceous deposit are found in an aromatised form with high heteroatomic concentrations.[188, 217] In the slow third stage of oxidation in the PetroOxy the aromatic oxidised products are reacting together to form the majority of the insoluble deposits on the surface. This is supportive of the SMORS mechanism proposed by Hardy
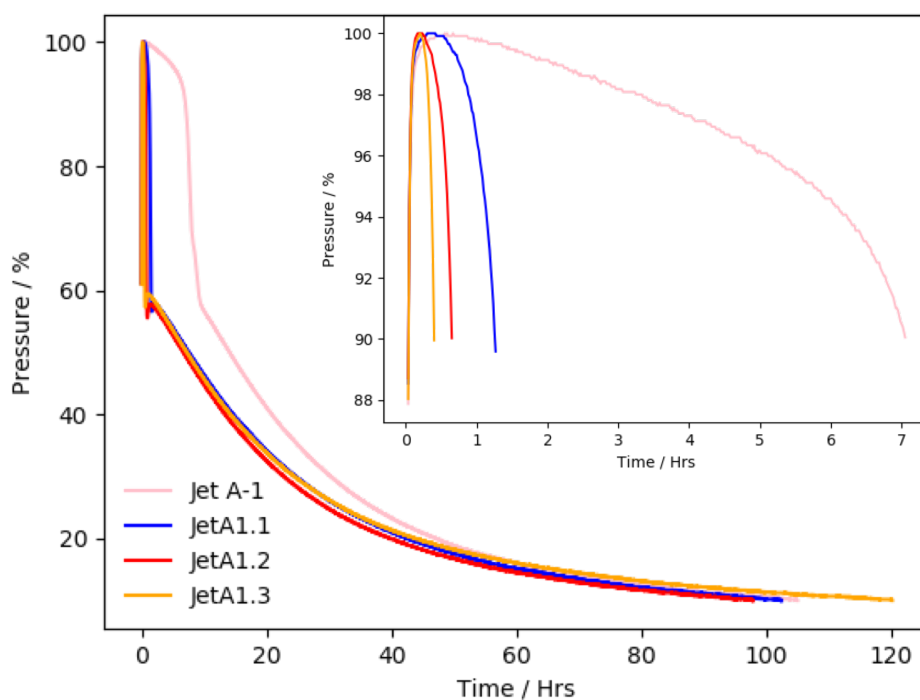
Fig. 4.4: PetroOxy plot of the 90% pressure drop for A group of fuels and to 10% drop in the insert.

and expanded by Beaver, which stated that the mechanisms proceed though electrophilic aromatic substitution and addition reactions, which can not occur in alkanes.[185, 279] Thus, the level of deposition seen in the PetroOxy test is linked to the concentration of aromatic and heteroatomic species in the fuel. An interesting artefact seen in almost all of the fuel data, is that as the mechanism switches from the rapid oxidation step to the slow agglomeration and deposition step there is an increase in the pressure, indicating that some volatile compounds are generated during the mechanism. This can be seen clearly in figure 4.5 where fuels A1.1-1.3 all demonstrate this phenomena. However, the base Jet A-1 does not, this is also observed in other Jet A-1 fuels with high aromatic and heteroatomic species concentrations. Suggesting that aromatic hydrocarbons, and heteroatomic derivatives, can oxidise and form deposits through electrophilic aromatic substitution mechanisms even in low concentrations of radicals.

Clearly the chemical composition of the non-aromatic hydrocarbon in the fuels also plays a role in the rate of oxidation. This is starkly demonstrated by the difference in the time taken to reach 90% pressure depletion for fuel D1 and
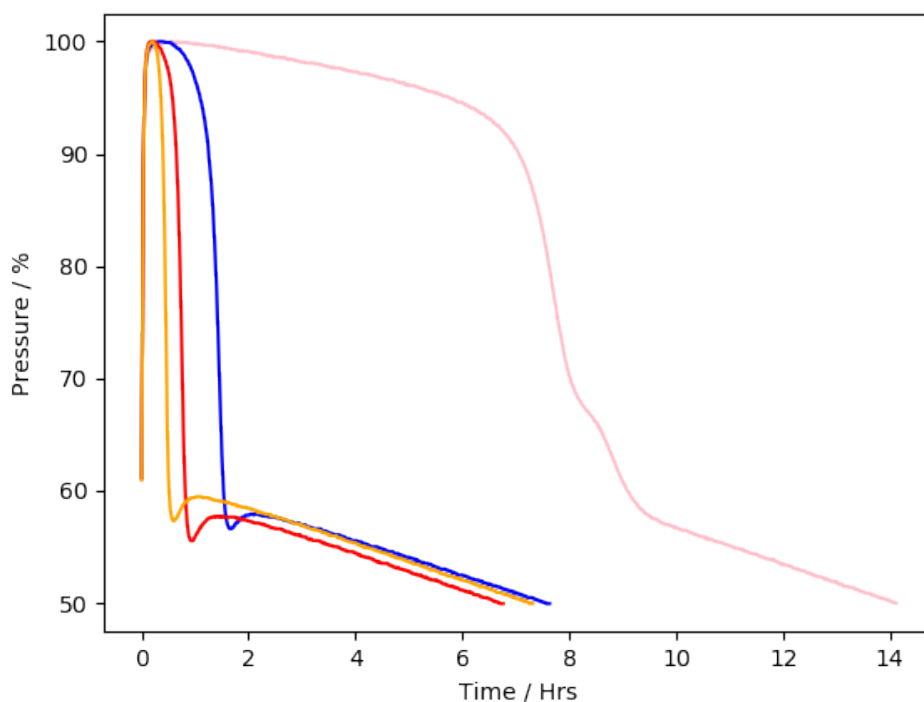
Fig. 4.5: PetroOxy plot of the 50% pressure drop for A group of fuels.

A1.2, with similar aromatic and sulfur concentrations, but very different alkane composition. D1 has the quickest oxidation, compared to A1.2 which has one of the longest, and takes almost double the length of time to reach a 90% pressure drop than D1. Whereas the time for the IP is 3 times longer for D1 compared to A1.2, 3hrs compared to 50mins, with this mostly attributed to the higher di-aromatic content in the D fuels. The major component of the hydrocarbon blend for the D fuels is cycloalkanes, compared to the A fuels, where the major component is n and iso-alkanes. This different chemical composition also leads to a dramatic difference in rate of the slow oxidation rate. This is interesting, as has been previously reported that the ratio of terminal carbons compared to C_2 carbons is the cause of this, as it is easier to abstract a hydrogen from a C_2 due to greater radical stabilisation.[138, 140] This, with the difference in aromatic composition, would provide the difference between the IP times. However, this cannot be the only cause for the observed difference in these tests, with cycloalkanes clearly having a different deposition mechanism to n and iso-alkanes. This could be caused by the aromatisation of the cycloalkanes, something which is much more difficult

for non-cyclic alkanes, with this contributing to the increased rate of deposition in the third stage of the test.

In the D group of fuels the order of the time taken to reach 90% drop was D4 = D3 > D2 > D1, with B1 which has no sulfur taking much longer to reach the 90% drop for comparison. D3 has the highest concentration of sulfur in the fuel at 300ppm. Sulfur, particularly the di-tert-butyl disulfide used in the blends, has been shown to slow the autoxidation of fuel by reacting with peroxides that form during oxidation or that are natively present in the fuel. As D4 has a third of the sulfur in the blend, and the same concentration D2 which it performs better than, the cause for them having the same thermal stability in the PetroOxy test must be more complex. D4 and D3 have different aromatic and hydrocarbon composition, with D4 not being based on the same base blend at the other D fuels, with D4 having a lower aromatic concentration. As seen in the A fuels, lower aromatic content lead to a decrease in the time taken to reach the second rapid oxidation step, but an increase in the time taken to reach a 90% drop overall. However, as D4 has a lower sulfur and aromatic concentrations it should have a shorter IP than D3 and D2. The ranking of the time for the IP in the D group of fuels is D2 = D4 = D3 > D1 with B1 having a much shorter time required to reach the 10% pressure drop. This can be seen in figure 4.6. This indicates that 100ppm of sulfur is enough to defer the start of the rapid second stage of oxidation beyond the 10% drop. For D2, which has 100ppm of sulfur, this rapid drop is observed at 15-20%. While D4, which also has 100ppm of sulfur, this change is not observed with the pressure having a sigmoidal shape. This is peculiar, as its lower aromatic and similar sulfur content to D2 should mean that it would have a similar thermal stability to that fuel. The fact that it doesn't means that the non-aromatic hydrocarbon component must being having an affect on the thermal stability. This was seen clearly earlier when the oxidation of D1 and A1.2 were compared. The third stage of the mechanism seen in the PetroOxy, where the deposition takes place, is much faster for D group of fuels than for the A group. Sulfur has been shown to be present in the deposit in the literature, with sulfur-oxygen bonds being in high concentration.[158, 188, 221] This coupled with the increased rate of oxidation and deposition indicates that the di-tert-butyl disulfide is being oxidised into sulfoxides, sulfones and sulfonic acids, which are progressively more reactive and polar leading to greater deposition. It is important to note that the deposit was also very dark, and was particularly difficult to remove, with it not being particularly soluble in the methanol or acetone. One reason for this is likely to be that the PetroOxy dish has a gold

surface, and sulfur-gold bonds are known to form readily and strongly, some that has been taken advantage of in self-assembled mono-layer.[280]
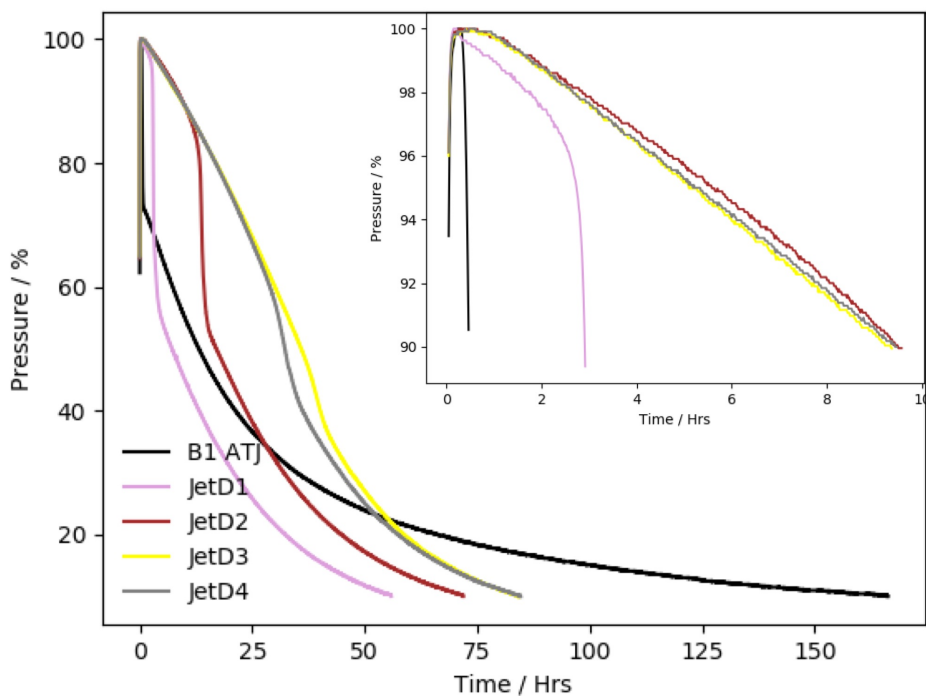
Fig. 4.6: PetroOxy plot of the 90% pressure drop for D group of fuels and to 10% drop in the insert.

The synthetic B group of fuels demonstrated very different oxidation and deposition behaviour to all of the other fuels investigated in the JETSCREEN program. The PetroOxy result for the B group of fuels the can be seen in figure 4.7. The three B groups of fuels have short IPs, with B3-CHCJ having the longest, but was still under an hour. This is surprising, as it has a high level of mono-aromatic (14.6%), but its IP is approximately ten times shorter than that of Jet A1 with slightly higher levels of aromatics. This would suggest that the nature of aromatic species effects the oxidation rate, with Jet A1 having some percentage of di-aromatics, but also that the response to increased aromatic concentration in the rate of oxidation is not linear. Fuels B1 had the longest IP of the three B groups of fuels, at 28 minutes, with B3 and B2 being closely behind at 22 and 18 minutes respectively. However, it is clear that all of the fuel oxidise quickly. The reason for the rapid IP is the lack of aromatics and natural antioxidants present in the B1 and B2 fuels which slows the IP and defers the start of the rapid oxidation step. However, fuel B3 and A1.2 have similar aromatic concentrations, and had similar IP

results in the PetroOxy test, so the difference fuels could be attributed to the difference between the non-aromatic component. The B3 fuel has a far higher cycloalkane component, and this would suggest that this results in an increase rate of oxidation, most likely a result of the ease of aromatisation.
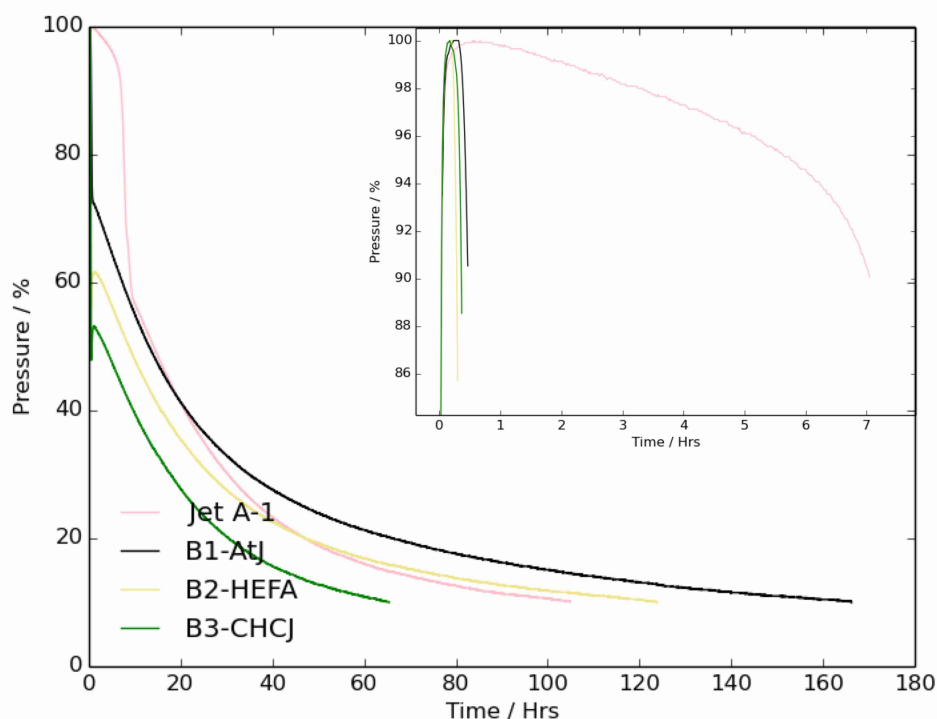
Fig. 4.7: PetroOxy plot of the 90% pressure drop for B group of fuels and to 10% drop in the insert.

The point at which the transition between the rapid radical driven stage of oxidation to the slower oxidative coupling driven stage of oxidation occurs at different levels of oxygen depletion. The point at which the change in the gradient in the curve changes as the hydrocarbon composition changes. Their is far greater variation in the point that this rate change occurs than in the other groups of fuels. This indicates that it it is linked to the variation in the composition of the non-aromatic component. The change in oxidation mechanism happens at 25% oxygen depletion for fuel B1, with it B2 demonstrating this transition at 44%, and for B3 it occurring at 53% oxygen depletion. This difference between the point of this transition for fuel B1 and all the other fuels of the JETSCREEN program is stark, with the transition occurring 15% before any other fuel tested. Fuel B1 is formed of 99% iso-alkanes, with GCxGC results showing that 75% the fuel is formed of alkanes with twelve carbons, meaning that with substantial branching they may have a high CH_3:CH_2 ratio.

The B2 fuel has a high percentage of iso-alkanes, but the GCxGC indicates that they have a broader range of molecular weights and coupled with the significant proportion of n-alkanes, means that it has a lower $CH_3:CH_2$ ratio. Fuel B3 has the highest concentration of cycloalkanes tested, with this resulting in the transition in oxidation mechanism occurring at the greatest depletion of any fuels, and indicates that this transition is linked to the $CH_3:CH_2$ ratio.

The three B group of fuels demonstrate very different oxygen consumption profiles for the slow third stage of oxidation. Fuel B1 had the slowest third stage of oxidation of all the fuels, taking approximately 170 hours to reach a 90% pressure drop, this is likely to be caused by the B1-AtJ fuel having a majority composition of iso-alkanes which are slower to oxidise than other alkanes. One reason for this could be that the high level of substitution of the alkane chains with carbon side chains places steric restraints on the oxidised iso-alkanes. This puts limits on the rates of coupling, condensation and cyclisation reactions. The B1-AtJ fuel demonstrated no deposition, and this coupled with the slow oxidation, supports the statement that the high iso-alkane composition slows coupling reactions. Thus, it cannot undergo aromatisation easily and leads to lower levels of deposition. The B2 fuel, which also had a high iso and n-alkane composition, demonstrated a similarly slow third oxidation profile. B2-HEFA took 123 hours to reach the point of 90% oxygen depletion, and also demonstrated no deposition, with light yellowy brown material present after oxidation, but which was easily removed. Thus, it was not chemically bound to the wall of the PetroOxy forming deposit. B3-CHCJ reached 90% oxygen depletion in 65 hours and the deposit formed after oxidation was a dark brown colour, more difficult to remove than the material from B2, and similar in nature to that formed by the A group of fuels. As such, this provided evidence for the oxidative coupling, electrophillic substitution and condensation reactions proposed to drive the deposition mechanisms of oxidation. As aromatic hydrocarbon, or cyclic hydrocarbons which are easily aromatised during oxidation, would be important for these reactions. The rate of oxygen consumption observed during this third stage of oxidation for fuel B3 was quickest of all the fuels tested during the JETSCREEN program. This suggests that the high cycloalkane concentration, highest for any fuel, and higher level of aromatic concentration leads to this deposit forming step being promoted by cyclic hydrocarbons.

When the fuels are thermally stressed in the PetroOxy a noticeable colour change occurs. This can be seen in figure 4.8. This colour change is linked

to the chemical change that occurs during oxidation. The fuels are clear and colourless when unstressed, meaning that they are absorbing in the the ultraviolet range, and are not interacting with the visible spectrum. When they are oxidised the fuels spectra red shifts and thus can now interacts with the visible light spectrum. The chemical changes that usually cause this is an increase in conjugation and delocalisation. This can occur through aromatisation or the formation of polar groups with resonance structures, such as the carbonyl functional group, which is found in aldehydes, ketones and acids. For this reason, it would not be expected for all of the fuels to exhibit the same colour change under thermal stressing. The fuels with high aromatic concentrations would expected to be darker as they more easily be oxidised into chemical species which appear in the visible range.
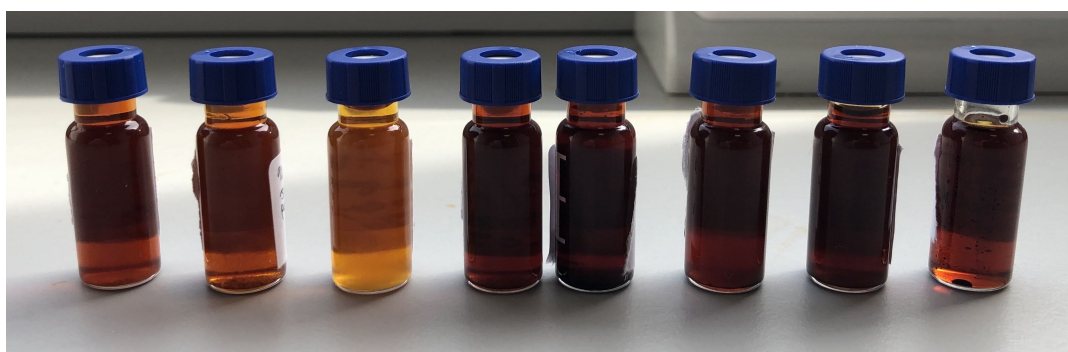
Fig. 4.8: Colour of JETCREEN fuels at 90% pressure depletion. left to right: A1.1, A1.2, A1.3, D1, D2, D3, D4 and Jet A-1. All fuels were colourless when unstressed.

This effect was observed in the A group of JETSCREEN fuels, with a increase in the aromatic concentration, resulting in darker colour changes when thermally stressed. This was more pronounced for the fuels with higher di-aromatics and multi-ringed Naphthalenes concentrations with the reference fuel Jet A1 and fuel A1.1 being noticeably darker than A1.2 and A1.3. When the D group of fuel were oxidised the same effect was observed, with these fuels being particularly dark in colour when thermally stressed. There was less discernible difference between the the colour of the D fuels when thermally stressed. This could be a results of all of these fuels having moderately high aromatic concentrations. However, they were darker than the low sulfur A group of fuels, so clearly sulfur has an effect on the colour change and thereby the oxidation. A reason for this is that the oxidation products of the sulfur species in the fuel, the sulfoxides, sulfones and sulfonic acid, can then be incorporated into aromatic oxidation products and these species have particularly strong absorbance in the visible region. The B group of fuels

demonstrated the striking affect that increased aromatic concentration in the fuel has on the colour change that occurs during oxidation. Fuels B1 and B2, with no aromatic component, were clear straw to yellow in colour after thermal stressing. However, the B3 fuel with 14.6% aromatic component, was a darker brown colour which was more similar to the colour of the higher aromatic concentration A group of fuels.

The thermally stressed JETSCREEN fuel samples were tested and characterised using FTIR. The results can be seen in figure 4.9 for the A group of fuels, figure 4.10 for the D group of fuels and figure 4.11 for the B group of fuels.
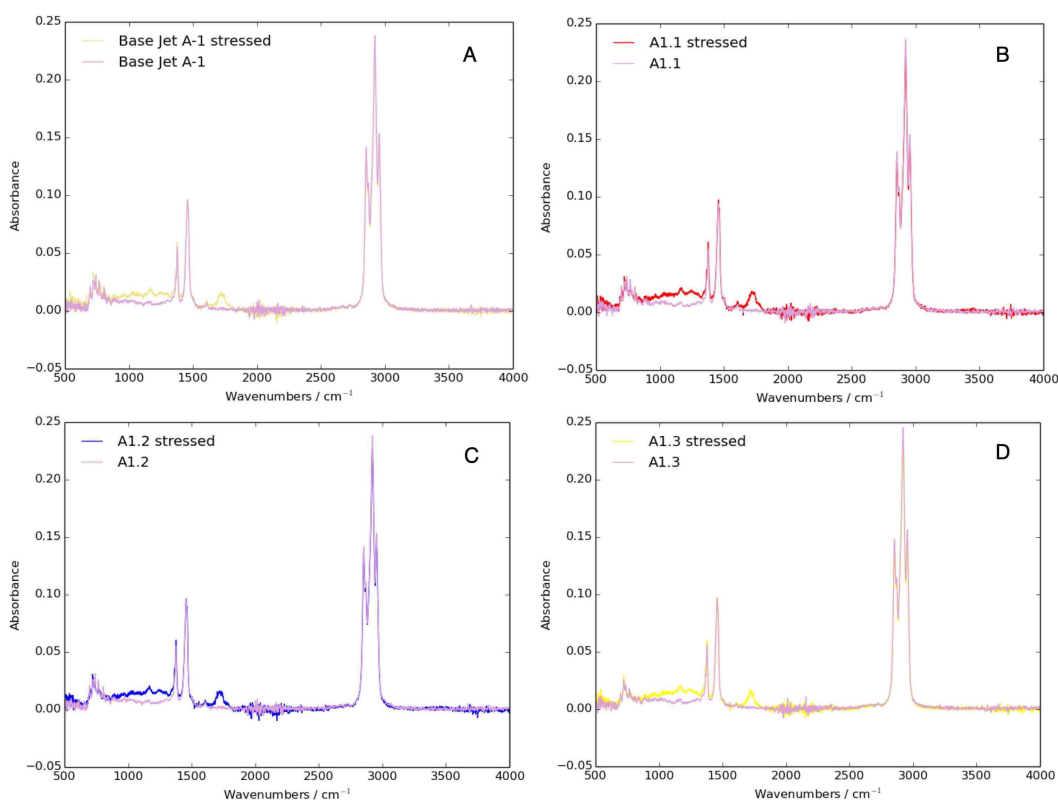
Fig. 4.9: Infrared absorbance spectra for the thermally stressed and unstressed JETSCREEN A group of fuels. Figure A is for the reference Jet-A1, B is fuel A1.1, C is A1.2 and D is fuel A1.3.

If we focus on the A group of fuels, the hydrocarbon C-H and C-C stretching and bending peaks are clearly visible in the spectra of the unstressed and stressed fuels at 1350-1500 and 2750-3000 cm^{-1}. There is no noticeable change in the intensity of the peaks as the fuels are oxidised. This is to be expected, as while the chemical composition of the fuel is changing through the oxidation process, the bulk of the fuel sample is still hydrocarbons. Compound-

ing this, is that a proportion of the oxidised have ended up in the insoluble deposits on the surface of the PetroOxy reactor. The most obvious change to occur during the oxidation is that there is a growth of a carbonyl peak at 1750 cm⁻¹. This indicates that aldehydes, ketones and carboxylic acids or the ester condensation products are being formed during oxidation. The only effect that the changing aromatic concentration seems to have, is that at the aromatic concentration increases, the number of peaks in the fingerprint region below 1000 cm⁻¹ increases. However, this change is minimal as the aromatic concentrations in the fuel is still a small compoent of the fuel.
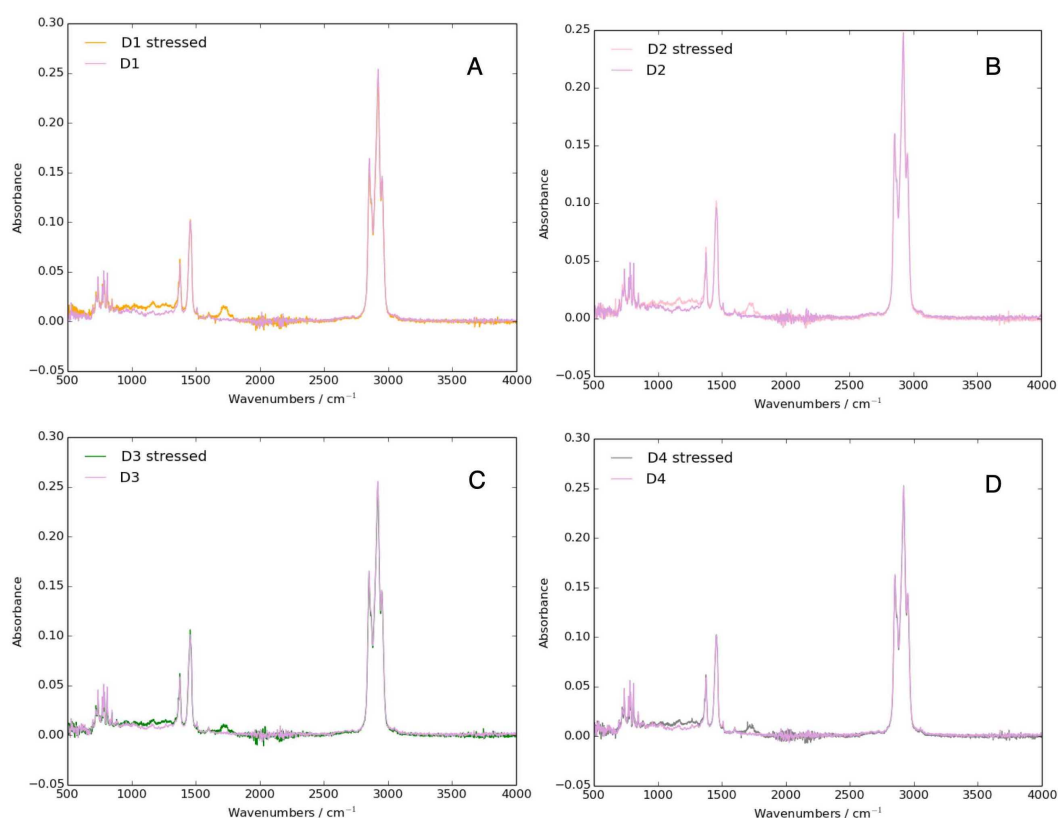
Fig. 4.10: Infrared absorbance spectra for the thermally stressed and unstressed JETSCREEN D group of fuels. Figure A is for Fuel D1, B is fuel D2, C is D3 and D is fuel D4.

The FTIR spectra for the D group of fuel, seen in figure 4.10, demonstrate similar results. The C-H and C-C stretching and bending peaks are at 1350-1500 and 2750-3000 cm⁻¹, with again there being no noticeable change in intensities of the peaks as the fuels are oxidised. There also a growth of a carbonyl stretch at 1750 cm⁻¹ as the fuel is oxidised. Interestingly, for fuel D3 which has the highest concentration of sulfur, this peak has a lower intensity. This could be caused by a couple of complementary processes. The first could be

that sulfur species in the fuel preferentially reacting with the oxidised products, particularly the peroxides formed, limiting the formation of oxygenated species with carbonyl groups. However, the oxidised sulfur species can then react with the oxygenated products, in a mechanism analogoues to one suggested by Zabarnick *et al* to form oxidised products with limited carbonyl bonds present. The sulfur-oxygen bonds absorb infrared at around 1350 cm^{-1}, which overlaps with where the C-H scissoring and rocking, and as such are not visible in the spectra so this hypothesis cannot be confirmed using the FTIR spectra. The D group of fuels have sharper definition in the fingerprint region with this most likely being the result of synthetic fuel they are derive from being chemically purer than the hydrotreated A group of fuels. The carbonyl peak at 1750 cm^{-1} indicates that aldehydes, ketones, carboxylic acids and ester are also formed during the oxidation of the D group of fuels.

The differences between the hydrocarbon composition of the B group of fuels is very clear from the FTIR spectra, which can be seen in figure 4.11. The aromatic species clearly present in B3-CHCJ around the 750 cm^{-1}, which is indicative of the out-of-the-plane bending of aromatic rings C-H bond. A sharp and pronounced carbonyl stretch is also present at 1750 cm^{-1} in the oxidised fuel, suggesting that the mono-aromatic component of the fuel can readily react to form aldehydes, ketones, acids and even the ester condensation products. It can be seen in the FTIR spectra of the B1 and B2 fuels that they have obvious variations in the hydrocarbon composition of each other. The B1 spectra has gem-dimethyl C-H stretches at 1350-1380 cm^{-1}, which suggests that the iso-alkanes have double subsitutions on some of the carbons, resulting even higher CH_3:CH_2 ratio. The C-H peaks at 1350-1500 and 2750-3000 cm^{-1} also have the inverse intensities to the other fuels investigated, with the peak at higher wavenumber in each set being more intense that the lower one. As this is a measure of bond strength, and the CH_3 bonds would be stronger than the CH_2 due to the lack of induction, this again suggests a high CH_3:CH_2 ratio. As fuel B2, while also having a high iso-alkanes concentration it has a broader range of molecular weights and much less substitution, this phenomena is not observed in the FTIR spectra. The spectra of the oxidised samples of both B1 and B2 fuels have a carbonyl stretches around 1750 cm^{-1}. However, they are less intense than for B3, and B1 is particularly unpronounced. This suggests that the assertion made previously, that the high iso-alkane component in this fuel, inhibits the oxidative coupling and condensation reactions. It also suggests that the iso-alkanes react slower than the n-alkanes because of this

steric inhibition, and this limits the formation of aldehyde, ketone and acid products. Hence, there is limited colour change and no deposition.
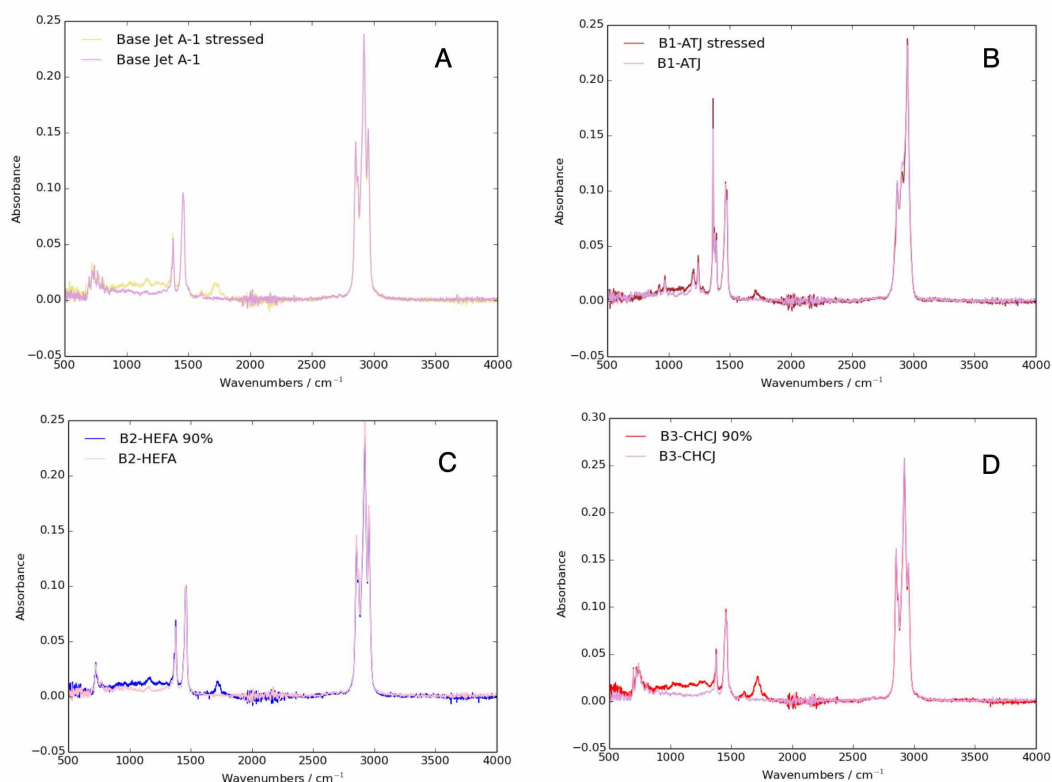
Fig. 4.11: Infrared absorbance spectra for the thermally stressed and unstressed B group of fuels compared to the reference Jet A1. Figure A is for Fuel Jet A1, B is fuel B1, C is B2 and D is fuel B3.

The GCMS trace for the JETSCREEN fuels can be seen in figure 4.12 for the A group of fuels, figure 4.13 for the D group of fuels, and figure 4.14 for the B group of fuels.

If we focus on the A group of fuels first, they all have very similar GCMS traces, with no notable difference between them. This is to be expected, with the bulk hydrocarbon composition being similar for all the A group of fuels, as seen by the GCxGC breakdown of the hydrocarbon speciation in figure 4.2. It is difficult to analysis the GCMS data in detail, and get chemical speciation of the oxidised products, due to the high number of chemically distinct chemical species present in the fuel. This means that comparing mass spectra to the NIST database give very poor agreement. However, it is clear that the main peak bands associated with the hydrocarbon components are present at 4, 7.5, 10, 12, 14, 15, 16 and 17 minutes. The cluster of peaks around this main band are oxidised products, with there being minimal

peaks at longer retention times, indicating that no polymeric species were in the thermally stressed liquid samples. However, these polymeric oxidative coupling, electrophillic substitution and condensation product are more likely to be found in the solid deposit which has not been analysed. Some classes of chemical species which were detectable in the GCMS results of all of the fuels tested were alcohols and anhydride acids. Aldehydes, ketones, carboxylic acids and esters were not found, but would need to have been present in the oxidation mechanism at some point to form the anhydride acids detected in the GCMS.
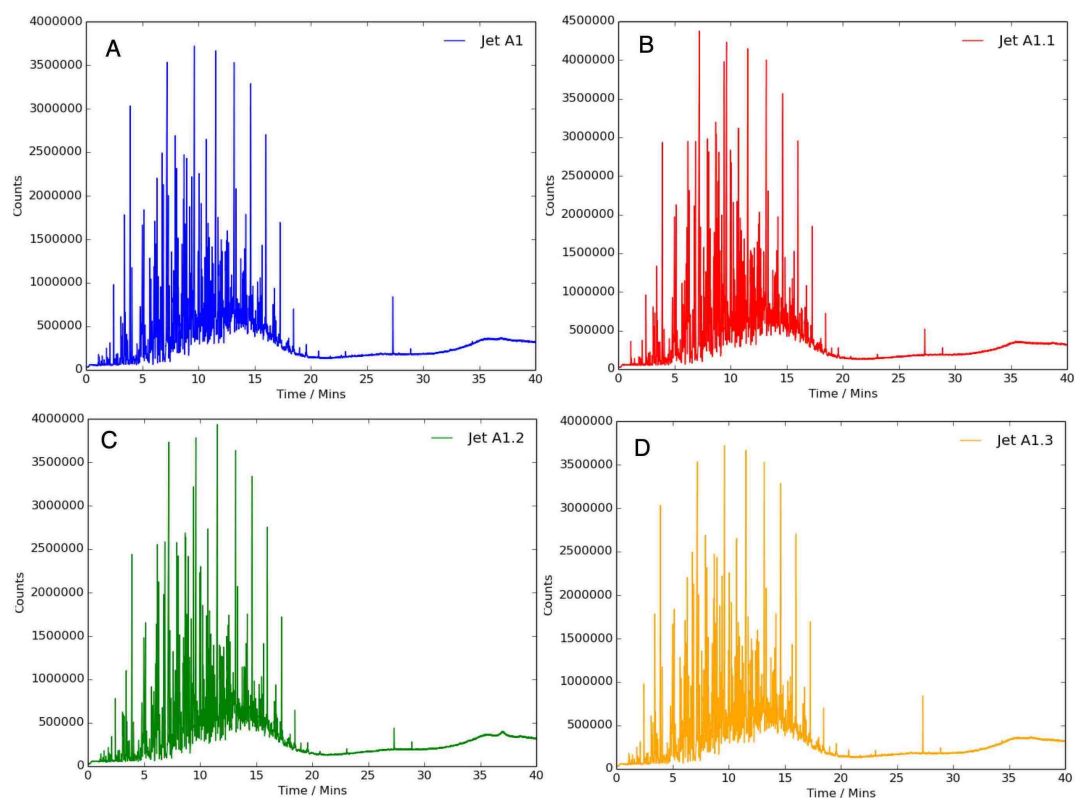
Fig. 4.12: GCMS trace for the thermally stressed A group of JETSCREEN fuels. Figure A is for the reference Jet-A1, B is fuel A1.1, C is A1.2 and D is fuel A1.3.

The D group of fuels, seen in figure 4.13, also have similar trace to each other. However, they have very different GCMS traces to the A group of fuels, with all of them having far more clustered peaks. Again this is to be expected, as they have the same hydrocarbon composition, with only D4 having a slightly lower concentration of aromatics. The GCMS traces suggest that the hydrocarbons present in the D group of fuel all have similar molecular weight. This is confirmed by the GCxGC results for the un-oxidised fuel, which show that 51% of the fuel consists og cycloalkanes with in the molecular weight range

of 12-15 carbons of size. The main peaks at 9, 13, 15, 16 and 17.5 minutes are likely to be caused by these cycloalkanes and they oxidised products are clustered around these peaks. However, agian more indepth analysis of the GCMS results is limited by the large number of chemical species in the traces, and that significant levels of deposition means most of the oxidised products at 90% depletion will not be present in the liquid samples.
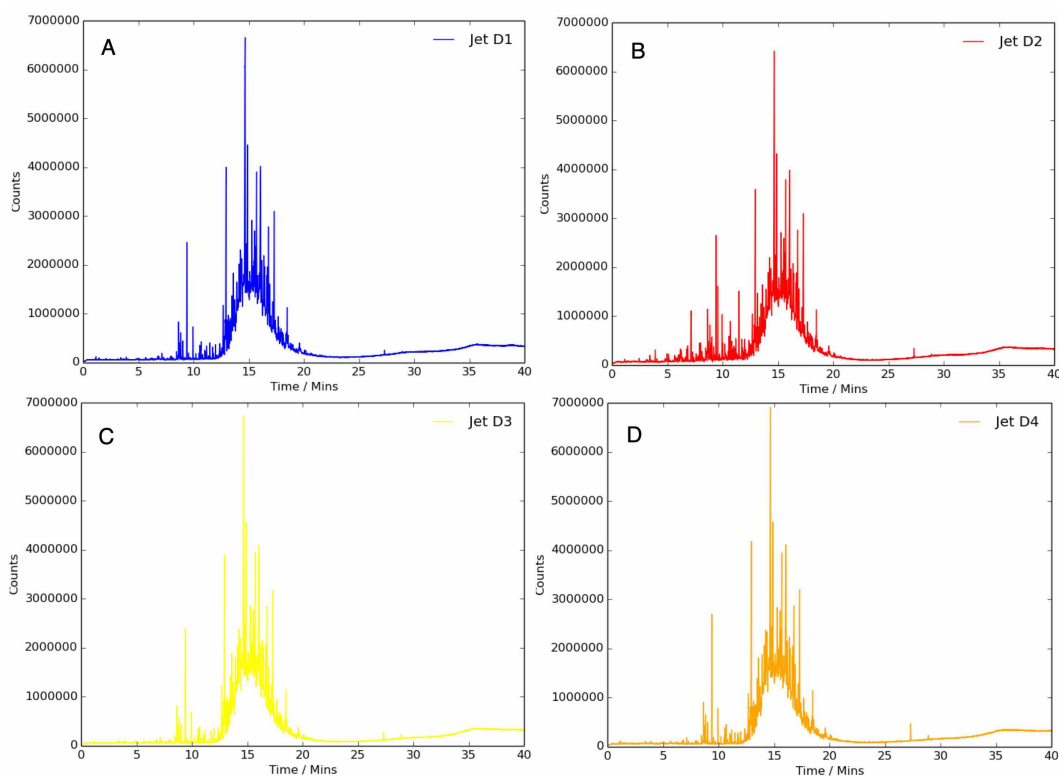
Fig. 4.13: GCMS trace for the thermally stressed D group of JETSCREEN fuels. Figure A is for Fuel D1, B is fuel D2, C is D3 and D is fuel D4.

The B group of fuels were derived from different production methods, with this being reflected in the results of the GCMS traces relative to each other, seen in figure 4.14. The GCMS trace of the oxidised B1-AtJ demonstrated that the hydrocarbon composition is very homogeneous, with the GCxGC results showing that 75% has a molecular weight of 12 carbons, and 16.5% has a molecular weight of 16 carbons. The trace also shows, coupled with the lack of deposition in this fuel, that the oxidised products are present in the sample with polymeric products clearly present above 20 minutes retention time. B2 and B3 do not have these polymeric products present their traces. The trace for B2 and B3 also demonstrate that both fuels are less homogeneous than B1, with the level of chemical noise as a result of this, potentially reducing the ability to observe the polymeric products. Fuel B2 is particularly non-

homogeneous. Fuel B3 has more clustered peaks, with more definition in the trace, with the GCxGC data indicating that 54.7% of the B3 fuel consists of cycloalkanes with molecular weights in the range of 10-14 carbons. However, even the more chemically pure B group of fuels were composed of too many chemical species for the oxidised samples to be analysed using GCMS.
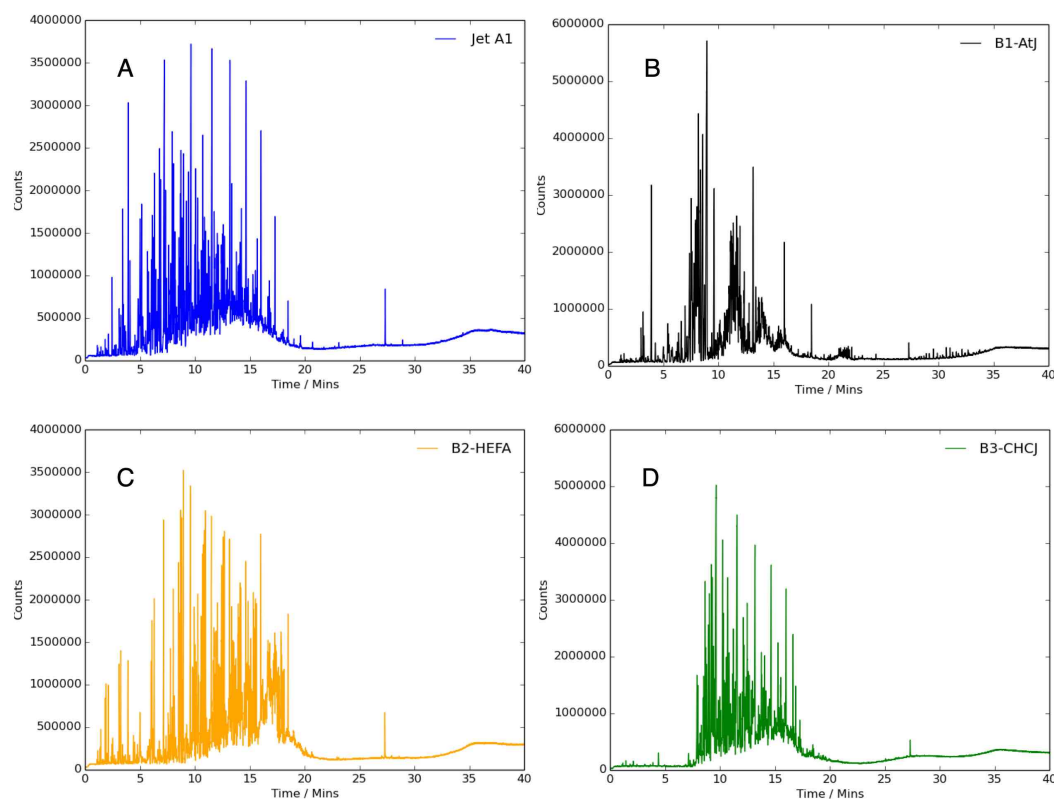
Fig. 4.14: GCMS trace for the thermally stressed B group of fuels compared to the reference Jet A1. Figure A is for Fuel Jet A1, B is fuel B1, C is B2 and D is fuel B3.

The study on the JETSCREEN fuels highlights the importance of understanding the role that a fuels chemistry has on it thermal stability. Particularly the effect that a fuel's hydrocarbon composition has on this phenomena, as fuel's with very different compositions, demonstrated quantitatively different thermal stability in the PetroOxy device. A number of conclusions can be drawn from the investigation into the autoxidation of aviation fuels using the PetroOxy. There is a general trend to the data for all tests with higher aromatic and sulfur concentrations resulting in greater levels of deposit formation. The JETSCREEN fuels also all demonstrated distinct regions of oxidation.

The first stage of oxidation in the PetroOxy is the induction period, where oxygen is consumed slowly, with the length and extent of the percentage drop

associated with this oxidation stage varying with the chemical composition of the fuel. However, for all fuels tested this stage had concluded by the point 10% of the oxygen had been consumed. Increasing the concentration of aromatic species in the fuel, had the effect of increasing the length of this induction period, which is in agreement with evidence in the literature.[140, 281]

The second stage of oxidation, which happens between 5% and 60% dependent on the chemical composition of the fuel, is a rapid consumption of oxygen with the gradient of the curve almost being vertical in some cases. This signifies that the reaction is proceeding through a radical chain mechanism where the primary oxidation products are formed. The colour of the fuel at this stage is usually dependent of the chemical composition, with those with high aromatic concentration starting to change colour, with this likely caused by the aromatic species in the fuel being preferentially oxidised. Not all fuels had this rapid oxidation stage, or demonstrated it to a much lesser extent, with fuels D3 and D4 having a more sigmoidal shape to the rate of oxygen consumption in the PetroOxy. This is most probably caused by their more complex chemical compositions, with high sulfur and di-aromatic concentrations, as well as high cycloalkane content. This behaviour can also be seen in other aviation fuels with unknown chemical composition tested in the PetroOxy, with the results being presented in the appendix.

The final stage of oxidation in the PetroOxy device is characterised by a slow consumption of oxygen. At this point the colour of all fuel samples has changes, the viscosity of the samples has changed, and deposition occurs for most fuels. The only fuels not to form deposit at this stage was the synthetic B1 and B2 fuel which had no aromatic or sulfur species present in it. The fuel B2 formed yellow silt at 90% oxygen consumption. During this final stage of oxidation, the rate of oxygen depletion varied for each fuel, and is clearly linked to the chemical composition of the fuels. From the literature, the mechanisms involved in this stage of oxidation are indicated to be the agglomeration and oxidative coupling reactions presented in the SMORS mechanism.[182–185] Higher aromatic concentrations in the fuel leads to an increase in the rate of this oxidative coupling mechanism, and in conventional fuel with high concentrations of polar and aromatic species, the radical and oxidative coupling mechanisms can happen concurrently.

There is a small pressure increase present in some of the fuels tested, when oxidation mechanism transitions from the rapid radical stage to the slow oxidative coupling stage, which can be seen in figure 4.5. This is not present in D group of fuels or the reference Jet A1 so clearly the chemical composition, particularly the concentration of sulfur and polar species, affects whether this linking step happens. It could be argued that the induction period is just the initiation of the radical chain reaction, seen in the rapid second stage of oxidation, and that they are driven by the same mechanism. Thus, the autoxidation of hydrocarbons in the PetroOxy can be simplified to two steps, characterised by the mechanism which drives them. A rapid first stage, driven by radical chain reactions, and a slower second stage driven by oxidative coupling reactions of the products formed in the first stage. Obviously, these reactions do not happen separately from each other, with both occurring at the same time to some extent. However, the observed rate of oxygen consumption in the PetroOxy can be attributed to the dominant reaction at that stage, caused by the relative rates and the concentration of oxygen and oxidised products. For example, as the oxidised hydrocarbon products are formed and the concentration of oxygen is depleted, it would be expect for the oxygen to react with the already oxidised products as they will be more easily oxidised further.

From the PetroOxy traces and the analysis of the the thermally stressed fuels, it is clear that the chemical composition of a fuel affects its thermal stability greatly, and that the hydrocarbon component is just as important for determining this property. However, it is also clear that even simple, chemically pure synthetic fuels, are too complex to understand how the hydrocarbon composition of these fuel affects the autoxidation behaviour from the outset. This is particularly true of the analysis of the products formed during the oxidation process. As such, we need to take a step back, and investigate hydrocarbon building blocks separately and in blends to gain a more fundamental understanding of the autoxidation process. The rest of this thesis will test pure hydrocarbons and their blends to understand their response to oxidation.

4.3 Autoxidation of hydrocarbons in the PetroOxy

To start this study, a half way between a chemically pure n-alkane and a representative synthetic fuel, BannerSol was oxidised in the PetroOxy device.

BannerSol is an industrial solvent, constructed from 5 n-alkane, with chain length C_{10}-C_{14}. These chain lengths would put the solvent in the lighter end of the jet fuel range, but it is representative of the n-alkanes present in aviation fuel. The PetroOxy trace can be seen in figure 4.15 and the FTIR spectra and GCMS trace for the thermally stressed BannerSol in figures 4.16 and 4.17 respectively. The PetroOxy results indicate that BannerSol has qualitatively the same autoxidation behaviour as the synthetic fuel, B1-AtJ-SPK, but reached 90% oxygen depletion in half the time. The reason for this differnece is caused by the BannerSol consisting of n-alkanes rather than iso-alkanes. As can be seen, this causes the transition between the rapid oxidation radical oxidation step and the slower oxidative coupling step to occur at 46% oxygen consumption, compared to B1 where this point happens at 25% depletion. Similar to the B1 fuel, the BannerSol has a short induction period, followed by a rapid radical oxidation step and a slow oxidative coupling step below 40% oxygen depletion, connected by a this pressure increase at the transition. The D group of fuels are also synthetic fuel blends, but with higher aromatic and sulfur concentrations, which affects the thermal stability. BannerSol resulted in minimal insoluble material to form instead, it formed a silt similar to the silt that formed during the oxidation of B2.
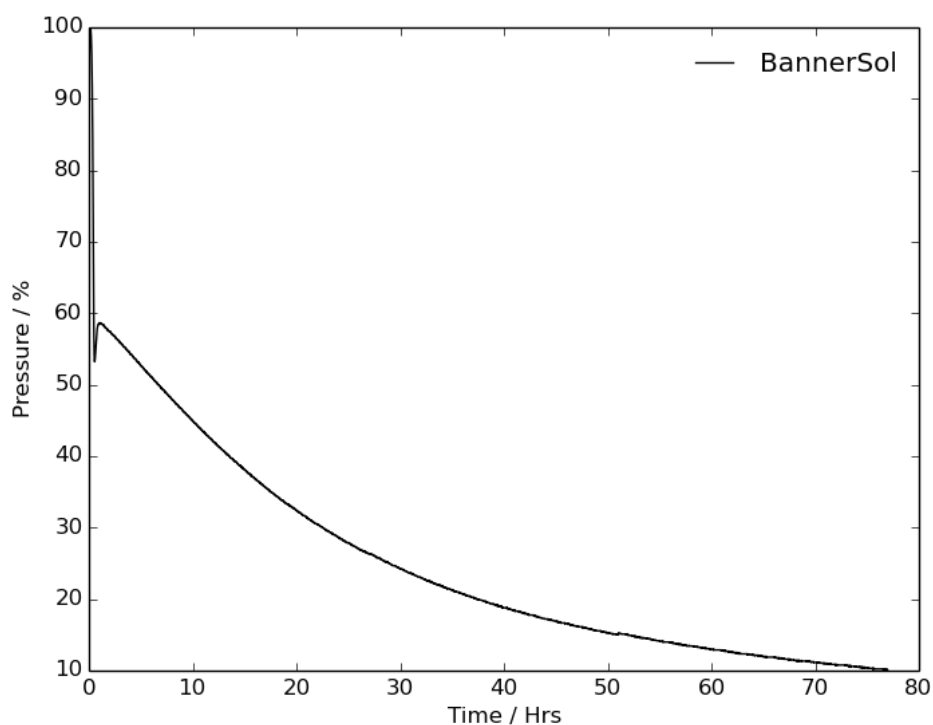
Fig. 4.15: PetroOxy plot of the 90% pressure drop for BannerSol.

The infrared spectra for the BannerSol thermally stressed to a 90% oxygen depletion can be seen in figure 4.16. The finger print region below 1000 cm^{-1} is much cleaner than that for the fuels, with a single peak at $\sim$ 750 cm^{-1}, which is the absorbance for the C-H bend in mono and disubstituted alkanes.[282] Because BannerSol is constructed from five n-alkane building blocks it is to be expected that a single sharp peak would appear in this region. As with the aviation fuels the C-H and C-C stretching and bending peaks are clearly present at 1350-1500 and 2750-3000 cm^{-1}. The thermally stressed BannerSol also has multiple overlapping carbonyl stretch around 1750 cm^{-1}. This would suggest that ketones and esters are present, and from the previous fuel studies, that anhydride acids could also be present in the thermally stressed sample. There is no O-H stretch above 3000 cm^{-1}, which means that if alcohols and carboxylic acids are formed during oxidation, they have all been consumed by 90% oxygen depletion in condensation reactions.
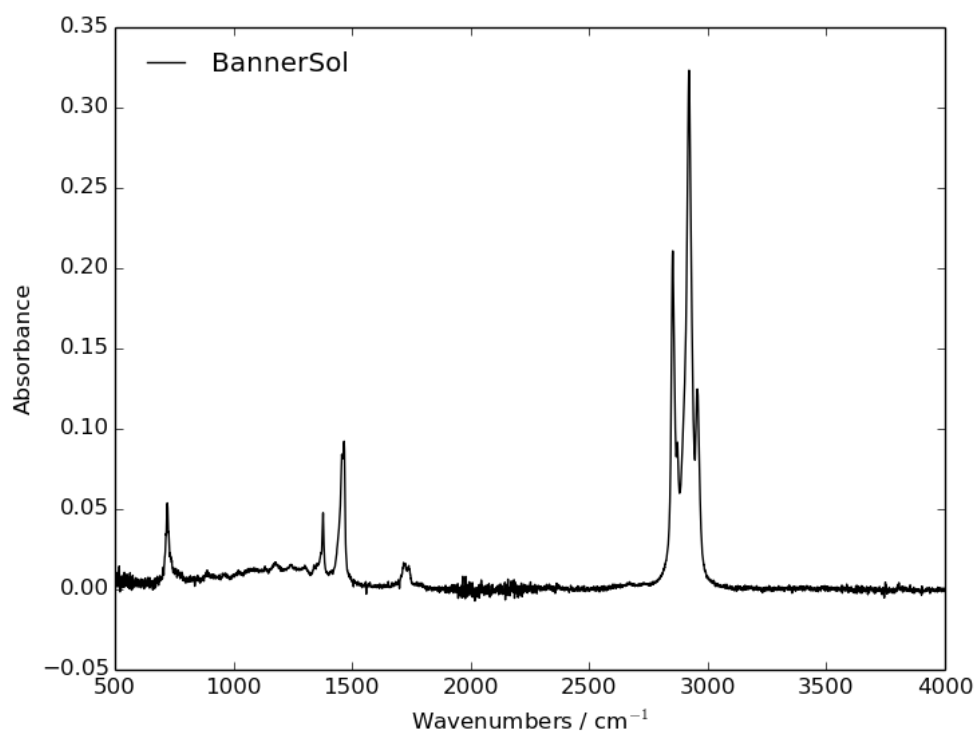
Fig. 4.16: FTIR for the thermally stressed BannerSol at 90% pressure drop.

The GCMS trace for the thermally stressed BannerSol, seen in figure 4.17, and due to its simplicity it give far more information than those for the JETSCREEN fuels. The five hydrocarbons that form the solvent can clearly be seen in the

five most intense peaks between minute 9 and 18. Numerous less intense peaks can be seen in the trace, with these being the oxidised products of n-alkanes, with alcohols, ketones, acids and anhydride acids present in the sample. The presence of ketones and anhydride acids is consistent with the Infrared analysis, but if alcohols and acids were in the fuel samples an O-H stretch above 3000 cm^{-1} would be expected. A reason for this could be that the GCMS trace is still complex and the comparison to the NIST database is poor. A significant number of peaks at higher molecular weight, above 20 minutes retention time, are also present. These would be a result of oxidative coupling and condensation reactions, with ester being one of the products, resulting in the consumption of the alcohols and acids in the fuel. As such there is some inconsistencies between analysis methods.
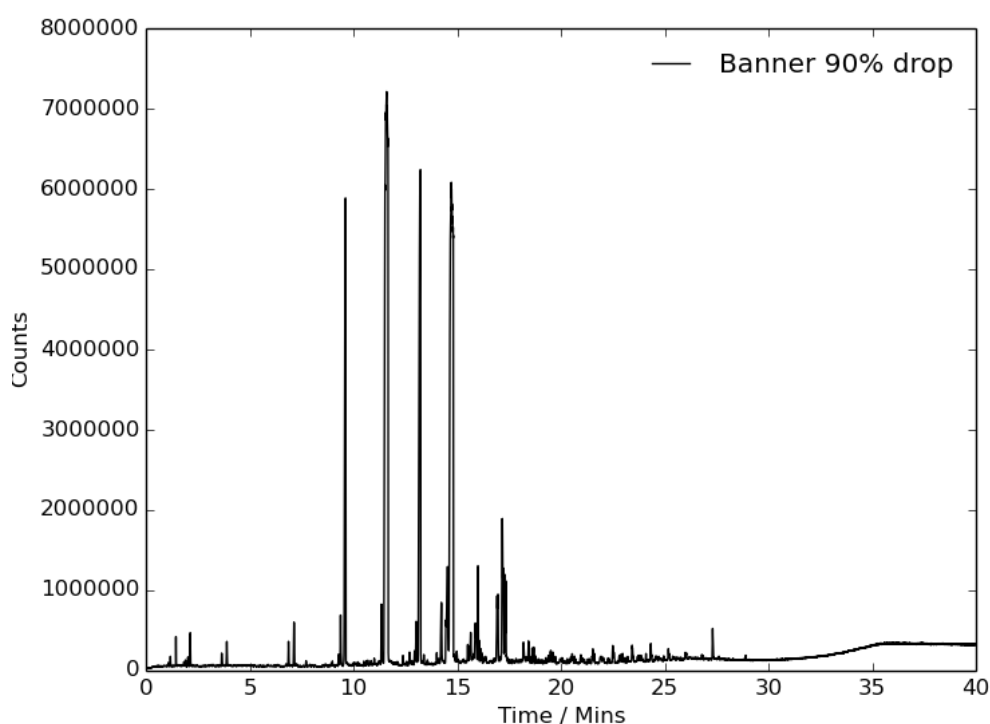
Fig. 4.17: GCMS for the thermally stressed BannerSol at 90% pressure drop.

4.3.1 Dodecane and n-alkanes

Multi-component industrial solvents, such as BannerSol, are still too complex to investigate and fully understand in this manner. Their use also limits our ability to build models of individual hydrocarbon components chemistry from

first principles. To start this study a number of n-alkanes were oxidised in the PetroOxy, with the samples heated to 170 °C at a starting pressure of 700 kPa, and the time taken to reach a 40% oxygen depletion measured.

The chain-length of the the n-alkanes was altered, in the range of C_7-C_{16}, during this test. An attempt was made to test hexane (C_6), but the pressure in the system when the sample was heated went above the safe limit of the device, and the test stopped. This was due to the hexane vaporising at this temperature and pressure. This effect was also seen in other light n-alkanes, seen in figure 4.18, with the effect being significant for hydrocarbons with chain-lengths below C_9.
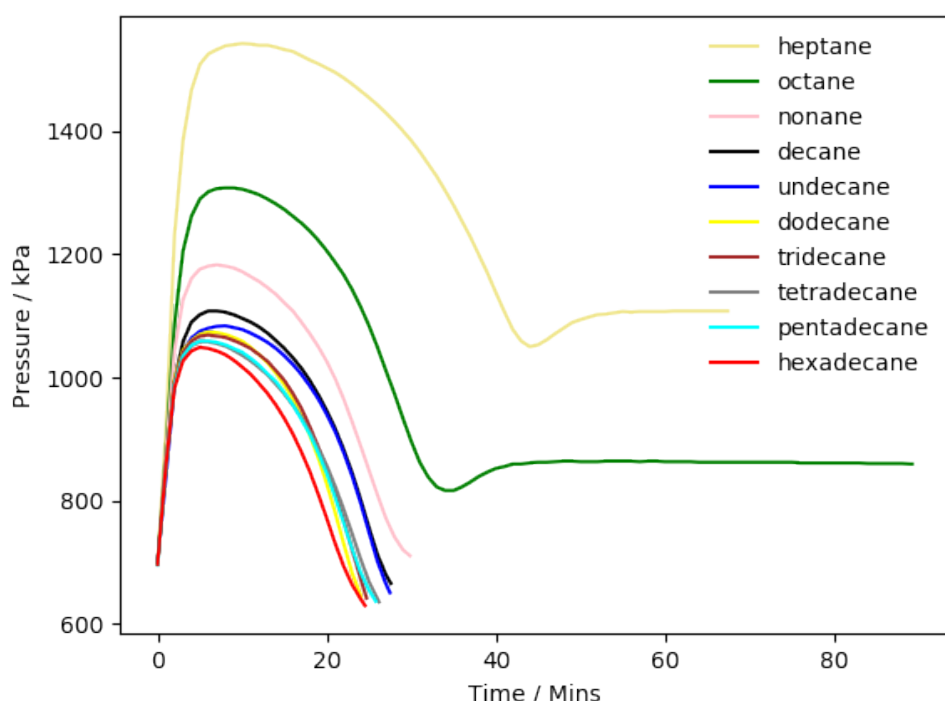
Fig. 4.18: PetroOxy plot of the time taken for n-alkanes of varying chain lengths to reach a 40% drop in kPa.

If the PetroOxy data is re-plotted using time versus the pressure as a percentage of the highest point of pressure in the test, it can also be seen that heptane and octane did not reach 40% depletion, before the tests was stopped. Instead the hydrocarbons had started the slow second stage of oxidation characterised by oxidative coupling and condensation reactions. This data can be seen in figure 4.19. This suggests that the length of the induction period is linked to the length of the hydrocarbon chain, which has

already been presented in the literature, but that the time taken for the second radical oxidation step is also affected by the chain length.[138, 140] This would help to explain the results seen for the oxidation of B1, with the transition to the slow mechanism occurs at 25% depletion, caused by the high $CH_3:CH_2$ ratio. This observation could also be caused by the carbon chain reaching an oxidative saturation, or that the shorter chain-length can promote cyclisation reactions, that are slower for larger n-alkanes.
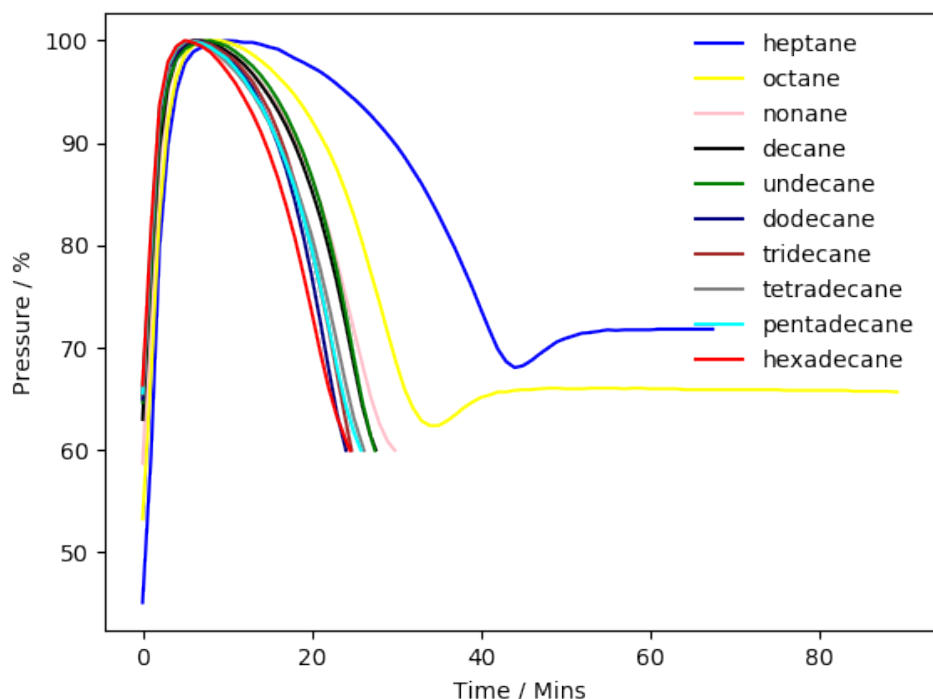
Fig. 4.19: PetroOxy plot of the time taken for n-alkanes of varying chain lengths to reach a 40% drop as a percentage of the total pressure.

Heptane and octane will only be present in aviation fuel is small quantities, as they are out of the distillation range for conventional fuels, and are unlikely to be included in the blend for synthetic fuels due to their poor physical properties for aviation. As such, if these lighter hydrocarbons are excluded from the PetroOxy trace in figure 4.20, we can see the affect of chain length on the oxidative stability in the jet range. The time taken to reach 40% oxygen depletion for all of the n-alkane tested is between 25 and 30 minutes. The order of the time for the n-alkane to reach 40% oxygen depletion was nonane > decane > undecane > tetradecane > pentadecane > tridecane > hexadecane > dodecane. A trend of the shorter the chain-length the slower the rate of oxidation emerges from this data. Octane and heptane also follow this trend.

However, at chain-lengths above C_{12} the time take begins to plateau, and the literature indicates that at longer chain lengths this plateau is reached.[138]
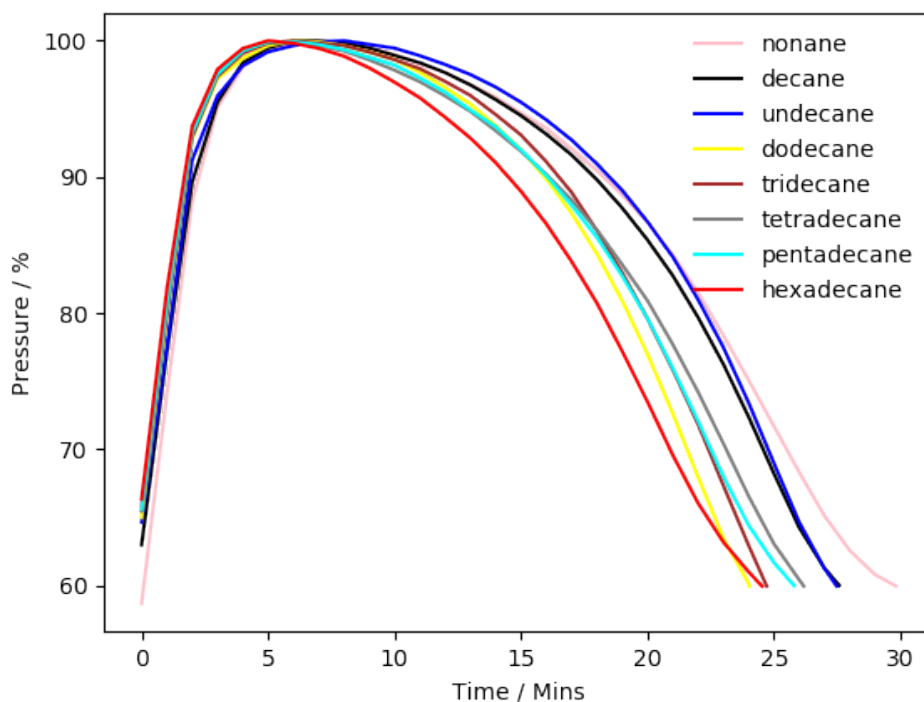
Fig. 4.20: PetroOxy plot of the time taken for n-alkanes Nonane to Hexadecane to reach a 40% drop.

To study the oxidation of the individual hydrocarbon building block of fuel in more detail and depth, dodecane was chosen as representative of the n-alkane component in aviation fuel, as it in the middle of the jet range and was available for reasonable cost from suppliers. Iso-alkane were not investigated in this study, due to the increased cost involved in obtained isomerically pure compounds, and that previous research has shown that the properties of alkanes can be estimated from the ratio of terminal and middle carbons.[139] Dodecane was thermally stressed in the PetroOxy at 170 °C to a range of oxygen depletions with the samples collected and analysed using FTIR and GCMS.

The PetroOxy trace for dodecane, oxidised to a 90% oxygen depletion, can be seen in figure 4.21. The induction period for dodecane at 170 °C is 16.3 minutes, with the rapid radical oxidation step being completed by 30 minutes and the transition to the second stage of the oxidation mechanism occurs at 48% oxygen consumption. Dodecane is oxidised to 90% oxygen depletion in

4101 minutes, or 68 hours, and as such the second slow stage of oxidation takes 4071 minutes. This is quicker than the time taken for BannerSol, which supports the finding that decreasing chain-length increases the thermal stability of an n-alkane, as BannerSol is in the C_{10}-C_{14} meaning that significant proportion of the solvent is made up of decane and undecane.
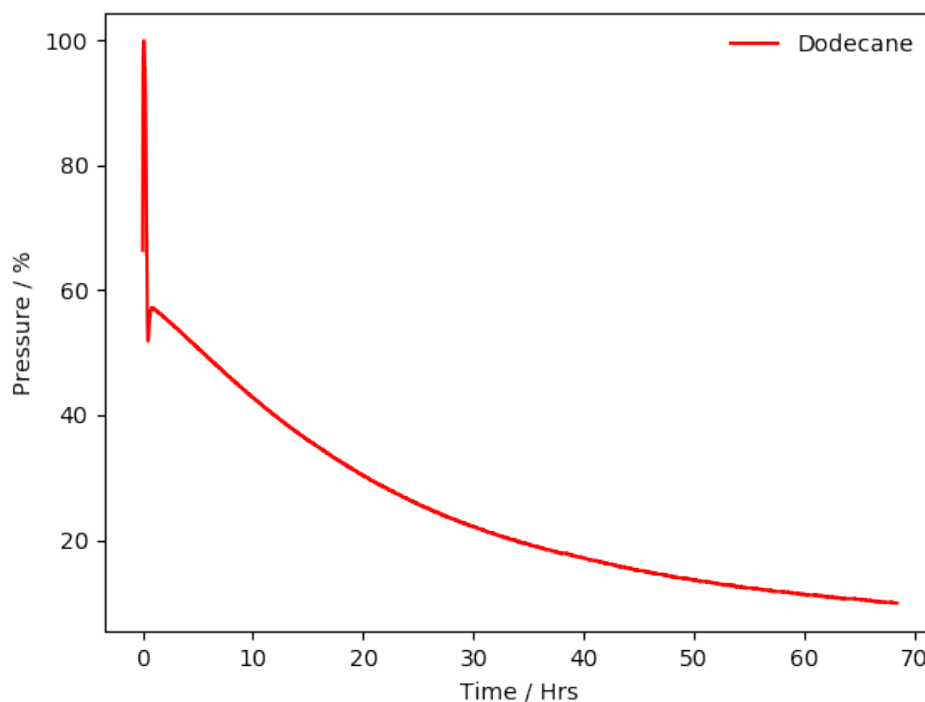
Fig. 4.21: PetroOxy plot of the time taken in hours for dodecane to reach 90% oxygen depletion.

The colour of the dodecane samples changed as they were progressively oxidised, which can be seen in figure 4.22.

The colour did not change as the dodecane was thermally stressed to 40% oxygen depletion, during which, the rapid radical oxidation mechanism occurs. After 50% of the oxygen has been consumed in the PetroOxy the colour of the dodecane changes from a colourless liquid to a light straw colour. This change occurs as the second slow stage of oxidation begins. This would support the proposition that the mechanism changes from a rapid radical chain mechanism, to a slower oxidative coupling SMORS mechanism, with the requisite colour change brought on by increased conjugation.
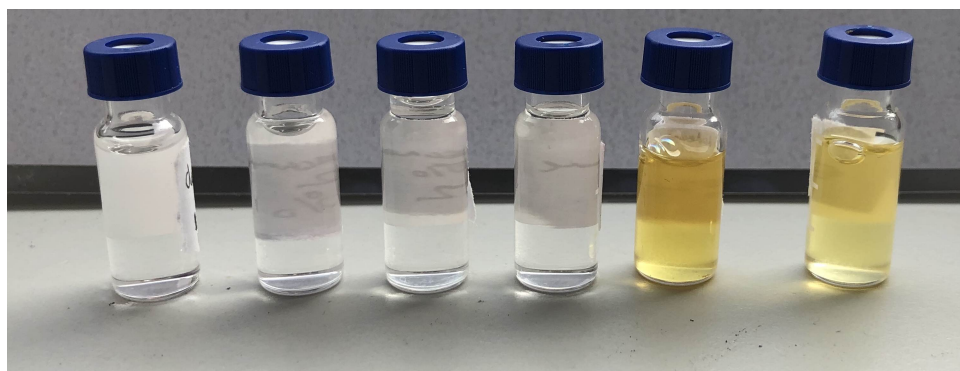
Fig. 4.22: Colour of dodecane at different levels of oxygen consumption left to right: 10%, 20%, 30%, 40%, 50% and 90%.

This change in oxidation mechanism, and the oxidation products being formed as a result, is even more obvious when the samples are analysed using infrared spectroscopy. The results of which can be seen in figure 4.23.
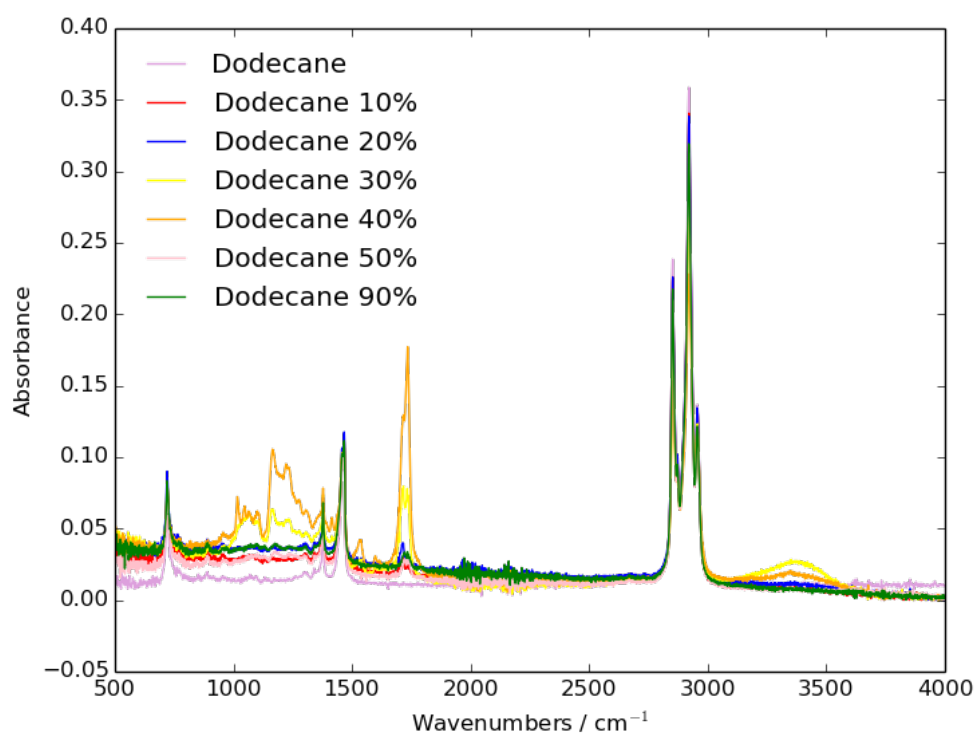
Fig. 4.23: Absorbance spectra for the thermally stressed dodecane at different stages of oxidation.

As the dodecane is increasingly oxidised the carbonyl peak at 1750 cm^{-1} and O-H peak at 3400 cm^{-1} increase in intensity. A number of peaks between 1000-1300 cm^{-1} also increase with intensity. After the change in oxidation

rate occurs above 50% oxygen consumption, the peaks in the 1000-1300 cm^{-1} range, and O-H peak above 3000 cm^{-1} disappear. The carbonyl peak also reduces in intensity and broadens out with a number of separate peaks present around this wavenumber. This suggests that at oxygen consumptions below 50%, alcohols, ketones and acids are the main products. Beyond this point, the picture is more complex, with esters and anhydride acids potentially being present. However, further study is required to investigate these products and the mechanisms that form them in more depth.

The dodecane samples at these stages of oxidation were also studied using GCMS with the results shown in figure 4.24.
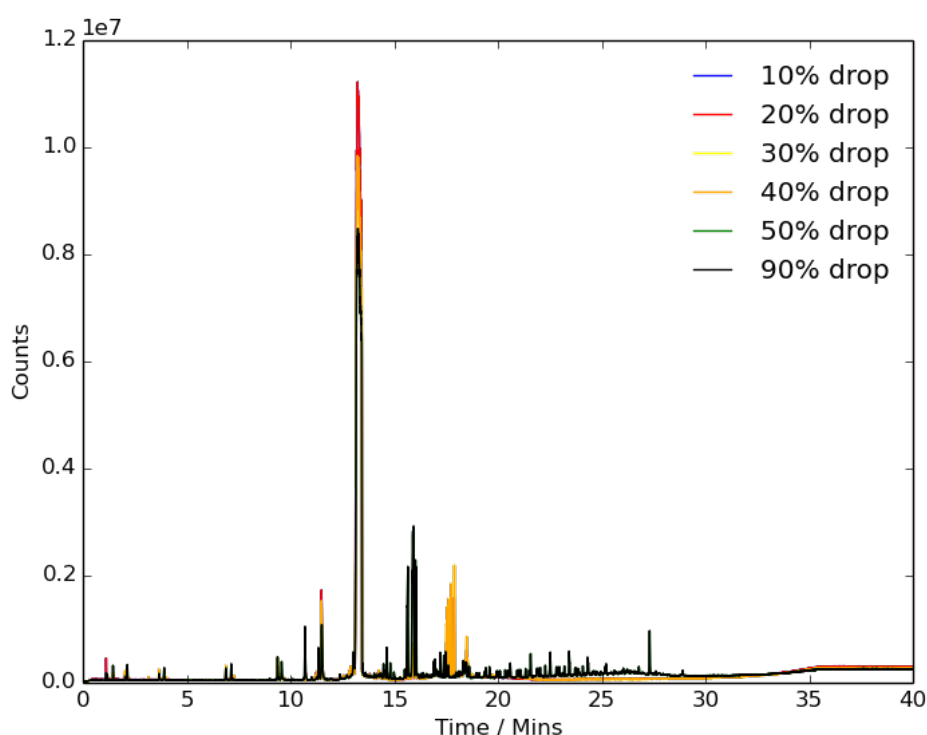
Fig. 4.24: GCMS traces for the thermally stressed dodecane at increasing stages of oxygen consumption.

The main peak caused by the dodecane can be seen at a retention time of 13.5 minutes. As the sample is progressively oxidised up to 40% oxygen depletion, a set peak at 17.5 minutes retention grows, this is caused by primary oxidation products such as alcohols, aldehydes, ketones and acids forming. These will be heavier, but also more polar, and thus have longer retention times due to an apolar solvent being used as the mobile phase. An interesting transition occurs above 50% oxygen consumption, and is clearly present in the GCMS

trace of the Dodecane oxidised to 90% oxygen consumption, with this set of peaks at 17.5 minutes being replaced by a set of peaks at high retention times. An intense set of peaks at 16 minutes also appears. This is caused by oxidative coupling and condensation reactions that have happened to the dodecane sample to result in higher molecular weight polymeric products and cyclic anhydride acids. These anhydride are ring closing reactions that can result is in a drop in molecular weight and polarity. This means that they can be eluted earlier in the GMCS. Numerous peaks below the main dodecane peak can also be seen, supporting this statement, as these are the by-products of the condensation and coupling reactions.

4.3.2 Decalin

To study the oxidation of the cycloalkane building block of fuels, decalin was chosen, as it is of a similar size to dodecane, and avoids any alkyl side chains that would complicate the results. In real fuels, a number of different cycloalkanes would be present, with many of them based around a cyclohexane base with various lengths of side-chains. However, to investigate the affect that just the specific chemical structure that cycloalkanes have on the thermal stability of aviation fuels, decalin was investigated. The decalin was thermally stressed to a range of oxygen depletions at 170°C in the PetroOxy, with the samples being analysed as before, using FTIR and GCMS. The results of decalin being oxidised to a 90% oxygen consumption can be seen in figure 4.25. The induction period of decalin is 11.08 minutes, with the time required to complete the rapid oxidation stage being 24 minutes, with the transition occurring when 64% of the oxygen has been consumed. The decalin took a similar amount of time to reach a 90% depletion of the oxygen as dodecane, with this happening in 73.6 hours, or 4417 minutes. This means that the second slow stage of oxidation takes 4393 minutes which is 322 minutes longer than the time required for dodecane. It is clear that the first stage of oxidation is quicker for decalin, and results in a greater incorporation of oxygen into the oxidised products, as seen by the greater oxygen depletion that occurs during this stage of the oxidation mechanism. However, the second stage of the oxidation mechanism is slower, this suggest that the cyclic structure inhibits the oxidative coupling and condensation reactions. One cause of this could be that the steric hindrance placed on the reaction by the ring structure slows these reactions. Another possibility could be that the decalin under goes aromatisation to form tetralin or other aromatic species.

This change in the hydrocarbon composition of the sample during testing could produce complex changes to the rate of the oxidation mechanisms.
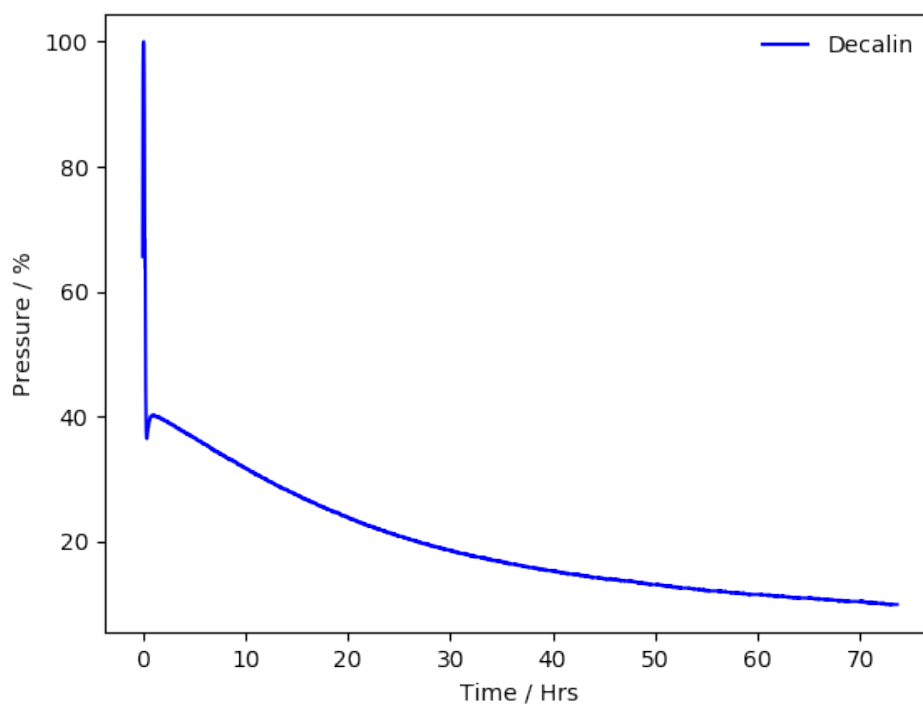
Fig. 4.25: PetroOxy plot of the time taken in hours for decalin to reach 90% oxygen depletion.

The colour of the decalin samples at various stages of oxygen consumption can be seen in figure 4.26.
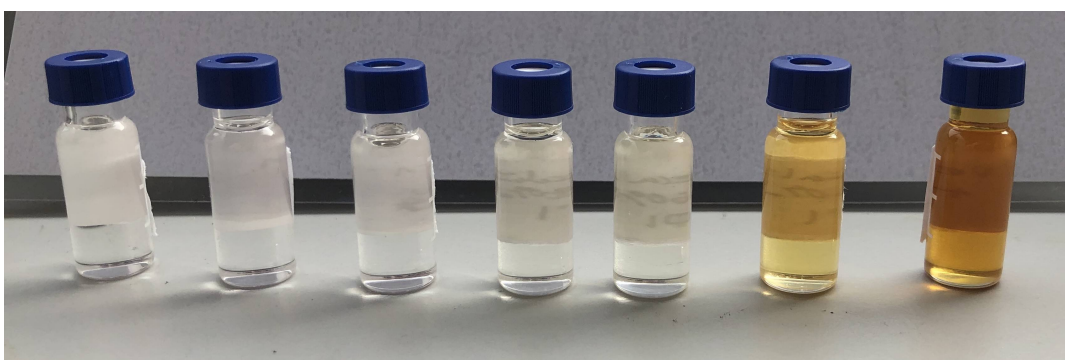
Fig. 4.26: Colour of decalin at different levels of pressure depletion left to right: 10%, 20%, 30%, 40%, 40%, 50%, 70% and 90%.

The decalin shows similar changes in colour to that shown by the dodecane. However, the transition from colourless to straw yellow occurs between 50

and 70% oxygen consumption, whereas this happened between 40-50% for dodecane. This colour change occurring at this oxygen consumption is inline with the observation that the change occurs as the hydrocarbon transition from the first stage of oxidation to the second oxidative coupling stage. This occurs at 64% oxygen consumption for decalin. The oxidised decalin samples are also darker in colour which supports the idea that the decalin undergoes aromatisation in the oxidation mechanism. When these aromatic products react together and are further oxidised they absorb strongly in the visible region.

FTIR spectra for the decalin at increasing levels of oxidation can be seen in figure 4.27. The difference in the hydrocarbon structure between decalin and dodecane can be seen clearly in the the infrared spectra.
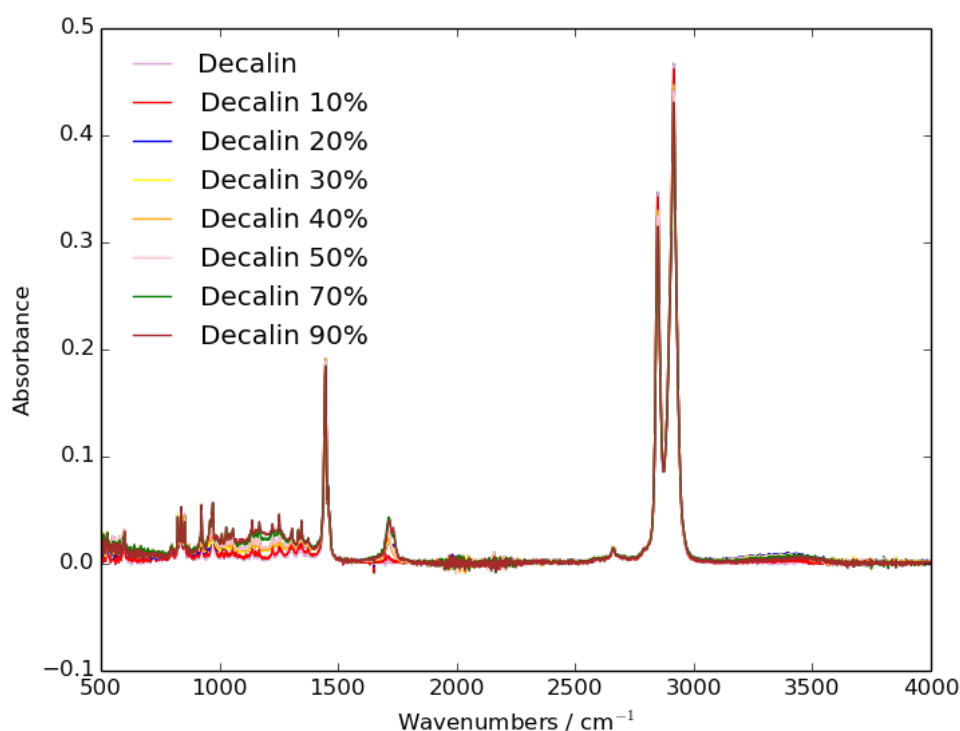
Fig. 4.27: Absorbance spectra for the thermally stressed decalin at different stages of oxidation.

The two C-H peaks at 2800 and 2950 cm^{-1} no longer have a shoulder at higher wavenumber, which they do in dodecane, and is caused by the terminal CH_3 group. When this knowledge is applied to the spectra of the B1-AtJ fuel, it become obvious that the iso-alkane is very highly branched, and the CH_3:CH_2 is in-favour of the terminal CH_3 groups. As the decalin is thermally stressed,

and exposed to greater levels of oxygen consumption, the carbonyl peak at 1750 cm^{-1} increases in intensity. This peak suggests that ketones, acids and esters are being formed in the oxidation of decalin. Coupled with the visual inspection of the samples, it would be suggested that the products formed above 70% oxygen consumption, are the aromatic Tetralones and polymeric oxidative coupling products. Unlike with the dodecane, the peak at 1750 cm^{-1}, and there is negligible growth of the O-H peak above 3000 cm^{-1}. This suggests that the acid species are not being formed, which could be caused by the high steric hindrance of the intermediates required to form the carboxylic acid group on the decalin ring, and how strained the O-C=O angle would be when formed. As such, it is more likely that the aromatisation of the decalin occurs, and that the oxidised products of these aromatic species oxidatively couple together to form extended oxidised aromatic systems. These species would have similar chemical formula as those proposed by Beaver *et al* providing some support for this theory.[182–185]

The GCMS trace for decalin at increasing levels of oxiation can be seen in figure 4.28.
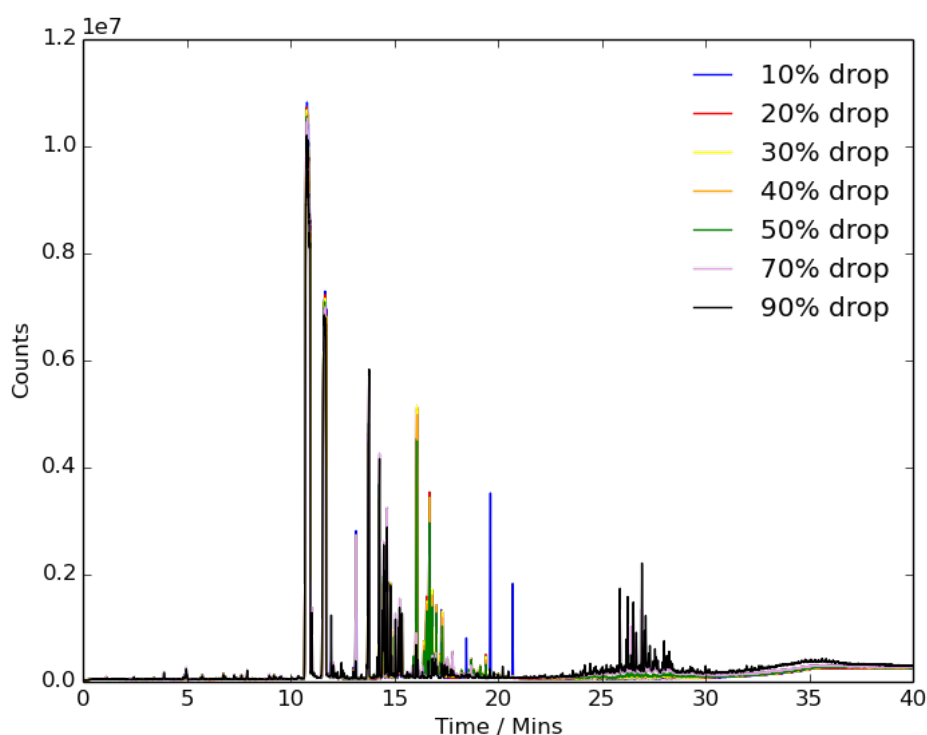
Fig. 4.28: GCMS for the thermally stressed decalin at increasing levels of oxygen depletion.

The results of these GCMS studies provide evidence in support for the theory that the decalin oxidises through a slightly modified mechanism because of its chemical structure. Or that at least the oxidative coupling and deposition during the second stage of oxidation is different. It is obvious that at higher degrees of oxidation there is a move to higher molecular weight products. The main decalin peak can be seen at a retention time of 11 minutes. In all of the GCMS traces, even when the decalin has undergone high thermal stressing, there is minimal number of peaks observable at times below the retention time of the main decalin peak. Of particular interest in the GMCS traces of decalin is the formation of a number of chemical species at retention times between 25 and 28.5 minutes, and the disappearance of peaks in retention time between 16 and 20 minutes. This is strong evidence of the oxiation products of decalin, which are likely to be aromatic in character, undergoing oxidative coupling reactions and that these reaction do not formed significant amounts of small molecular weight side products.

If decalin undergoes significant aromatisation during the oxidation mechanism, and there is high concentration of aromatic species in the sample at high level of oxygen depletions, this could provide a reason for the rate of oxygen consumption in the second stage of oxidation being slower than for dodecane. However, from the data collected from the PetroOxy tests, it is also clear that the autoxidation mechanisms for alkanes are very similar and have a number of key details in common. They both undergo two stages of oxidation observed in the fuels, with a rapid radical driven stage of oxidation, where the primary oxidation products are formed and the physical properties of the fuels are not significantly affected. The second slow stage of oxidation occurs, which is driven by slower oxidative coupling reactions, where the colour changes and deposition occurs. It appears to be at this stage that the two classes of alkanes diverge from each other, with the decalin forming visibly darker colour changes and heavier products. The point at which the oxidation mechanism transitions is also different for the two alkanes, with the point that this occurs linked to the CH_3:CH_2 ratio. Despite these differences, the alkanes seem to have similar primary oxidation mechanism, with the slight difference an interesting area to study using theoretical chemistry.

4.3.3 Toluene

The mono-aromatic aromatic building block of aviation fuel was also investigated using the PetroOxy device. However, unlike the alkane classes, limits on the volume of aromatics allowed in aviation fuel are in place.[7, 8] The reason for investigating the aromatic component in isolation is that it, from the the study of the JETSCREEN fuels, it is clearly the hydrocarbon class that most dominates the thermal stability behaviour of an aviation fuel. Future development of the fuel for high temperature operating condition may mean that the limit on the concentration of aromatics in the fuel may be lifted. This could allow for the density of the fuels to be improved, without the negative impact on the thermal stability, due to the reduction in the concentrations of heteroatomic species when compared to conventional fuels. As such, it is important to study aromatic hydrocarbons in isolation, to understand their behaviour in high temperature conditions.

When toluene was thermally stressed in the PetroOxy, it exhibited a very different oxidation profile to the alkane classes previously studied, both quantitatively and qualitatively. The results of toluene oxidised to a 90% oxygen depletion in the PetroOxy are presented in figure 4.29.

The time taken to reach a 90% pressure drop was 147.5 hours, or 8850 minutes, which was double the time taken for the alkanes dodecane and decalin. The induction period of the toluene also took 653.35 minutes, which is on a completely different time frame to that for the alkanes, and suggest that a different reaction is occurring. This is even more clear when the time required to reach the change in oxidation rate is compared to for alkanes, with the time required being 4800 minutes, which is longer than the total test for the alkanes. The second stage of oxidation is slightly more rapid, but is still slow, and took 4050 minutes. As both rates of oxidation are slow, it can be suggested that the toluene is acting as an antioxidant. However, deposition occurs throughout the oxidation process, suggesting that the oxidised products react with each other. This would support the proposal by Beaver *et al* who suggested that phenols and oxidised aromatics can react through electrophillic aromatic substitution reactions.[182–185] This is supported by the observation that deposition occurs throughout the oxidation. The most likely reason for the profile seen in the data is that the oxidative coupling reactions and antioxidant reactions are competing with the radical chain reactions and thus are inhibiting the rapid oxidation.
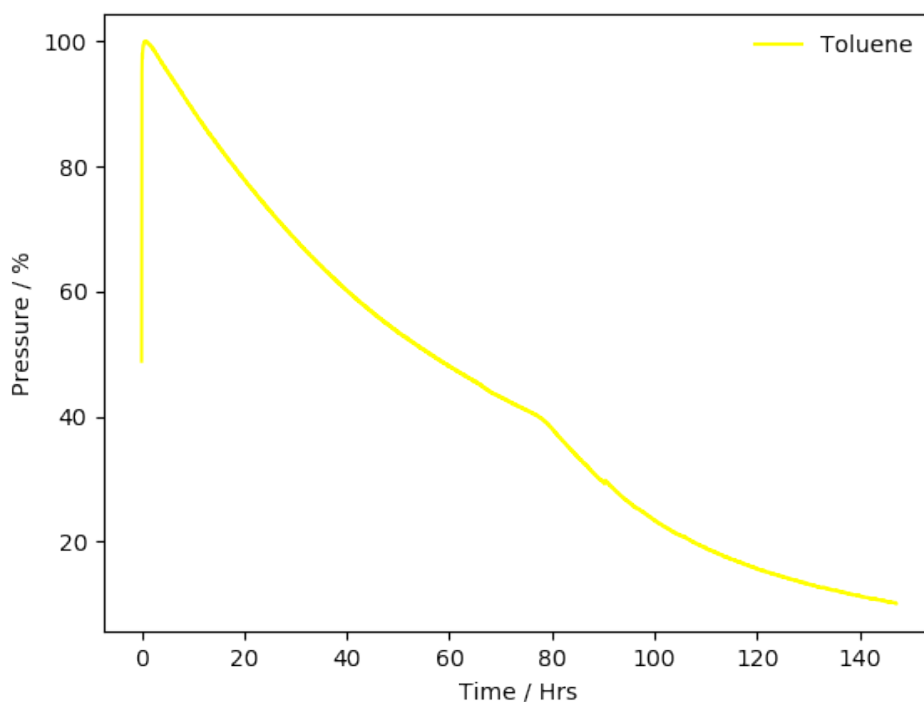
Fig. 4.29: PetroOxy plot of the time taken in hours for toluene to reach 90% oxygen depletion.

The colour of the thermally stressed toluene samples at increasing oxidation can be seen in figure 4.30. The colour of the samples gets progressively darker as the level of oxidation increases, determined by the level of head-space oxygen depletion, until the pressure has dropped over 70%. At this point oxidised products formed in the fuel have precipitated out of solution and forms a dark insoluble sediment. At this point, heavy levels of deposition occurs, resulting in even more of the precipitate and sediment to be reduced from the solution, resulting in the solution at 90% oxygen depletion to be light than previous samples.

The oxidised samples of toluene, unlike the oxidised sample of the other hydrocarbons tested, changed colour immediately under thermal stressed conditions. This, with the rate of the oxygen consumption in the PetroOxy, suggests that the toluene oxidises differently to the alkanes species. The colour change in the other hydrocarbons tested only occurred once during the second stage of oxidation, characterised by oxidative coupling reactions, and as such it is likely that the toluene can oxidise through this mechanism
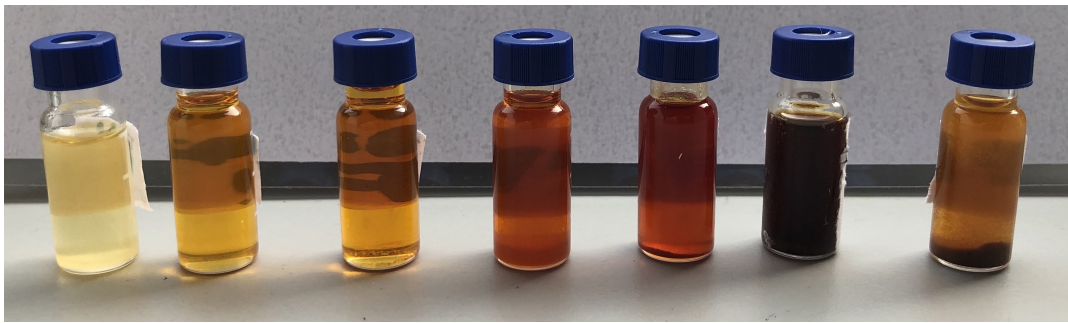
Fig. 4.30: Colour of toluene at different levels of pressure depletion left to right: 10%, 20%, 30%, 40%, 40%, 50%, 70% and 90%.

from the start. This is because it aromatic structure allows for these reactions to occur more easily.

The FTIR studies of the thermally stressed toluene samples at different levels of oxygen depletion can be seen in figure 4.31.
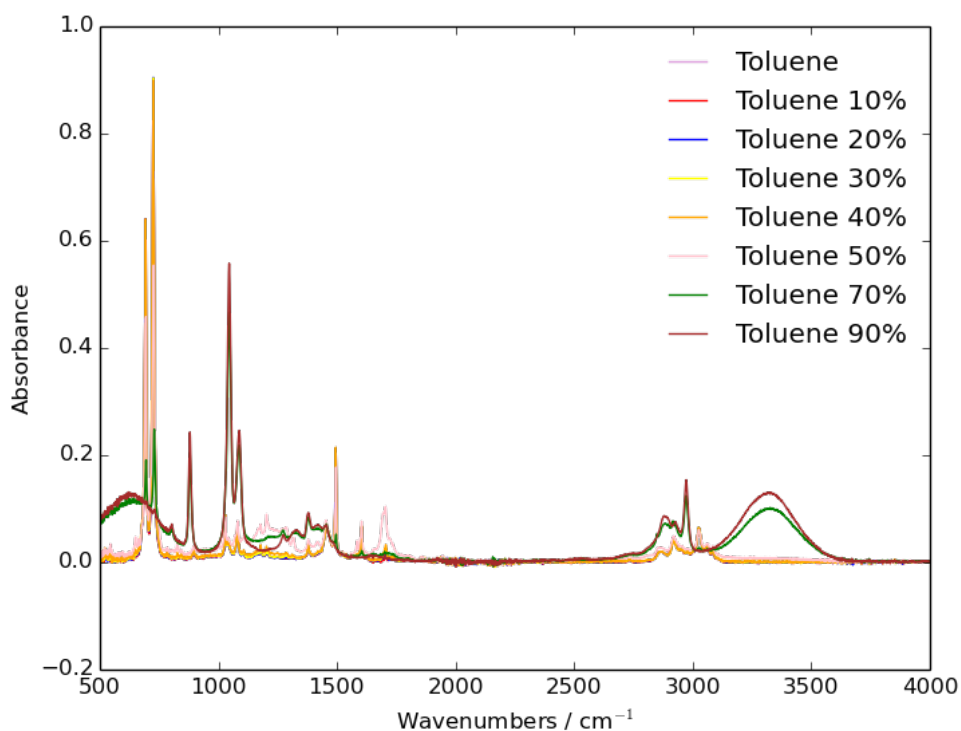
Fig. 4.31: Absorbance spectra for the thermally stressed toluene at different stages of oxidation.

The progression of the formation of oxidised products is particularly clear to see in the thermal stressing of toluene. As the toluene is thermally stressed

up to a 50% oxygen drop, the intensity of the carbonyl C=O stretch increases, indicating that aldehydes and ketones are being formed during the oxidation mechanism. At a 70% pressure drop and above, this carbonyl stretch has disappeared, and has been replaced by a broad stretch between 3200-3600 cm^{-1}. However, the oxidised products of toluene are difficult to investigate with FTIR, as the spectra of benzoic acid does not have a broad O-H peak at 3200-3600 cm^{-1}. This is because the O-H vibration and the aromatic delocalisation from the ring cancel each other out, resulting in the peak to be reduced, this is compounded by the effect of intermolecular interactions reducing the vibration.[282] The peak would be visible if ultra fast measurements are carried out. However, we can confirm the presence of benzoic acid in the oxidised toluene in the samples below 70% oxygen depletion from the GCMS studies, discussed below. This means that the broad stretch that appears at 3200-3600 cm^{-1} above 70% depletion cannot be caused by benzoic acid.

The two most obvious species causing this peak would be alcohols or water. The rest of the spectra gives excellent agreement with the formation of alcohol. When this evidence is taken into consideration with the visual analysis of the colour and constancy of the sample in figure 4.30, this would imply that above 70% oxygen depletion the oxidative coupling products have precipitated out of solution, and the dominant species left are alcohols and water. The reason that the very dark brown solution that is formed at 70% oxygen consumption does not have an intense absorbance is that it formed of a suspension. Thus, the small particles scatter the infrared radiation, making FTIR an ineffective technique for analysing the sample. This is even more severe at 90% drop, as the particles have completely precipitated out of solution or formed deposit of the PetroOxy surface.

The GCMS trace for the thermally stressed toluene samples at the increasing levels of oxygen consumption can be seen in figure 4.32. The first thing that is obvious from the data, and support the visual and infrared studies, is that the significant deposition above 70% oxygen consumption depletes the concentration of oxidised products in the toluene sample. The main peak for the toluene can be seen at a retention time of 3.5 minutes, with the oxidised products at longer retention times appearing from 10% oxygen consumption. By the time 90% oxygen has been consumed in the test, the main peaks remaining are the three peaks at 1, 3.5 and 13.5 minutes, with the peak at 27.5 minutes being the Triphenylphosphine oxide standard. The peak at 13.5 is the alcohol that can clearly be seen in the infrared spectra in figure

4.31. However, as most of the products of the oxidation process are now found in the deposit, the information gained from the GCMS results at this exposure time is of less interest than for the other hydrocarbons tested. Of more interest is comparing the GCMS traces below 50% oxygen depletion to the FTIR results at the same stages. Due to the nature of the column used in the GCMS studies, carboxylic acid groups present in the trace will be stretched and form a broad slope up to the peak. This can clearly be seen in the GCMS traces up to 50% oxygen depletion, in the 13-13.5 time range, with this peak disappearing after this point. This supports the infrared findings, which suggested that benzoic acid is formed during the oxidation.
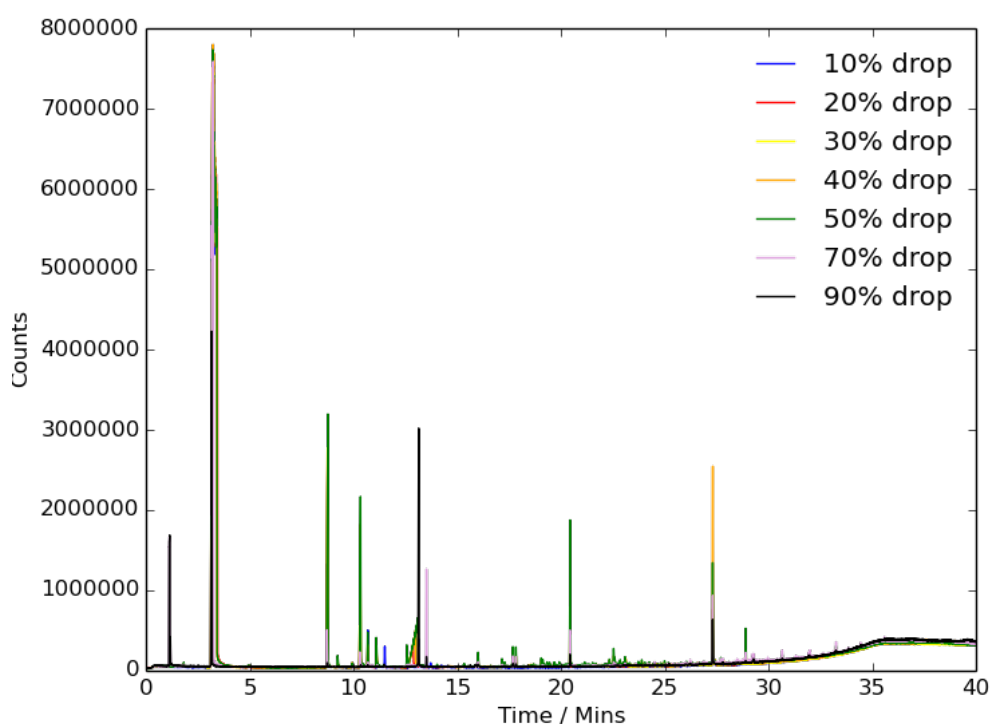
Fig. 4.32: GCMS for the thermally stressed toluene at increasing pressure drop.

From all of the data available, the toluene undergoes a different oxidation mechanism to that of the alkanes, with both the oxidative coupling reactions and the radical oxidation reaction happening concurrently to each other in the first stage of oxidation in the PetroOxy. During the second stage of oxidation, from the evidence present in the FTIR and GCMS, much of the toluene has been reacted and mainly lightly oxidised alcohols are present. They would persist because the oxygen concentration at this point may be too low to oxidise the remaining alcohols to carbonyls and acids, or because

the alcohols are in a form that is unreactive. The findings from this study also supports those seen in the literature that aromatics in the fuel slow the rate of oxidation, as seen by the longer time required to reach 90% oxygen consumption, but results in greater levels of deposition on the PetroOxy device. From these studies, it can also be seen that this deposition begins to occur almost instantly, meaning that the oxidation mechanism is more complex than for the alkanes studied. These diffrences are of interest to study using computational chemistry.

4.4 PetroOxy investigations into hydrocarbon blends

Aviation fuels used in service and being developed for future use are blends of a number of different hydrocarbon components. As such, to get a representative picture of the way the different hydrocarbon components oxidise when they are blended together, simple hydrocarbon blends of the pure components were tested using the PetroOxy device. The first, rapid radical chain reaction driven, stage of the autoxidation mechanism was selected to investigate for this study. This is because it is more important to understand this stage for the prediction of an aviation fuel's thermal stability, as the tests at higher levels of oxygen depletion represent area of much longer retention time, with stagnate flow in the fuel systems. The time taken to reach a 40% oxygen depletion is plotted as a function of the percentage of decalin, or toluene in the next section, in the blend. The complete PetroOxy data for these tests can be found in the appendix. However, as we are more interested in the trends that increasing the concentration of a hydrocarbon in the blend, only the final test time is plotted here. The affect of increasing the ratio of decalin in a blend with dodecane can be seen in figure 4.33, where it has been plotted against the time to reach 40% oxygen depletion in seconds.

The relationship between the time taken to reach a 40% oxygen drop is linear with the percentage of decalin in the blend. As the concentration of decalin increases the time required to complete this first radical stage of the oxidation mechanism reduces. As was found in the study of the JETSCREEN fuels, and seen in the literature, this relationship is likely caused by the ratio of CH_3 and CH_2 carbons.[138, 140] The CH_1 site and the restrictive ring structure, also is likely to have an impact of the rate of oxidation, with the exact intricacies
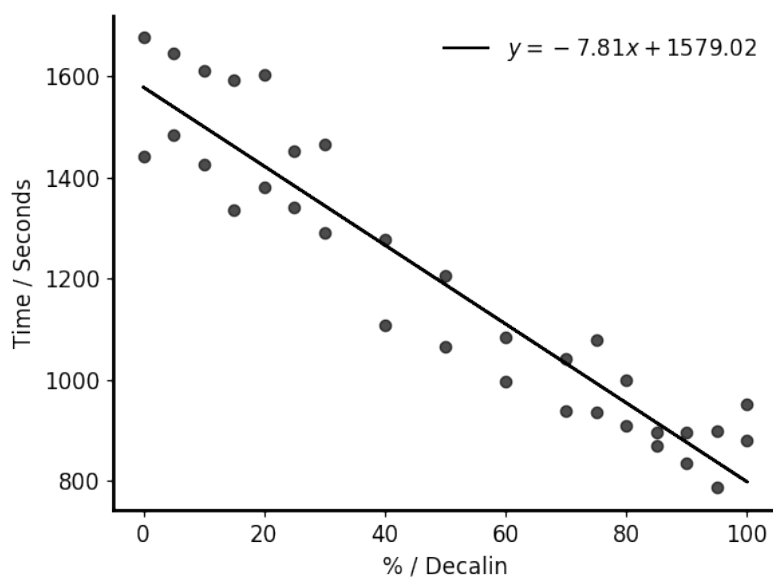
Fig. 4.33: Plot of time in seconds for dodecane:decalin mixtures to reach 40% pressure drop as a function of decalin concentration.

needing study using theoretical chemistry. However, the relationship observed in this study allows us to predict how an aviation fuel with a known alkane composition would behave, as its response to thermal stressing should be linear to the concentration of the cycloalkanes in the blend.

Aviation fuels are formed of more complex hydrocarbon mixtures than just alkanes. As such, it is important to understand how blending alkanes with aromatic hydrocarbons effects the thermal stability, and if this can be linked to the observations seen in the JETSCREEN experiments. This is also important to understand now, as there is an opportunity for aviation fuel to develop, by including a great proportion of aromatic hydrocarbons in them. However, it is not understood what affect that this can have on the thermal stability. As such, dodecane and decalin were blended with toluene, with the percentage of toluene increased by five percent up to the point it was thirty percent of the blend. On top of this 50:50 and 30:70 percent blends were tested, as was pure toluene. The results were plotted as a function of the log of time in seconds, as otherwise the 30:70 and 100% toluene measurements could not reasonably fit in the same data range.

The dodecane:toluene blend is plotted as a function of the log of time in seconds in figure 4.34. There is a clear linear trend in this data from increasing
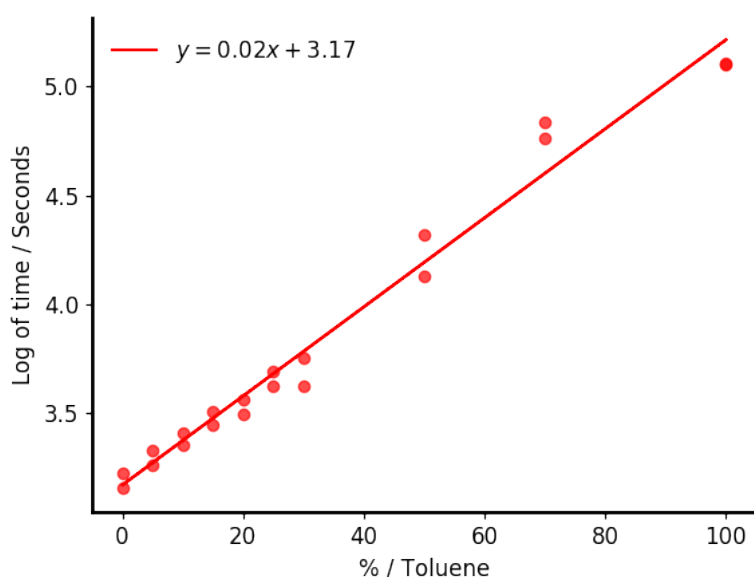
Fig. 4.34: Plot of the log of time in seconds for dodecane:toluene mixtures to reach 40% pressure drop as a function of toluene concentration.

the concentration of toluene in the blend, with this resulting in an exponential increase in the time required to reach 40% oxygen depletion. The most clear reason for this is that the aromatic toluene acts as an antioxidant, slowing the oxidation of the more quickly oxidisable dodecane, by donating a hydrogen to the alkyl and peroxyl radicals formed during autoxidation.

The decalin:toluene blend is plotted as a function of the log of time in second in figure 4.35. This data has a deviation from the linear trend seen in the dodecane:toluene blend. One reason for this could be that toluene is a poorer antioxidant for decalin, as the stability of the radical products and intermediates are closer in energy than for dodecane, or the transition states in the reaction pathways are higher in energy. However, it could also be due to the observation seen in the PetroOxy studies, where decalin appears to undergo aromatisation.

This deviation from the exponential relationship can be seen if the data for the decalin and dodecane blend with toluene are plotted on the same graph, seen in figure 4.36. The decalin has a noticeable deviation from a linear trend as a function of the log of time. However, the agreement is good up to 70% toluene volume in the blend, and as such if the concentration of aromatics in a fuel is increased to 50% by volume in fuel blend you would expect that
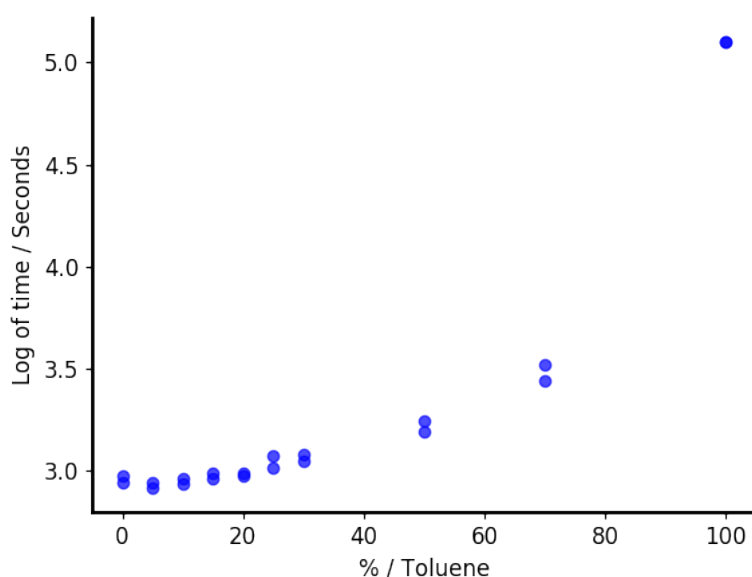
Fig. 4.35: Plot of the log of time in seconds for decalin:toluene mixtures to reach 40% pressure drop as a function of toluene concentration.

the response of the fuel to thermal stressing can be predicted using this relationship. To confirm that this relationship is observed in aviation fuels, more complex mixtures are needed to be tested in the future, with ternary blends of these three hydrocarbon being the most obvious place to start for any future work.

However, despite the deviation at higher aromatic concentration, it is clear that the increase in aromatic concentration below 50% by volume as an exponential increase in the time required for 40% of the oxygen to be consumed. This can be used to explain the observations seen in the JETSCREEN testing, particularly for the A group of fuels, where a small increase in the concentration of aromatics lead to a noticeable increase in the time required for a fuel to complete the rapid stage of oxidation. This exponential relationship is likely caused by the aromatic hydrocarbon acting as antioxidants in the fuel. Thus increasing their concentration increases this effect. This phenomenon is likely to be even more enhanced for di-aromatics and poly-aromatic species, such as naphthalenes, and thus the reference Jet A1 has a particularly long induction period. This hypothesis could be tested further, by investigating the affect of changing the structure of the aromatic hydrocarbon in the blend, on the inhibition of radical oxidation mechanism.
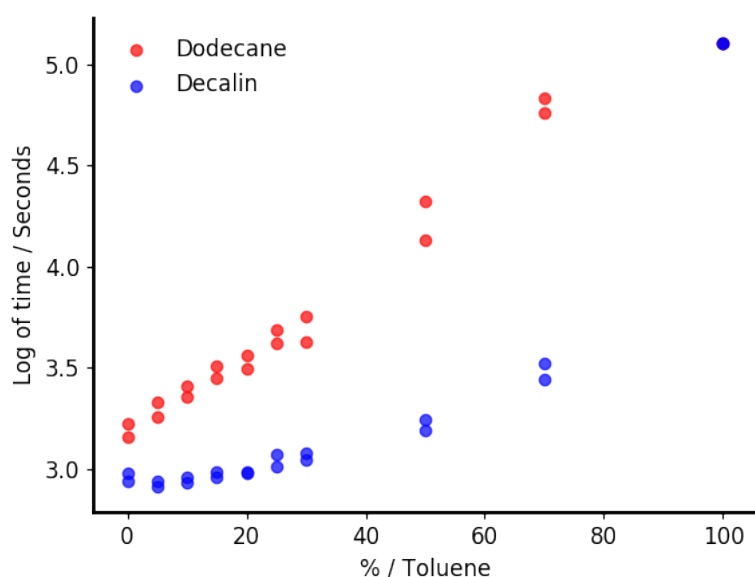
Fig. 4.36: Plot of the log of time in seconds for alkane:toluene mixtures to reach 40% pressure drop as a function of toluene concentration.

4.5 Building pseudo-detailed mechanism for hydrocarbon oxidation

The experimental work carried out in this thesis have been carried out in support of the principal aim of this study, namely to develop an updated pseudo-detailed mechanism for the autoxidation of hydrocarbons, which can incorporate the effect of changing chemical structure. The PetroOxy investigations show that the oxidation mechanism often had two stages with rates which are distinct from each other. However, increasing the concentration of aromatic hydrocarbons in the fuel affects this differentiation, and causes the oxidation to have a more steady transition in rate. The first stage is attributed to the formation of alcohols, ketones and other primary oxidation products, with the rate of the mechanism being dominated by the build up and reaction of radical species in the fuel. The second stage of oxidation results in the formation of insoluble material and deposits and is characterised by a range of oxidative coupling reactions. These two stages have different kinetics and are controlled by different chemistry. It is clear that the hydrocarbon composition of a fuel affects the rate of oxidation in both stages of the mechanism. As such, it is important to decide which stage of oxidation to develop a model for, and the best methodology is to study the mechanism

Computational quantum chemistry calculations have been used in this thesis to construct the expanded pseudo-detailed mechanisms for the separate classes of hydrocarbons. The reason for using these calculations is that they allow us to get chemically accurate results to predict the activation barrier and pre-exponential factor for the Arrhenius equation. These can then be used in a number of modelling approaches to study larger scale systems. Quantum chemistry also give us the opportunity to develop a detailed understanding of the causes of these observed differences in the autoxidation of hydrocarbons. Changes in the electronic and steric effects will be seen prominently in the changes in the activation energy and the pre-exponential factor, with large steric strain resulting in an increase in the E_a and a reduction in the A.

4.5.1 Methodology

This section will focus on developing a kinetic mechanism to study the effect that changing the hydrocarbon composition of an aviation fuel has on the first stage of autoxidation. There were a number of reasons for selecting this primary stage of oxidation to study. The first was that the reactants and products of these reactions are small and finite in nature, rather than being polymeric in nature. This makes computationally modelling them easier. Thus, the picture is less confusing and the calculations are less computationally expensive to study with quantum chemistry calculations. The second reason for selecting the primary stage of oxidation is that these mechanism are likely driven mostly by the chemistry of the hydrocarbon species. The second stage of oxidation has more complex physical and transport processes involved in the formation of insoluble sediments and deposits, with it not even being clear why one forms over the other. The temperature of the wall, surface of the wall, solvent properties and mixing caused by turbulence all are going to have an effect on this second stage of oxidation. As such, studying it purely with quantum chemistry methods would be inadequate. Instead, proper CFD modelling would need to be considered.

The final reason for focusing on the first stage of oxidation is a practical one. Significantly more effort in the literature has been applied to modelling this stage of oxidation. Thus, there is a better starting point for starting developing a more chemically detailed and rigorous model for this stage of oxidation. Moreover the autoxidation of hydrocarbons also has applications in other fields, including industrial catalysis, biology and the beverage industry, rather

the the more narrow applications of a model for the second stage of oxidation. Thus, the findings that result from this thesis have greater potential impact in the wider scientific community. Thus, to better understand the role that hydrocarbon composition has on the rate of autoxidation, and to provide insight into the fundamental mechanisms behind hydrocarbon oxidation, a pseudo-detailed mechanism of oxidation up to the formation of the initial oxidation products will be constructed. The starting point was to use previous models developed by Kuprowicz *et al* to select a set of reactions that are of importance for the oxidation process.[14] The reaction steps that do not purely involve hydrocarbons and their oxidised products were removed from the mechanism and it was extended by populating it with a selection of other potentially important oxidation reactions. The complete base mechanism can be seen in in table 4.5, with alteration for different classes of hydrocarbon being discussed at the time.

Reaction steps 3, 4, 5, 9, 10, 11 and 12 come directly from the pseudo-detailed mechanism proposed in [14]. Reaction steps 25 and 26 as well as 6 and 17 are expansions of individual steps in that mechanism.[14] The other reactions are thought to be important steps towards the formation of the primary oxidation products of ketones, aldehydes and alcohols. The peroxide and peroxyl radical species are crucial intermediates in this mechanism, and will be studied in more depth in chapter 5. Importantly, this mechanism will also look at the formation of alkenes in the fuel. These are potential products of the autoxidation. They can react rapidly with other oxidised products present in the fuel *via* oxidative coupling reactions. They have been shown in the literature to have poor thermal stability properties, so calculating the energies and kinetics for their routes to formation is important for future expansions of the mechanism to study the second stage of oxidation.

The next step is to select a methodology to use to build the extended pseudo-detailed mechanism from computational chemistry calculations. Constructing the mechanism for each hydrocarbon, and for the reactions involving two hydrocarbon groups reacting with each other, will require optimisation and frequency calculations to be preformed for the reactants, products and transition states. Thus, a minimum of 447 calculations need to be performed if the optimisation and frequency calculations converge first time. As these calculations involve complex open shell electronic structures, and transition states that are difficult to locate, in reality the number of calculations will be much higher. Compounding this problem is that these systems are large,

Tab. 4.5: Detailed mechanism for the oxidation of hydrocarbons, R can indicate dodecane, decalin or toluene.

No	Reaction Schematic
1	$RH \rightarrow R + H$
2	$RH + O_2 \rightarrow R + HOO$
3	$RH + OH \rightarrow R + H_2O$
4	$R + O_2 \rightarrow RO_2$
5	$RO_2 + RH \rightarrow RO_2H + R$
6	$RO + RO \rightarrow ROH + R{=}O$
7	$RO + R \rightarrow ROH + alkene$
8	$R + R \rightarrow RH + alkene$
9	$R + R \rightarrow R\text{-}R$
10	$RO_2H \rightarrow RO + OH$
11	$RO + RH \rightarrow ROH + R$
12	$RO \rightarrow R_{prime} + C{=}O$
13	$R + OH \rightarrow alkene + H_2O$
14	$RO + OH \rightarrow R{=}O + H_2O$
15	$ROH + OH \rightarrow RO + H_2O$
16	$RO_2H + OH \rightarrow RO_2 + H_2O$
17	$RO + RO \rightarrow ROOR$
18	$R + RH \rightarrow RH + R_{prime}$
19	$RO_2 + R \rightarrow ROOR$
20	$ROOR \rightarrow RO + RO$
21	$RO + R \rightarrow R{=}O + RH$
22	$RO_2 + RO \rightarrow ROOH + R{=}O$
23	$RO_2 + ROH \rightarrow ROOH + RO$
24	$RO + R \rightarrow ROR$
25	$RO_2 + RO_2 \rightarrow ROOOOR$
26	$ROOOOR \rightarrow RO + RO + O_2$
27	$RO_2H + RO_2H \rightarrow RO_2 + RO + H_2O$

with between 100-400 electrons in the systems selected, dependant of the chemical structure investigated. This means that constructing the mechanism from high cost post-Hartree-Fock wave function methods is not feasible at the present moment, even though recent advances put these methods within reach for systems of this size.[283, 284] This limits the level of theory that can be used for this work to Density Functional Theory. However here, there are many different choices for the functional and basis sets. Previous work has looked at bench-marking functionals against coupled cluster methods (CCSD), for the reactions of radicals.[285, 286] In these studies, B3LYP performed surprisingly well, particularly for geometries of the system when compared to CCSD. This, coupled with the fact that many kinetics databases use B3LYP

calculations as a starting point, means that this functional offers a good level of accuracy at reasonable computational cost.[287, 288]

The reason it has been used in previous kinetics databases is because of the excellent agreement with calculated geometries from CCSD(T), the gold standard of computational chemistry, as well as experimental bond lengths. This allows the calculated geometries to be used as good initial trial geometries, and thereby trial wave functions, for calculations at higher level of theory. The hybrid GGA family of functionals, which B3LYP is a member, has also shown to give a surprisingly good accuracy of barrier heights when compared to even more complex functionals and wave function methods.[289] It was originally thought to be caused by singlet diradical character in the systems studied. Then, symmetry breaking within the functional helps to describe this. However, Mahler *et al* suggested other possibilities, they state that the highly parameterised functionals such as M06-2X have numerical errors in their description of the gradient and exact exchange corrections. This would lead to errors in the barrier heights and other properties of interest.[289] In contrast, the B3LYP functional and other simpler GGA functionals benefit from a cancellation of errors which works in chemists favour. This is because the energy from pure functionals underestimates the barrier height, whereas the Hartree-Fock energy over estimates it. Thus, hybrid functionals like B3LYP end up in the middle. The reason for this improvement is the inclusion of the exact exchange from Hartree-Fock improves the description of the kinetic energy term.[290] The other benefit of using B3LYP over more parameterised functionals, is that it has not been developed for a particular set of reaction families. This results in it being applicable to be applied to different sets of potential chemistries.[291, 292] This allows for the mechanism developed to be expanded in future, to include metals, sulfur, and nitrogen chemistry, without having to change methodology.

Due to this possible improvement in the level of theory and the accuracy of the calculations used to construct this mechanism in future, Dunning's correlation consistent triple zeta basis set, cc-pVTZ, was selected for this thesis.[62–66] This is because these basis sets were built to improve in accuracy as the description of correlation in your methods improved. This will allow future improvements in the scalability of multi-reference and coupled cluster methods can be taken advantage of. The drawback of using this basis set, and building in this future contingency, is that cc-pVTZ is a very large basis set. This increases the computational expense of the calculations, the amount of time

and resources required to run the computation, and thus limits the size of the mechanism.

The proceeding sections of this thesis will be dedicated to presenting the results of building the pseudo-detailed mechanism for the individual hydrocarbon classes, the alterations made to each mechanism caused by the specific hydrocarbons chemical structure, and the effects this has on the calculated values. The three hydrocarbons selected are the same as those used in the experimental studies; dodecane, decalin and toluene. As discussed previously, these are representative of the molecular weight and chemical structure of the hydrocarbon species found in aviation fuel. Again studies of iso-alkanes and alternative aromatic structure have not been carried out due to limits on time and computational resources. As discussed in the experimental results of the experimental studies, the ratio of n-alkanes to iso-alkanes is likely to only result in small and predictable changes in the rate of oxidation.[138, 140] The affect of changing the aromatic structure has been shown to be more profound. However, time constraints means that studying this is beyond the scope of the thesis. More discussion on the possible effect of this change will be presented in chapter 6.

4.5.2 Dodecane

The extended pseudo-detailed mechanism for the autoxidation of dodecane can be seen in table 4.6. Dodecane has twelve carbons. As such, a decision was made which carbon would be used as the active site for the reactions. The calculations used to build this mechanism were carried out on the terminal carbon on the chain. This is the most easily accessible for hydrogen abstraction and is the least sterically hindered site. This simplifies the calculation of transition states for reaction involving multiple R groups. The change in the rate of reaction from abstracting from the other sites can be parameterised using the observations from Chatelain *et al.*[138] However, despite this mechanism being built using the reactions from the terminal carbon, the formation of dodecene was carried out on the C2 carbon, as were the formation of carbonyl groups. The reaction energy for both the formation of a ketone and an aldehyde were calculated, with a noticeable difference between them. dodecane was the only hydrocarbon studied that could form an aldehyde and a ketone and as such this was the only mechanism that had this alteration.

Tab. 4.6: Detailed mechanism for the oxidation of dodecane, With E_a having units of kcal mol^{-1} and A for unimolecular reactions has units of s^{-1} and L mol^{-1} s^{-1} for bimolecular reactions. The mechanism was constructed using B3LYP/cc-pVTZ/pcm=heptane calculations in Gaussian09 and corrections to the thermodynamic data was done through the GoodVibes software.[121, 122, 125]

No	Reaction Schematic	A	E_a
1	$RH \rightarrow R + H$	8.2×10^{13}	94.2
2	$RH + O_2 \rightarrow R + HO_2$	2.7×10^{12}	38.1
3	$RH + OH \rightarrow R + H_2O$	2.5×10^{12}	5
4	$R + O_2 \rightarrow RO_2$	6.7×10^{11}	0
5	$RO_2 + RH \rightarrow RO_2H + R$	2.6×10^{12}	18.1
6	$RO + RO \rightarrow ROH + R=O$	2.2×10^{12}	16.9
7	$RO + R \rightarrow ROH + alkene$	5.2×10^{11}	29.9
8	$R + R \rightarrow RH + alkene$	7.1×10^{11}	17.3
9	$R + R \rightarrow R\text{-}R$	4.7×10^{11}	0
10	$RO_2H \rightarrow RO + OH$	1.9×10^{13}	34.3
11	$RO + RH \rightarrow ROH + R$	1.9×10^{12}	5.3
12	$RO \rightarrow R_{prime} + C=O$	2.5×10^{13}	9.3
13	$R + OH \rightarrow alkene + H_2O$	1.9×10^{12}	0
14	$RO + OH \rightarrow R=O + H_2O$	1.6×10^{12}	0
15	$ROH + OH \rightarrow RO + H_2O$	2.8×10^{12}	0
16	$RO_2H + OH \rightarrow RO_2 + H_2O$	2.5×10^{12}	0
17	$RO + RO \rightarrow RO_2R$	$1.4 \times 10_{12}$	0
18	$R + RH \rightarrow RH + R_{prime}$	1.2×10^{12}	15.8
19	$RO_2 + R \rightarrow RO_2R$	7.8×10^{11}	0
20	$RO_2R \rightarrow RO + RO$	2.8×10^{13}	25.4
21	$RO + R \rightarrow R=O_{ketone} + RH$	2.2×10^{12}	7.1
22	$RO + R \rightarrow R=O_{aldehyde} + RH$	1.5×10^{12}	10.4
23	$RO_2 + RO \rightarrow RO_2H + R=O$		
24	$RO_2 + ROH \rightarrow RO_2H + RO$		
25	$RO + R \rightarrow ROR$	1.1×10^{12}	0
26	$RO_2 + RO_2 \rightarrow ROOOOR$	1.7×10^{11}	0
27	$ROOOOR \rightarrow RO + RO + O_2$	2.6×10^{13}	0.8
28	$RO_2H + RO_2H \rightarrow RO_2 + RO + H_2O$		

The calculations for reaction step 8 were carried out using the singlet surface at first. An interesting result from these calculations was that the transition state was barrierless using this surface. However, when the triplet surface was used, the reaction did have a barrier. This inconsistency in the energies calculated for the two surfaces is caused by the electronic structure of these bi-radical species being inherently multi-reference in nature, and not being properly described by DFT. This is a known problem with modelling

reactions such as these, and introduces uncertainties into the values calculated. As such, in future the extended mechanism could be optimised prior to use in larger scale modelling to improve agreement with experimental data, with sensitivity analysis being carried out to test the rigour of the calculated values.

In the extended pseudo-detailed mechanisms presented in this chapter the barrier heights and pre-exponential factors for bi-radical systems are calculated using the triplet surface. This is because these results give a more accurate description of the shape of the barrier, in that they predict one to be present, for this level of theory. The gaps in the mechanism are due to the transition state calculations not being completed at the time of writing. This is because these reactions are either highly multi-reference in nature, or the barrier is low lying, and thus difficult to locate. For reaction 23 and 28, this problem is treated in more detail using multi-reference methods in chapter 5. The rate determining steps for this reaction mechanism are 1, 2 and 10 with barriers of 94.2, 38.1 and 34.3 kcal mol^{-1} respectively. These are the only reactions in the mechanism to have barrier over 30 kcal mol^{-1}. They are important reactions as they either initiate the reactions, in the case of reaction steps 1 and 2, or are crucial early chain branching reactions that can accelerate the autoxidation of dodecane in the case of reaction 10. The homolytic fission of dodecane peroxide has been linked to be so important in the fuel that it is treated in more detail in chapter 5.

4.5.3 Decalin

When building an extended pseudo-detailed mechanism for the autoxidation of decalin, it needs to be decided which isomer is used for the study, with a choice of trans-decalin or cis-decalin to use. The experimental studies in this thesis were carried out using decalin which was a mixture of these two isomers. However, to save time and computational resources, only one isomer will be studied. In this study we have used trans-decalin, as it has been shown by Heyne *et al* to be the most stable form.[293] However, this is likely to introduce some inaccuracy into our model as you would expect some to be in the cis-decalin form. With the energy required to transition between the two isomers being 14 kcal mol^{-1} it would be expected that the ratio of the isomers in the fuel to remain unchanged during storage at room temperatures. Also, like with dodecane, we have chosen to use a sterically

unhindered position on the decalin ring as the active site for the reactions. The pseudo-detailed mechanism built using this set of circumstances can be seen in table 4.7. Again, the gaps in the mechanism are caused by the transition states of these reaction steps not being completed at the time of submission.

Tab. 4.7: Detailed mechanism for the oxidation of decalin, With E_a has units of kcal mol^{-1} and A for unimolecular reactions has units of s^{-1} and L mol^{-1} s^{-1} for bimolecular reactions. The mechanism was constructed using B3LYP/cc-pVTZ/pcm=heptane calculations in Gaussian09 and corrections to the thermodynamic data was done through the GoodVibes software.[121, 122, 125]

No	Reaction Schematic	A	E_a
1	$RH \rightarrow R + H$	7.8×10^{13}	94.8
2	$RH + O_2 \rightarrow R + HO_2$	1.3×10^{12}	23.9
3	$RH + OH \rightarrow R + H_2O$	4.4×10^{12}	0
4	$R + O_2 \rightarrow RO_2$	9.0×10^{11}	0
5	$RO_2 + RH \rightarrow RO_2H + R$	2.5×10^{12}	18.3
6	$RO + RO \rightarrow ROH + R=O$		
7	$RO + R \rightarrow ROH + alkene$	1.7×10^{12}	5.8
8	$R + R \rightarrow RH + alkene$	1.9×10^{12}	15.4
9	$R + R \rightarrow R\text{-}R$	6.7×10^{11}	0
10	$RO_2H \rightarrow RO + OH$	1.5×10^{13}	32.5
11	$RO + RH \rightarrow ROH + R$		
12	$R + OH \rightarrow alkene + H_2O$	3.7×10^{12}	0
13	$RO + OH \rightarrow R=O + H_2O$	5.6×10^{12}	0
14	$ROH + OH \rightarrow RO + H_2O$	5.9×10^{12}	19.1
15	$RO_2H + OH \rightarrow RO_2 + H_2O$	5.9×10^{12}	0
16	$RO + RO \rightarrow RO_2R$	$5.4 \times 10_{12}$	0
17	$R + RH \rightarrow RH + R_{prime}$	1.5×10^{12}	14.8
18	$RO_2 + R \rightarrow RO_2R$	1.0×10^{12}	0
19	$RO_2R \rightarrow RO + RO$	6.6×10^{12}	25.1
20	$RO + R \rightarrow R=O_{ketone} + RH$	2.1×10^{12}	11.7
21	$RO_2 + RO \rightarrow RO_2H + R=O$	3.8×10^{12}	11.3
22	$RO_2 + ROH \rightarrow RO_2H + RO$		
23	$RO + R \rightarrow ROR$	1.0×10^{12}	0
24	$RO_2 + RO_2 \rightarrow ROOOOR$	1.7×10^{11}	0
25	$ROOOOR \rightarrow RO + RO + O_2$	2.6×10^{13}	0.8
26	$RO_2H + RO_2H \rightarrow RO_2 + RO + H_2O$		

The chemical difference of decalin enforced by cyclic chemical structure has resulted in an extended pseudo-detailed mechanism which has 26 reactions, with some which are possible for dodecane, are not possible for decalin. These include the formation of an aldehyde product, which is reaction 22 in

table 4.6, or the decomposition of the alkoxide radical into formaldehyde and an alkane radical seen in reaction 12 of the dodecane mechanism. This was not calculated as the formation of formaldehyde would result in the breaking of two C-C bonds and the formation of 2 alkane radicals. This would undoubtedly have a large barrier and would not be feasible. As such ring opening reactions have also not been included in the mechanism at this stage. However, it could be possible that an analogous reaction could occur, particularly in the second stage of oxidation. This would result in the formation of an ether as the ring undergoes rearrangement and recombines. This is less likely to happen for 6-membered rings, as the result of this reaction would be the formation of a 7-membered ring, which is thermodynamically unfavoured. As such, it has not been calculated, as the low likelihood of the reaction means that dedicating computational resources to this reaction is a low priority.

The initiation step for the abstraction of hydrogen by dissolved oxygen, step 2, is 14.2 kcal mol^{-1} lower in energy than that for the same reaction in dodecane. This could account for some of the observations seen in the PetroOxy studies, with cycloalkanes oxidising more rapidly, as the Boltzmann distribution at 170 °C has 99% of the reaction proceeding through the decalin route. However, this only takes the difference in the energy barrier into account, and the pre-exponential and concentration of reactants is also important and can be accessed using higher scale modelling. The mechanism is missing steps toward aromatisation, which has been shown to be important in the PetroOxy studies, and would be an obvious next step. This work could be driven by mechanistic investigations, as carried out in the organic chemistry field, to determine if oxidation or aromatisation occurs first in the mechanism. Notably, the transition state are all low lying hydrogen transfer reactions, and indicates that the barriers are very low. The multi-reference systems where there were issues optimising in for dodecane were optimised in for decalin. However, they were predicted to be barrierless, which is an artefact of these reactions being highly multi-reference in nature and DFT failing to describe the problems correctly. Again, these reactions are examined in more detail in chapter 5.

4.5.4 Toluene

The extended pseudo-detailed mechanism for the autoxidation of toluene can be seen in table 4.8. The core mechanism is constructed from 27 reactions. Toluene is not being able to form a ketone due to it only having a single carbon

site in the benzylic side-chain. The benzylic carbon was selected as the site for reaction, as it has been shown to be the most reactive site on aromatic hydrocarbons. The gaps in the mechanism are due to the transition states calculations not being complete at the time of submission. The literature indicates that the number of these sites could be the cause of aromatic hydrocarbons relative reactivity to each other.[134] More discussion of this effect will be given in chapter 6.

The toluene pseudo-detailed mechanism was supplemented with the formation of alkanes on the side-chain, rather than just between the aromatic ring and the benzylic carbon, as this is an important set of reactions to model. For this ethylbenzene was used as a surrogate aromatic hydrocarbon and can bee seen in the lower section of table 4.8. The reason for carrying out these calculations, and adding them to the pseudo-detailed mechanism, is that the styrene product formed during these reactions is a species which is particularly problematic for thermal stability since it can undergo rapid polymerisation. As such, predicting the rate of formation of styrene is important for future modelling investigations into the second stage of oxidation. The barrier for the formation of styrene through the disproportionation of two hydrocarbon radicals is 7.7 kcal mol^{-1} lower than the same reaction for toluene. This difference is caused by the formation of the alkene on the toluene system breaks the aromaticity of the system. Thus there is a large penalty to this happening. Similarly, the reaction in step 30 is almost barrierless, with only step 28 being an outlier with the cause unknown.

The initiation step for the abstraction of hydrogen by dissolved oxygen, step 2, is 15.3 kcal mol^{-1} lower in energy than that for the same reaction in dodecane and 1.1 kcal mol^{-1} lower than decalin. The Boltzmann distribution at 170 °C has 99% of the reaction proceeding through the toluene route when compared to dodecane and 77% when compared to decalin. However, this only takes the difference in the energy barrier into account, and the pre-exponential and concentration of reactants is also important. The reasoning for this facile extraction of hydrogen from the toluene is caused by the aromatic stabilisation of the radical formed, which means the mechanism slows after this point compared to the other hydrocarbons. An important step missed for all of the mechanisms, but from the PetroOxy studies is particularly important for toluene, is the formation of acids. These are likely to be the final products formed prior to the start of the second stage of oxidation and prediction their

Tab. 4.8: Detailed mechanism for the oxidation of toluene, With E_a has units of kcal mol^{-1} and A for unimolecular reactions has units of s^{-1} and L mol^{-1} s^{-1} for bimolecular reactions. The mechanism was constructed using B3LYP/cc-pVTZ/pcm=heptane calculations in Gaussian09 and corrections to the thermodynamic data was done through the GoodVibes software.[121, 122, 125]

No	Reaction Schematic	A	E_a
1	$RH \rightarrow R + H$	2.5×10^{13}	86.0
2	$RH + O_2 \rightarrow R + HO_2$	6.7×10^{11}	22.8
3	$RH + OH \rightarrow R + H_2O$		
4	$R + O_2 \rightarrow RO_2$	1.0×10^{12}	0
5	$RO_2 + RH \rightarrow RO_2H + R$	4.1×10^{13}	14.6
6	$RO + RO \rightarrow ROH + R=O$	2.7×10^{12}	3.4
7	$RO + R \rightarrow ROH + alkene$	1.7×10^{12}	9.0
8	$R + R \rightarrow RH + alkene$	1.9×10^{12}	26.2
9	$R + R \rightarrow R\text{-}R$	7.9×10^{11}	0
10	$RO_2H \rightarrow RO + OH$	1.9×10^{13}	33.1
11	$RO + RH \rightarrow ROH + R$	2.2×10^{12}	4.1
12	$RO \rightarrow R_{prime} + C=O$	3.6×10^{13}	21.6
13	$R + OH \rightarrow alkene + H_2O$	2.7×10^{12}	8.2
14	$RO + OH \rightarrow R=O + H_2O$	3.4×10^{12}	0
15	$ROH + OH \rightarrow RO + H_2O$	5.4×10^{12}	0.4
16	$RO_2H + OH \rightarrow RO_2 + H_2O$	5.5×10^{12}	5.3
17	$RO + RO \rightarrow RO_2R$	$1.8 \times 10_{12}$	0
18	$R + RH \rightarrow RH + R_{prime}$	1.3×10^{12}	16.4
19	$RO_2 + R \rightarrow RO_2R$	1.6×10^{12}	0
20	$RO_2R \rightarrow RO + RO$	2.1×10^{13}	24.4
21	$RO + R \rightarrow R=O_{aldehyde} + RH$	1.7×10^{12}	9.0
22	$RO_2 + RO \rightarrow RO_2H + R=O$	2.0×10^{12}	12.2
23	$RO_2 + ROH \rightarrow RO_2H + RO$	2.1×10^{12}	16.2
24	$RO + R \rightarrow ROR$	1.2×10^{12}	0
25	$RO_2 + RO_2 \rightarrow ROOOOR$	1.6×10^{12}	0.8
26	$ROOOOR \rightarrow RO + RO + O_2$	1.3×10^{14}	0
27	$RO_2H + RO_2H \rightarrow RO_2 + RO + H_2O$		
28	$RO + R \rightarrow ROH + alkene$ (styrene)	1.8×10^{12}	9.2
29	$R + R \rightarrow RH + alkene$ (styrene)	1.6×10^{12}	18.5
30	$R + OH \rightarrow alkene + H_2O$ (styrene)	2.8×10^{12}	0.4

concentration is important to improve the prediction of any future models developed for this stage of oxidation.

4.5.5 Modelling hydrocarbon interactions

To develop the extended pseudo-detailed mechanism for the use in the prediction of an aviation fuels it is required that the mechanism can model the behaviour of hydrocarbon components when they are blended together. This is of particular interest to this thesis, as it is clear that the aromatic hydrocarbons bahave as antioxidants. As such, developing an extended pseudo-detailed mechanism to understand the cause of this behaviour would be useful, as the PetroOxy test indicate that the antioxidant potential of toluene is not the same when used with dodecane and decalin. The same carbon positions and conformers of dodecane, decalin and toluene were selected for this study as those used in the individual mechanisms and the gaps in the mechanism are due to the calculations not being finished at the time of submission. The extended pseudo-detailed mechanism for the interaction of alkanes can be seen in table 4.9 and the mechanism for the interaction of toluene with the individual alkanes can be seen in table 4.10. Unlike for the interaction of alkanes, the mechanism for the aromatic interactions was not constructed the other way, i.e. changing which species donates the hydrogen. The reason for this is that it is clear from the PetroOxy data that aromatics are acting as antioxidants in the fuel, so the rate of reaction going the other way is negligible.

An obvious effect seen in the mechanism for the reactions of toluene with alkanes is that the hydrogen abstraction in step 1 is significantly lower than that for the individual alkanes. The barrier for this reaction step is 6.1 kcal mol^{-1} lower for the reaction of toluene with dodecane when compared to the similar dodecane step 18 and is 3.5 kcal mol^{-1} lower for decalin compared to step 17 in that mechanism. This difference mean that 99% of the dodecane radical will react with the toluene rather than anther dodecane species and 98% of decalin will react with toluene. This is the likely cause of the antioxidant behaviour of aromatics in the fuel, as while they are they are still present in the fuel, they can act as a sink for the radicals formed. An interesting result observed in this mechanism is that the disproportionation to from an alkene on the alkane fragment is disfavoured compared to reaction of alkanes in isolation. As the barrier is approximately 5 kcal mol^{-1} higher when they are reacting with toluene. The likely cause of this is that the aromatic radical is stabilised, relative to the purely alkane system, and as such the barrier to formation is higher. This supports the idea that the aromatics act as radical sinks in the fuel.

Tab. 4.9: Detailed mechanism for the oxidation of alkanes, dodecane and decalin, reacting with each other. E_a has units of kcal mol^{-1} and A for unimolecular reactions has units of s^{-1} and L mol^{-1} s^{-1} for bimolecular reactions. The mechanism was constructed using B3LYP/cc-pVTZ/pcm=heptane calculations in Gaussian09 and corrections to the thermodynamic data was done through the GoodVibes software.[121, 122, 125]

No	Reaction Schematic	A	E_a
	R_a = dodecane / R_b = decalin		
1	$R_a + R_bH \rightarrow R_aH + R_b$	6.2×10^{12}	14.9
2	$R_a + R_b \rightarrow$ R-R	3.8×10^{11}	0
3	$R_a + R_b \rightarrow R_aH$ + alkene	1.6×10^{12}	15.9
4	$R_aO + R_bO \rightarrow R_aOH + R_b$=O	3.2×10^{12}	0.17
5	$R_aO + R_bH \rightarrow R_aOH + R_b$	2.5×10^{12}	5.5
6	$R_aO + R_b \rightarrow R_aOH$ + alkene	1.6×10^{12}	5.3
7	$R_aO + R_b \rightarrow R_a$=O + R_bH	1.4×10^{12}	11.5
8	$R_aO_2 + R_bH \rightarrow R_aO_2H + R_b$	2.3×10^{12}	18.9
9	$R_aO_2 + R_bO \rightarrow R_aO_2H + R_b$=O	2.7×10^{12}	11.0
10	$R_aO_2 + R_bOH \rightarrow R_aO_2H + R_bO$		
11	$R_aO_2 + R_b \rightarrow RO_2R$	1.2×10^{12}	0
12	$R_aO + R_bO \rightarrow RO_2R$	$1.8 \times 10_{12}$	0
13	$RO_2R \rightarrow R_aO + R_bO$	2.2×10^{13}	26.1
14	$R_aO + R_b \rightarrow$ ROR	6.7×10^{11}	0
15	$R_aO_2 + R_bO_2 \rightarrow$ ROOOOR	1.4×10^{12}	1.5
16	ROOOOR $\rightarrow R_aO + R_bO + O_2$	1.2×10^{14}	1.2
17	$R_aO_2H + R_bO_2H \rightarrow R_aO_2 + R_bO + H_2O$		
	R_b = decalin / R_a = dodecane		
1	$R_b + R_aH \rightarrow R_bH + R_a$		
2	$R_b + R_a \rightarrow$ R-R	3.8×10^{11}	0
3	$R_b + R_a \rightarrow R_bH$ + alkene	1.5×10^{12}	15.6
4	$R_bO + R_aO \rightarrow R_bOH + R_a$=O	2.8×10^{12}	2.1
5	$R_bO + R_aH \rightarrow R_bOH + R_a$	2.3×10^{12}	7.3
6	$R_bO + R_a \rightarrow R_bOH$ + alkene	4.5×10^{12}	4.1
7	$R_bO + R_a \rightarrow R_b$=O + R_aH	1.7×10^{12}	0
8	$R_bO_2 + R_aH \rightarrow R_bO_2H + R_a$	2.7×10^{12}	21.2
9	$R_bO_2 + R_aO \rightarrow R_bO_2H + R_a$=O		
10	$R_bO_2 + R_aOH \rightarrow R_bO_2H + R_aO$	3.1×10^{12}	18.9
11	$R_bO_2 + R_a \rightarrow RO_2R$	1.1×10^{12}	0
12	$R_bO + R_aO \rightarrow RO_2R$	$1.6 \times 10_{12}$	0
13	$RO_2R \rightarrow R_bO + R_aO$	2.3×10^{13}	26.4
14	$R_bO + R_a \rightarrow$ ROR	9.5×10^{11}	0
15	$R_bO_2 + R_aO_2 \rightarrow$ ROOOOR		
16	ROOOOR $\rightarrow R_bO + R_aO + O_2$		
17	$R_bO_2H + R_aO_2H \rightarrow R_bO_2 + R_aO + H_2O$		

Tab. 4.10: Detailed mechanism for the oxidation of alkanes, dodecane and decalin, reacting with toluene. E_a has units of kcal mol^{-1} and A for unimolecular reactions has units of s^{-1} and L mol^{-1} s^{-1} for bimolecular reactions. The mechanism was constructed using B3LYP/cc-pVTZ/pcm=heptane calculations in Gaussian09 and corrections to the thermodynamic data was done through the GoodVibes software.[121, 122, 125]

No	Reaction Schematic	A	E_a
R_a = dodecane / R_c = toluene			
1	$R_a + R_cH \rightarrow R_aH + R_c$	1.1×10^{12}	9.7
2	$R_a + R_c \rightarrow$ R-R	7.7×10^{11}	0
3	$R_a + R_c \rightarrow$ alkene + R_cH	1.2×10^{12}	20.6
4	$R_aO + R_cO \rightarrow R_aOH + R_c{=}O$	3.3×10^{12}	3.1
5	$R_aO + R_cH \rightarrow R_aOH + R_c$	2.3×10^{12}	4.7
6	$R_a + R_cO \rightarrow$ alkene + R_cOH	2.2×10^{12}	7.2
7	$R_a + R_cO \rightarrow R_aH + R_c{=}O$	1.7×10^{12}	9.8
8	$R_aO_2 + R_cH \rightarrow R_aO_2H + R_c$	2.3×10^{12}	14.8
9	$R_aO_2 + R_cO \rightarrow R_aO_2H + R_c{=}O$	1.7×10^{12}	11.0
10	$R_aO_2 + R_cOH \rightarrow R_aO_2H + R_cO$		
11	$R_aO_2 + R_c \rightarrow RO_2R$	1.3×10^{12}	0
12	$R_aO + R_cO \rightarrow RO_2R$	$1.2 \times 10_{12}$	0
13	$RO_2R \rightarrow R_aO + R_cO$	3.2×10^{13}	25.2
14	$R_aO + R_c \rightarrow ROR$	9.3×10^{11}	0
15	$R_aO_2 + R_cO_2 \rightarrow ROOOOR$	1.1×10^{12}	0
16	$ROOOOR \rightarrow R_aO + R_cO + O_2$	7.7×10^{13}	2.0
17	$R_aO_2H + R_cO_2H \rightarrow R_aO_2 + R_cO + H_2O$		
R_b = decalin / R_c = toluene			
1	$R_b + R_cH \rightarrow R_bH + R_c$	9.7×10^{11}	11.3
2	$R_b + R_c \rightarrow$ R-R	3.8×10^{11}	0
3	$R_b + R_c \rightarrow$ alkene + R_cH	1.4×10^{12}	20.5
4	$R_bO + R_cO \rightarrow R_bOH + R_c{=}O$	3.5×10^{12}	3.7
5	$R_bO + R_cH \rightarrow R_bOH + R_c$		
6	$R_b + R_cO \rightarrow$ alkene + R_cOH	2.8×10^{12}	4.3
7	$R_b + R_cO \rightarrow R_bH + R_c{=}O$	2.7×10^{12}	16.0
8	$R_bO_2 + R_cH \rightarrow R_bO_2H + R_c$	2.3×10^{12}	15.5
9	$R_bO_2 + R_cO \rightarrow R_bO_2H + R_c{=}O$	3.1×10^{12}	14.3
10	$R_bO_2 + R_cOH \rightarrow R_bO_2H + R_cO$	2.9×10^{12}	17.9
11	$R_bO_2 + R_c \rightarrow RO_2R$	6.7×10^{12}	0
12	$R_bO + R_cO \rightarrow RO_2R$	$2.5 \times 10_{12}$	0
13	$RO_2R \rightarrow R_bO + R_cO$	1.5×10^{13}	24.5
14	$R_bO + R_c \rightarrow ROR$	9.4×10^{11}	0
15	$R_bO_2 + R_cO_2 \rightarrow ROOOOR$	1.3×10^{12}	0
16	$ROOOOR \rightarrow R_bO + R_cO + O_2$	1.1×10^{14}	2.8
17	$R_bO_2H + R_cO_2H \rightarrow R_bO_2 + R_cO + H_2O$		

4.6 Summary

It is clear from the investigations carried out using the PetroOxy device that the autoxidation mechanism proceeds through multiple stages. This is in agreement with findings in the literature, where a three stage deposition mechanism is discussed across a number of devices. These mechanisms postulate that there is an induction period followed by a period of rapid deposition and a final stage where deposition levels off. However, IFPEN have discussed this mechanism in terms of liquid phase oxidation rather than deposition. Where they see an initial induction period, where oxygen isn't being consumed followed by a rapid oxidation stage. It is at this point that they postulate that small oxygenated and volatile products are released. During a third stage of oxidation the rate slows as it has reached a steady rate. Interestingly, the third stage is where deposition occurs in the PetroOxy device, just before which an increase in pressure in the PetroOxy test occurs.

The findings from this thesis and literature imply that the induction period in the deposition mechanism combines the slow induction period in the oxidation mechanism, which occur up to roughly 10% oxygen depletion, and the rapid oxidation step where the significant amounts of oxygen is consumed. After this point the primary oxidation products have been formed. These species are partially soluble, and as can be seen by the test carried out in this thesis, this oxidation leads to a colour change in the samples. The PetroOxy tests then demonstrate deposit growth inline with the second stage of the deposition mechanism proposed. However, because of the limitation of sample size and static condition used in the test, the third stage of the deposition mechanism where deposit growth levels out is not reached. This observation seen in previous studies could also be attributed to the loss of heat transfer into the fuel, due to the build up of deposit which has lower heat transfer coefficient, observed through the increase in wall temperature.

This chapter has focused on the effect that the hydrocarbon composition of an aviation fuel has on its thermal stability. This has been done to develop a fundamental understanding of its role in the autoxidation mechanism and aid in future development of the fuel. To investigate this, pure hydrocarbons and fuels with known chemical composition were tested using the PetroOxy device, with it clear that the hydrocarbon composition has a dramatic effect. The ratio of n, iso and cycloalkanes present in the fuel can have an affect,

with the rate of the autoxidation mechanism being affected by the ratio of the CH_3 to CH_2 carbons present in the fuel blend. The response of increasing the percentage of aromatic in a fuel blend is more complex. However, the result of the testing of the JETSCREEN fuels and pure hydrocarbon blends indicate that they act as antioxidants, and exponentially increase the time to complete the rapid oxidation mechanism. The results of testing toluene in isolation point to it oxidising through a different mechanism to the alkanes tested.

This chapter has also presented an extended pseudo-detailed mechanism, where kinetic parameters for the oxidation of individual classes of hydrocarbons have been calculated, using quantum chemistry methods. Constructing the mechanism using this approach, allows us to develop fundamental insight into the chemical mechanism which govern the first stage of oxidation of the hydrocarbons in fuel, and how their chemical structure affects this. Mechanism were also built to simulate the hydrocarbon classes reacting with each other in order to allow us to simulate in larger scale modelling work the antioxidant behaviour of aromatic hydrocarbons. From the testing using the PetroOxy, and the analysis of the products formed, this model needs further expansion to include to formation of carboxylic acids and acid anhydrides.

A clear issue with the mechanism is that these reactions are multi-reference in nature, this is also seen in the literature, and is the reason that modelling thermal stability is such a challenge. This multi-reference nature of the reaction originates from the fact that they are bi-radical systems and as such could be described as a singlet or a triplet ground state. One example of this can be seen in the reaction of RO + R, in the dodecane mechanism, where this reaction was barrierless on the singlet surface but had a barrier of 28.5 kcal mol^{-1} on the triplet surface. The true energy will be somewhere in between and multi-reference methods are required to study this further. The next chapter will apply these methods to studying the reactions of peroxides and peroxyl radicals.

Studying Peroxides using Multi-reference Methods

As was discussed in the previous chapter, the autoxidation mechanism involves a number of reaction steps. These contain bi-radical singlets and systems which are inherently multi-reference in nature. As such, all of the reaction steps in the Pseudo-detailed mechanism presented in chapter 5 should be treated using the multi-reference methods discussed in chapter 2. However, this would be incredibly computationally expensive. These methods scale factors as N^6. This means doubling the number of electrons will make the calculations N^6 times more expensive. Therefore, the feasibility of carrying out these calculations in a reasonable time frame for larger molecules becomes intractable. This chapter will focus on applying these computationally expensive methods to one set of reactions, namely those involving peroxides and peroxyl radicals. However, before presenting the results of this study, it is important to discuss why these reactions were chosen, and to present a more detailed introduction to some electronic structure theory briefly discussed briefly in chapter 2.

The reason for choosing peroxides and peroxyl radicals for this more in-depth and rigorous study, is because of their importance in the autoxidation mechanism. Therefore, understanding their role in this process in a fundamental way is vital. They have been linked to be involved in the initiation, chain-branching and product formation steps in the oxidation process. The reason for this reactivity is due to the peroxides oxygen-oxygen single bond is relatively unstable and will break apart to form two radicals. These radicals can then abstract hydrogens from the hydrocarbon component of the fuel. Peroxides can initiate the autoxidation process, or as they are expected to be formed in the oxidation mechanism, the two radicals formed from the oxygen-oxygen bond splitting can form a chain branch in the mechanism. The peroxides and peroxyl radicals have also been linked to play a role in the reactions which form the primary oxidation products, which can then begin to agglomerate together due to their polarity, and react further to form the insoluble species which cause the gums and deposits. These reactions are complex and can go through a number of possible mechanism, but both involve 2 peroxides or

peroxyl radicals reacting together to form polar non-radical products. These reactions are outlined in the figure 5.1.

$$ROOH \longrightarrow RO^\bullet + {}^\bullet OH$$
$$2ROOH \longrightarrow RO^\bullet + ROO^\bullet + H_2O$$
$$RO^\bullet + ROO^\bullet \longrightarrow R=O + ROOH$$
$$2ROO^\bullet \longrightarrow RO^\bullet + RO^\bullet + O_2$$
$$2RO^\bullet \longrightarrow R=O + ROH$$
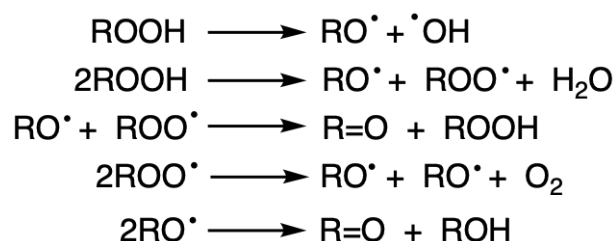
Fig. 5.1: proposed chemical reactions involving peroxides

These reaction have been extensively researched previously, both experimentally and computationally, but despite this there are some unanswered questions. One issue with previous research into the reactions of peroxides is in the treatment of the electronic spin states of the peroxides and peroxyl radicals during the reactions.[294, 295] If we take the case of the homolytic fission of a peroxide, which can be seen in figure 5.2. When the two oxygens are bonded, the 2 electrons in the bonding orbital are of the opposite spin to each other, due to the Pauli exclusion principle. This means that the peroxide is in a singlet multiplicity state. The multiplicity of a molecule can be determined from the total spin angular momentum (S) of the system, 2S+1 where S is 0. For the case of a molecule with every electron paired up, this gives 1, or a singlet as the multiplicity. This is the sum of the spin states of the electrons in the system. As electrons can have α or β spin, and each orbital can have one α and one β spin electron in it, the multiplicity is usually the number of unpaired electrons in the system.

$$ROOH \longrightarrow RO^\uparrow \quad {}^\downarrow OH$$
Singlet Multiplicity
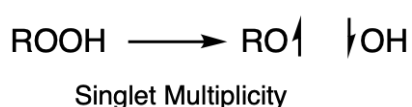
Fig. 5.2: spin configuration of the homolytic fission of peroxides

The reason that this is important for the homolytic fission of peroxides, is that when the oxygens are bonded they are paired in the same spatial orbital, but the opposite spin configuration. When the bond is broken they are now no longer paired together and thus we have formed 2 unpaired electron and a biradical system. Instinctively this means that we consider the multiplicity of the system to now be a triplet. However, chemical reaction must obey all physical principles, including the conservation of momentum. The conservation of spin angular momentum is also required for a reaction to be allowed. This means

that the overall spin state of the system cannot change during a reaction, and as electron spin flips are forbidden, meaning there cannot be a change from singlet to triplet multiplicity during the homolytic fission of the peroxide. Instead the system must be treated as an open shell singlet, with the two unpaired electrons in the opposite spin states, centred on the individual fragments.

This makes the problem inherently multi-reference in nature and using single reference methods such as Hartree-Fock, or methods with high chemical accuracy such as coupled cluster theory (CCSD), to investigate these reactions computationally will fail. This is due to the standard implementations of these theories being unable to treat the α and β electrons separately and produce the correct electronic structure. When a bond is homolytically broken in Hartree-Fock theory, instead of it being treated as a covalent bond, it has ionic properties with a positive and negative fragment formed. This inability to describe the electronic structure in a qualitatively correct way is the origin of the static electron correlation discussed in chapter 2.

The failure to describe the problem correctly causes a number of issues. The first is a fundamental issue, as not describing the reactions with the correct theoretical approach means that we will lack knowledge of the true mechanism, or of the products formed. The other is a more practical issue. The treatment of the homolytic fission of peroxides as an ionic problem means that the energy needed to break the bond will be overestimated. This is due to the two ionic fragments being more attached to each other than the two radical fragments would be due to long range coulombic interactions. As such, any model developed using these theories would overestimate the barrier to reaction, and thus would demonstrate slower rates of autoxidation than would be seen in experimental studies. A diagrammatic way of showing static correlation can be seen in the figure 5.3, where we can see that the energy calculated using a single reference method like Hartree-Fock fails describe the long range states correctly, and as such the energy never reaches an asymptote.

As is seen in figure 5.3, the inclusion of a static correlation improves the shape of the potential energy surface when the bond is breaking. However, as discussed in chapter 2, static correlation correction to the wave function does not fully describe the true potential energy surface, due to the mean field approach. This is called dynamic correlation, and refers to the errors in describing the motion of the electrons in models. It's caused by the electrons
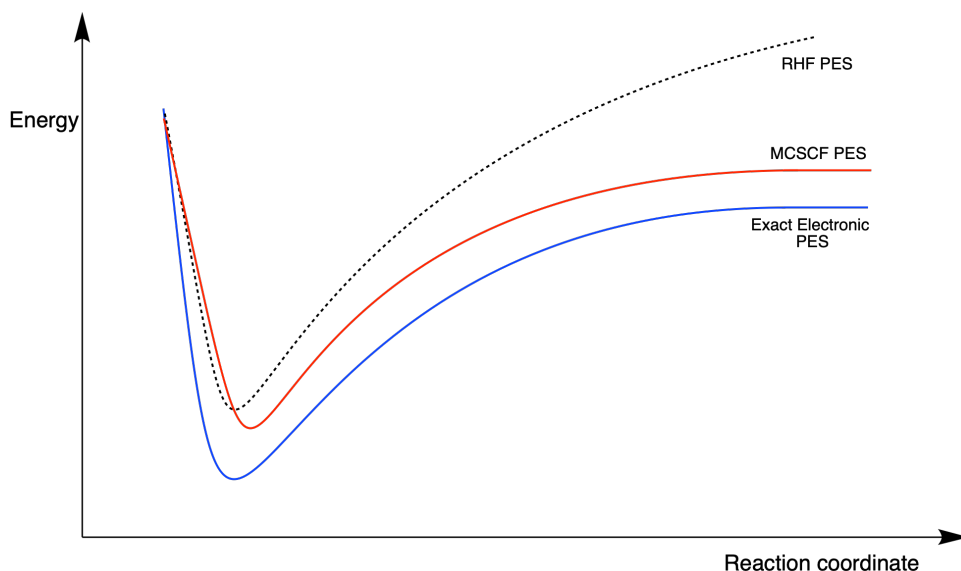
Fig. 5.3: potential energy surface (PES) of HF and MCSCF energy, demonstrating static correlation

being treated as an average of positions. This means that the two electron terms are overestimated, such as the coulombic and exchange components of the of the Fock operator, as they are not being treated as point charges. This causes the repulsive interactions at the point charges to be lower than in reality for them to be higher in the space between the points. As such, the electrons will take up unphysical locations, and the energy of the system will be higher than the true energy of the system. This is important if we consider what is physically happening in the homolytic fission of a peroxide. The two fragments with their respective electrons are being pulled apart. This involves calculating the position of the electrons as the orbitals change during the fission. Treating them with this mean field approach leads to overestimation's in the energy required to break the bond as electrons in the two fragments will be interacting with each other in a none physical way. If we look at our imagined potential energy surface from 5.3, again in figure 5.4, we can see that inclusion of static and dynamic correlation gets us in principle close to the true energy of the system.

The issue is that, as discussed this is prohibitively computationally expensive, as it involves carrying out full configuration interaction (CI) at the basis set limit for each point on the energy surface. For anything but diatomic molecules carrying out these calculations are not possible, and as such we need to carry out limited CI calculations with smaller basis sets, hence some of the
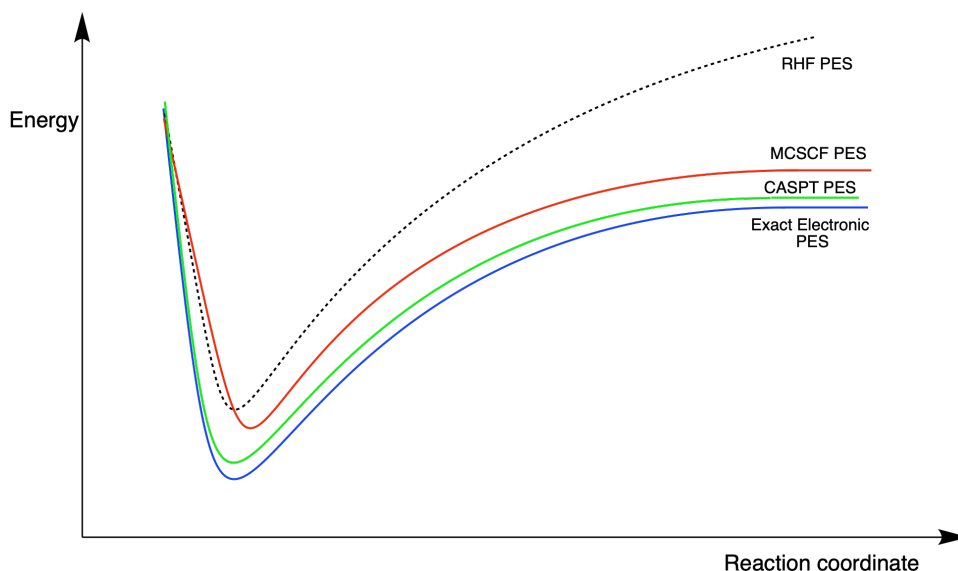
Fig. 5.4: potential energy surface (PES) of HF, MCSCF and CASPT energy, demonstrating the effect of static and dynamic correlation

correlation energy is not recovered and we do not calculate the exact potential energy surface.

For the self-reaction of peroxides, seen in figure 5.5, we can see that there is no issue due to there being no change in multiplicity between the reactants and the products. During this reaction two peroxides form another peroxide, a carbonyl, and a water molecule. Thereby providing a route to breakdown peroxides into non-radical products. However, when the rules of the conversation of spin angular momentum is applied, we can see that the intermediates formed during this process are open shell diradicals. This includes the transition states and as such locating them during optimisation searches using single reference methods is particularly difficult. The self-reaction of peroxides can progress through 2 mechanisms, a two step mechanism, where high energy peroxyl and alkoxy radicals are formed. The reaction can also proceed through a single step concerted reaction. During this mechanism, the hydrogen of peroxide 1 moves on to terminal oxygen of the peroxide 2, and extracts a hydrogen from the carbon site of peroxide 2. This leads to the formation of the products in a single step. However, this transition state is likely to be higher in energy due to it needing to be highly ordered and conformationally strained.

The self-reaction of the peroxyl reactions is more complex and presents some issues with current models presented in the literature. If we look at this
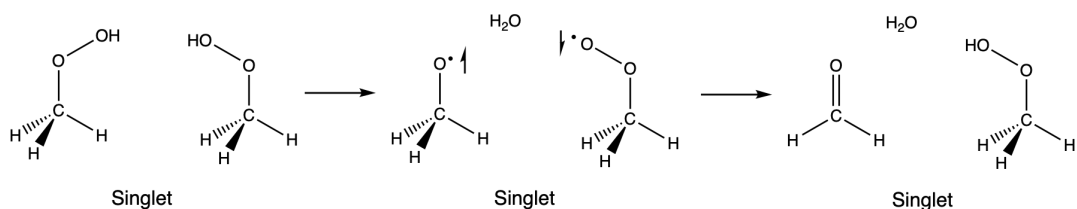
Fig. 5.5: Multi step reaction pathway between two peroxides radicals, showing the role that an open shell diradical has in the reaction

reaction in more detail, seen in figure 5.6, the issues become clear. Like with the self-reaction of peroxides, the mechanism can proceed through a multi step process, or a concerted mechanism. For the four oxygen intermediate to form the two peroxyl radicals must have opposite spin. Thus, the system has singlet multiplicity which it must maintain throughout. When the tetraoxide intermediate decomposes the unpaired electronic spins must add up to a singlet. As such, either a very high energy unstable triplet carbonyl is formed, or a highly reactive singlet oxygen. Oxygen is normally found in its triplet form. However, singlet oxygen can be formed through chemical reactions. As singlet oxygen has the same multiplicity as the hydrocarbons in the fuel it can react rapidly and accelerate the oxidation process. Coupled to this, the products of the self-reactions of peroxides are polar oxygenated hydrocarbons that can react together to form insoluble gums and deposits. Because of this incredible autoxidation acceleration potential, understanding the mechanism and electronic structure of this reaction is of vital importance to the future development of aviation fuel, and being able to understand how it behaves under thermal stressing.
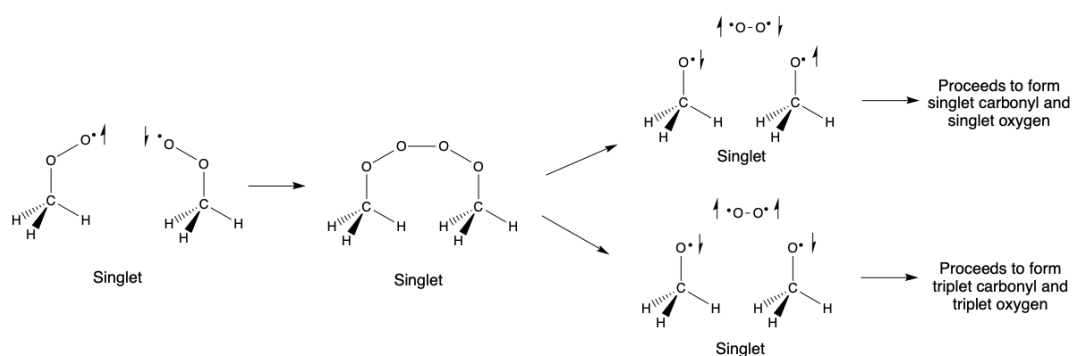
Fig. 5.6: Multi step reaction pathway between two peroxyl radicals, and the spin configurations of the possible pathways

This chapter will provide some solutions to these issues, by applying high level computational techniques, such as multi-reference self consistent field

theory (MCSCF) and complete active space perturbation theory (CASPT). Broken symmetry spin unrestricted DFT (BS-UDFT) will also be used because of the high computational expense of theses methods. This implementation of DFT allows the α and β electron and orbitals to be treated independent from each other. This is achieved by symmetry breaking the wave function, through mixing of the highest occupied molecular orbitals (HOMOs) and lowest unoccupied molecular orbitals (LUMOs), destroying the αβ and spatial symmetry. Thus, the α and β orbitals can have different spatial components to the orbitals. In the case of the homolytic fission of a peroxide, the α and β electrons can be on separate oxygen atoms at some distance apart. BS-DFT can still suffer from spin contamination, which is the artificial mixing of spin states rather than the real mixing of spin-orbit interactions, as the ground state spin has some components of the excited state wavefucntion. Spin contamination can be determined from the expectation value of the total spin operator. If we take the doublet spin state the expectation value would be $\langle S^2 \rangle = \frac{1}{2}(\frac{1}{2} + 1) = 0.75$. However, it could be significantly higher than this if the system has high multi-reference character and thus BS-DFT cannot be described using these methods.

BS-DFT is still single reference and as such does not completely describe the multi-reference reactions, but is does greatly improve the description at a fraction of the computational cost. For this reason, the BS-UDFT calculations will be used to improve the description of the reactions of peroxides and peroxyl radicals from chapter 5, as carrying out MCSCF and CASPT calculations would be computationally intractable at this point. This allows us to better understand the complex electronic structure of these systems and get us closer to the true kinetics of the reactions. Similarly to chapter 5, this methodology will be applied to n-alkane, cycloalkane and aromatic systems, in order to understand the affect of changing hydrocarbon structure has on the relative rates of these reactions.

5.1 The homolytic fission of Peroxides

The homolytic fission of peroxides is a vitally important reaction in the autoxidation of aviation fuels and appears in most kinetics models. However, as we have discussed above, this is an inherently multi-reference reaction. Thus, it is important we apply multi-reference methods to this problem. The first step

was to select and work with a test system to troubleshoot any issues with the methodology and to understand the physical mechanisms at play.

Methyl peroxide

Methyl peroxide was selected for this testing as it is the smallest hydrocarbon peroxide species. An initial test of the multi-reference nature of the problem can be seen by showing the singlet and triplet potential energy surface using the standard implementation of DFT in the Gaussian 09 program, seen in figure 5.7. These calculations were carried out with the moderately sized basis of 6-311G (d,p). Moreover, the C-O-O-H dihedral angle was frozen to avoid hydrogen bonding in the separated fragments.
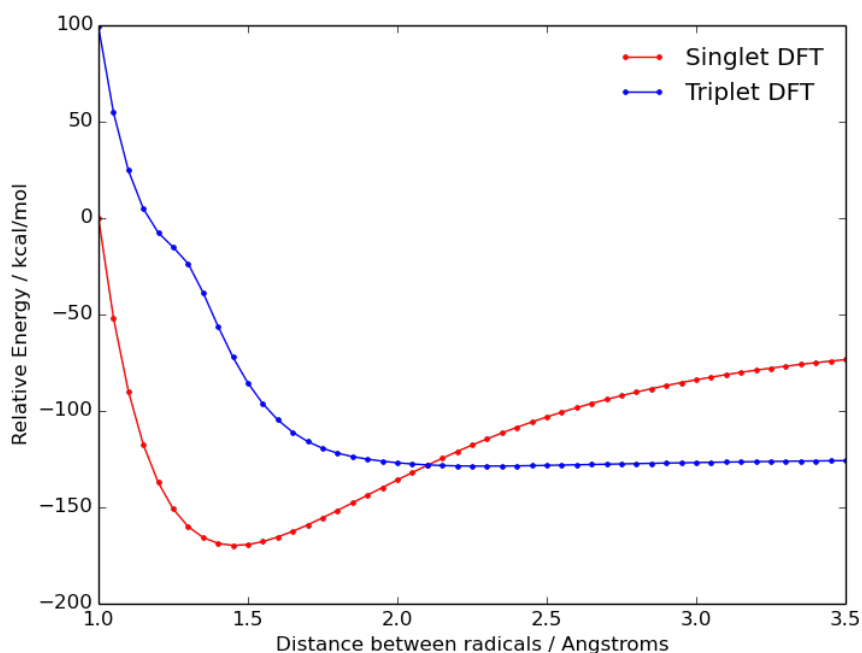
Fig. 5.7: DFT scans of the singlet and triplet surfaces for the homolytic fission of methyl peroxide, calculated at the B3LYP/6-311G (d,p) level of theory.

As would be expected, the singlet surface is the lowest energy when the peroxide oxygen-oxygen is at its equilibrium bond distance. When the bond is extended the triplet potential energy surface drops below the singlet surface. From this point the singlet energy keeps increasing, whereas the triplet energy decreases to an asymptotic value. This should not happen as the singlet surface should be a range separated diradical. Moreover, electrons

are fermions and thus indistinguishable. therefore, quantitatively the two surfaces should be degenerate at long range. However, the singlet and triplet surfaces do not converge to the same point, because the singlet system has significant ionic character and does not converge towards an asymptote. The physical reason for this is that the calculation tries to pull apart two oppositely charged fragments, which is energetically unfavourable, and thus leads to a synthetically high energy barrier to homolytic fission. The discontinuity in the triplet surface at bond distances below 1.3 Å is due to the O-O bond approaching the covalent radius.[296] This discontinuity can also be seen in some of the higher level calculations. However, as we are correctly describing the system at the bonding distance and of the separated fragments, this is has minimal effects on the results.

Because the standard implementation of DFT fails to describe the homolytic fission of peroxides BS-UDFT was used to improve the results for the spin unrestricted singlet surface. These calculations were carried out with the larger basis set cc-pVTZ, and the oxygen-oxygen bond distance was scanned to 4 Å, the results can be seen in figure 5.8. The results were qualitatively and quantitatively the same as those produced using the standard implementation of DFT, with the singlet failing to reach an asymptote value because it still has some ionic character. The reason for this is that the spin contamination discussed previously, is particularly high in these species. Thus, BS-DFT breaks down in describing this highly multi-reference system.

To correctly model this system, the MOLPRO program was used to carry out MCSCF and CASPT2 calculations, as the implementation of multi-reference methods in this program is particularly efficient. As these methods are computationally expensive they were carried out with the smaller def2-SVP basis set as implemented in MOLPRO. Unlike DFT, MCSCF is not a black box method. As a consequence, a number of parameters need to be choosen. The most important of these parameters is the active space. This is the number of electrons that are included in the CI component of calculations, and consequently the number of orbitals to be used in the CI portion of the calculation. The way that this is usually decided is through a second order Møller-Plesset perturbation theory calculation (MP2). The natural orbitals used in perturbation theory describe the electron occupancy well. As such, the converged orbitals generated in the MP2 calculations can be used to determine the occupation of the orbitals in MCSCF, and generate the active space. Orbitals with occupancy significantly below 2 indicate that they have
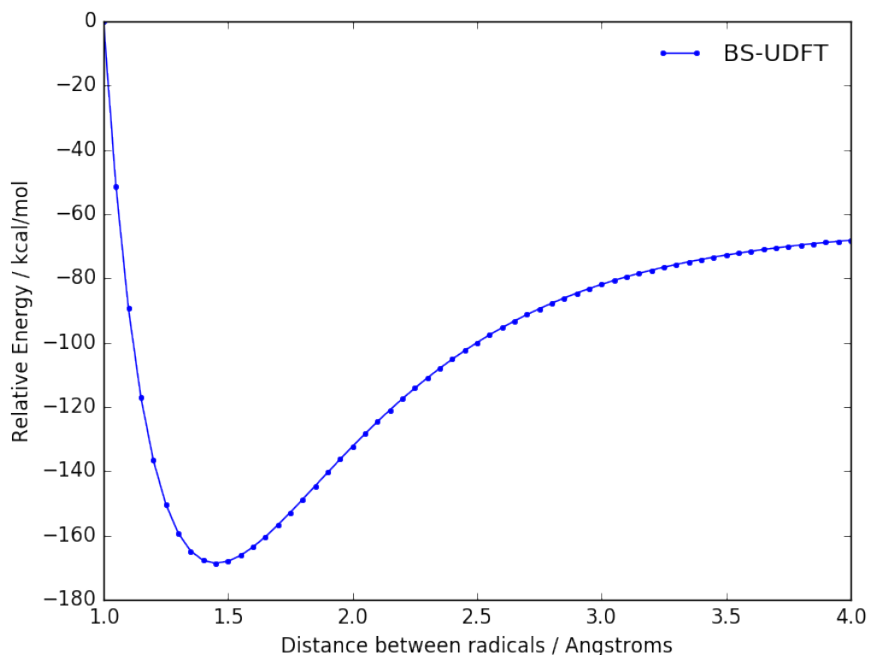
Fig. 5.8: BS-UDFT scan of the singlet surface for the homolytic fission of methyl peroxide, calculated at the UB3LYP/cc-pVTZ level of theory.

partial occupancy. These are not described correctly by single reference methods, and are important to be included in the active space.

In practice, having as large an active space as possible would be best. However, this would be very expensive computationally. For the methyl peroxide system, this would mean that 26 electrons would be included in the active space with a minimum of 14 orbitals, this would take an unfeasible amount of computational time. This active space would also likely be insufficient to describe the bond breaking because only one unoccupied orbital being included. Between 2 and 6 unoccupied orbitals are usually needed to correctly model this process. This could produce an active space of 26 electrons and 19 orbitals. For this reason not all electrons in the system are included in the active space. We can cut this number down by only including those likely to take part in the bond breaking. This is decided from the MP2 natural orbital occupancy and energies, with low energy non-interacting orbitals such as the hydrogen 1s, not included. For the methyl peroxide system, the number of occupied orbitals used can be constrained to 8, This means 16 electrons are included in the active space. Please note that if 8 occupied orbitals and 2 unoccupied orbitals were selected to take part in the active space, this would

be written as CAS(16,10). This is the labelling system used in the rest of this chapter. A MCSCF scan with active space CAS(16,10) can be seen in figure 5.9. These were all carried out with natural orbitals and the standard MOLPRO basis set, avPDZ, and is compared to the Hartree-Fock energy at the same geometry.
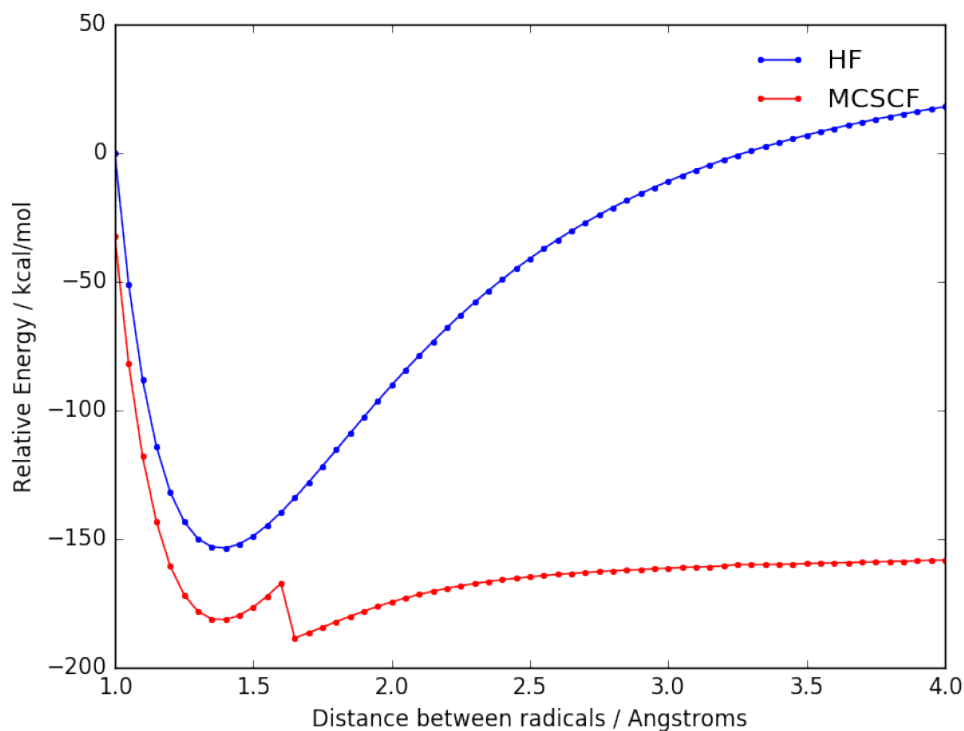
Fig. 5.9: MCSCF scan of the singlet surface for the homolytic fission of methyl peroxide, with and active space of (16,10), compared to Hartree-Fock.

The results of this scan demonstrates that the selection of active space can have a large affect on the qualitative results, such as the shape of the potential energy surface, and quantitative results such as the predicted energy barrier to fission. Figure 5.9 shows that CAS(16,10) has a discontinuity in the MCSCF scan, which is not present in the HF scan, indicating that it is not a geometry change but instead an issue with the active space. This can be seen in the sharp change in the orbital energies and printed occupations between the 2 steps. When MCSCF calculations with an active space of CAS(16,11), and the 2 highest unoccupied orbitals have their occupancy restricted to either 0 or 2, the results produced a potential energy surface with the correct asymptote and produced a barrier to fission in this case in agreement with the literature, with a value of 46 kcal mol^{-1}.[11] However, this does not qualitatively describe our system correctly, as the resulting CI vectors demonstrated significant ionic

character. Hence the importance of checking the qualitative and quantitative results of MCSCF calculations.

One parameter that can have a large affect on the results in MCSCF calculations is the type of orbitals that are selected for generating the active space. Up to this point natural orbitals generated by the MP2 calculations have been selected to generate the active space. However, as seen in previous calculations, they fail to describe the wave function and the CI vectors correctly. Canonical orbitals, or the pseudo-canonical orbitals implemented in MOL-PRO, can also be used in the MCSCF calculation. The power of canonical orbitals is that they do not enforce double occupancy in singlet ground state. Further calculations were carried out to decide upon the best set of orbitals for continuing this study with. MCSCF scans were carried out on a set of active spaces, CAS(12,8) and CAS(10,8), using natural orbital and canonical orbital variants of the basis set. The scans are given in figures 5.10 and 5.11. The quantitative results obtained were analysed, as were the CI vectors, to determine the occupancy of the orbitals and location of the unpaired α and β.
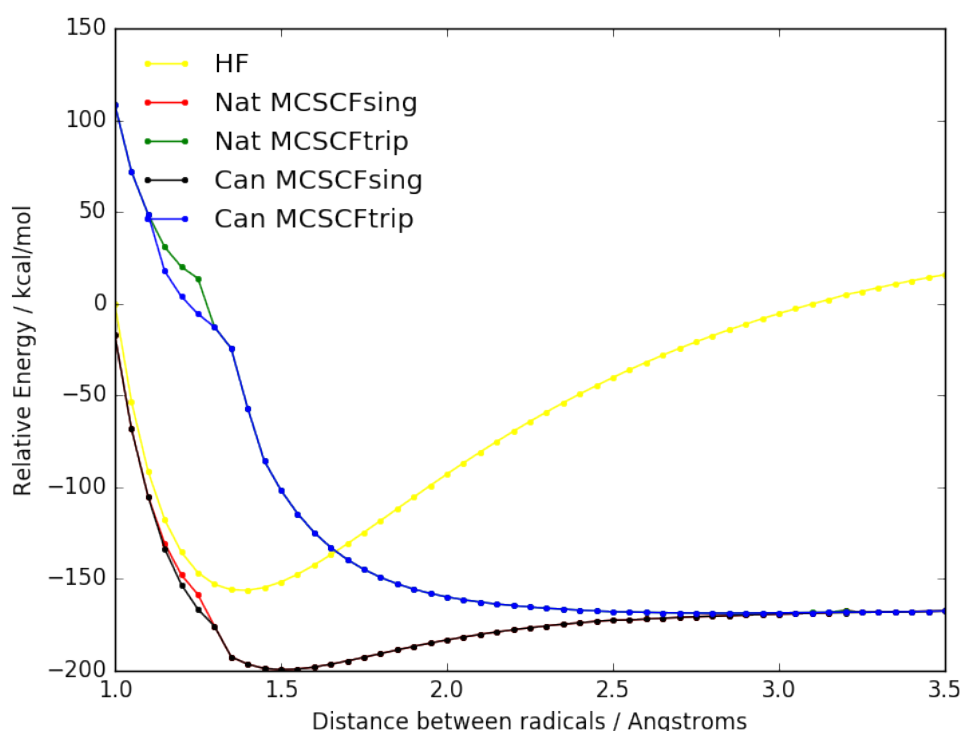
Fig. 5.10: Scan of the homolytic fission of methyl peroxide, using natural and canonical orbitals, and an active space of (12,8)
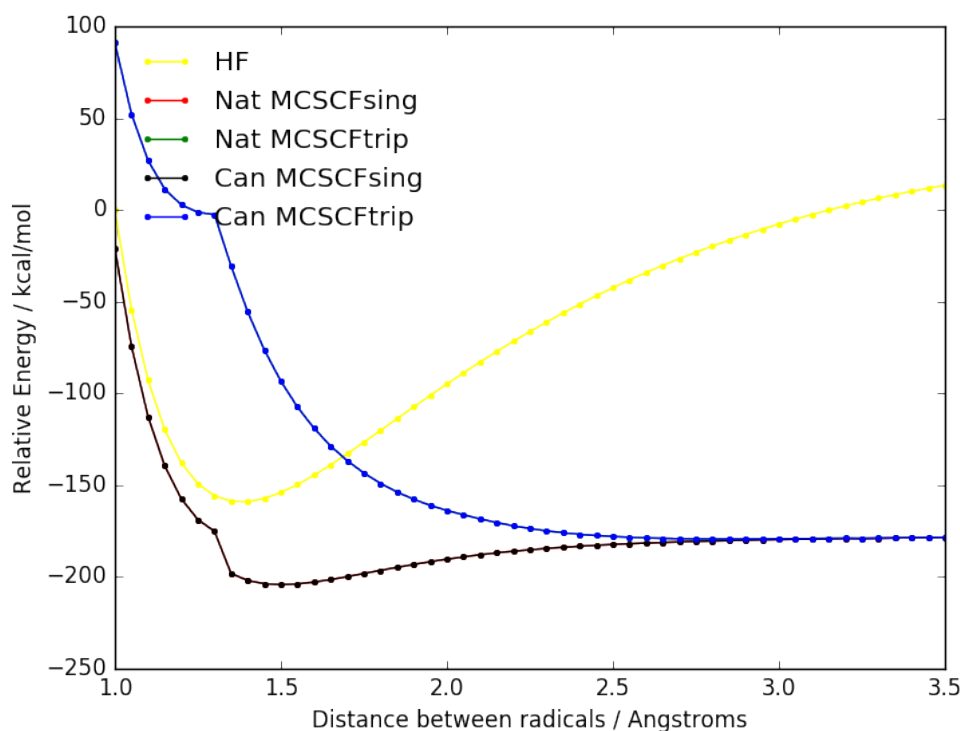
Fig. 5.11: Scan of the homolytic fission of methyl peroxide, using natural and canonical orbitals, and an active space of (10,8)

The singlet and triplet surface for both the CAS(12,8) and CAS(10,8) active spaces were generated. The results of these scans indicate that as the two fragments are pulled apart the singlet and triplet surfaces converge together. This gives confidence that the MCSCF level of theory is correctly describing the system. given that, at long range separations the singlet should have the same energy as a triplet. The second observation, is that the difference in energy between the singlet and triplet surfaces generated using the two sets of orbitals is trivial, indeed they give quantitatively the same result. The two types of orbitals (natural and canonical) used to generate the active spaces also achieved the same quantitative results when predicting the barrier to homolytic fission, with 25 kcal mol^{-1} for the CAS(12,8) scan and 35 kcal mol^{-1} for the CAS(10,8). The smaller active space of CAS(10,8) actually achieved the better agreement with literature values. As such, a smaller active space would be preferential given the computational cost attached to increasing the active space unnecessarily.

Whilst analysis of the energies gives similar results between the canonical and natural orbitals, the CI vectors generated during the last step of the scan for

each set of orbitals, seen in table 5.1, demonstrates that the qualitative results for the two systems are different. The natural orbitals produce closed shell singlets. The linear combination of the weighting of the two most important configurations results in single occupancy of the frontier orbitals, allowing it to match the triplet state. On the other hand the most important configurations for the canonical orbitals are antisymmetric singularly occupied orbitals. These two sets of CI vectors produce the same result, but the canonical set is qualitatively more correct and allows us to understand the electronic structure of the problem in a more intuitive way.

Tab. 5.1: CI vectors of for CAS(10,8) with Canonical and natural orbitals.

CI vectors for singlet state			
Canonical orbitals		Natural orbitals	
2222ba00	-0.6933	22222000	0.7071
2222ab00	0.6933	22220200	-0.6914
22b2a200	0.0848	22202020	-0.0544
22a2b200	-0.0848	22200220	0.0532
2202ba20	0.0508	22022002	-0.0506
2202ab20	-0.0508		
CI vectors for triplet state			
Canonical orbitals		Natural orbitals	
2222aa00	0.9805	2222aa00	0.9890
22a2a200	0.1199	2220aa20	-0.0761
2202aa20	-0.0719	2202aa02	-0.0707

Using canonical orbitals also allows us to investigate the correctness of the active space selected and the results obtained. This is important as limiting the size of the active space below full CI can introduce inconsistencies in the description of the wave function as a function of distance. As a consequence inconsistent results will be obtained. This can be seen in the results of the potential energy surfaces and CI vectors of the two active spaces using the canonical orbitals, CAS(10,8) and CAS(12,8), in figure 5.12 and table 5.2. The CAS(12,8) active space more accurately predicted the barrier to homolytic fission than the CAS(10,8), getting close to the 45 kcal mol^{-1} experimental value. However, the CI vectors show that a significant component of the singlet states, approximately 0.38 of the total contribution, originates from a combination of doubly occupied frontier orbitals. This introduces significant ionic character into the wave function which artificiality increase the energy of the system. As such, despite the prediction of the barrier to homolytic fission being closer to the experimental value, this active space is incorrect to

continue with as it is partially un-physical. This demonstrates one of the main reasons that MCSCF methods are not black box, as selection of orbitals and active space can have a large affect on the results and their validity.
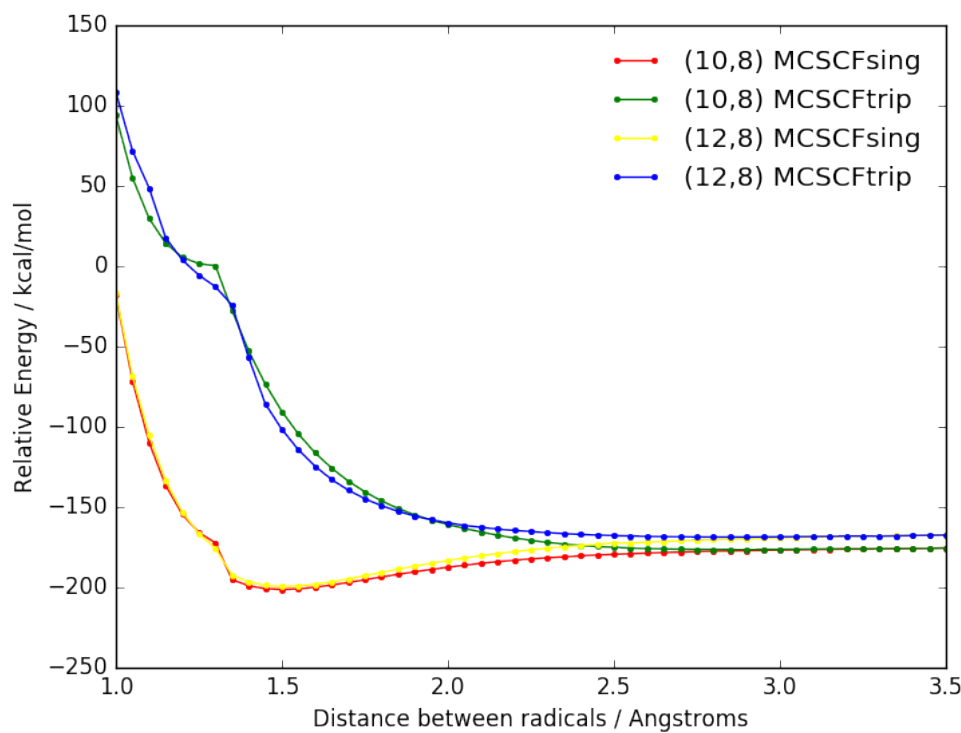
Fig. 5.12: MCSCF scan of the homolytic fission of methyl peroxide, comparing the results for the active spaces (12,8) and (10,8) using the canonical def2-SVP basis set.

The most important result from the physically correct CAS(10,8) active space is that it underestimates the barrier to fission by 10 kcal mol^{-1}. However, we know that this is due to the MCSCF method only recovering the static correlation, and poorly treating the dynamic correlation. Incorporating the movement of the electrons at the equilibrium bond distance, and as the bond is being pulled apart, is important to describe the breaking of a chemical bond. As such, the second order Rayleigh-Shrödinger perturbation corrections was applied to MCSCF calculations, referred to as CASPT2. The inclusion of dynamic correlation into the system allowed us to get within 2 kcal mol^{-1} of the quoted literature value of 46 kcal mol^{-1}, predicting the barrier to be 48 kcal mol^{-1}, using the same active space.[11] The results of the MCSCF and CASPT scans, with an active space of CAS(10,8) and canonical orbitals, can be seen in figure 5.13. This is within chemical accuracy and also allows us to have confidence in our selection of active space, as it appears to describe the

Tab. 5.2: CI vectors for CAS(10,8) and CAS(12,8) active spaces with canonical orbitals.

CI vectors for singlet state			
CAS(10,8)		CAS(12,8)	
2222ba00	-0.6933	2222ba00	0.5940
2222ab00	0.6933	22222ab0	-0.5940
22b2a200	0.0848	22202200	0.3868
22a2b200	-0.0848	22222020	-0.361
2202ba20	0.0508		
2202ab20	-0.0508		
CI vectors for triplet state			
CAS(10,8)		CAS(12,8)	
2222aa00	0.9805	2222aa00	0.9928
22a2a200	0.1199	2220aa20	-0.0812
2202aa20	-0.0719		

system qualitatively and quantitatively correctly. The results also demonstrate how poorly the active space and orbitals used are at describing the system when the oxygen-oxygen bond distance is below the covalent radius in the triplet state. The large jump in energy in the CASPT triplet surface is a result of a triplet state being lower in energy at this point of the surface than our target one, so was calculated in the CASPT instead. As the active space poorly describe it at this point, it results in a large discontinuity, and the error at this point of the surface. However as stated before, this region is not of interest to this work, nor does it play a role in the convergence of the system.

An interesting aside is that the energy required to make the vertical electronic transition from the singlet state to the triplet state at bond equilibrium distance of 1.45 Å is 4.2 eV, but is spin forbidden. This corresponds to a wavelength of 295 nm, and once the peroxide is on the triplet surface, fission of the bond is barrierless. This wavelength is in the UV B range, which has been linked to causing the initiation of radical reactions in the fuel.

The results of this study clearly indicate that MCSCF and CASPT2 are very powerful tools for investigating the electronic structure and kinetics of radical reactions in the fuel, as they are intrinsically multi-reference. In this study, the experimental values for the homolytic fission of methyl peroxide were able to be reproduced. Moreover, from this a methodology for future study and greater understanding for the reasoning for this was gained. This give us the
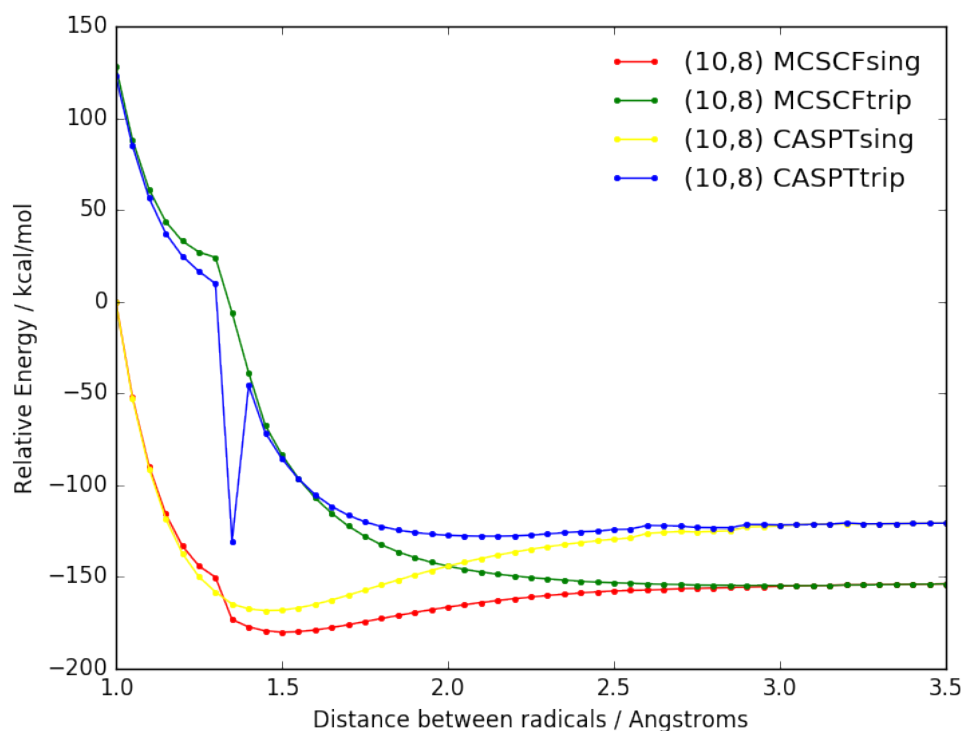
Fig. 5.13: MCSCF and CASPT2 scan of the homolytic fission of methyl peroxide, using canonical orbitals, and an active spaces of (10,8)

confidence to apply this methodology to other systems with consistency, by analysing the CI vectors, geometry and energy barrier. This methodology can now be applied to the homolytic fission of peroxides derived from other hydorcarbons, namely cyclohexane and toluene.

Cyclohexane peroxide

A BS-UDFT scan using the B3LYP functional and cc-pVTZ basis set was carried out in Gaussian 09, the results of which are presented in figure 5.14. The barrier to homolytic fission of the oxygen-oxygen bond was 65 kcal mol^{-1}. However, the carbon-carbon bond next to the peroxide centre on the cyclohexane ring was extended and started to dissociate during the scan of the O-O bond distance. This would lead to an increase in the energy of the system increasing and is the most likely cause of the high energy barrier. This presents a problem, as to achieve the convergence using BS-UDFT, a number of the internal coordinates such as the COOH and CCOO dihedrals

were frozen. This will also result in an increase of the energy of the system and an increased barrier to fission. The unrestricted scan could not be carried out, as this is a complex geometry, which has some multi-reference nature to the problem. As such, the Gaussian program would alter the geometry to achieve a lower energy, but un-physical solution
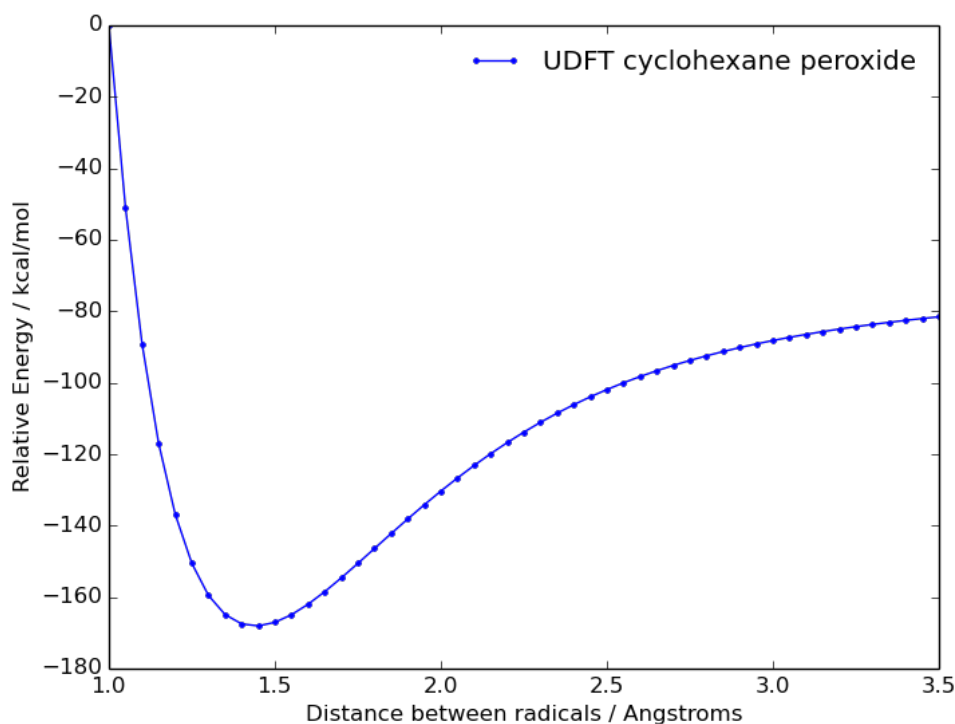
Fig. 5.14: Scan of the singlet surface for the homolytic fission of cyclohexane peroxide using BS-UB3LYP/cc-pVTZ. The geometry was highly constrained to achieve convergence, and lead to partial C-C bond breaking in the ring.

The results from the scan are coupled with the change in the electron density throughout the scan. At the equilibrium bond distance the electron density is evenly distributed across the molecule, with slight increases on the terminal oxygen and a decrease on the carbon bound to the oxygen. This will be caused by the electronegativities of the respective atoms and those they are bonded to. When the bond has been fissured and the O-O distance is at its greatest extension, the electron density increases on the oxygen atoms and decreases on the carbon atom bound to the oxygen. However, these values only represent the overall electron density, and not the spin density or the electronic structure of the broken bond state. For this reason, MCSCF and CASPT2 are needed to be used to better describe the system, and understand

the multi-reference nature of the problem. The BS-DFT calculations also fail to accurately predicted the bond strength, with similar systems demonstrating a barrier of approximately 30-40 kcal mol^{-1}. As such the data produced is of insufficient accuracy for use in kinetic mechanisms. At the time of writing, the CASPT2 calculations investigating the homolytic fission of the cyclohexane peroxide are incomplete, with there being issues in the selection of active space and the coordinate system used to description the molecule. However, they are being prepared for future publication.

Toluene peroxide

A BS-UB3LYP scan for the toluene peroxide system with the cc-pVTZ basis set was carried out in Gaussian 09, which can be seen in figure 5.15. Two surfaces are plotted in figure 5.15. In the first one calculated, represented by the blue data, an unrestricted scan was carried out. However, in this scan as the O-O bond was extended the C-C-O angle decreased to form a cyclic epoxide group. This would cause the aromaticity of the system to be disturbed, so is an artefact of the single reference method being used, as this is highly unlikely to happen. As such the C-C-O angle and C-O-O-H dihedral angle, as otherwise the OH fragment formed water, was restricted and a second scan was carried out. The results of this are shown by the red data. Due to geometry being restricted, the energy of the system is higher, seen in the energy of the equilibrium bond length being higher than for the unrestricted scan. The scan also fails to reach an asymptote and has a barrier to fission of approximately 90 kcal mol^{-1}. This is exceptionally high, and as aromatics have been shown to have lower barriers to fission, must be incorrect.[11]

The electron density changes in the system as the O-O bond is broken highlights this issue, with aromaticity clearly being effected by the methodology selected. In the bound state, the electron density was based mostly on the oxygens and there was a partial positive charge on the carbons bound to them, there was also partial negative charges in the ortho and para positions of the methyl peroxide group. This stands up to basic chemical reasoning as the resonance structures would place electron density in those positions. However, as the O-O bond was broken, there was no particular trend in the location of the electron density on the aromatic ring. The partial negative charges on the oxygens increased and the partial positive charge of the methyl carbon decreased, but the two ortho position had different partial
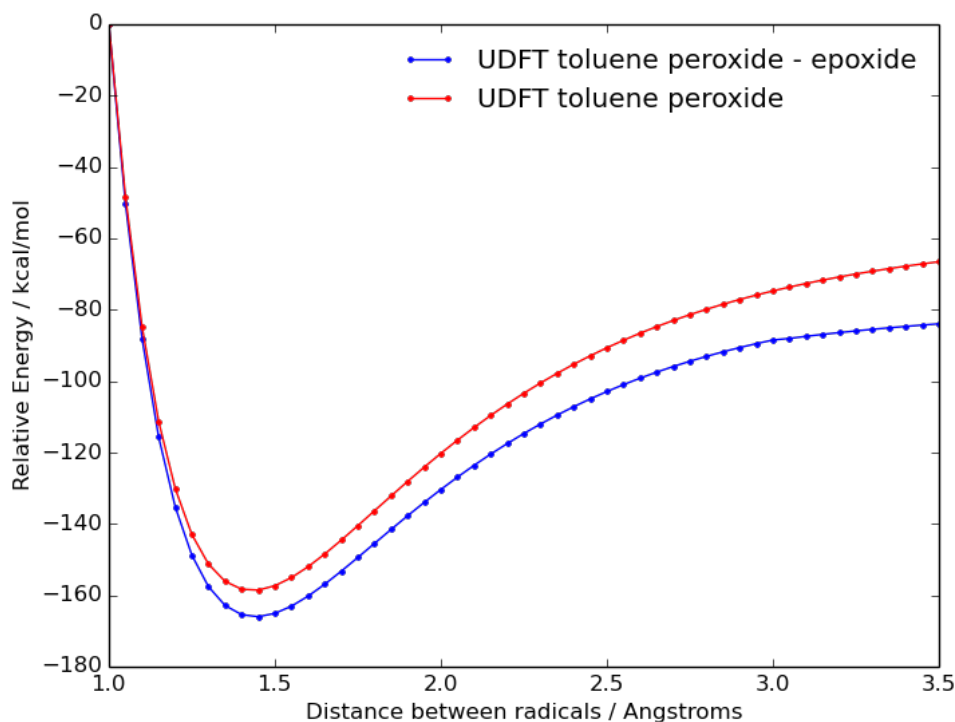
Fig. 5.15: Scan of the singlet surface for the homolytic fission of toluene peroxide using BS-UB3LYP/cc-pVTZ. It was found that is the molecule was not constrained during the search, an toluene peroxide was formed, as such a contained scan was carried out.

charges, and one was the same as the meta positions. This does not stand up to chemical reasoning, and suggests that method is failing to describe the system. Because the numerical results and the electronic structure description being of insufficient accuracy to understand, MCSCF and CASPT2 will be used to improve the results. At the time of writing, the CASPT2 calculations investigating the homolytic fission of the cyclohexane peroxide are incomplete, with the issue being caused by the coordinate system used to describe the molecule. However, they are being prepared for future publication.

5.2 The self-reaction of Peroxides

As discussed previously, in this chapter and in chapters 3 and 4, the self-reaction of peroxides is an important reaction in the oxidation of hydrocarbons. However, the exact mechanism of this reaction is not very well understood, in particular it is not clear whether it proceeds through a multi-step mechanism

with a number of intermediates and transition states, or through a single concerted mechanism. The multi-step mechanism will involve the generation of radicals in the fuel. Moreover, it is a complex multi-reference electronic structure problem, whereas the concerted mechanism forms no radicals during the reaction. As such, an understanding of which mechanism is dominant, and the implications that this has for the kinetics of autoxidation is important. To investigate this, BS-UDFT calculations were carried out to optimise the stationary points of the reaction surface, and investigate the kinetics of the mechanism.

Methyl peroxide

As with the homolytic fission of peroxides, the first step was to investigate this reaction using our test system from the previous section, methyl peroxide. The two-step mechanism and a one-step concerted pathway were investigated. These calculations were carried out in the Gaussian 09 program using the BS-UB3LYP/cc-pVTZ/PCM=heptane level of theory, with the HOMO and LUMO orbitals mixed in order to help optimisation of the higher energy intermediates and transition states, which is expected to be an open shell singlets. The results can be seen in figure 5.16.

The results of these calculations demonstrate clearly that these reactions are feasible in the fuel, as a barrier to reaction of +33.6 kcal mol^{-1} for the multi-step mechanism and +37.8 kcal mol^{-1} for the concerted mechanism. This is lower than that for the homolytic fission of peroxides. This means that, when the concentration of peroxides in the fuel increases, this deactivation mechanism is likely to become the dominant pathway. The calculated energy difference of the barriers between the two possible pathways is 4.2 kcal mol^{-1}. As such, at the temperatures present in the thermally stressed fuel, 99% of the reaction will proceed through the two-step mechanism. When we interrogate this two-step mechanism more, it becomes clear that the products of the first step are highly reactive alkoxy and peroxyl radicals. These could react together to form non-radical products. On the other hand they could react just as easily with other species in the fuel. As both of these outcomes are possible, and will depend on the level of mixing in the fuel system as well as the kinetics of each single step reaction, the result of the reaction of two peroxides could be chain branching and the formation of two radical chain reactions.

Fig. 5.16: BS-UDFT reaction surface of the self-reaction of peroxides via the concerted and two step mechanism, carried out using the Gaussian 09 program at the BS-UB3LYP/cc-pVTZ/pcm=heptane level of theory. Reprinted with permission from [297].

It is noted that the transitions states and diradical intermediates for the two step mechanism were of particular difficultly to optimise. As a consequence they had to be carried out using a constrained search initially, before being re-optimised without the constraints using the better guess for the transition state. Another important note about the calculations is that the transition state between the peroxyl and alkyl oxide radical fragments and the final product could not be located even using the improved guess state from the constrained search. Both of the issues are likely to be an artefact of the level of theory. This problem optimising the radical species, coupled with the spin density of the intermediates indicates that these are highly multi-reference systems. As the barrier to hydrogen abstraction will likely to be lower in energy than that for the first step in the mechanism, or does exist as the hydrogen abstraction reaction is barrierless, this will not be the rate determining step and the overall barrier to reaction stands at +33.6 kcal mol^{-1}. The radical intermediates formed after the first step are higher in energy than the reactants. However, since they are radical species, this will contribute to

the reaction progressing to quickly to the final products or in chain branching reactions.

Cyclohexane peroxide

The same set of BS-DFT calculations were carried out for the cyclohexane peroxide with the reaction surface presented below in figure 5.17. The transition state linking the initial reactants and the first set of radical intermediates is +32.2 kcal mol^{-1}, compared to the energy of transition state for the concerted mechanism, which is +38 kcal mol^{-1}. Thus, at the lower temperatures present in the autoxidation process, >99% of the reaction would proceed through the lower multi-step mechanism. This is similar to the methyl peroxide system, indicating that alkanes have similar chemistry available to them. The transition state of the concerted mechanism is somewhat higher in energy than that for the methyl peroxide system. This is due to the greater steric hindrance placed on the transition state, produced by the larger hydrocarbon group, and as such it is higher in energy. This steric hindrance will also lead to a decrease in the pre-exponential factor. The result of both of these factors is a slow rate of reaction than for the methyl peroxide system. The steric hindrance does not effect the energy of the transition state for the first step of the multi-step reaction, as the transition state it self does not require a highly constrained molecular projection, and the reactive site is projected out of the molecule.

The results of the BS-DFT calculations also show that the intermediates formed after the first step and the final products are relatively more stable in energy than those for the methyl peroxide. This is likely to be caused by the inductive electron stabilising effects of the hydrocarbon group, as it is a larger hydrocarbon group but it is also a secondary hydrocarbon, and as shown by IFPEN this effects the rate of reactions of alkanes in a measurable and linear way.[139] The importance of this result, is that it is clear that changing the hydrocarbon component in the fuel has an affect on the rate of these reactions, and it is important to understand the role of its chemistry in more fundamental depth to help future development.

Fig. 5.17: BS-UDFT reaction surface of the self-reaction of cyclohexane peroxides via the concerted and two step mechanism, carried out using the Gaussian 09 program at the BS-UB3LYP/cc-pVTZ/pcm=heptane level of theory.

Toluene peroxide

As with the homolytic fission of peroxides, BS-DFT calculations were carried for the toluene peroxide system, to generate the reaction surface for the self-reaction of toluene peroxides which can be seen in figure 5.18. The transition state between the reactants and the first set of intermediates has not be located in an unconstrained search. Preliminary results, using a constrained optimisation, indicate that the transition state is higher in energy than that for the concerted mechanism which is +34 kcal mol^{-1}. This is a significant change from the methyl peroxide and cyclohexane peroxide systems, where 99% progressed through the multi-step route, meaning that a drop in the number of radical species formed during the reaction and decreased levels of chain branching. However, the transition state for the concerted mechanism is lower in energy than that for the methyl peroxide and the cyclohexane peroxide systems. This is likely due to the aromatic toluene having a fixed structure, which is projected out of the way of the transition state. Thus, the

steric hindrance imposed of the system is lower than than for the alkanes. The aromaticity of the system also allowing for electron density to be spread over the molecule, thus stabilising the transition state. This suggests that the mono-aromatic hydrocarbon components in the fuel are going to be more reactive in the fuel under kinetic control, leading to greater deposition, as already shown in the literature.[147]
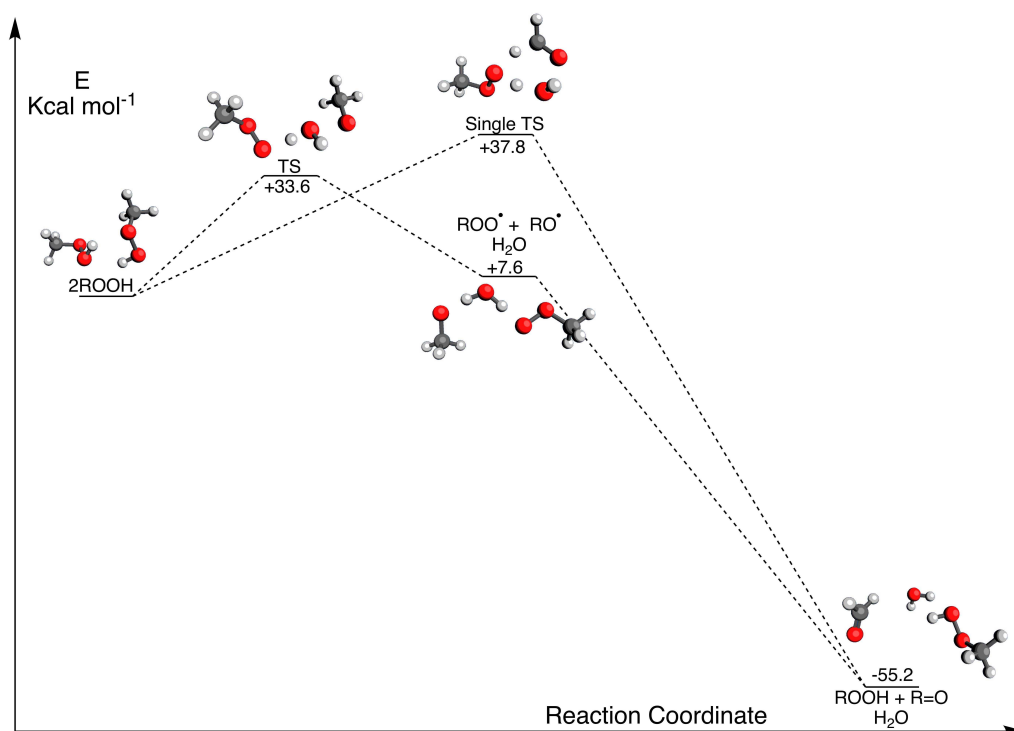

Fig. 5.18: BS-UDFT reaction surface of the self-reaction of toluene peroxides via the concerted and two step mechanism, carried out using the Gaussian 09 program at the BS-UB3LYP/cc-pVTZ/pcm=heptane level of theory.

The aromaticity of the system means that the intermediates and final products formed have a higher relative energy than for the cyclohexane system. For the radical intermediates, this is somewhat surprising, as it could be expected that they would be stabilised by the aromatic ring. Thus, the alkoxide is stabilised by the aromatic ring, but the peroxyl radical is electronically isolated from the ring because of the CH_2 group. Stabilisation in the cyclohexane system could occur through inductive effects, resulting in products and intermediates which are relatively lower in energy. Of course the failure of BS-DFT to describe the system properly cannot be completely discounted either.

5.3 The self-reaction of Peroxyl radicals

A reaction of even more interest, and potentially even more importance to the oxidation of aviation fuel, is the self-reaction of the peroxyl radicals. As stated earlier, this reaction has been linked to the formation of the deposit precursors, and appears in most models of autoxidation. The mechanism for the self-reaction of peroxyl radicals was proposed by Russell in 1957, and has been studied in a number of different fields.[294, 295, 298, 299] It has been applied to the aviation field previously, both experimentally, and using modelling approaches.[14, 185] However, it is a complex electronic structure problem, which requires high level theoretical methods in order to be fully understood. Starting from the point that the multiplicity of the reaction must be conserved, it can be deduce that either a high energy triplet carbonyl must be formed, or reactive singlet oxygen. This reaction was investigated using our test system from the previous sections, methyl peroxide.

Methyl peroxyl radical

The two step mechanism and one-step concerted pathway for the self-reaction of peroxyl radicals were investigated using the Gaussian 09 program at the BS-UB3LYP/cc-pVTZ/PCM=heptane level of theory. The HOMO and LUMO orbitals were mixed in order to help with the optimisation of the higher energy intermediates and transition states which are expected to be open shell singlets. These optimisations were carried out in the singlet multiplicity state. Thus, if the carbonyl triplet is formed as is suggest by a recent publication, this will not be seen in these calculations.[300] The results can be seen in figure 5.19.

The BS-UDFT results indicate that the energy barrier for the concerted mechanism is +35 kcal mol^{-1}, with the highest point on the two-step mechanism having a barrier of +17.5 kcal mol^{-1}, making the energy barrier difference between the two routes +17.5 kcal mol^{-1}. The energy barrier on the two step pathway is taken as the difference in energy between the tetraoxide intermediate and the singlet oxygen and alkoxy radicals, which is +17.5 kcal mol^{-1}. Here, it is assumed that the reaction to form the final products is barrierless. This means that the energy required to form highly reactive singlet oxygen is +17.5 kcal mol^{-1}, and the radical products formed in the reaction can react with
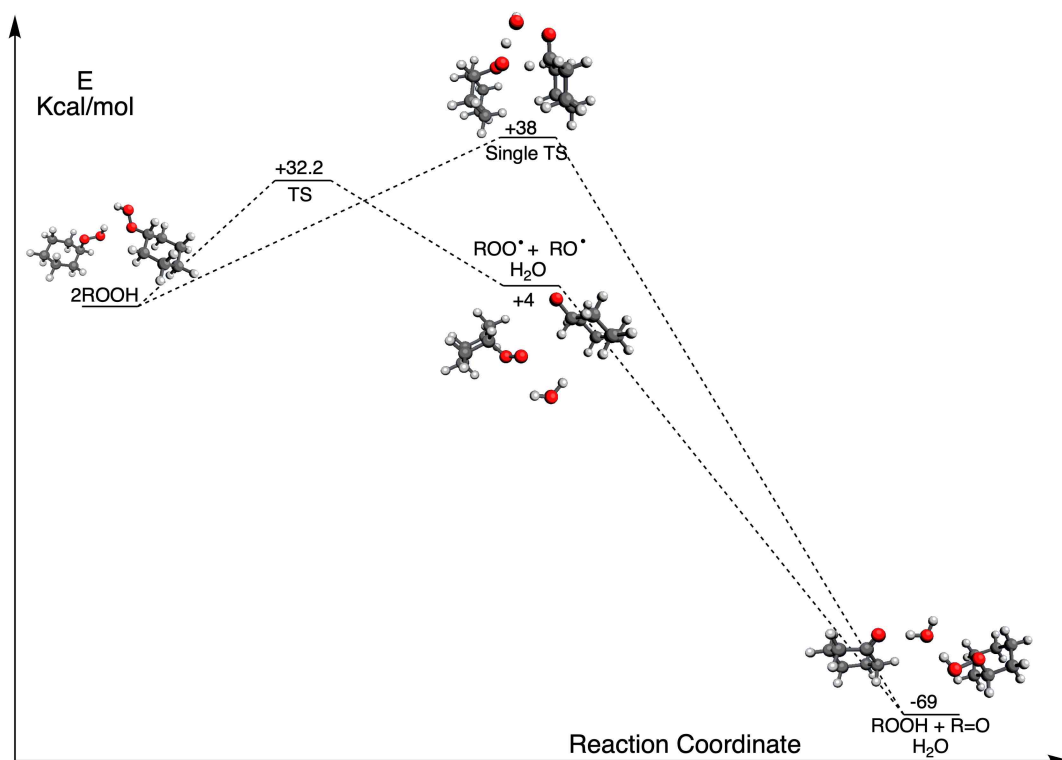
Fig. 5.19: BS-UDFT reaction surface of the self-reaction of peroxyl radicals via the concerted and two step mechanism, carried out using the Gaussian 09 program at the BS-UB3LYP/cc-pVTZ/pcm=heptane level of theory.

each other easily, or with other species in the fuel in chain branching reactions. However, the transition state for the two-step pathway was particularly difficult to locate, and could only be done so using a constrained optimisation. As such, it may not be representative of the actual kinetics of the reaction, and is likely an artefact of treating a highly multi-reference system with a single reference method.

In the first step of the multi-step mechanism, a pre-reaction complex of the two peroxyl fragments forms exothermically, with the resulting tetraoxide complex is 4 kcal mol^{-1} lower in energy than the fragments. This species can then split apart to form oxygen and two alkoxide fragments. Because the conservation of spin angular momentum, these fragments can have two possible spin configurations. We are not able to interpret the difference between these two states using UDFT, as they would have the same spin density. However, as this is a system consisting of purely first row elements. Thus inter-system crossing to stabilise a triplet alkoxide or aldehyde formed as a result of this decomposition reaction is unlikely. The most probable product formed is

singlet oxygen. Thus, singlet oxygen can be generated in the system with a barrier of +17.5 kcal mol^{-1}. This singlet oxygen would then be able to react directly with the other species present in the fuel. This would greatly increase the rate of oxidation, and leading to new radical chain reactions are initiated. The final products in the self-reaction of methyl peroxyl radicals are -65.6 kcal mol^{-1} lower in energy than the reactants. Thus, this is a facile mechanism for the formation of singlet oxygen.

Cyclohexane peroxyl radical

BS-DFT calculations were carried out for the cyclohexane peroxyl radical system as well, with the reaction surface presented in figure 5.20.
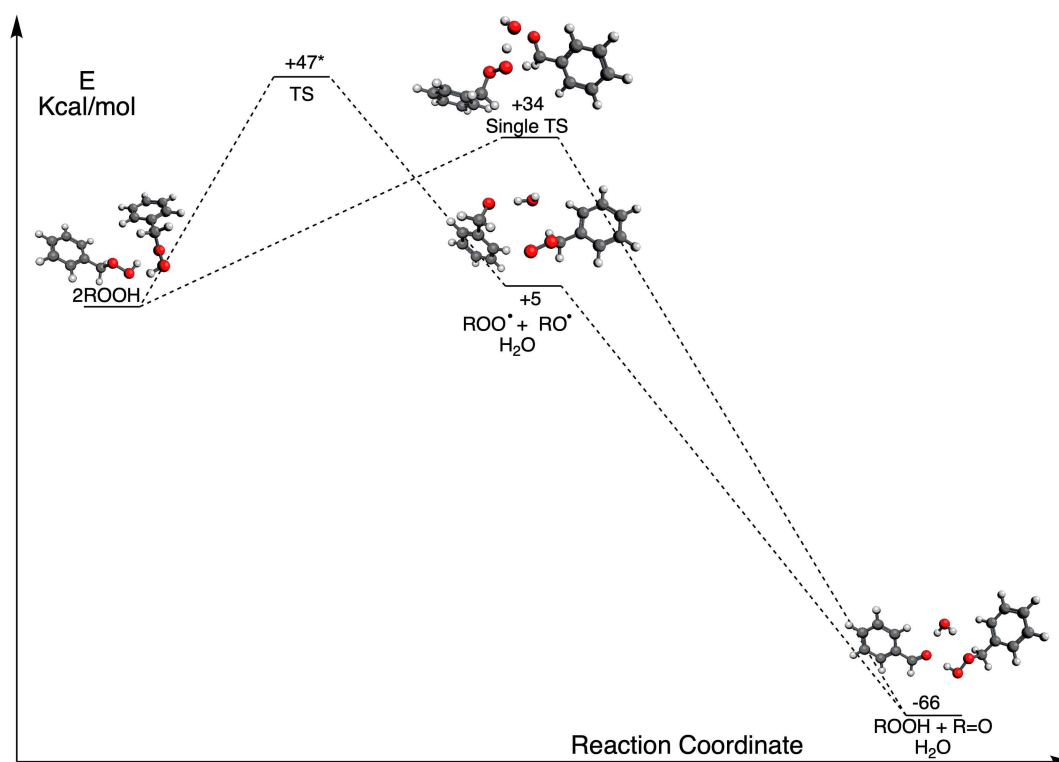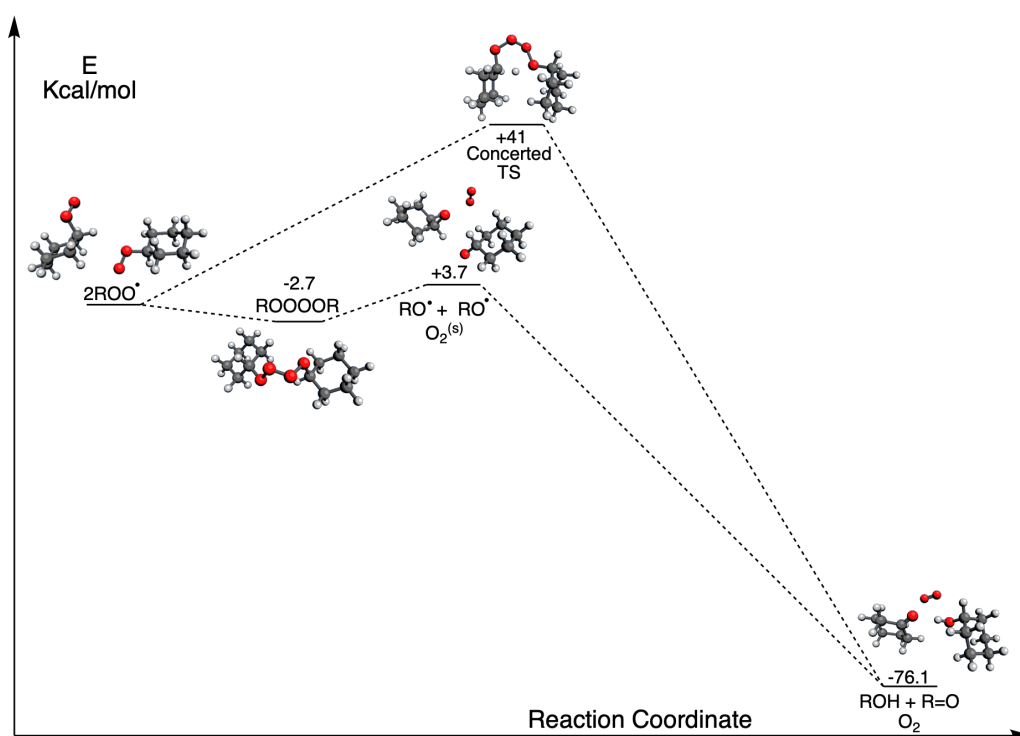

Fig. 5.20: BS-UDFT reaction surface of the self-reaction of cyclohexane peroxyl radicals via the concerted and two step mechanism, carried out using the Gaussian 09 program at the BS-UB3LYP/cc-pVTZ/pcm=heptane level of theory.

The reaction barrier for the concerted mechanism for the cyclohexane peroxyl radical is +41 kcal mol^{-1}. This is 6 kcal mol^{-1} higher than for the methyl peroxyl radical system. Thus, is would lead to a slower rate of oxidation through this route. This increase in the energy barrier is caused by the bulkier cyclohexane

placing greater steric strain on the transition state. As in the self-reaction of peroxides case, this is because forming the transition state requires the system be in a highly ordered geometry without any electronic stabilisation of the transition state. The cyclohexane ring is already ordered, and has limits on its conformational freedom. This extra strain leads a substantial increase in the energy barrier. With all else being equal, at the temperatures in the autoxidation region, this will lead to the methyl peroxyls being preferentially oxidised to the cyclohexane peroxyls through the concerted mechanism at a ratio of 99:1.

The more interesting and significant results can be seen in the relative energy difference for the two step mechanism compared to methyl peroxyl system. The formation of tetraoxide intermediate was higher in energy than for the methyl peroxyl system, -2.7 kcal mol^{-1} compared to -4 kcal mol^{-1}, but was still exothermic overall. Again this increase in the energy is caused by the greater reduction in the conformational freedom placed on the cyclohexane system compared to the methyl system. When this intermediate breaks apart to form the alkoxide radicals and singlet oxygen the reaction is +3.7 kcal mol^{-1} uphill from the reactant and +6.4 kcal mol^{-1} from the tetraoxide intermediate. This is a 11.1 kcal mol^{-1} reduction from the +17.5 kcal mol^{-1} barrier for the methyl peroxyl system. Contributions from a reduction in the steric hindrance compared to the tetraoxide intermediate and inductive electronic stabilisation of the alkoxide radicals by the cyclohexane rings result in this lowering in the energy of the alkoxide intermediates and singlet oxygen compared to the methyl peroxyl system. Thus, the rate determining step of the formation of singlet oxygen, and alkoxide radicals which can take part in chain branching mechanisms, is +6.4 kcal mol^{-1}. The breakdown of the highly ordered tetraoxide intermediate will also have positive entropic contributions through the formation of three molecules. This contribution will be present in the pre-exponential factor, and would be expected to be larger for the cyclohexane system, as it has less conformational freedom compared to the methyl peroxyl system. As such, this reaction offer a potential mechanism of autoxidation rate enhancement, through a facile route. No transition state linking the alkoxide intermediates to the non-radical products was not located through an unconstrained search. However, it is likely to be higher in energy than the one found for the methyl peroxyl radical system due to the greater steric hindrance of the cyclohexane.

Toluene peroxyl radical

The BS-DFT reaction surface for the aromatic toluene peroxyl radical self-reaction can be seen in figure 5.21. The reaction barrier for the concerted mechanism is +39 kcal mol^{-1}. This is 4 kcal mol^{-1} higher than for the methyl peroxyl radical system but 2 kcal mol^{-1} lower than the cyclohexane system. Again, this barrier is higher than the methyl peroxyl system because greater steric strain is placed on the transition state in the toluene peroxyl system. However, it is less strained than in the cyclohexane case, as there is limited clashing between the hydrogens of the two separate rings. The radicals present in the toluene peroxyl system cannot be significantly stabilised by the aromatic ring, as it is too distant from the ring to take part in resonance. Thus, resonance does not help lower the energy of the transition state.
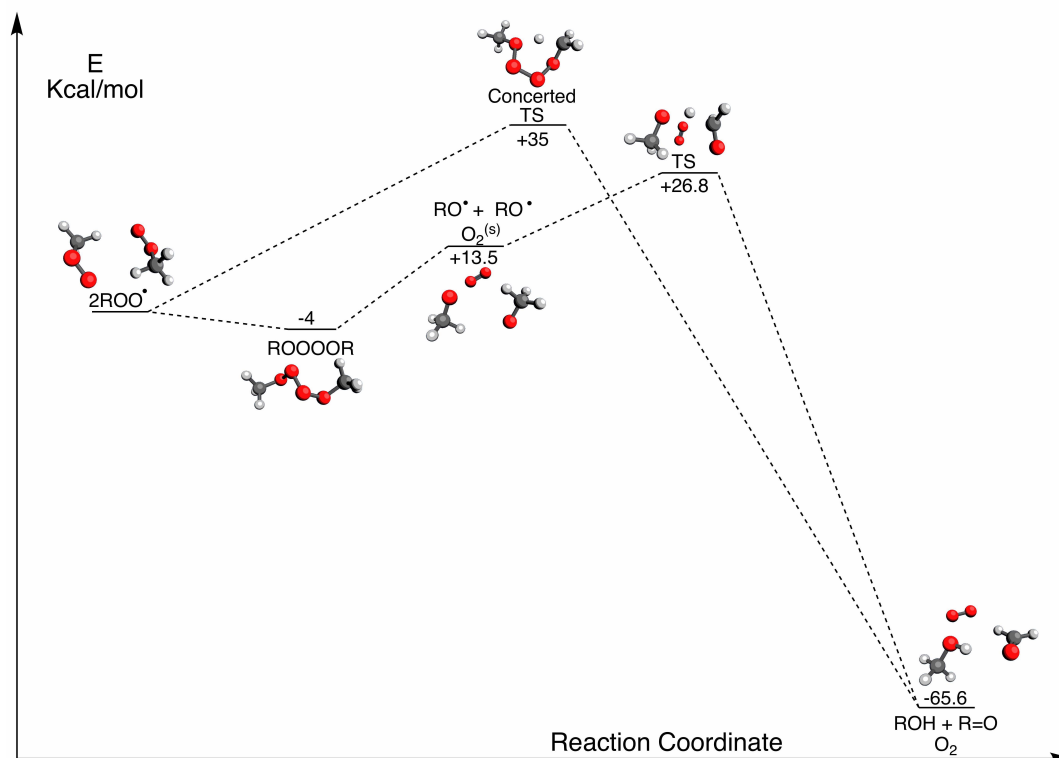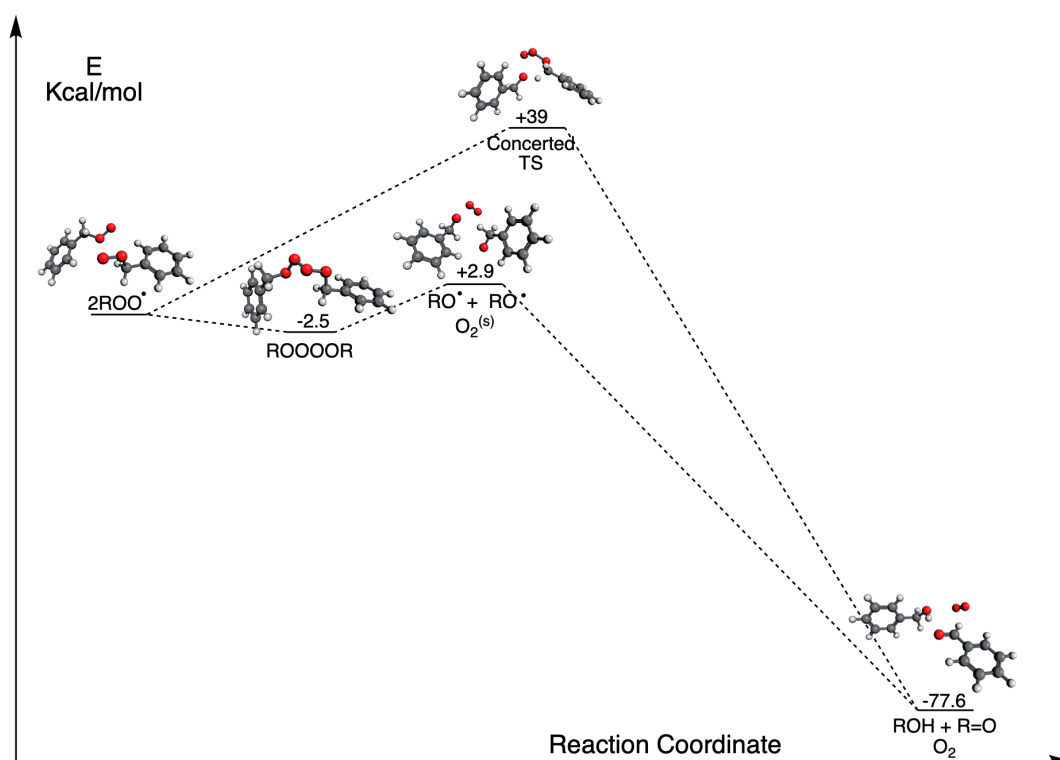

Fig. 5.21: BS-UDFT reaction surface of the self-reaction of toluene peroxyl radicals via the concerted and two step mechanism, carried out using the Gaussian 09 program at the BS-UB3LYP/cc-pVTZ/pcm=heptane level of theory.

The formation of the tetraoxide intermediate is exothermic, by -2.5 kcal mol^{-1}, but is higher in energy than the methyl peroxyl system. As with the cyclo-hexane case this will be a result of the greater reduction in conformational

freedom. The relative energy is higher than the cyclohexane case by 0.2 kcal mol^{-1}, but this is below the accuracy limits of most computational chemistry methods. The alkoxide and singlet oxygen intermediate are +5.4 kcal mol^{-1} energetically uphill from the tetraoxide and +2.9 kcal mol^{-1} from the peroxyl radical reactants. This is the lowest energy intermediate for any of the hydrocarbons studied. This is will be due to the alkoxide radicals being stabilised by the aromatic ring, as the radical centre is close enough to interact through resonance, unlike with the peroxyl radical. The alkoxide radicals formed during this step can then react with each other to form the final products, which are -77.6 kcal mol^{-1} lower in energy than the reactants, or with other species in the fuel. As such, like with the cyclohexane system, the self-reaction of toluene peroxyl radicals offers a low energy route to the formation of singlet oxygen *in-situ* in the fuel and possible chain branching mechanisms. The transition state linking the alkoxide intermediates to the non-radical products was not located through an unconstrained search. However, while the concerted transition state is higher in energy than the methyl peroxyl radical system, it is expected that the transition state between the intermediates and the final products is likely to be lower. This is because the aromatic ring will be able to provide stabilisation of this state, which it cannot do to the concerted transition due to the distances involved meaning that the radical is electronically isolated.

5.4 Inclusion of reactions into pseudo-detailed kinetic mechanisms

The results of the self-reaction of peroxide and peroxyl radicals from this chapter have been used to calculate Arrhenius parameters to improve pseudo-detailed mechanism for use in kinetic solvers. This kinetic modelling has been carried out by collaborators in the Blakey group and has been published or submitted for publication.[297, 301] In the first paper, published in Energy and Fuels [297], the self-reaction of hydrogen peroxides was applied to help understand the effect of deoxygenation and the removal of oxygenated species from fuel have on the thermal stability. This work was carried out as part of the DeOx program funded through the Horizon 2020 Clean Sky 2 program (grant number 71791). Similar findings to previous studies concluded that the deoxygenation of the fuel, *via* nitrogen purging, was effective, but only for a short amount of time. Moreover, oxygen removal could not be achieved through absorption from solution by zeolites. However, the removal

of polar species from a marginal fuels, resulted in a dramatic improvement in the thermal stability of the fuel and a reduction in the High Reynolds thermal stability (HiReTS) number from 1500 to approximately 400, turning this fuel into one with good thermal stability. The results of the HiReTS study can be seen in figure 5.22. As can be seen, removing the polar species was of far more importance to improving an aviation fuels thermal stability than removing the dissolved oxygen. Neither zeolite tested demonstrated selectivity in removing the polar species from the marginal fuel.
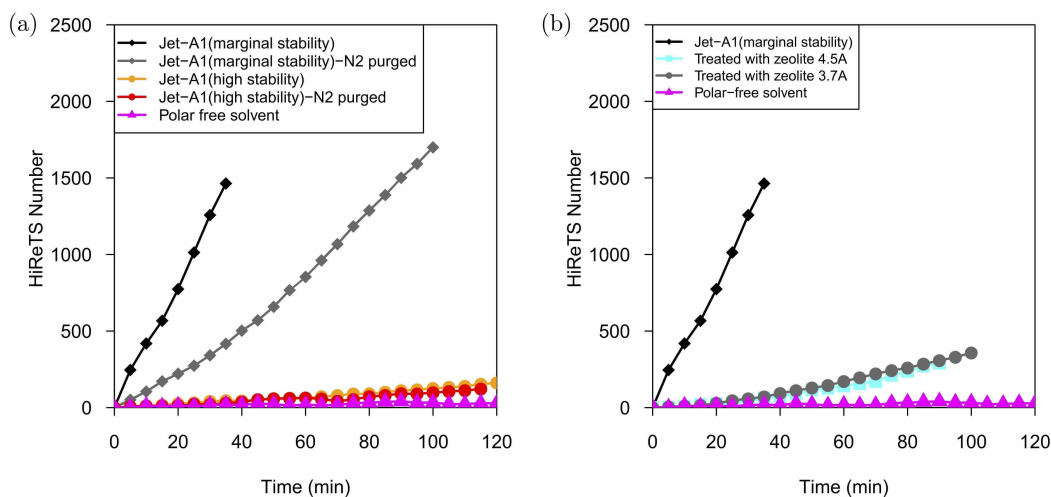
Fig. 5.22: The results of HiReTS testing after nitrogen purging and the zeolite treatment of two fuels, one marginal with high polar concentration and the other with high thermal stability, compared to a solvent with no polar species present. Reprinted with permission from [297].

However, the two fuels tested in the HiReTs were found to have similar chemical composition, with concentrations determined by GC x GC studies carried out at Intertek UK and collaborators at the University of Dayton Research Institute (UDRI). Metal speciation was carried out by the University of Sheffield mass spectrometry services using a Spectro-Ciros-Vision ICP-OES spectrometer. The results are shown in table 5.3.

The 2 fuels had almost identical chemical composition, with the only significant difference being in the concentration of hydroperoxides present in the fuels before testing. It is clear from the HiReTS results presented in figure 5.22 and the chemical composition breakdown of the fuel in table 5.3 that the peroxide concentration is an important species in determining the thermal stability of an aviation fuel. The paper by Alborzi *et al* proposed that in fuels with significant peroxide concentrations, deoxygenation is ineffective, because the peroxide acts as a native source of oxygen and can initiate oxidation. In

Tab. 5.3: Chemical composition of fuels used in the DeOx program. Fuel A has marginal thermal stability and Fuel B has high thermal stability if the HiReTS test. Reprinted and adapted with permission from [297].

Chemical	Fuel A	Fuel B
n-paraffins	20.67m/m%	19.56m/m%
iso-paraffins	24.77m/m%	25.83m/m%
cyclics	30.84m/m%	31.92m/m%
alkylbenzenes	16.18m/m%	15.12m/m%
indans and tetralins	2.15m/m%	2.1m/m%
naphtalenes	1.33m/m%	1.28m/m%
antioxidant	25 mg/L	25 mg/L
acidity	0.08 mg/100g	0.072 mg/100g
Sulfur	835 mg/kg	812 mg/kg
Nitrogen	12 mg/kg	12 mg/kg
total hydroperoxides	13.8 μM	4.1 μM
dissolved Fe	115 ppb	110 ppb
dissolved Cu	50 ppb	38 ppb
dissolved Zn	48 ppb	64 ppb
HiReTS Nu	1500	200

fuels with high polar concentrations, the low peroxide concentration limits the reactions which can occur in the secondary oxidation process, as peroxide and peroxyl radicals have been shown to be important in the formation of insoluble material.[15, 182–184] This paper presented work from this thesis, investigating the self-reaction of peroxides, and proposed a route to the production of radical peroxyl and alkoxide species which can under-go initiation and chain branching reactions. This has been discussed in more detail in a previous section in this chapter.

A second paper by Alborzi *et al*, which at the time of writing has been submitted to *Fuel*, investigated the role of peroxides in the autoxidation process and its effect on the initiation and propagation steps. This paper includes calculated Arrhenius parameters from the reactions in this chapter to improve the pseudo-detailed mechanism proposed by Kuprowicz *et al*.[14, 301] The current rate parameters for that Basic Autoxidation Scheme (BAS) mechanism from the paper by Kuprowicz *et al* were used to predict the oxygen depletion in a test of BannerSol in an Isothermal Tube Reactor (ITTR) at 150 °C when the hydrogen peroxide concentration was at the lower limits of what is found in aviation fuel and hydrocarbon solvents. The model was compared to the experimental results, which can be seen in figure 5.23, with the value for the

energy input for the homolytic fission of hydroperoxides being set at 39 and 30 kcal mol^{-1}.[14] When the activation barrier presented in the paper by Kuprowicz *et al* is used, insufficient oxidation occurs. It was therefore be concluded that the energy required to break the bond being too high. However, lowering the barrier to 30 kcal mol^{-1} does not lead to a significant improvement in the rate of autoxidation initiation. Therefore the conclusion must be drawn that the autoxidation mechanism is not described adequately. This is particularly true of the peroxide species in the fuel and their role in the initiation and chain branching steps.
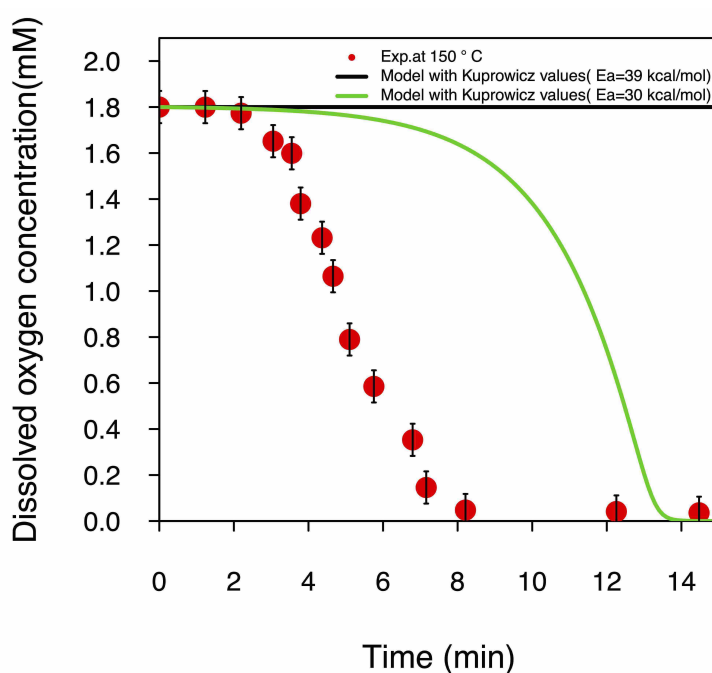
Fig. 5.23: Experimental and predicted oxygen depletion of BannerSol being heated in the Isothermal Tube Reactor (ITTR). The predicted values were calculated using the BAS mechanism from Kuprowicz *et al*, with the activation energy for the homolytic fission of peroxides set at 39 and 30 kcal mol^{-1}.[14] Reprinted with permission from [301].

To improve on the description of autoxidation, the barrier heights and pre-exponential factors for the reactions in the BAS used as part of the pseudo-detailed mechanism presented by Kuprowicz *et al* were recalculated, using quantum chemistry work not presented in this thesis. New reactions for the self-reaction of peroxides and peroxyl radicals were incorporated into the BAS mechanism, with the Arrhenius parameters calculated from results presented previously in this chapter with the barriers and pre-exponential factor then being optimised post-calculation prior to implementation into a kinetic mechanism. The values calculated and used from this chapter can

be seen in table 5.4. These new reaction steps offer new routes for the consumption of peroxides, and generation of chain branching radicals.

Tab. 5.4: Calculated and optimised Arrhenius parameters for methyl peroxide and peroxyl radicals originating from this thesis used in the paper by Alborzi *et al.*[301] E_a has units of kcal mol^{-1} and A has units of s^{-1}. The mechanism was constructed using BS-UB3LYP/cc-pVTZ level of theory in Gaussian09.

Reaction Schematic	A	E_a
Arrhenius parameters calculated in this chapter used in [301]		
$RO_2H \rightarrow RO + OH$	1×10^{12}	36
$RO_2H + RO_2H \rightarrow RO_2 + RO + H_2O$	5.6×10^{12}	28.12
$RO_2 + RO_2 \rightarrow RO + RO + O_2$	1.4×10^{12}	17.5
$RO + RO + O_2 \rightarrow R=O + ROH + O_2$	1.47×10^{14}	13.3
Other calculated Arrhenius parameters in [301]		
$RH \rightarrow R + H$	1×10^{14}	94.2
$RH + O_2 \rightarrow R + OOH$	1.1×10^{9}	65
$R + O_2 \rightarrow ROO$	3.1×10^{12}	0
$RO_2 + RH \rightarrow RO_2H + R$	1×10^{10}	11.5
$RO + RH \rightarrow ROH + R$	4.9×10^{13}	7.1
$HO + RH \rightarrow H_2O + R$	2.5×10^{13}	0
$RO \rightarrow R + CH_2O$	6.5×10^{12}	13.7
$R + R \rightarrow R-R$	6.5×10^{13}	0
$RO + RO \rightarrow ROOR$	7.8×10^{13}	0
$RO_2 + R \rightarrow ROOR$	1.37×10^{14}	0

The updated BAS mechanism was implemented into a MATLAB programme developed by Alborzi to integrate the ordinary differential equations for each chemical kinetic step.[301] ITTR experiments on BannerSol were carried out at 3 temperatures, 135, 140 and 150 °C, and the updated BAS model was integrated in the MATLAB programme at these three temperatures. The results can be seen in figure 5.24. The kinetic model has better agreement with experimental values at higher temperature. As thermochemistry frequency calculations were carried out at the standard 298.15 K, and the behaviour at higher temperatures was extrapolated from this point, this would be the opposite to what is expected. This is especially true as the thermochemistry correction applied in the base Gaussian code has issue with the low frequency vibrations. The likely cause is that the DFT calculations over estimate the barrier heights, and as such at higher temperature when more energy is available to overcome the barrier, and the effect of this error is minimised. The inclusion of the self-reaction of peroxides and peroxyl radicals helps to describe a more complete picture of the the autoxidation process and give a

more accurate description of the role of peroxides and peroxyl radicals in this process. Importantly it better models the rapid oxygen consumption after the induction period is complete. As postulated earlier in this chapter, this is likely to be caused by the production of radical species during these self-reactions, which can undergo chain branching reaction to increase the oxidation rate.
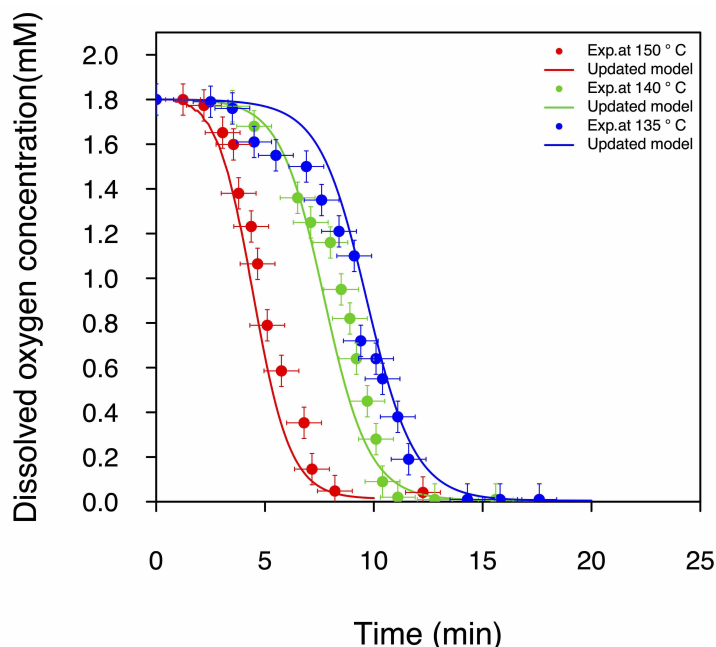
Fig. 5.24: Experimental and predicted oxygen depletion in an Isothermal Tube Reactor (ITTR) at temperatures of 130 °C, 140 °C and 150 °C. The predicted values were calculated using the BAS mechanism from Alborzi *et al*, using the quantum chemistry calculated Arrhenius parameters from this chapter. Reprinted with permission from [301].

The updated BAS mechanism was also used by Alborzi *et al* to predict the concentration of the peroxides formed in the BannerSol as it is thermally stressed in the ITTR at 150 °C.[301] The results of this modelling can be seen in figure 5.25. The model has good agreement at predicting the formation of peroxides at the temperature tested. As the oxygen is consumed the concentration of peroxides in BannerSol increases. This could imply that the oxygen is being incorporated into the peroxides, or that peroxides are being regenerated as quickly as they are being consumed, in that case radical species are generated in these reactions to accelerate the oxidation. Our calculations and experiments cannot distinguish between these options, and more work is required to confirm what the exact mechanism is, either experimentally or computationally.
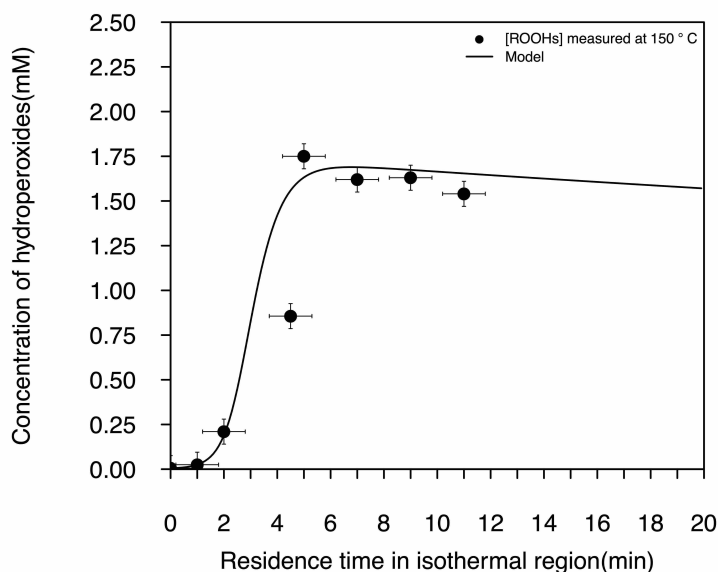
Fig. 5.25: Experimental and predicted peroxide concentration in an Isothermal Tube Reactor (ITTR) at 150 °C. The predicted values were calculated using the BAS mechanism from Alborzi *et al*, using the quantum chemistry calculated Arrhenius parameters from this chapter. Reprinted with permission from [301].

5.5 Summary

In this chapter, the oxidation mechanism of peroxides and peroxyl radicals have been investigated using computational chemistry techniques, in order to understand the complex electronic structure that involved in these reactions. It has been found that these reactions are inherently multi-reference in nature, involving bi-radical reactant, intermediates and products. These reactions are important to understand as they key species in the autoxidation mechanism with their concentration and reactivity affecting the rate of oxidation and the formation of insoluble species. As shown in this chapter, single reference method such as DFT have difficultly in describing the homolytic fission of peroxides, as they treat the bond breaking reaction as ionic and thus over estimates the barrier. However, even when the correct barrier is calculated, the rate of reaction for this reaction step is insufficient to describe the experimentally observed oxidation rate.

This has lead to two new sets of reactions to be introduced into the pseudo-detailed mechanism, with the Arrhenius parameters calculated from quantum chemistry calculations, and implemented into kinetic mechanisms. The results

of this study have been submitted to publication. These new sets of reactions, the self-reaction of peroxides and peroxyl radicals, result in the oxidation rate being predicted with good agreement with experiment. The reason for this is that they offer a labile route to the formation of radical species, which can take part in chain branching mechanisms, and can greatly increase the rate of autoxidation. These reaction progress through reactions with barriers between 10-20 kcal mol^{-1} lower in energy that the homolytic fission of the peroxide O-O bond. Thereby their inclusion in the pseudo-detailed mechanism leads to improved predictions.

However, the results from this chapter lead to some interesting findings. The first is that the fate of the peroxyl and alkoxide radicals formed during these reactions is important to model and predict. The current model has them reacting with fuel species and thereby increasing the rate of reaction, as well as reacting with fuel phenol and nitrogen species to form deposit precursors. However, as speculated by Beaver *et al* they have also been linked to be important species in the formation of insoluble SMORS products, and as such these reactions will compete with the initiation step.[15] The second finding from this chapter is that these reaction could offer a labile route to the chemical formation of singlet oxygen. This form of oxygen is highly reactive, and can react with the fuel directly, thus can initiate autoxidation and greatly increase the rate of oxidation. Some literature indicates that relativistic effects allow for a spin flipping mechanism to promote the formation of triplet oxygen. However, in small organic systems this seem unlikely, but this possibility could be investigated further using relativistic multi-reference methods and *in-situ* spectroscopy to determine the spin state of the oxygen formed.

Discussion

<div style="text-align: right">6</div>

This thesis has presented some experimental and theoretical models investigating the autoxidation of a number of different chemicals and in different thermally stressed conditions. As such, it is important to offer a general discussion of the implications that some of these results have, and how this effects our knowledge of the autoxidation mechanism. This discussion will start by reviewing the autoxidation mechanism and offering an extended and complimentary picture of this.

6.1 Evidence for a two step oxidation mechanism

The literature review, made it clear that the experimental device and the operating conditions used for studying studies effected our understanding of the results observed, and the type of reaction mechanisms that are driving the autoxidation. An example of this is that fuels with high aromatic or natural antioxidant concentrations were shown to slow the oxidation rate by increasing the length of the induction period. However, when these fuels were tested in experimental rigs with long residence times or if the fuels had undergone significant pre-heating, they would demonstrate increased deposition and a drop of thermal stability. It is clear that there are two separate, but linked, oxidation pathways for these processes. Thus, investigating only one does not help us fully understand a fuel's response to thermal stress, and it fails to investigate the complete reaction space of the autoxidation process. With either the radical driven mechanism or the agglomeration and oxidative coupling driven mechanism being ignored.

The PetroOxy thermal stability tester has allowed us to investigate aviation fuels, and pure hydrocarbon components of such fuels, in the different expermental regimes seen in other testing. An example of the data collected can be seen in figure 6.1. The initial regime, covering the induction period and the rapid consumption of oxygen, is characteristic of radical chain reactions, and provides insight into the initiation and radical autoxidation mechanism. It also shows how different fuels behave in this regime. The fuel is being thermally stressed in an oxygen-rich environment, compared to other testing,
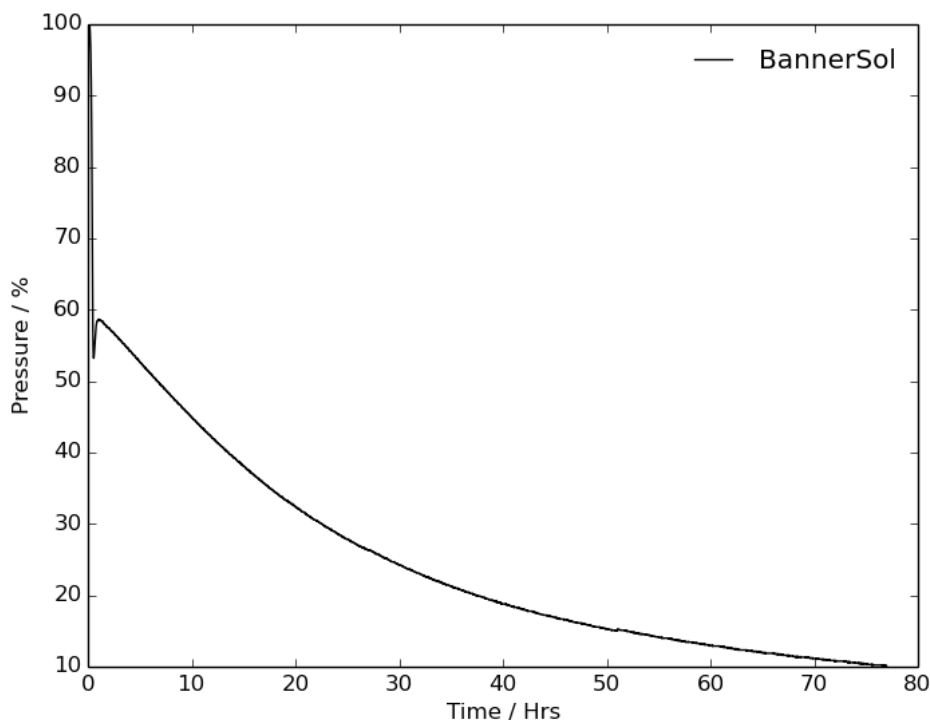
Fig. 6.1: PetroOxy plot of the 90% pressure drop for BannerSol.

and compared to real fuel systems. Hence the shorter time frame for these reactions to occur. However, as the reactions appear to show Arrhenius type behaviour, it is valid to use this data to interpret how a fuel will behave when it is in an oxygen-rich environment at the start of oxidation. Support for this has been presented in the literature review. Here temperatures below 350 °C demonstrated linear Arrhenius behaviour. Above this a change in mechanism to the pyrolysis regime occurred.

Peroxides and peroxyl radicals are of vital importance in describing this radical oxidation mechanism, as demonstrated by the modelling results in the previous chapter. They are involved in the formation of the oxidation products during this first stage of oxidation. The products formed at the end of this step are alcohols, aldehydes, ketones and carboxylic acids. Evidence of the formation of these compound can be seen in the analysis of the thermally stressed samples at this stage of oxidation. Independently the FTIR and GCMS clearly show that carbonyl and hydroxyl species are formed during this first stage of oxidation. The reactions of peroxide and peroxyl species allow for the formation of radical species through a very facile reaction

mechanism, particularly when compared to the homolytic fission of O-O or C-H bonds. These routes will accelerate the autoxidation mechanism and can help describe the rapid drop in the oxygen partial pressure in the PetroOxy device. Compounding this rate increase caused by the formation of radicals, is the complex electronic structure of the self-reaction of peroxyl radicals also provides a route to the formation of singlet oxygen *in-situ*. Singlet oxygen is highly reactive and can initiate the autoxidation reaction directly.

At longer test times a discontinuity can be observed in the rate of oxygen consumption. This also coincides with a change in colour of the sample towards a dark brown colour and eventually the formation of deposits. The testing conditions at this point are similar to experimental tests with long residence times Such tests lead to low oxygen environments where deposition occurs as oxidative coupling and condensation reactions become the dominant mechanism. At this point there are similarities to the SMORS mechanism proposed by Hardy *et al* and developed by Beaver *et al*.[15, 180–185] The conditions in this part of the PetroOxy test is analogous to the laminar sub-layer near wall flow present in turbulent conditions which will be at a high temperature due to its proximity to the hot wall. This is where most of the oxidation and deposition occurs. The reasoning provided for this observation is that in these regions of the flow there are increased residence times and higher temperatures in the fuel close to the wall, thus increased oxidation and deposition occurs. The PetroOxy allows for us to investigate this regime in isolation, making a more repeatable and reliable test than a full flowing fuel experiment. Thus, allowing us to investigate how a fuel behaves under extreme operating conditions. It is during this second stage of oxidation that deposition occurs in the PetroOxy. However, not all fuels or hydrocarbon samples formed deposit, with fuels which are blends of purely n and iso-alkanes forming minimal or no deposit at all. This would also signify that aromatic hydrocarbons, or cycloalkanes that are more easily undergo aromatisation, take part in the SMORS mechanism and result in greater levels of deposition because of this.

These mechanisms are summarised in figure 6.2. This figure attempts to link the rapid oxidation step with the deposit forming step, and builds on the work presented in the literature.[14, 15] The unified mechanism highlights the importance that peroxide and peroxyl species have in this process, as they are required in the SMORS mechanism suggested by Beaver *et al.* Moreover, the radicals and singlet oxygen formed during their self-reaction can

accelerate the first stage of oxidation through initiation and chain-branching reactions.[182–184]
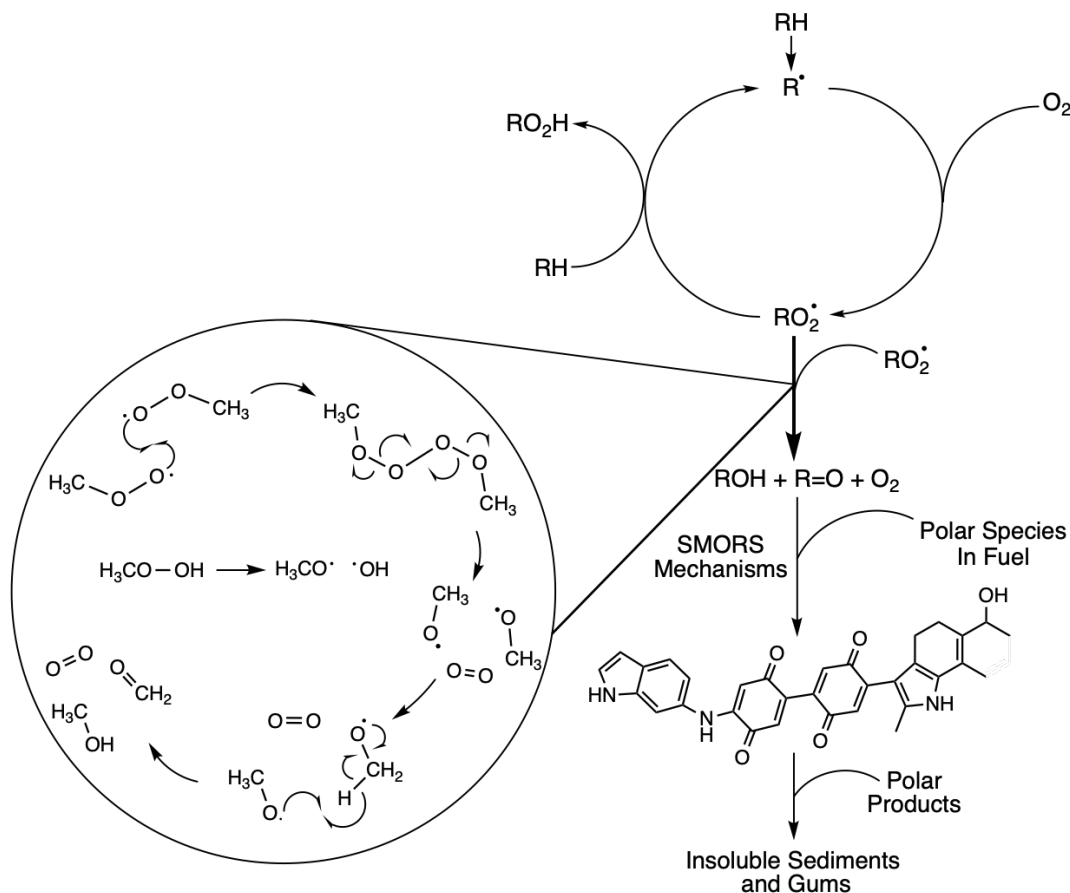
Fig. 6.2: A possible unified mechanism for the oxidation of hydrocarbons, linking the initial rapid radical oxidation with the slow secondary oxidation step that forms deposits, through the reaction of peroxides. This builds on previous work and is supported by our findings. [14, 15, 295]

An interesting note about the deposits formed during the second oxidation stage is that the deposit was not always methanol soluble. In particular the deposit formed at high oxygen depletion by fuels with high sulfur or polar concentrations was particularly difficult to remove. This observation could be explained by assuming that at high temperatures, and prolonged contact with the gold surface of the PetroOxy, the oxidised sulfur species in the fuels form strong chemical bonds with the gold. This is a known phenomenon [280]. As such, this shows that the second stage of oxidation is clearly more complex than just the SMORS mechanism, with a number of transport and surface interactions involved in forming the deposit. This is outside the scope of this thesis, which has focused on understanding the radical mechanism which

govern autoxidaiton, but offer a possible future direction for research to be carried out.

6.2 Aromatics antioxidant behaviour in fuel

Our studies of the JETSCREEN fuels highlighted that the aromatic component of an aviation fuel reacts in a different way to the alkane components. This was seen even more dramatically in the studies of the chemically pure hydrocarbons and their blends in Chapter 4. The affect of the addition of toluene to dodecane and decalin was more easily described as producing an exponential increase in the time taken to complete the first stage of oxidation, because of the increase in the induction period. However, at higher concentrations of aromatic molecules the rate of oxygen consumption during the rapid radical stage of the mechanism can also be affected. In contrast, slowing in the oxidation rate is not observed in the second stage of oxidation for the JETSCREEN fuels, in this phase deposition occurs, it is characterised by the greater levels of oxygen depletion. As discussed above, deposition is caused by the aromatic species undergoing electrophilic aromatic substitution reactions, as well as other oxidative coupling reactions. Thus, at this stage of oxidation they facilitate the SMORS mechanism and other routes to deposition. Interestingly, the time needed to reach 90% oxygen consumption for pure toluene was slower than the pure alkanes. However, this could be attributed a very slow consumption rate up to 60% depletion. In this earlier stage of oxidation the aromatic hydrocarbons are able to slow the oxidation by acting as antioxidants. This is in competition with the oxidative coupling reactions resulting in the shape of the oxygen consumption seen in the PetroOxy data. In fuels, where the concentration of the aromatic component is limited, the induction period is extended until the aromatics have been consumed.

However, it is clear from the literature that phenolic species and other classes of antioxidants in the fuel also present the same deposition issues in the the later stages of oxidation. However, because of the heteroatomic nature of many of these antioxidants, they introduce uncertainty in the autoxidation behaviour of a fuel, as the blending of two fuels does not produce a linear response in thermal stability testing. Moreover, they can negatively impact a number of other properties of the fuel. As such, aromatic hydrocarbons such as toluene which appears to have antioxidant characteristics, offers an opportunity for use in novel fuels developed for high thermal load environments.

This antioxidant behaviour of toluene and other aromatic hydrocarbons is caused by the facile removal of a hydrogen atom from the methyl group. This is analogous to the removal of the phenolic hydrogen in antioxidants. Both families of species share the same aromatic ring backbone. Thus, it is likely due to this aromaticity that they show similar antioxidant behaviour. Evidence for this antioxidant behaviour has been seen in the literature. Work by Taylor even attempted to provide some explanation about why some aromatics had better antioxidant behaviour than other.[134]
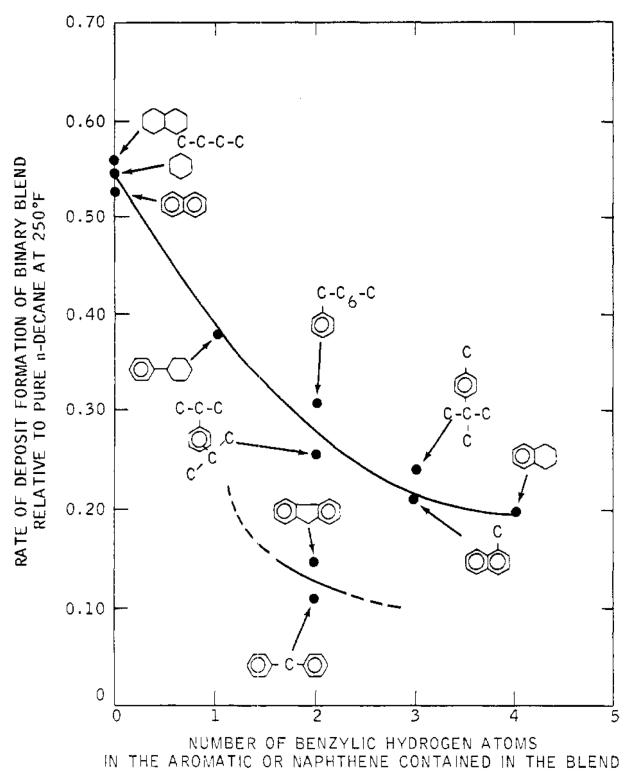
Fig. 6.3: Effect of aromatic structure on deposition rate seen by Taylor in 1969 (taken from [134])

Taylor linked the number of benzylic hydrogen atoms to the rate of deposit formation. This trend is plotted in figure 6.3. The higher the number of benzylic hydrogens, the slower the rate of deposition. Thus, the more hydrogen atoms the aromatic has to donate to the radicals the greater its capability for use as an antioxidant. However, it is clear from Taylor's own work that this is not a complete description, as the author proposed two trend lines. One trend was observed for aromatic species with benzylic hydrogens attached to a single aromatic system. Another trend was observed for benzylic hydrogen atoms attached to two aromatic systems. However, in the model proposed no reasoning is accounted for, and the trend line for aromatic hydrocarbons

attached to two aromatics systems is based on only two points. These two molecules demonstrate different antioxidant behaviour, even given that they have the same number of benzylic hydrogens. The limitations of Taylor's model are even more clear when more recent findings are taken into account. Work by groups at IFPEN and RMIT has shown that different isomers of xylene and trimethylbenzene have different induction periods in the PetroOxy device and thus demonstrated different antioxidant potential.

However, even with this incomplete picture with respect to the cause of this antioxidant potential of aromatic hydrocarbons, the behaviour is dramatic. Quantum chemistry calculations were carried out to better understand the observed antioxidant behaviour of aromatics, to put some context to its extent, and provide some understanding of the cause. Hydrogen abstraction calculations were carried out, with dodecane as the test case, with the dodecane radical and dodecane peroxyl radical reacting with a number of possible hydrogen donors. The donors were, butylated hydroxytoluene represented by AH, m-toluidine represented by NH, toluene represented by PhH and dodecane represented by RH. The results of these calculation can be seen in the reaction surface in figure 6.4.

As can be seen in figure 6.4, the reaction of toluene as the hydrogen donor with dodecane peroxyl radical, has a higher reaction barrier than the reactions involving butylated hydroxytoluene and m-toluidine. However, it is significantly lower than dodecane. Thus, it would slow the reaction of dodecane peroxyl radicals in a blend of the two when compared to a dodecane reference. The antioxidant potential of toluene is even more stark when the reaction of dodecane radical is assessed. The reaction barrier for the reaction of toluene with dodecyl radical is lower than for the m-toluidine case and is only 1.2 kcal mol^{-1} higher than the barrier for the reaction involving butylated hydroxytoluene. This provides some evidence for the exponential effect observed from increasing the percentage of toluene in a 1:1 blend with alkanes. Thus, at higher concentrations the probability of the dodecane radical abstracting a hydrogen from toluene compared to reacting with dissolved oxygen in the fuel is increased. Thus, while the reaction with oxygen is barrierless, the low concentration limits the rate for this reaction, and the rate is slowed by the aromatics in the fuel.
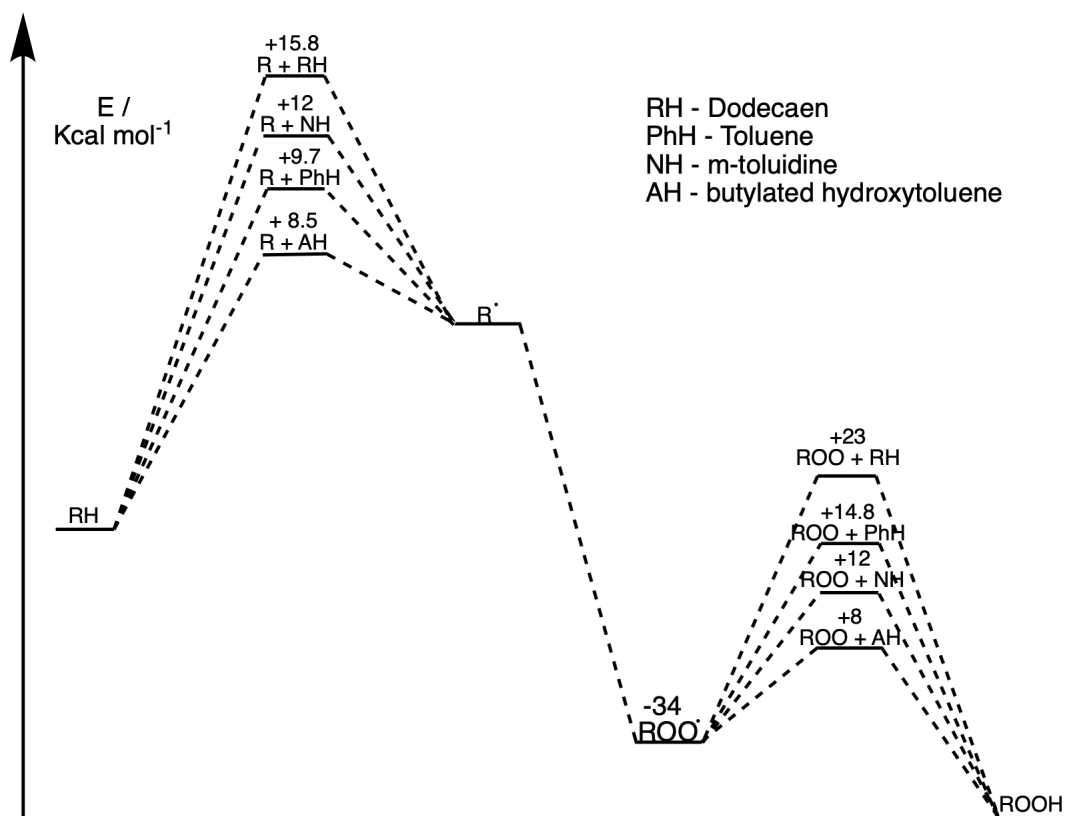
Fig. 6.4: Reactions surface comparing the barrier heights of dodecane reacting with toluene, as well as an two polar antioxidant additives, AH standing for butylated hydroxytoluene and NH standing for m-toluidine. The barriers heights for reaction with dodecane are also plotted for context. For simplicity, the change in energy of the separate products is not plotted.

One outcome from this study could be that the aromatics antioxidant potential of aromatics could be parameterised, Thus their behaviour, when blended into a fuel, could be predicted and optimised for the properties desired.

6.3 Benefits of quantum chemistry in mechanism development

An important outcome of this thesis is the demonstration of quantum chemistry methods in the development a fundamental understanding of autoxidation at the molecular scale and its application in producing pseudo-detailed kinetic mechanisms. Using these quantum chemistry methods, this thesis was able to show detailed chemical differences between different hydrocarbon species, and obtain an understanding for these changes in reactivity.

An interesting observation, is the fact that many of these reactions involve open shell bi-radical singlets, these reactions are highly multi-reference in nature. This was seen in the disproportionation reaction of two alkyl radicals to an alkane and alkene. When the transition state of this reactions was calculated in the singlet spin state the reaction was barrierless. However, a reaction barrier was present when the transition state was calculated in the triplet spin state. Both of these results are a consequence of using single reference methods to carry out the optimisation. Thus, the true energy of the system is likely somewhere between these two extremes. As such, the reaction barrier and pre-exponential factors calculated in this thesis for use in the pseudo-detailed kinetic mechanisms represent the upper bound of the true kinetic parameters. The other effect of using these single reference methods is that we cannot fully understand the intricacies and electronic structure of the reactions in the autoxidation mechanism.

In fact, some transition states proved to be a challenge to locate. Constrained searches were required to provide a good starting trial wave function for unconstrained optimisations. The complex electronic structure of these radical systems causes this complication for all reactions modelled have open shell configurations to some extent. As such, there are intrinsic errors in how some of these reactions are described, which can be seen in the calculated kinetic values of these reactions. The disproportionation reaction discussed earlier in this section is one example of this. The energy calculated for the triplet transition state is too high. However, this behaviour can be expected to be seen to some extent in all reactions, and provides a level of errors to the calculated data. It is generally regarded that DFT calculations show error in calculated results compared to experimental values of around 10%. However, this is for closed shell systems. For the open shell systems studied in this thesis this error may be as high as 15-20%. significant effort is spent on solving these complex electronic structure problems in computational chemistry these errors in the calculated values are likely to decrease to within chemical accuracy of 1 kcal mol^{-1} over the next decade.[302]

For this reason, a selection of reactions were investigated further using multi-reference methods and the broken symmetry implementation of unrestricted DFT in Chapter 5. The reactions in question were the self-reaction of per-oxides and peroxyl radicals, as well as the homolytic fission of peroxides, because these reactions are important to model the primary stage of oxida-tion. The intention of this work was to improve the accuracy of the kinetic data

obtained from the calculated values, as well as gain an understanding of the electronic structure of these systems and the challenges they represent.

Selecting the active space proved a challenge for carrying out the multi-reference calculations. This is a known problem with this theory. Defining the geometry also represented a challenge, as the Z-matrix implementation used in MOLPRO results in undefined coordinates for larger molecules. This meant that significant restrictions had to be placed on the cyclohexane and toluene system to generate the potential energy surfaces. However, the calculated barrier for the breaking of the oxygen-oxygen bonds using the CASPT2 level of theory was accurate to within 1 kcal mol^{-1} of the experimental values, when the data was available. Importantly, MCSCF and CASPT2 was also able to correctly describe the bi-radical singlet nature of these systems, unrestricted single reference methods model them with significant ionic character to the wave function instead. As such, we can be confident that our results were obtained by correctly describing the problem. This then allows us to use this method with confidence in future.

The investigations into the self-reaction of peroxides demonstrate that these reactions offer a facile route to the formation radical species, which can then take part in chain-branching reactions. The self-reaction of peroxyl radicals also results in the formation of radicals that can the proceed to react further in chain-branching mechanisms. However, this reaction also potentially results in the formation of singlet oxygen in the fuel, which can react directly with oxidised hydrocarbons, and initiate autoxidation. The result of these reactions is the acceleration of the rate of autoxidation. This is observed in the experimental data, where an improvement in the accuracy of the model when compared with validation data is achieved when these two reactions are included in the pseudo-detailed mechanism.[297, 301]

An interesting artefact of this study is that the reactions of toluene peroxide and peroxyl were very facile which could mean that they preferentially de-compose through these routes. This supports findings in the literature, which found these reactions were of particular interest when compared to similar reactions for the peroxyl and peroxide species of alkanes and interestingly also for the BHT derivatives.[147] However, these observed differences have not been implemented yet into the pseudo-detailed mechanism prepared for publication at the time of writing. The pseudo-detailed mechanism has also not been updated to take into account that potentially two distinct oxygen

species are now present in the fuel, triplet and singlet oxygen, with different reactivities and concentrations. The formation of our understanding of the detailed chemical differences between the behaviour of different hydrocarbons in the same reaction were only possible with high level quantum chemistry calculations. However, these detailed chemical differences can be implemented into pseudo-detailed mechanisms as demonstrated in Chapter 4. The result would be a kinetic model which can adapt to a change in the chemical composition of the fuel. This is possible because the model has an understanding of how the different chemical classes will behave due to autoxidation built into it, rather than these predictions being based on historical evidence from experiments. Through this we gain an understanding of how to mitigate the issue of thermal stability.

Conclusion

<div style="text-align: right">**7**</div>

7.1 Summary of results

1. This thesis is the first to apply quantum chemistry techniques in a systematic way to develop a methodology for constructing a detailed kinetic mechanism from first principles for the autoxidation of aviation fuel.

2. Using these methods it has been possible to demonstrate that highly complex problems, such as autoxidation, can be studied and modelled in this way and that chemically detailed understanding can be obtained from this approach.

3. This methodology can be applied to other complex problems. The increase in computational resources and efficiency of quantum chemistry calculations, means that this can become common place.

4. Quantum chemistry techniques have been used to update and expand the currently accepted pseudo-detailed mechanism. The new mechanism includes three distinct classes of hydrocarbon. The results of these calculations are currently being prepared for publication.

5. The self-reaction of peroxides and peroxyl radicals has been included in the updated reaction mechanism, greatly improving the modelling of oxygen consumption such that the model can now be validated using experimental results.

6. The results from modelling these reactions propose a route to singlet oxygen formation during oxidation. This would rapidly increase the rate of autoxidation.

7. The results from this work have been applied by the wider Blakey group in large scale modelling. The resulting work has been or is being prepared for publication [297, 301, 303].

8. The development of models for the individual hydrocarbon components of fuel, coupled with chemically purer fuels in the future, allow for off the shelf mechanisms to be tailored to specify predict the thermal stability of a fuel.

9. Synthetic and highly hydrotreated fuels, without any polar minor components, have a better thermal stability and result in less deposition.

10. The thermal stability properties of these fuels can be tailored by altering the percentage of aromatics and cycloalkanes in the fuel predictably.

11. Cycloalkanes reduce the induction period of a fuel, but slow the secondary stage of oxidation, when compared to n-alkanes.

12. Aromatics increase the induction period and the secondary stage of oxidation by acting like antioxidants in the fuel. However, they result in a greater level of deposition. However, their use in chemically purer fuels can result in improvements in the thermal stability of a fuel compared to conventional fuels.

7.2 Outlook

The chemical composition of aviation fuel is changing. The growing use and development of synthetic fuels means it is becoming chemically purer. As such, current limits of the concentration of aromatics in conventional fuel, alternative fuels and its blends, place constraints on the development of high thermal stability fuels. The removal of the polar species that affect the thermal stability dramatically nullifies the issues seen in the literature of aromatics reducing the thermal stability of the fuel. The aromatic component of the fuel can act as an antioxidant in the fuel, improving storage stability, with increases in deposition only occurring at very high residence times. The improved thermal properties of these chemically purer fuels will allow them to become a driver for new engine frameworks that can operate at high temperature with greater efficiencies. Legacy engine designs could be enabled to use this fuel, with admittedly different properties to current drop-in fuels, through additive packages at the airport to ensure backwards compatibility of the novel fuels.

The thermal stability of simple two-component blends of aromatics, cyclo and n-alkanes were investigated in this thesis, exploring the vertices of this chemical space. However, an obvious next step would be complete this chemical space by investigating the ternary blends of these hydrocarbon classes. This could be used, in conjunction with theoretical chemical modelling, to predict the autoxidation of blends with known hydrocarbon composition by class prior to its testing. As such a longer-term ambition of this work should be to construct this chemical map of thermal stability and compare it to fuels with known chemical composition to determine the agreement with the behaviour predicted by these ternary blends.

The analysis carried out in this study was limited to simple post-testing techniques, such as FTIR and GCMS. However, the chemical sciences offer a number of other potential techniques to study the oxidation mechanism and characterise the products formed. Modern *In-situ* spectroscopy techniques offer a way to study complex systems, such as autoxidation, in real-time and follow the progress of the processes that govern it. The proposed formation of singlet oxygen in the fuel during oxidation offers an obvious candidate to start with these studies by using fluorescence techniques, as would be the growth and/or depletion of the carbonyl stretch at different stage of the oxidation process, using *in-situ* FTIR studies. These studies could be carried out in either a static bomb reactor, similar to a PetroOxy, or an isothermal flowing reactor like the ITTR in Sheffield.

This thesis has presented a methodology for studying autoxidation using quantum chemistry calculations, where the results were used to construct pseudo-detailed mechanisms. This has involved finding stationary points along the potential energy surface. Moreover, using the energy of the transition states and reactants the kinetics of a reaction were predicted. However, this is time-consuming as locating a transition state represents a substantial challenge. This is particularly true if the spin state of the involved species is poorly described using single reference methods. As such, with the advances in quantum chemistry codes and computational resources observed already during this PhD and the expectation that it continues improve in the future, It is very likely that, in future, the reactions will be modelled using unconstrained scans along the reaction coordinates to obtain a description of the complete reaction surface relatively quickly. This will allow researchers to develop a greater understanding of the kinetics of a reaction, but would sacrifice some description of the transition state. An interesting alternative to this approach,

would be to use machine learning to generate these potential energy surface. Machine learning has been applied recently to study a number of chemical systems and other complex problems, such as deriving Newtonian mechanics from observations.[304, 305]

From chapter 4 and 5, it is clear that the many of the reactions involved in the autoxidation process are highly multi-reference in nature. Thus, single reference methods are not sufficient to fully understand them. As such, a logical next step would be to develop potential energy surfaces for the open shell bi-radical reactions presented in this thesis using multi-reference methods, whether that be the MCSCF/CASPT2 methodology used in this thesis or newer methods such as MRACPF, SORCI, adaptive sampling CI or UHF-DLPNO-CCSD. Treatment of these reactions using these methods would not only describe the systems in a physically more correct manner, but would also help achieve better kinetic data for pseudo-detailed mechanisms.

The work in this thesis has focused on the primary radical driven oxidation stage. However, this is clearly only half the story, and the slow deposition stage that is dominated by the oxidative coupling and condensation reactions needs to be studied in more detail. Similar to the *in-situ* analysis suggested for studying the primary oxidation mechanism, the chemical nature of the deposit can be investigated at each step of the oxidation mechanism, to determine how it changes at greater levels of oxidation. Thermal gravimetric analysis, X-ray photoelectron spectroscopy, microscopy, X-ray diffraction techniques, as well as a number of other material characterisation and analysis methods could be used for these studies. The deposition steps would also benefit from the modelling approach applied in this thesis, as current models have limited chemical information in them, and thus cannot respond to chemical changes in the fuel. This would require improvements in the understanding of the chemical reactions that govern this process, as well as, better descriptions of the physical transport mechanisms that are important in the formation of deposition.

The multi-disciplinary approach to studying autoxidation carried out in this thesis offers a number of benefits. It allows for knowledge from other fields to be applied to thermal stability and the utilisation of cutting edge techniques to study complex problems. As a general point, research carried out this way can generate more interesting results, and can have higher impact in the academic field and provide more insight for the public.

Published work originating from this thesis

8.1 Journal articles

1. Ehsan Alborzi, Phil Gadsby, Mohammed S. Ismail, Abdolkarim Sheikhansari, **Matthew R. Dwyer**, Anthony J. H. M. Meijer, Simon G. Blakey and Mohamed Pourkashanian, "Comparative Study of the Effect of Fuel Deoxygenation and Polar Species Removal on Jet Fuel Surface Deposition" , *Energy and Fuels*, 2019, **33**, 1825-1836.

2. Ehsan Alborzi, **Matthew R Dwyer**, Christopher M Parks, Abdolkarim Sheikhansari, Anthony J Meijer, Simon G Blakey, Mohammed Pourkashanian, "Construction of a Reduced Chemical Kinetic Mechanism for Autoxidation of n-Paraffinic Solvent- A Model for Aviation Fuel", submitted to FUEL.

8.2 Conference papers

1. **Matthew R. Dwyer** Simon G. Blakey, Ehsan Alborzi, Anthony J. H. M. Meijer, "The role of hydrocarbon composition on the thermal stability of aviation fuel", *International symposium of stability, handling and use of fuels*, **IASH 2017**, Rome, 10-14 Sept. 2017

2. **Matthew R. Dwyer** Simon G. Blakey, Ehsan Alborzi, Anthony J. H. M. Meijer, "Investigating the autoxidation accelerating reactions of peroxides and peroxyl radicals using quantum chemistry calculations", *International symposium of stability, handling and use of fuels*, **IASH 2019**, Long Beach, 8-12 Sept 2019

8.3 Conference posters

1. **Matthew R. Dwyer** Simon G. Blakey, Ehsan Alborzi, Anthony J. H. M. Meijer, "Investigating the role of peroxides in the oxidation of aviation fuel using quantum chemistry" *MOLEC*, Dinard, France, 26-31 Aug 2018.

2. **Matthew R. Dwyer** Simon G. Blakey, Ehsan Alborzi, Anthony J. H. M. Meijer, "The role of hydrocarbon composition on the thermal stability of aviation fuel", *Young Modellers Forum*, Greenwich, UK, 24 Nov 2017.

3. **Matthew R. Dwyer** Simon G. Blakey, Ehsan Alborzi, Anthony J. H. M. Meijer, "The role of hydrocarbon composition on the thermal stability of aviation fuel", *ANUMOCP 2017*, Sheffield, UK, July 2017.

4. **Matthew R. Dwyer** Simon G. Blakey, Ehsan Alborzi, Anthony J. H. M. Meijer, "Methodologies for hydrocarbon autoxidation mechanism generation", *ECATS*, Athens, Greece, 7-9 Nov 2016.

5. **Matthew R. Dwyer** Simon G. Blakey, Ehsan Alborzi, Anthony J. H. M. Meijer, "Methodologies for hydrocarbon autoxidation mechanism generation", *UK Theoretical Chemistry Summer School 2016*, Oxford, UK, Sept 2016.

Bibliography

(1) IEA, *IEA World Energy Outlook, 2016*, tech. rep., IEA, 2016 (cit. on pp. 1, 2).

(2) R. N. Hazlett, *Thermal Oxidation Stability of Aviation Turbine Fuels*, 1991, p. 163, DOI: `10.1520/MONO1-EB` (cit. on pp. 1, 10, 11, 94, 96, 133).

(3) ICAO, *ICAO Annual Report, 2017*, tech. rep., ICAO, 2017 (cit. on pp. 2, 3).

(4) R.-R. plc, *The Jet Engine*, Rolls-Royce plc, Derby, Uk, 1996 (cit. on p. 2).

(5) L. Rye, S. Blakey and C. W. Wilson, "Sustainability of supply or the planet: a review of potential drop-in alternative aviation fuels", *Energy & Environmental Science*, 2010, **3**, 17, DOI: `10.1039/b918197k` (cit. on p. 3).

(6) IATA, *IATA Alternative Fuels Report, 2015*, tech. rep., IATA, 2015 (cit. on p. 3).

(7) A. International, *ASTM D1655-12 - Standard Specification for Aviation Turbine Fuels*, tech. rep., ASTM International, 2019, p. 23 (cit. on pp. 4, 6, 14, 74, 183).

(8) M. of Defence, *Defence Standard 91-91*, tech. rep., Ministry of Defence, 2015, p. 38 (cit. on pp. 4, 183).

(9) A. International, *D324119 - Standard Test Method for Thermal Oxidation Stability of Aviation Turbine Fuels*, tech. rep., ASTM International, 2019, p. 25 (cit. on pp. 5, 6).

(10) L. J. Spadaccini, D. R. Sobel and H. Huang, "Deposit Formation and Mitigation in Aircraft Fuels", *Journal of Engineering for Gas Turbines and Power*, 2001, **123**, 741–746, DOI: `10.1115/1.1383772` (cit. on pp. 5, 134, 135, 137).

(11) E. T. Denisov and I. B. Afanas'ev, *Oxidation and Antioxidants in Organic Chemistry and Biology*, CRC Press, Boca Raton, 2005, DOI: `https://doi.org/10.1201/9781420030853` (cit. on pp. 6, 107, 131, 219, 223, 227).

(12) J. L. Bolland, "Kinetic Studies in the Chemistry of Rubber and Related Materials. I. The Thermal Oxidation of Ethyl Linoleate", *Procc. Roy. Soc.*, 1946, **A185**, 218–236 (cit. on p. 7).

(13) L. Bateman, "Olefin oxidation", *Q. Rev. Chem. Soc.*, 1954, **8**, 147–167 (cit. on p. 7).

(14) N. J. Kuprowicz, S. Zabarnick, Z. J. West and J. S. Ervin, "Use of measured species class concentrations with chemical kinetic modeling for the prediction of autoxidation and deposition of jet fuels", *Energy and Fuels*, 2007, **21**, 530–544, DOI: `10.1021/ef060391o` (cit. on pp. 7, 103, 118, 122, 123, 194, 234, 241, 242, 249, 250).

(15) C. G. Kabana, S. Botha, C. Schmucker, C. Woolard and B. Beaver, "Oxidative Stability of Middle Distillate Fuels. Part 1: Exploring the Soluble Macromolecular Oxidatively Reactive Species (SMORS) Mechanism with Jet Fuels", *Energy & Fuels*, 2011, **25**, 5145–5157, DOI: `10.1021/ef200964z` (cit. on pp. 8, 86, 87, 92, 94, 96, 241, 246, 249, 250).

(16) A. B. F. Wiki, *A Barrel Full of Oil*, 2019, `http://abarrelfull.wikidot.com/crude-oil-types` (visited on 06/19/2019) (cit. on p. 10).

(17) U. S. E. I. Administration, *U.S. Energy Information Administration, based on Energy Intelligence Group—International Crude Oil Market Handbook*, tech. rep., United States Energy Information Administration, 2013 (cit. on p. 10).

(18) P. 2015, *Petroleum benchmarks*, 2015, `http://www.petroleum.co.uk/benchmarks` (visited on 06/19/2019) (cit. on p. 10).

(19) M. Beychok, *Petroleum benchmarks*, 2019, `https://en.wikipedia.org/wiki/Oil_refinery` (visited on 07/22/2019) (cit. on p. 12).

(20) A. International, *D756619 - Standard Specification for Aviation Turbine Fuel Containing Synthesized Hydrocarbons*, tech. rep., ASTM International, 2019, p. 35 (cit. on pp. 12, 74).

(21) L. de Broglie, "XXXV. A tentative theory of light quanta", *The London, Edinburgh, and Dublin Philosophical Magazine and Journal of Science*, 1924, **47**, 446–458, DOI: `10.1080/14786442408634378` (cit. on p. 19).

(22) P. Atkins and J. Paula, *Physical Chemistry. 9th Edition*, W. H. Freeman Co., New York, 2010 (cit. on pp. 19, 21).

(23) J. A. Pople, *Quantum chemical models*, Nobel prize lecture (cit. on pp. 19, 36, 37).

(24) M. Born, W. Heisenberg and P. Jordan, "Zur Quantenmechanik II", *Zeitschrift für Physik*, 1925, **35**, English translation in: B. L. van der Waerden, Sources of Quantum Mechanics, 557–615 (cit. on p. 20).

(25) M. Born and P. Jordan, "Zur Quantenmechanik", *Zeitschrift für Physik*, 1925, **34**, English translation in: B. L. van der Waerden, Sources of Quantum Mechanics, 858–888 (cit. on p. 20).

(26) W. Heisenberg, "Über quantentheoretische Umdeutung kinematischer und mechanischer Beziehungen", *Zeitschrift für Physik*, 1925, **33**, English translation in: B. L. van der Waerden, Sources of Quantum Mechanics, 879–893 (cit. on p. 20).

(27) E. Schrödinger, "Quantisierung als Eigenwertproblem (Erste Mitteilung)", *Annalen der Physik*, 1926, **79**, 361–376 (cit. on p. 20).

(28) E. Schrödinger, "Quantisierung als Eigenwertproblem (Zweite Mitteilung)", *Annalen der Physik*, 1926, **79**, 489–527 (cit. on p. 20).

(29) E. Schrödinger, "Quantisierung als Eigenwertproblem (Dritte Mitteilung)", *Annalen der Physik*, 1926, **80**, 437–490 (cit. on p. 20).

(30) E. Schrödinger, "Quantisierung als Eigenwertproblem (Vierte Mitteilung)", *Annalen der Physik*, 1926, **81**, 109–139 (cit. on p. 20).

(31) E. Schrödinger, "Über das Verhältnis der Heisenberg-Born-Jordanschen Quantenmechanik zu der meinen", *Annalen der Physik*, 1926, **79**, 734–756 (cit. on p. 20).

(32) E. Schrödinger, "An Undulatory Theory of the Mechanics of Atoms and Molecules", *Phys. Rev.*, 1926, **28**, 1049–1070, DOI: `10.1103/PhysRev.28.1049` (cit. on p. 20).

(33) E. Schrödinger, "Der stetige Übergang von der Mikro- zur Makromechanik", *Die Naturwissenschaften*, 1926, **14**, 664–666 (cit. on p. 20).

(34) A. Szabo and N. S. Ostlund, *Modern Quantum Chemistry*, Dover Publications incorporated, Mineola, New York, 1996 (cit. on p. 21).

(35) I. N. Levine, *Quantum Chemistry, 4th edition*, Prentice Hall, Englewood cliffs, NJ, 1991 (cit. on p. 21).

(36) M. Born and R. Oppenheimer, "Zur Quantentheorie der Molekeln", *Annalen der Physik*, 1927, **389**, 457–484, DOI: `10.1002/andp.19273892002` (cit. on p. 23).

(37) M. Born and R. Oppenheimer, "Zur Quantentheorie der Molekeln - English translation", *Quantum chemistry - classic scientific papers*, 2000, **1**, 1–24 (cit. on p. 23).

(38) P. A. M. Dirac, "A new notation for quantum mechanics", *Mathematical Proceedings of the Cambridge Philosophical Society*, 1939, **35**, 416–418, DOI: `10.1017/S0305004100021162` (cit. on p. 26).

(39) P. Echenique and J. L. Alonso, "A mathematical and computational review of Hartree–Fock SCF methods in quantum chemistry", *Molecular Physics*, 2007, **105**, 3057–3098, DOI: `10.1080/00268970701757875` (cit. on p. 28).

(40) D. R. Hartree, "The Wave Mechanics of an Atom with a Non-Coulomb Central Field. Part I. Theory and methods", *Mathematical Proceedings of the Cambridge Philosophical Society*, 1928, **24**, 89–111 (cit. on p. 28).

(41) D. R. Hartree, "The Wave Mechanics of an Atom with a Non-Coulomb Central Field. Part II. Some Results and Discussion", *Mathematical Proceedings of the Cambridge Philosophical Society*, 1928, **24**, 111–132, DOI: `10.1017/S0305004100011920` (cit. on p. 28).

(42) D. R. Hartree, "The Wave Mechanics of an Atom with a Non-Coulomb Central Field. Part III. Term vlaues and intensities in series in optical spectra", *Mathematical Proceedings of the Cambridge Philosophical Society*, 1928, **24**, 426–437 (cit. on p. 28).

(43) D. R. Hartree, "The Wave Mechanics of an Atom with a Non-Coulomb Central Field. Part IV. Further results relating to terms of the optical spectrum", *Mathematical Proceedings of the Cambridge Philosophical Society*, 1929, **25**, 310–314 (cit. on p. 28).

(44) J. C. Slater, "Note on Hartree's Method", *Phys. Rev.*, 1930, **35**, 210–211, DOI: 10.1103/PhysRev.35.210.2 (cit. on p. 28).

(45) J. A. Gaunt, "A Theory of Hartree's Atomic Fields", *Mathematical Proceedings of the Cambridge Philosophical Society*, 1928, **24**, 328–342, DOI: 10.1017/S0305004100015851 (cit. on p. 28).

(46) J. C. Slater, "The Theory of Complex Spectra", *Phys. Rev.*, 1929, **34**, 1293–1322, DOI: 10.1103/PhysRev.34.1293 (cit. on pp. 30, 31, 46).

(47) E. U. Condon, "The Theory of Complex Spectra", *Phys. Rev.*, 1930, **36**, 1121–1133, DOI: 10.1103/PhysRev.36.1121 (cit. on pp. 31, 46).

(48) P.-O. Löwdin, "Quantum Theory of Many-Particle Systems. I. Physical Interpretations by Means of Density Matrices, Natural Spin-Orbitals, and Convergence Problems in the Method of Configurational Interaction", *Phys. Rev.*, 1955, **97**, 1474–1489, DOI: 10.1103/PhysRev.97.1474 (cit. on p. 31).

(49) C. C. J. Roothaan, "New Developments in Molecular Orbital Theory", *Rev. Mod. Phys.*, 1951, **23**, 69–89, DOI: 10.1103/RevModPhys.23.69 (cit. on p. 36).

(50) J. C. Slater, "The Self Consistent Field and the Structure of Atoms", *Phys. Rev.*, 1928, **32**, 339–348, DOI: 10.1103/PhysRev.32.339 (cit. on p. 36).

(51) V. Fock, "„Selfconsistent field" mit Austausch für Natrium", *Zeitschrift für Physik*, 1930, **62**, 795–805, DOI: 10.1007/BF01330439 (cit. on p. 36).

(52) V. Fock, "Näherungsmethode zur Lösung des quantenmechanischen Mehrkörperproblems", *Zeitschrift für Physik*, 1930, **61**, 126–148, DOI: 10.1007/BF01340294 (cit. on p. 36).

(53) L. A. Curtiss, K. Raghavachari, P. C. Redfern, V. Rassolov and J. A. Pople, "Gaussian-3 (G3) theory for molecules containing first and second-row atoms", *The Journal of Chemical Physics*, 1998, **109**, 7764–7776, DOI: 10.1063/1.477422 (cit. on p. 36).

(54) J. A. Pople and R. K. Nesbet, "Self-Consistent Orbitals for Radicals", *The Journal of Chemical Physics*, 1954, **22**, 571–572, DOI: 10.1063/1.1740120 (cit. on p. 37).

(55) J. A. Pople, D. P. Santry and G. A. Segal, "Approximate Self-Consistent Molecular Orbital Theory. I. Invariant Procedures", *The Journal of Chemical Physics*, 1965, **43**, S129–S135, DOI: 10.1063/1.1701475 (cit. on p. 37).

(56) J. A. Pople and G. A. Segal, "Approximate Self-Consistent Molecular Orbital Theory. II. Calculations with Complete Neglect of Differential Overlap", *The Journal of Chemical Physics*, 1965, **43**, S136–S151, DOI: 10.1063/1.1701476 (cit. on p. 37).

(57) R. Krishnan, J. S. Binkley, R. Seeger and J. A. Pople, "Self-consistent molecular orbital methods. XX. A basis set for correlated wave functions", *The Journal of Chemical Physics*, 1980, **72**, 650–654, DOI: 10.1063/1.438955 (cit. on p. 37).

(58) P. Hoggan, M. B. Ruiz Ruiz and T Özdoğan, "Molecular integrals over slater-type orbitals. From pioneers to recent developments", *Quantum Frontiers of Atoms and Molecules*, 2011, 61–89 (cit. on p. 37).

(59) M. Putz, *Quantum Frontiers of Atoms and Molecules*, Nova Science Publishers, 2011 (cit. on p. 37).

(60) F. Weigend and R. Ahlrichs, "Balanced basis sets of split valence, triple zeta valence and quadruple zeta valence quality for H to Rn: Design and assessment of accuracy", *Phys. Chem. Chem. Phys.*, 2005, **7**, 3297–3305, DOI: 10.1039/B508541A (cit. on p. 37).

(61) F. Weigend and R. Ahlrichs, "Balanced basis sets of split valence, triple zeta valence and quadruple zeta valence quality for H to Rn: Design and assessment of accuracy", *Phys. Chem. Chem. Phys.*, 2005, **7**, 3297–3305, DOI: 10.1039/B508541A (cit. on p. 37).

(62) K. A. Peterson, D. E. Woon and T. H. Dunning, "Benchmark calculations with correlated molecular wave functions. IV. The classical barrier height of the H+H2→H2+H reaction", *The Journal of Chemical Physics*, 1994, **100**, 7410–7415, DOI: 10.1063/1.466884 (cit. on pp. 37, 196).

(63) T. H. Dunning, "Gaussian basis sets for use in correlated molecular calculations. I. The atoms boron through neon and hydrogen", *The Journal of Chemical Physics*, 1989, **90**, 1007–1023, DOI: 10.1063/1.456153 (cit. on pp. 37, 196).

(64) D. E. Woon and T. H. Dunning, "Gaussian basis sets for use in correlated molecular calculations. III. The atoms aluminum through argon", *The Journal of Chemical Physics*, 1993, **98**, 1358–1371, DOI: 10.1063/1.464303 (cit. on pp. 37, 196).

(65) R. A. Kendall, T. H. Dunning and R. J. Harrison, "Electron affinities of the first-row atoms revisited. Systematic basis sets and wave functions", *The Journal of Chemical Physics*, 1992, **96**, 6796–6806, DOI: 10.1063/1.462569 (cit. on pp. 37, 196).

(66) E. R. Davidson, "Comment on "Comment on Dunning's correlation-consistent basis sets"", *Chemical Physics Letters*, 1996, **260**, 514 –518, DOI: `https://doi.org/10.1016/0009-2614(96)00917-7` (cit. on pp. 37, 196).

(67) P. O. Löwdin, *Advances in chemical physics 1st ed*, John Wiley & sons Inc, 1959, vol. 2 (cit. on p. 38).

(68) E. Valderrama, E. V. Ludeña and J. Hinze, "Analysis of dynamical and nondynamical components of electron correlation energy by means of local-scaling density-functional theory", *The Journal of Chemical Physics*, 1997, **106**, 9227–9235, DOI: `10.1063/1.474024` (cit. on p. 38).

(69) E. Ramos-Cordoba, P. Salvador and E. Matito, "Separation of dynamic and nondynamic correlation", *Phys. Chem. Chem. Phys.*, 2016, **18**, 24015–24023, DOI: `10.1039/C6CP03072F` (cit. on p. 38).

(70) E. R. Davidson, S. A. Hagstrom, S. J. Chakravorty, V. M. Umar and C. F. Fischer, "Ground-state correlation energies for two- to ten-electron atomic ions", *Phys. Rev. A*, 1991, **44**, 7071–7083, DOI: `10.1103/PhysRevA.44.7071` (cit. on p. 38).

(71) H.-J. Werner, "Third-order multireference perturbation theory The CASPT3 method", *Molecular Physics*, 1996, **89**, 645–661, DOI: `10.1080/002689796173967` (cit. on pp. 39, 51).

(72) P. Celani and H.-J. Werner, "Multireference perturbation theory for large restricted and selected active space reference wave functions", *The Journal of Chemical Physics*, 2000, **112**, 5546–5557, DOI: `10.1063/1.481132` (cit. on pp. 39, 51).

(73) H. Werner and P. J. Knowles, "A second order multiconfiguration SCF procedure with optimum convergence", *The Journal of Chemical Physics*, 1985, **82**, 5053–5063, DOI: `10.1063/1.448627` (cit. on pp. 43, 51).

(74) P. J. Knowles and H.-J. Werner, "An efficient second-order MC SCF method for long configuration expansions", *Chemical Physics Letters*, 1985, **115**, 259 –267, DOI: `https://doi.org/10.1016/0009-2614(85)80025-7` (cit. on pp. 43, 51).

(75) H. Werner and P. J. Knowles, "An efficient internally contracted multiconfiguration–reference configuration interaction method", *The Journal of Chemical Physics*, 1988, **89**, 5803–5814, DOI: `10.1063/1.455556` (cit. on p. 43).

(76) D. A. Kreplin, P. J. Knowles and H.-J. Werner, "Second-order MCSCF optimization revisited. I. Improved algorithms for fast and robust second-order CASSCF convergence", *The Journal of Chemical Physics*, 2019, **150**, 194106, DOI: `10.1063/1.5094644` (cit. on p. 43).

(77) H. Werner and W. Meyer, "A quadratically convergent MCSCF method for the simultaneous optimization of several states", *The Journal of Chemical Physics*, 1981, **74**, 5794–5801, DOI: `10.1063/1.440892` (cit. on p. 43).

(78) H. Werner and W. Meyer, "A quadratically convergent multiconfiguration–self-consistent field method with simultaneous optimization of orbitals and CI coefficients", *The Journal of Chemical Physics*, 1980, **73**, 2342–2356, DOI: `10.1063/1.440384` (cit. on p. 43).

(79) J. Olsen, B. O. Roos, P. Jörgensen and H. J. A. Jensen, "Determinant based configuration interaction algorithms for complete and restricted configuration interaction spaces", *The Journal of Chemical Physics*, 1988, **89**, 2185–2192, DOI: `10.1063/1.455063` (cit. on p. 48).

(80) P. A. Malmqvist, A. Rendell and B. O. Roos, "The restricted active space self-consistent-field method, implemented with a split graph unitary group approach", *The Journal of Physical Chemistry*, 1990, **94**, 5477–5482, DOI: `10.1021/j100377a011` (cit. on p. 48).

(81) B. O. Roos, P. R. Taylor and P. E. Sigbahn, "A complete active space SCF method (CASSCF) using a density matrix formulated super-CI approach", *Chemical Physics*, 1980, **48**, 157 –173, DOI: `https://doi.org/10.1016/0301-0104(80)80045-0` (cit. on p. 48).

(82) L. M. Cheung, K. R. Sundberg and K. Ruedenberg, "Dimerization of carbene to ethylene", *Journal of the American Chemical Society*, 1978, **100**, 8024–8025, DOI: `10.1021/ja00493a050` (cit. on p. 48).

(83) K. Ruedenberg, M. W. Schmidt, M. M. Gilbert and S. Elbert, "Are atoms intrinsic to molecular electronic wavefunctions? III. Analysis of FORS configurations", *Chemical Physics*, 1982, **71**, 65 –78, DOI: `https://doi.org/10.1016/0301-0104(82)87006-7` (cit. on p. 48).

(84) P. G. Szalay, T. Müller, G. Gidofalvi, H. Lischka and R. Shepard, "Multiconfiguration self-consistent field and multireference configuration interaction methods and applications", *Chemical Reviews*, 2012, **112**, 108–181, DOI: `10.1021/cr200137a` (cit. on p. 50).

(85) E. Fermi, "Un Metodo Statistico per la Determinazione di alcune Prioprietà dell'Atomo", *Rend. Accad. Naz. Lincei*, 1927, **6**, 602–607 (cit. on p. 51).

(86) L. H. Thomas, "The calculation of atomic fields", *Mathematical Proceedings of the Cambridge Philosophical Society*, 1927, **23**, 542–548, DOI: `10.1017/S0305004100011683` (cit. on p. 51).

(87) P. Hohenberg and W. Kohn, "Inhomogeneous Electron Gas", *Phys. Rev.*, 1964, **136**, B864–B871, DOI: `10.1103/PhysRev.136.B864` (cit. on p. 53).

(88) W. Kohn, *Electronic structure of matter - Wave functions and density functionals*, Nobel prize lecture (cit. on p. 53).

(89) E. H. Lieb, "The stability of matter: from atoms to stars", *Bull. Amer. Math. Soc. (N.S.)*, 1990, **22**, 1–49 (cit. on pp. 53, 54).

(90) M. Levy and J. P. Perdew, "In defense of the Hohenberg–Kohn theorem and density functional theory", *International Journal of Quantum Chemistry*, 1982, **21**, 511–513, DOI: `10.1002/qua.560210213` (cit. on pp. 53, 54).

(91) W. Kohn and L. J. Sham, "Self-Consistent Equations Including Exchange and Correlation Effects", *Phys. Rev.*, 1965, **140**, A1133–A1138, DOI: `10.1103/PhysRev.140.A1133` (cit. on p. 55).

(92) E. J. Baerends, O. V. Gritsenko and R. van Meer, "The Kohn–Sham gap, the fundamental gap and the optical gap: the physical meaning of occupied and virtual Kohn–Sham orbital energies", *Phys. Chem. Chem. Phys.*, 2013, **15**, 16408–16425, DOI: `10.1039/C3CP52547C` (cit. on p. 58).

(93) R. van Meer, O. V. Gritsenko and E. J. Baerends, "Physical Meaning of Virtual Kohn–Sham Orbitals and Orbital Energies: An Ideal Basis for the Description of Molecular Excitations", *Journal of Chemical Theory and Computation*, 2014, **10**, 4432–4441, DOI: `10.1021/ct500727c` (cit. on p. 58).

(94) D. Ceperley, "Ground state of the fermion one-component plasma: A Monte Carlo study in two and three dimensions", *Physical Review B*, 1978, **18**, 3126–3138, DOI: `10.1103/PhysRevB.18.3126` (cit. on p. 60).

(95) D. M. Ceperley and B. J. Alder, "Ground State of the Electron Gas by a Stochastic Method", *Phys. Rev. Lett.*, 1980, **45**, 566–569, DOI: `10.1103/PhysRevLett.45.566` (cit. on p. 60).

(96) E. Wigner, "Effects of the electron interaction on the energy levels of electrons in metals", *Transactions of the Faraday Society*, 1938, **34**, 678, DOI: `10.1039/TF9383400678` (cit. on p. 60).

(97) J Harris and R. O. Jones, "The surface energy of a bounded electron gas", *Journal of Physics F: Metal Physics*, 1974, **4**, 1170–1186, DOI: `10.1088/0305-4608/4/8/013` (cit. on p. 60).

(98) D. C. Langreth and J. P. Perdew, "The exchange-correlation energy of a metallic surface", *Solid State Communications*, 1975, **17**, 1425–1429, DOI: `10.1016/0038-1098(75)90618-3` (cit. on p. 60).

(99) O. Gunnarsson and B. I. Lundqvist, "Exchange and correlation in atoms, molecules, and solids by the spin-density-functional formalism", *Phys. Rev. B*, 1976, **13**, 4274–4298, DOI: `10.1103/PhysRevB.13.4274` (cit. on p. 60).

(100) D. C. Langreth and M. J. Mehl, "Beyond the local-density approximation in calculations of ground-state electronic properties", *Phys. Rev. B*, 1983, **28**, 1809–1834, DOI: `10.1103/PhysRevB.28.1809` (cit. on p. 61).

(101) A. D. Becke, "Density-functional exchange-energy approximation with correct asymptotic behavior", *Phys. Rev. A*, 1988, **38**, 3098–3100, DOI: `10.1103/PhysRevA.38.3098` (cit. on p. 61).

(102) J. P. Perdew, J. A. Chevary, S. H. Vosko, K. A. Jackson, M. R. Pederson, D. J. Singh and C. Fiolhais, "Atoms, molecules, solids, and surfaces: Applications of the generalized gradient approximation for exchange and correlation", *Phys. Rev. B*, 1992, **46**, 6671–6687, DOI: `10.1103/PhysRevB.46.6671` (cit. on p. 61).

(103) A. D. Becke, "Density-functional thermochemistry. III. The role of exact exchange", *The Journal of Chemical Physics*, 1993, **98**, 5648–5652, DOI: `10.1063/1.464913` (cit. on p. 62).

(104) C. Lee, W. Yang and R. G. Parr, "Development of the Colle-Salvetti correlation-energy formula into a functional of the electron density", *Phys. Rev. B*, 1988, **37**, 785–789, DOI: `10.1103/PhysRevB.37.785` (cit. on p. 62).

(105) J.-D. Chai and M. Head-Gordon, "Long-range corrected hybrid density functionals with damped atom–atom dispersion corrections", *Phys. Chem. Chem. Phys.*, 2008, **10**, 6615–6620, DOI: `10.1039/B810189B` (cit. on p. 62).

(106) A. D. Becke, "Perspective: Fifty years of density-functional theory in chemical physics", *The Journal of Chemical Physics*, 2014, **140**, 18A301, DOI: `10.1063/1.4869598` (cit. on p. 62).

(107) H. S. Yu, S. L. Li and D. G. Truhlar, "Perspective: Kohn-Sham density functional theory descending a staircase", *The Journal of Chemical Physics*, 2016, **145**, 130901, DOI: `10.1063/1.4963168` (cit. on p. 62).

(108) H. Eyring, "The Activated Complex in Chemical Reactions", *The Journal of Chemical Physics*, 1935, **3**, 107–115, DOI: `10.1063/1.1749604` (cit. on pp. 63, 64).

(109) M. G. Evans and M. Polanyi, "Some applications of the transition state method to the calculation of reaction velocities, especially in solution", *Trans. Faraday Soc.*, 1935, **31**, 875–894, DOI: `10.1039/TF9353100875` (cit. on pp. 63, 64).

(110) S. Kozuch and J. M. L. Martin, "The Rate-Determining Step is Dead. Long Live the Rate-Determining State!", *ChemPhysChem*, 2011, **12**, 1413–1418, DOI: `10.1002/cphc.201100137` (cit. on pp. 63, 66).

(111) D. Chandler and D. E. Manolopoulos, "Reaction rate theory: summarising remarks", *Faraday Discuss.*, 2016, **195**, 699–710, DOI: `10.1039/C6FD00229C` (cit. on p. 64).

(112) R. Levine, "The steric factor in transition state theory and in collison theory", *Chemical Physics Letters*, 1990, **175**, 331 –337, DOI: `https://doi.org/10.1016/0009-2614(90)80120-3` (cit. on p. 64).

(113) H. Ryu, J. Park, H. K. Kim, J. Y. Park, S.-T. Kim and M.-H. Baik, "Pitfalls in Computational Modeling of Chemical Reactions and How To Avoid Them", *Organometallics*, 2018, **37**, 3228–3239, DOI: `10.1021/acs.organomet.8b00456` (cit. on p. 64).

(114) J. L. Bao, J. Zheng and D. G. Truhlar, "Kinetics of Hydrogen Radical Reactions with Toluene Including Chemical Activation Theory Employing System-Specific Quantum RRK Theory Calibrated by Variational Transition State Theory", *Journal of the American Chemical Society*, 2016, **138**, PMID: 26841076, 2690–2704, DOI: `10.1021/jacs.5b11938` (cit. on p. 64).

(115) B. Peters, "Common Features of Extraordinary Rate Theories", *The Journal of Physical Chemistry B*, 2015, **119**, 6349–6356, DOI: `10.1021/acs.jpcb.5b02547` (cit. on p. 64).

(116) S. J. Klippenstein, "From theoretical reaction dynamics to chemical modeling of combustion", *Proceedings of the Combustion Institute*, 2017, **36**, 77 –111, DOI: `https://doi.org/10.1016/j.proci.2016.07.100` (cit. on p. 64).

(117) S. J. Klippenstein, L. B. Harding and B. Ruscic, "Ab Initio Computations and Active Thermochemical Tables Hand in Hand: Heats of Formation of Core Combustion Species", *The Journal of Physical Chemistry A*, 2017, **121**, PMID: 28758403, 6580–6602, DOI: `10.1021/acs.jpca.7b05945` (cit. on p. 64).

(118) D. G. Truhlar, B. C. Garrett and S. J. Klippenstein, "Current Status of Transition-State Theory", *The Journal of Physical Chemistry*, 1996, **100**, 12771–12800, DOI: `10.1021/jp953748q` (cit. on p. 64).

(119) J. Ochterski, *Thermochemistry in Gaussian*, tech. rep., Guassain, 2000 (cit. on p. 64).

(120) P. L. Houston, *Chemical kinetics and reaction dynamics*, Dover Publications, Mineola, N.Y, 2006 (cit. on p. 64).

(121) R. Paton, I. Funes-Ardoiz, G. Luchini, J. V. Alegre-Requena, Y. Guan and J. Rodríguez-Guerra, *GoodVibes*, 2019, `https://github.com/bobbypaton/GoodVibes` (visited on 09/12/2019) (cit. on pp. 65, 198, 200, 203, 205, 206).

(122) S. Grimme, "Supramolecular Binding Thermodynamics by Dispersion-Corrected Density Functional Theory", *Chemistry – A European Journal*, 2012, **18**, 9955–9964, DOI: `10.1002/chem.201200497` (cit. on pp. 65, 198, 200, 203, 205, 206).

(123) M. Mammen, E. I. Shakhnovich, J. M. Deutch and G. M. Whitesides, "Estimating the Entropic Cost of Self-Assembly of Multiparticle Hydrogen-Bonded Aggregates Based on the Cyanuric Acid·Melamine Lattice", *The Journal of Organic Chemistry*, 1998, **63**, 3821–3830, DOI: `10.1021/jo970944f` (cit. on p. 65).

(124) I. M. Alecu, J. Zheng, Y. Zhao and D. G. Truhlar, "Computational Thermochemistry: Scale Factor Databases and Scale Factors for Vibrational Frequencies Obtained from Electronic Model Chemistries", *Journal of Chemical Theory and Computation*, 2010, **6**, 2872–2887, DOI: `10.1021/ct100326h` (cit. on p. 65).

(125) Y.-P. Li, J. Gomes, S. Mallikarjun Sharada, A. T. Bell and M. Head-Gordon, "Improved Force-Field Parameters for QM/MM Simulations of the Energies of Adsorption for Molecules in Zeolites and a Free Rotor Correction to the Rigid Rotor Harmonic Oscillator Model for Adsorption Enthalpies", *The Journal of Physical Chemistry C*, 2015, **119**, 1840–1850, DOI: `10.1021/jp509921r` (cit. on pp. 65, 198, 200, 203, 205, 206).

(126) R. F. Ribeiro, A. V. Marenich, C. J. Cramer and D. G. Truhlar, "Use of Solution-Phase Vibrational Frequencies in Continuum Models for the Free Energy of Solvation", *The Journal of Physical Chemistry B*, 2011, **115**, 14556–14562, DOI: `10.1021/jp205508z` (cit. on p. 65).

(127) F. R. Mayo and a. a. Miller, "Oxidation of Unsaturated Compounds. II. Reactions of Styrene Peroxide", *Journal of American Chemical Society*, 1956, **78**, 1023 (cit. on p. 69).

(128) F. R. Mayo, "Free-radical autoxidations of hydrocarbons", *Accounts Chem. Res.*, 1968, **1**, 193–201, DOI: `10.1021/ar50007a001` (cit. on p. 69).

(129) J. A. Howard and K. U. Ingold, "Absolute Rate Constants for Hydrocarbon Autoxidation: I. Styrene", *Canadian Journal of Chemistry*, 1965, **43**, 2729–2736, DOI: `10.1139/v65-383` (cit. on p. 69).

(130) J. a. Howard and K. U. Ingold, "Absolute Rate Constants for Hydrocarbon Autoxidation: Iii. A-Methylstyrene, B-Methylstyrene, and Indene", *Canadian Journal of Chemistry*, 1966, **44**, 1113–1118, DOI: `10.1139/v66-168` (cit. on p. 69).

(131) J. a. Howard and K. U. Ingold, "Absolute rate constants for hydrocarbon autoxidation. VI. Alkyl aromatic and olefinic hydrocarbons", *Canadian Journal of Chemistry*, 1967, **45**, 793–802, DOI: `10.1139/v67-132` (cit. on p. 69).

(132) J. A. Howard and K. U. Ingold, "Absolute rate constants for hydrocarbon oxidation. XII. Rate constants for secondary radicals", *Can.J.Chem.*, 1968, **46**, 2661–2666 (cit. on p. 69).

(133) J. A. Howard and S. Korcek, "Absolute Rate Constants for Hydrocarbon Autoxidation. Part XX. Oxidation of Some Organic Sulfides", *Canadian Journal of Chemistry*, 1971, **49**, 2178–2182, DOI: `10.1139/v71-356` (cit. on pp. 69, 101).

(134) W. F. Taylor, "Kinetics of Deposit Formation from Hydrocarbons", *I & EC Product Research and Development*, 1969, **8**, 375–380 (cit. on pp. 69, 71, 72, 134, 152, 202, 252).

(135) W. F. Taylor, "Deposit Formation from Deoxygenated Hydrocarbons. I. General Features", *Product R&D*, 1974, **13**, 133–138, DOI: `10.1021/i360050a011` (cit. on pp. 69, 137).

(136) J. W. Frankenfeld and W. F. Taylor, "Deposit Formation from Deoxygenated Hydrocarbons. 4. Studies in Pure Compound Systems", *Industrial & Engineering Chemistry Product Research and Development*, 1980, **19**, 65–70, DOI: `10.1021/i360073a016` (cit. on p. 69).

(137) K. U. Ingold and D. A. Pratt, "Advances in radical-trapping antioxidant chemistry in the 21st century: A kinetics and mechanisms perspective", *Chemical Reviews*, 2014, **114**, 9022–9046, DOI: `10.1021/cr500226n` (cit. on p. 69).

(138) K. Chatelain, A. Nicolle, A. Ben Amara, L. Catoire and L. Starck, "Wide Range Experimental and Kinetic Modeling Study of Chain Length Impact on n-Alkanes Autoxidation", *Energy and Fuels*, 2016, **30**, 1294–1303, DOI: `10.1021/acs.energyfuels.5b02470` (cit. on pp. 70, 72, 128, 143, 154, 173, 174, 188, 197).

(139) K. Chatelain, A. Nicolle, A. Ben Amara, L. Starck and L. Catoire, "Structure–Reactivity Relationships in Fuel Stability: Experimental and Kinetic Modeling Study of Isoparaffin Autoxidation", *Energy & Fuels*, 2018, **32**, 9415–9426, DOI: `10.1021/acs.energyfuels.8b01379` (cit. on pp. 70, 129, 130, 174, 231).

(140) A. Ben Amara, S. Kaoubi and L. Starck, "Toward an optimal formulation of alternative jet fuels: Enhanced oxidation and thermal stability by the addition of cyclic molecules", *Fuel*, 2016, **173**, 98–105, DOI: `10.1016/j.fuel.2016.01.040` (cit. on pp. 70–72, 143, 145, 154, 167, 173, 188, 197).

(141) E. L. Wong and D. A. Bittker, *Effect of hydrocarbon fuel type on fuel thermal stability*, tech. rep., Lewis Research Centre, 1983, p. 11 (cit. on pp. 71, 113, 134).

(142) J. Igarashi, R. K. Jensen, J. Lusztyk, S. Korcek and K. U. Ingold, "Autoxidation of Alkylnaphthalenes. 2. Inhibition of the Autoxidation of n-Hexadecane at 160 °C", *Journal of the American Chemical Society*, 1992, **114**, 7727–7736, DOI: `10.1021/ja00046a019` (cit. on pp. 71, 73).

(143) J. Igarashi, J. Lusztyk and K. U. Ingold, "Autoxidation of Alkylnaphthalenes. 1. Self-Inhibition during the Autoxidation of 1-and 2-Methylnaphthalenes Puts a Limit on the Maximum Possible Kinetic Chain Length", *Journal of the American Chemical Society*, 1992, **114**, 7719–7726, DOI: `10.1021/ja00046a018` (cit. on pp. 71, 73).

(144) D. C. Mielczarek, M. Matrat, A. B. Amara, Y. Bouyou, P. Wund and L. Starck, "Toward the Accurate Prediction of Liquid Phase Oxidation of Aromatics: A Detailed Kinetic Mechanism for Toluene Autoxidation", *Energy and Fuels*, 2017, **31**, 12893–12913, DOI: `10.1021/acs.energyfuels.7b00416` (cit. on pp. 72, 128, 129).

(145) M. J. Dewitt, Z. West, S. Zabarnick, L. Shafer, R. Striebich, A. Higgins and T. Edwards, "Effect of Aromatics on the Thermal-Oxidative Stability of Synthetic Paraffinic Kerosene", 2014 (cit. on pp. 72, 73, 143).

(146) E. Corporan, T. Edwards, L. Shafer, M. J. DeWitt, C. Klingshirn, S. Zabarnick, Z. West, R. Striebich, J. Graham and J. Klein, "Chemical, Thermal Stability, Seal Swell, and Emissions Studies of Alternative Jet Fuels", *Energy & Fuels*, 2011, **25**, 955–966, DOI: `10.1021/ef101520v` (cit. on pp. 72, 73, 143).

(147) S. P. Heneghan and S. Zabarnick, "Oxidation of jet fuels and the formation of deposit", *Fuel*, 1994, **73**, 35–43, DOI: `10.1016/0016-2361(94)90185-6` (cit. on pp. 72, 233, 256).

(148) C. D. S. Blakey, S. Yusuf and C Wilson, "Effect of aromatic content on thermal stability of Jet Fuels", *IASH, 13th International Conference on Stability, Handling and Use of Liquid Fuels, Rhodes, Greece*, 2013, 1–14 (cit. on p. 73).

(149) E. G. Jones and L. M. Balster, "Interaction of a Synthetic Hindered-Phenol with Natural Fuel Antioxidants in the Autoxidation of Paraffins", *Energy & Fuels*, 2000, **14**, 640–645, DOI: `10.1021/ef990216q` (cit. on pp. 73, 74, 77).

(150) B. D. Batts and A. Fathoni, "A Literature Review on Fuel Stability Studies with Particular Emphasis on Diesel Oil", *Energy & Fuels*, 1991, **5**, 2–21, DOI: `10.1021/ef00025a001` (cit. on pp. 75, 85, 92, 94–96, 98, 99).

(151) A. Z. Fathoni and B. D. Batts, "A literature review of fuel stability studies with a particular emphasis on shale oil", *Energy & Fuels*, 1992, **6**, 681–693, DOI: `10.1021/ef00036a001` (cit. on pp. 75, 92, 94–96, 98–100).

(152) D. J. Abdallah, L. Kreno, F. P. Disanzo, R. G. Gaughan, W Mark, P. P. Wells, D. H. Hoskin, K. M. Penn, B. Brown and D. Wiseman, "Impact of additives on jet fuel thermal stability", *IASH 2013, the 13TH INTERNATIONAL SYMPOSIUM ON STABILITY, HANDLING AND USE OF LIQUID FUELS, Rhodes, Greece*, 2013 (cit. on pp. 75, 76, 84, 111).

(153) P. M. Rawson, C.-A. Stansfield, R. L. Webster and D. Evans, "Re-addition of antioxidant to aged MEROX and hydroprocessed jet fuels", *Fuel*, 2015, **139**, 652–658, DOI: `10.1016/j.fuel.2014.09.048` (cit. on pp. 76, 131).

(154) M. R. E., J. M. Hughes, Begue, N. J. and K. M. Myers, "Assessment of the effectiveness of antioxidant additions to Jet A", *IASH, 12th International Conference on Stability, Handling and Use of Liquid Fuels, Florida, USA*, 2011, 1–28 (cit. on p. 77).

(155) R. Dinkov, G. Hristov, D. Stratiev and V. Boynova Aldayri, "Effect of commercially available antioxidants over biodiesel/diesel blends stability", *Fuel*, 2009, **88**, 732–737, DOI: `10.1016/j.fuel.2008.09.017` (cit. on p. 77).

(156) J. S. Ervin and S. Zabarnick, "Computational Fluid Dynamics Simulations of Jet Fuel Oxidation Incorporating Pseudo-Detailed Chemical Kinetics", *Energy & Fuels*, 1998, **12**, 344–352, DOI: `10.1021/ef970132m` (cit. on pp. 78, 117, 119).

(157) S. Kerkering, W. Koch and J. T. Andersson, "In fl uence of Phenols on the Oxidation Stability of Home Heating Oils / FAME Blends", 2015, 8–14, DOI: `10.1021/ef502260d` (cit. on p. 78).

(158) R. Epping, S. Kerkering and J. T. Andersson, "Influence of Different Compound Classes on the Formation of Sediments in Fossil Fuels During Aging", *Energy & Fuels*, 2014, **28**, 5649–5656, DOI: `10.1021/ef501230c` (cit. on pp. 78, 79, 103, 155).

(159) S. P. Heneghan, C. R. Martel, T. F. Williams and D. R. Ballal, "Effects of Oxygen and Additives on the Thermal Stability of Jet Fuels", *Turbo Expo: Power for Land, Sea, and Air*, 1993, V002T05A005, DOI: `10.1115/93-GT-130` (cit. on pp. 79, 84).

(160) E. G. Jones, W. J. Balster and L. M. Balster, "Evaluation of the Effectiveness of a Metal Deactivator and Other Additives in Reducing Insolubles in Aviation Fuels", *Turbo Expo: Power for Land, Sea, and Air*, 1996, V003T06A035, DOI: `10.1115/96-GT-204` (cit. on pp. 79, 84).

(161) E. G. Jones, L. M. Balster and W. J. Balster, "Quantitative Evaluation of Jet-Fuel Fouling and the Effect of Additives", *Energy & Fuels*, 1995, **9**, 906–912, DOI: `10.1021/ef00053a025` (cit. on p. 79).

(162) G. Karavalakis, D. Hilari, L. Givalou, D. Karonis and S. Stournas, "Storage stability and ageing effect of biodiesel blends treated with different antioxidants", *Energy*, 2011, **36**, 369–374, DOI: `10.1016/j.energy.2010.10.029` (cit. on pp. 79, 80, 131).

(163) W. W. Focke, I. van der Westhuizen, A. L. Grobler, K. T. Nshoane, J. K. Reddy and A. S. Luyt, "The effect of synthetic antioxidants on the oxidative stability of biodiesel", *Fuel*, 2012, **94**, 227 –233, DOI: `https://doi.org/10.1016/j.fuel.2011.11.061` (cit. on pp. 79, 80).

(164) S. Kerkering, W. Koch and J. T. Andersson, "Influence of Phenols on the Oxidation Stability of Home Heating Oils/FAME Blends", *Energy & Fuels*, 2015, **29**, 793–799, DOI: `10.1021/ef502260d` (cit. on p. 80).

(165) M. Wijtmans, D. A. Pratt, J. Brinkhorst, R. Serwa, L. Valgimigli, G. F. Pedulli and N. A. Porter, "Synthesis and reactivity of some 6-substituted-2,4-dimethyl-3-pyridinols, a novel class of chain-breaking antioxidants", *Journal of Organic Chemistry*, 2004, **69**, 9215–9223, DOI: `10.1021/jo048842u` (cit. on pp. 80, 96).

(166) L. Valgimigli and D. A. Pratt, "Maximizing the Reactivity of Phenolic and Aminic Radical-Trapping Antioxidants: Just Add Nitrogen!", *Accounts of Chemical Research*, 2015, **48**, 966–975, DOI: `10.1021/acs.accounts.5b00035` (cit. on pp. 80, 81).

(167) E. A. Haidasz, R. Shah and D. A. Pratt, "The Catalytic Mechanism of Di-arylamine Radical-Trapping Antioxidants", *Journal of the American Chemical Society*, 2014, **136**, 16643–16650, DOI: `10.1021/ja509391u` (cit. on pp. 80, 81).

(168) B. D. Beaver, L. Gao, M. G. Fedak, M. M. Coleman and M. Sobkowiak, "Model Studies Examining the Use of Dicyclohexylphenylphosphine to Enhance the Oxidative and Thermal Stability of Future Jet Fuels", *Energy & Fuels*, 2002, **16**, 1134–1140, DOI: `10.1021/ef020028r` (cit. on pp. 80, 81).

(169) B. D. Beaver, C. B. Clifford, M. G. Fedak, L. Gao, P. S. Iyer and M., "High Heat Sink Jet Fuels. Part 1. Development of Potential Oxidative and Pyrolytic Additives for JP-8", *Energy & Fuels*, 2006, **20**, 1639–1646, DOI: `10.1021/ef050352x` (cit. on pp. 80–82).

(170) M. Sobkowiak, C. Burgess Clifford and B. Beaver, "High Heat Sink Jet Fuels. 2. Stabilization of a JP-8 with Model Refined Chemical Oil/Light Cycle Oil (RCO/LCO)-Derived Stabilizers", *Energy & Fuels*, 2007, **21**, 982–986, DOI: `10.1021/ef060422f` (cit. on pp. 80–82).

(171) B. Beaver, M. Sobkowiak, C. Burgess Clifford, Y. Wei and M. Fedek, "High Heat Sink Jet Fuels. 3. On the Mechanisms of Action of Model Refined Chemical Oil/Light Cycle Oil (RCO/LCO)-Derived Stabilizers for JP-8", *Energy & Fuels*, 2007, **21**, 987–991, DOI: `10.1021/ef0604238` (cit. on pp. 80–82).

(172) E. Bendary, R. Francis, H. Ali, M. Sarwat and S. E. Hady, "Antioxidant and structure–activity relationships (SARs) of some phenolic and anilines compounds", *Annals of Agricultural Sciences*, 2013, **58**, 173 –181, DOI: `https://doi.org/10.1016/j.aoas.2013.07.002` (cit. on p. 81).

(173) J. A. Waynick, "The Development and Use of Metal Deactivators in the Petroleum Industry: A Review", *Energy & Fuels*, 2001, **15**, 1325–1340, DOI: `10.1021/ef010113j` (cit. on pp. 82, 83, 108, 109).

(174) S. G. Pande and D. R. Hardy, "Effects of Extended Duration Testing and Time of Addition of N,N'-Disalicylidene-1,2-propanediamine on Jet Fuel Thermal Stability As Determined Using the Gravimetric JFTOT", *Energy & Fuels*, 1998, **12**, 129–138, DOI: `10.1021/ef970096r` (cit. on p. 83).

(175) S. Zabarnick and R. R. Grinstead, "Studies of Jet Fuel Additives using the Quartz Crystal Microbalance and Pressure Monitoring at 140.degree.C", *Industrial & Engineering Chemistry Research*, 1994, **33**, 2771–2777, DOI: `10.1021/ie00035a029` (cit. on p. 84).

(176) S. Zabarnick and S. D. Whitacre, "Aspects of Jet Fuel Oxidation", *Turbo Expo: Power for Land, Sea, and Air*, 1997, V002T06A029, DOI: `10.1115/97-GT-219` (cit. on p. 84).

(177) L. M. Balster, S. Zabarnick, R. C. Striebich, L. M. Shafer and Z. J. West, "Analysis of polar species in jet fuel and determination of their role in autoxidative deposit formation", *Energy and Fuels*, 2006, **20**, 2564–2571, DOI: `10.1021/ef060275l` (cit. on pp. 85, 86).

(178) R. C. Striebich, J. Contreras, L. M. Balster, Z. West, L. M. Shafer and S. Zabarnick, "Identification of Polar Species in Aviation Fuels using Multidimensional Gas Chromatography-Time of Flight Mass Spectrometry", 2009, **49**, 5474–5482, DOI: `10.1021/ef900386x` (cit. on pp. 85, 86).

(179) S. Zabarnick, Z. J. West, L. M. Shafer, S. S. Mueller, R. C. Striebich and P. J. Wrzesinski, "Studies of the Role of Heteroatomic Species in Jet Fuel Thermal Stability: Model Fuel Mixtures and Real Fuels", *Energy & Fuels*, 2019, **33**, 8557–8565, DOI: `10.1021/acs.energyfuels.9b02345` (cit. on pp. 85, 86, 96, 97).

(180) D. R. Hardy and M. A. Wechter, "Insoluble sediment formation in middle distillate diesel fuel: further evidence concerning the role of in situ fuel acidity", *Fuel*, 1990, **69**, 720–724, DOI: `10.1016/0016-2361(90)90036-P` (cit. on pp. 86, 87, 96, 135, 249).

(181) D. R. Hardy and M. A. Wechter, "Characterization of Soluble Macromolecular Oxidatively Reactive Species (SMORS) from Middle Distillate Diesel Fuels: Their Origin and Role in Instability", *Energy Fuels*, 1994, **8**, 782–787, DOI: `10.1021/ef00045a036` (cit. on pp. 86–88, 96, 135, 249).

(182) M. Sobkowiak, J. M. Griffith, B. Wang and B. Beaver, "Insight into the mechanisms of middle distillate fuel oxidative degradation. Part 1: On the role of phenol, indole, and carbazole derivatives in the thermal oxidative stability of fischer-tropsch/petroleum jet fuel blends", *Energy and Fuels*, 2009, **23**, 2041–2046, DOI: `10.1021/ef8006992` (cit. on pp. 86–88, 90, 94, 96, 167, 181, 183, 241, 249, 250).

(183) P. Aksoy, Ö. Gül, R. Cetiner, D. a. Fonseca, M. Sobkowiak, S. Falcone-Miller, B. G. Miller and B. Beaver, "Insight into the Mechanisms of Middle Distillate Fuel Oxidative Degradation. Part 2: On the Relationship between Jet Fuel Thermal Oxidative Deposit, Soluble Macromolecular Oxidatively Reactive Species, and Smoke Point", *Energy & Fuels*, 2009, **23**, 2047–2051, DOI: `10.1021/ef8007008` (cit. on pp. 86–88, 90, 94, 96, 167, 181, 183, 241, 249, 250).

(184) Gül, R. Cetiner, J. M. Griffith, B. Wang, M. Sobkowiak, D. A. Fonseca, P. Aksoy, B. G. Miller and B. Beaver, "Insight into the Mechanisms of Middle Distillate Fuel Oxidative Degradation. Part 3: Hydrocarbon Stabilizers to Improve Jet Fuel Thermal Oxidative Stability", *Energy & Fuels*, 2009, **23**, 2052–2055, DOI: `10.1021/ef800701u` (cit. on pp. 86–88, 91, 94, 96, 167, 181, 183, 241, 249, 250).

(185) B. Beaver, L. Gao, C. Burgess-Clifford and M. Sobkowiak, "On the mechanisms of formation of thermal oxidative deposits in jet fuels. Are unified mechanisms possible for both storage and thermal oxidative deposit formation for middle distillate fuels?", *Energy and Fuels*, 2005, **19**, 1574–1579, DOI: `10.1021/ef040090j` (cit. on pp. 86, 87, 89, 94, 96, 135, 153, 167, 181, 183, 234, 249).

(186) W. F. Taylor and J. W. Frankenfeld, "Deposit Formation from Deoxygenated Hydrocarbons. 3. Effects of Trace Nitrogen and Oxygen Compounds", *Industrial & Engineering Chemistry Product Research and Development*, 1978, **17**, 86–90, DOI: `10.1021/i360065a021` (cit. on pp. 92, 93).

(187) J. W. Frankenfeld and W. F. Taylor, "Storage Stability of Synfuels from Oil Shale . 1 . General Features of Sediment Formation in Model Fuel Systems", 1983, **3**, 608–614 (cit. on pp. 93–96, 99, 130, 131).

(188) R. N. Hazlett, P. Kirklin and P. David, *Physicochemical Aspects of Aviation Fuel Thermal Stability*, tech. rep., 1992, p. 16, DOI: `10.1520/STP15038S` (cit. on pp. 93, 103, 152, 155).

(189) G. W. Mushrush, E. J. Beal, D. R. Hardy and J. M. Hughes, "Nitrogen compound distribution in middle distillate fuels derived from petroleum, oil shale, and tar sand sources", *Fuel Processing Technology*, 1999, **61**, 197 –210, DOI: `https://doi.org/10.1016/S0378-3820(99)00056-9` (cit. on pp. 94, 132).

(190) J. W. Frankenfeld, W. F. Taylor and D. W. Brinkman, "Storage Stability of Synfuels from Oil Shale . 3 . Studies with Actual Shale-Derived Middle Distillates", 1983, 622–627 (cit. on pp. 94–96).

(191) J. W. Frankenfeld and W. F. Taylor, "Storage Stability of Synfuels from Oil Shale. 2. Effects of Nitrogen Compound Type and the Influence of Other Nonhydrocarbons on Sediment Formation in Model Fuel Systems", 1983, **22**, 615–621 (cit. on pp. 94–96, 102).

(192) M. C. Loeffler and N. C. Li, "Role of nitrogen- and sulphur-containing compounds in the ageing of liquid fuels", *Fuel*, 1985, **64**, 1047–1053 (cit. on pp. 94, 95, 98, 100).

(193) M. N. Siddiquee and A. de Klerk, "Heterocyclic Addition Reactions during Low Temperature Autoxidation", *Energy & Fuels*, 2015, **29**, 4236–4244, DOI: `10.1021/acs.energyfuels.5b00767` (cit. on pp. 96, 101).

(194) R. E. Kauffman, "The Effects of Different Sulfur Compounds on Jet Fuel Oxidation and Deposition", 2016, **119** (cit. on pp. 98, 101).

(195) W. F. Taylor, "Deposit Formation from Deoxygenated Hydrocarbons. II. Effect of Trace Sulfur Compounds", *Industrial & Engineering Chemistry Product Research and Development*, 1976, **15**, 64–68, DOI: `10.1021/i360057a012` (cit. on p. 98).

(196) W. F. Taylor and T. J. Wallace, "KINETICS OF DEPOSIT FORMATION FROM HYDROCARBONS - Effect of Trace Sulfur Compounds", *Industrial & Engineering Chemistry Product Research and Development*, 1968, **7**, 198–202 (cit. on p. 98).

(197) G. W. Mushrush, R. N. Hazlett, R. E. Pellenbarg and D. R. Hardy, "Role of Sulfur Compounds in Fuel Instability: A Model Study of the Formation of Sulfonic Acids from Hexyl Sulfide and Hexyl Disulfide", 1991, 258–262 (cit. on pp. 98, 100, 103).

(198) W. F. de Souza, I. R. Guimarães, M. C. Guerreiro and L. C. Oliveira, "Catalytic oxidation of sulfur and nitrogen compounds from diesel fuel", *Applied Catalysis A: General*, 2009, **360**, 205–209, DOI: `10.1016/j.apcata.2009.03.023` (cit. on p. 98).

(199) J. M. Bauldreay and C.-H. Ang, "Reduced sulfur aviation fuels – A worldwide challenge", *IASH 2003, the 8TH INTERNATIONAL SYMPOSIUM ON STABILITY, HANDLING AND USE OF LIQUID FUELS, Steamboat Springs, Colorado*, 2003 (cit. on pp. 98, 100).

(200) C. von Mühlen, C. A. Zini, E. B. Caramão and P. J. Marriott, "Applications of comprehensive two-dimensional gas chromatography to the characterization of petrochemical and related samples", *Journal of Chromatography A*, 2006, **1105**, 28TH INTERNATIONAL SYMPOSIUM ON CAPILLARY CHROMATOGRAPHY AND ELECTROPHORESIS, 39 –50, DOI: `https://doi.org/10.1016/j.chroma.2005.09.036` (cit. on p. 98).

(201) V. V. Lobodin, W. K. Robbins, J. Lu and R. P. Rodgers, "Separation and Characterization of Reactive and Non-Reactive Sulfur in Petroleum and Its Fractions", *Energy & Fuels*, 2015, **29**, 6177–6186, DOI: `10.1021/acs.energyfuels.5b00780` (cit. on p. 98).

(202) D. D. Link, J. P. Baltrus, K. S. Rothenberger, P. Zandhuis, D. K. Minus and R. C. Striebich, "Class- and Structure-Specific Separation, Analysis, and Identification Techniques for the Characterization of the Sulfur Components of JP-8 Aviation Fuel", *Energy & Fuels*, 2003, **17**, 1292–1302, DOI: `10.1021/ef0300747` (cit. on p. 98).

(203) R. W. Hiley and J. F. Pedley, "Storage stability of petroleum-derived diesel fuel: 2. The effect of sulphonic acids on the stability of diesel fuels and a diesel fuel extract", *Fuel*, 1988, **67**, 469 –473, DOI: `https://doi.org/10.1016/0016-2361(88)90341-9` (cit. on p. 99).

(204) R. D. Offenhauer, J. A. Brennan and R. C. Miller, "Sediment Formation in Catalytically Cracked Distillate Fuel Oils", *Industrial & Engineering Chemistry*, 1957, **49**, 1265–1266, DOI: `10.1021/ie50572a032` (cit. on p. 99).

(205) R. B Thompson, L. W. Druge and J. A. Chenicek, "Stability of Fuel Oils in Storage: Effect of Sulfur Compounds", *Industrial & Engineering Chemistry*, 1949, **41**, 2715–2721, DOI: `10.1021/ie50480a016` (cit. on p. 100).

(206) G. H. Denison, "Oxidation of Lubricating Oils", *Industrial & Engineering Chemistry*, 1944, **36**, 477–482, DOI: `10.1021/ie50413a028` (cit. on p. 100).

(207) G. W. Mushrush, "Fuel instability 2: organo-sulfur hydroperoxide reactions", *Fuel Science and Technology International; (United States)*, 1992, **10:10** (cit. on pp. 100, 103).

(208) S. R. Daniel and F. C. Heneman, "Deposit formation in liquid fuels: 4. Effect of selected organo-sulphur compounds on the stability of Jet A fuel", *Fuel*, 1983, **62**, 1265 –1268, DOI: `https://doi.org/10.1016/S0016-2361(83)80007-6` (cit. on p. 100).

(209) D. W. Naegeli, "The Role of Sulfur in the Thermal Stability of Jet Fuel", *Turbo Expo: Power for Land, Sea, and Air*, 1999, V002T02A053, DOI: `10.1115/99-GT-298` (cit. on p. 100).

(210) K. D.R., R. Clark and P. Wolveridge, "Fuels for Jet Engines: The Importance of Thermal Stability", *Aircraft Engineering and Aerospace Technology*, 1997, **59**, 6796–6806, DOI: `10.1108/eb036544` (cit. on pp. 101, 102).

(211) P. Rawson and S. Abanteriba, "Sulfur Deposit Formation In Jet Fuel At High Thermal Stressing Temperatures", *IASH, 13th International Conference on Stability, Handling and Use of Liquid Fuels, Rhodes, Greece*, 2013, 1–15 (cit. on p. 101).

(212) J.-P. R. Chauvin, M. Griesser and D. A. Pratt, "Hydropersulfides: H-Atom Transfer Agents Par Excellence", *Journal of the American Chemical Society*, 2017, **139**, 6484–6493, DOI: `10.1021/jacs.7b02571` (cit. on p. 101).

(213) P. M. Rawson, R. L. Webster, D. Evans and S. Abanteriba, "Contribution of sulfur compounds to deposit formation in jet fuels at 140 °C using a quartz crystal microbalance technique", *Fuel*, 2018, **231**, 1 –7, DOI: `https://doi.org/10.1016/j.fuel.2018.05.084` (cit. on pp. 101, 143).

(214) O. K. Bhan, D. W. Brinkman, J. B. Green and B. Carley, "Storage stability of marine diesel fuels", *Fuel*, 1987, **66**, 1200 –1214, DOI: `https://doi.org/10.1016/0016-2361(87)90057-3` (cit. on pp. 101, 131, 132).

(215) I. Bergeron, J.-P. Charland and M. Ternan, "Color Degradation of Hydrocracked Diesel Fuel", *Energy & Fuels*, 1999, **13**, 686–693, DOI: `10.1021/ef980214q` (cit. on p. 102).

(216) R. E. Morris and G. W. Mushrush, "Fuel instability model studies: the liquid-phase cooxidation of thiols and indene by oxygen", *Energy & fuels*, 1991, **5**, 744–748 (cit. on p. 102).

(217) Y. K. Sharma, H. C.Chandola, K. M.Agrawal and I. D. Singh, "Studies on the stability and sediment precursors in visbreaker middle distillate.", *American Chemical Society Division of Fuel Chemistry*, 1994, **39**, 923–932 (cit. on pp. 103, 152).

(218) M. A. Wechter and D. R. Hardy, "Effects of Dodecylbenzenesulfonic Acid on Insolubles Production in Mid-Distillate Diesel Fuel Blends", *Energy & Fuels*, 1996, **10**, 117–120, DOI: `10.1021/ef950167r` (cit. on p. 103).

(219) G. W. Mushrush, E. J. Beal, E. Slone and D. R. Hardy, "Reaction of Organosulfur Compounds with Naturally Occurring Peroxides in Jet Fuel", *Energy & Fuels*, 1996, **10**, 504–508, DOI: `10.1021/ef950179c` (cit. on p. 103).

(220) R. N. Hazlett, J. A. Schreifels, W. M. Stalick, R. E. Morris and G. W. Mushrush, "Distillate fuel insolubles: formation conditions and characterization", *Energy & Fuels*, 1991, **5**, 269–273, DOI: `10.1021/ef00026a008` (cit. on p. 103).

(221) S. Zabarnick, "Studies of Jet Fuel Thermal Stability and Oxidation Using a Quartz Crystal Microbalance and Pressure Measurements", *Industrial & Engineering Chemistry Research*, 1994, **33**, 1348–1354, DOI: `10.1021/ie00029a034` (cit. on pp. 103, 155).

(222) S. Zabarnick and D. K. Phelps, "Density Functional Theory Calculations of the Energetics and Kinetics of Jet Fuel Autoxidation Reactionss", *Energy & Fuels*, 2006, **20**, 488–497, DOI: `10.1021/ef050348l` (cit. on pp. 103, 104, 107, 108, 113, 125).

(223) T. Punniyamurthy, S. Velusamy and J. Iqbal, "Recent advances in transition metal catalyzed oxidation of organic substrates with molecular oxygen", *Chemical Reviews*, 2005, **105**, 2329–2363, DOI: `10.1021/cr050523v` (cit. on p. 104).

(224) A. K. Frizen, S. L. Khursan, S. V. Kolesov and Y. B. Monakov, "A Quantum-chemical study of the mechanism of formation of styrene polymerization centers under initiation by the ferrocene—benzoyl peroxide system", *Russian Journal of Physical Chemistry B*, 2009, **3**, 674–678, DOI: `10.1134/S1990793109040277` (cit. on pp. 104–106).

(225) J. Haber, *Selectivity in Heterogeneous Catalytic Oxidation of Hydrocarbons*, American Chemical Society, 1996, ch. 2, pp. 20–34, DOI: `10.1021/bk-1996-0638.ch002` (cit. on p. 104).

(226) H. J. H. Fenton, "LXXIII.—Oxidation of tartaric acid in presence of iron", *J. Chem. Soc., Trans.*, 1894, **65**, 899–910, DOI: `10.1039/CT8946500899` (cit. on p. 105).

(227) W. Koppenol, "The centennial of the Fenton reaction", *Free Radical Biology and Medicine*, 1993, **15**, 645 –651, DOI: `https://doi.org/10.1016/0891-5849(93)90168-T` (cit. on p. 105).

(228)B. Ensing, F. Buda and E. J. Baerends, "Fenton-like chemistry in water: Oxidation catalysis by Fe(III) and H2O2", *Journal of Physical Chemistry A*, 2003, **107**, 5722–5731, DOI: 10.1021/jp0267149 (cit. on p. 106).

(229)F. Buda, B. Ensing, M. C. M. Gribnau and E. J. Baerends, "DFT study of the active intermediate in the Fenton reaction", *Chemistry - A European Journal*, 2001, **7**, 2775–2783, DOI: 10.1002/1521-3765(20010702)7:13<2775::AID-CHEM2775>3.0.CO;2-6 (cit. on p. 106).

(230)B. Ensing, F. Buda, M. C. M. Gribnau and E. J. Baerends, "Methane-to-methanol oxidation by the hydrated iron(IV) oxo species in aqueous solution: A combined DFT and CarParrinello molecular dynamics study", *Journal of the American Chemical Society*, 2004, **126**, 4355–4365, DOI: 10.1021/ja038865a (cit. on p. 106).

(231)Z. J. West, R. K. Adams and S. Zabarnick, "Homogeneous Catalysis of Liquid-Phase Hydroperoxide Decomposition in Hydrocarbons", *Energy & Fuels*, 2011, **25**, 897–904, DOI: 10.1021/ef101678s (cit. on pp. 106, 108, 109, 111, 113).

(232)C. R. Council, "CRC Literature Survey on the Thermal Oxidation Stability of Jet Fuel", *Coordinating Research Council and CRC-Aviation Group on Oxidation Stability of Gas Turbine Fuels. Literature Survey Panel*, 1979 (cit. on pp. 106, 109).

(233)W. F. Taylor, "Kinetics of Deposit Formation from Hydrocarbons - III Heterogeneous and Homogenous Metal Effects", *Journal of Applied Chemistry*, 1968, **18**, 251–254 (cit. on pp. 106, 109, 110).

(234)J. S. Mills and D. R. Kendall, "The Quantification and Improvement of the Thermal Stability of Aviation Turbine Fuel", *Journal of Engineering for Gas Turbines and Power*, 1986, **108**, 381–386, DOI: 10.1115/1.3239915 (cit. on pp. 106, 111, 132, 135).

(235)J Colbert and C. J. Nowack, "US Navy Evaluaion of the High Reynolds' Number Thermal Stability (HiReTS) Test Unit", *Naval Air Systems Command - tech. rep.*, 2003 (cit. on pp. 106, 107).

(236)F. Pradelle, S. L. Braga, A. R. F. A. Martins, F. Turkovics and R. N. C. Pradelle, "Gum Formation in Gasoline and Its Blends: A Review", *Energy & Fuels*, 2015, **29**, 7753–7770, DOI: 10.1021/acs.energyfuels.5b01894 (cit. on pp. 107–109).

(237)C. C. Pereira and V. M. D. Pasa, "Effect of Alcohol and Copper Content on the Stability of Automotive Gasoline", *Energy & Fuels*, 2005, **19**, 426–432, DOI: 10.1021/ef049849h (cit. on pp. 107–109).

(238)R. E. Morris, T. Evans, J. M. Hughes, J. E. Colbert, R. A. Kamin and C. J. Nowack, "Oxidation of JP-5 in Single and Multipass Flow Testing", *IASH 2005, the 9TH INTERNATIONAL SYMPOSIUM ON STABILITY, HANDLING AND USE OF LIQUID FUELS, Sitges, Spain*, 2005 (cit. on p. 107).

(239) P. Lahtinen, E. Lankinen, M. Leskelä and T. Repo, "Insight into copper oxidation catalysts: Kinetics, catalytic active species and their deactivation", *Applied Catalysis A: General*, 2005, **295**, 177–184, DOI: `10.1016/j.apcata.2005.08.013` (cit. on p. 107).

(240) R. E. Morris, J. M. Hughes and J. E. Colbert, "The Impact of Copper on the Liquid-Phase Oxidation of Jet Fuel for Advanced Aircraft", *Energy & Fuels*, 2004, **18**, 490–496, DOI: `10.1021/ef0301093` (cit. on p. 108).

(241) L. S. Teixeira, J. C. Souza, H. C. dos Santos, L. A. Pontes, P. R. Guimarães, E. V. Sobrinho and R. F. Vianna, "The influence of Cu, Fe, Ni, Pb and Zn on gum formation in the Brazilian automotive gasoline", *Fuel Processing Technology*, 2007, **88**, 73 –76, DOI: `https://doi.org/10.1016/j.fuproc.2006.08.008` (cit. on p. 110).

(242) A. A. Haidar, "Effect of the Copper and Iron Concentration on Gum Formation in Gas Oil of Baiji Refinery", *Journal of Chemistry and Chemical Engineering*, 2011, **5**, 652–656 (cit. on p. 110).

(243) S. Jain and M. Sharma, "Correlation development for effect of metal contaminants on the oxidation stability of Jatropha curcas biodiesel", *Fuel*, 2011, **90**, 2045 –2050, DOI: `https://doi.org/10.1016/j.fuel.2011.02.002` (cit. on p. 110).

(244) J. P. Adjimani and P. Asare, "Antioxidant and free radical scavenging activity of iron chelators", *Toxicology Reports*, 2015, **2**, 721–728, DOI: `10.1016/j.toxrep.2015.04.005` (cit. on p. 111).

(245) J. Smith, "The Effect of Metals and Alloys on the Thermal Stability of Avtur 50", *Aircraft Engineering and Aerospace Technology*, 1967, **39**, 19–26, DOI: `10.1108/eb034253` (cit. on p. 112).

(246) E. G. Jones, L. M. Balster and W. J. Balster, "Autoxidation of Aviation Fuels in Heated Tubes: Surface Effects", *Energy & Fuels*, 1996, **10**, 831–836, DOI: `10.1021/ef9502012` (cit. on p. 112).

(247) J. S. Ervin, T. A. Ward, T. F. Williams and J. Bento, "Surface Deposition within Treated and Untreated Stainless Steel Tubes Resulting from Thermal-Oxidative and Pyrolytic Degradation of Jet Fuel", *Energy & Fuels*, 2003, **17**, 577–586, DOI: `10.1021/ef020180t` (cit. on p. 112).

(248) S. Eser, R. Venkataraman and O. Altin, "Deposition of Carbonaceous Solids on Different Substrates from Thermal Stressing of JP-8 and Jet A Fuels", *Industrial & Engineering Chemistry Research*, 2006, **45**, 8946–8955, DOI: `10.1021/ie060968p` (cit. on p. 112).

(249) R. N. Hazlett, J. M. Hall and M. Matson, "Reactions of Aerated N-Dodecane Liquid Flowing over Heated Metal Tubes", *Product R&D*, 1977, **16**, 171–177, DOI: `10.1021/i360062a013` (cit. on p. 112).

(250) I. L. Stavinoha, D. W. Naegeli and L. McInnis, "The role of surface composition in fuel deposition", *Division of fuel chemistry*, 1990, **35**, 1315–1323 (cit. on p. 113).

(251) E. J. Szetela, A. J. Giovanetti and S. Cohen, "Fuel Deposit Characteristics at Low Velocity", *Journal of Engineering for Gas Turbines and Power*, 1986, **108**, 460–464, DOI: `10.1115/1.3239930` (cit. on p. 113).

(252) A. J. Giovanetti and E. J. Szetela, "Long-term deposit formation in aviation turbine fuel at elevated temperature", *Journal of Propulsion and Power*, 1986, **2**, 450–456, DOI: `10.2514/3.22928` (cit. on p. 113).

(253) G. Despande, A. Michael, P. R. Solomon and R. Malhotra, 198th ACS National Meeting, Symposium on the Chemical Aspects of Hypersonic Propulsion, Miami FL, 1989 (cit. on p. 114).

(254) J. L. Krazinski, S. P. Vanka, J. A. Pearce and W. M. Roquemore, "A Computational Fluid Dynamics and Chemistry Model for Jet Fuel Thermal Stability", *Journal of Engineering for Gas Turbines and Power*, 1992, **114**, 104–110, DOI: `10.1115/1.2906291` (cit. on p. 114).

(255) V. R. Katta and W. M. Roquemore, "Numerical method for simulating fluid-dynamic and heat-transfer changes in jet-engine injector feed-arm due to fouling", *Journal of Thermophysics and Heat Transfer*, 1993, **7**, 651–660, DOI: `10.2514/3.474` (cit. on p. 114).

(256) V. R. Katta, E. G. Jones and W. M. Roquemore, "Modeling of Deposition Process in Liquid Fuels", *Combustion Science and Technology*, 1998, **139**, 75–111, DOI: `10.1080/00102209808952082` (cit. on pp. 114, 115).

(257) S. Zabarnick, "Pseudo-Detailed Chemical Kinetic Modeling of Antioxidant Chemistry for Jet Fuel Applications", 1998, **0624**, 547–553 (cit. on pp. 117–119, 143).

(258) N. J. Kuprowicz, J. S. Ervin and S. Zabarnick, "Modeling the liquid-phase oxidation of hydrocarbons over a range of temperatures and dissolved oxygen concentrations with pseudo-detailed chemical kinetics", *Fuel*, 2004, **83**, 1795 –1801, DOI: `https://doi.org/10.1016/j.fuel.2004.03.013` (cit. on pp. 120, 121).

(259) T. Doungthip, J. S. Ervin, S. Zabarnick and T. F. Williams, "Simulation of the Effect of Metal-Surface Catalysis on the Thermal Oxidation of Jet Fuel", *Energy & Fuels*, 2004, **18**, 425–437, DOI: `10.1021/ef030098d` (cit. on p. 120).

(260) Z. H. Sander, Z. J. West, J. S. Ervin and S. Zabarnick, "Experimental and Modeling Studies of Heat Transfer, Fluid Dynamics, and Autoxidation Chemistry in the Jet Fuel Thermal Oxidation Tester (JFTOT)", *Energy & Fuels*, 2015, **29**, 7036–7047, DOI: `10.1021/acs.energyfuels.5b01679` (cit. on pp. 123, 124, 134).

(261) A. Ben Amara, A. Nicolle, M. Alves-Fortunato and N. Jeuland, "Toward predictive modeling of petroleum and biobased fuel stability: Kinetics of methyl oleate/n-dodecane autoxidation", *Energy and Fuels*, 2013, **27**, 6125–6133, DOI: 10.1021/ef401360k (cit. on pp. 126, 127, 143).

(262) N Sebbar, H Bockhorn and J. W. Bozzelli, "Structures, thermochemical properties (enthalpy, entropy and heat capacity), rotation barriers, and peroxide bond energies of vinyl, allyl, ethynyl and phenyl hydroperoxides", *Phys. Chem. Chem. Phys.*, 2002, **4**, 3691–3703, DOI: 10.1039/b111303h (cit. on p. 131).

(263) I. N. Grishina, I. M. Kolesnikov, S. T. Bashkatova and A. Marvan, "Kinetics of gum deposition during storage of diesel fuel", *Petroleum Chemistry*, 2007, **47**, 131–133, DOI: 10.1134/S0965544107020120 (cit. on p. 131).

(264) J. W. Bauserman, G. W. Mushrush and D. R. Hardy, "Organic Nitrogen Compounds and Fuel Instability in Middle Distillate Fuels", *Industrial & Engineering Chemistry Research*, 2008, **47**, 2867–2875, DOI: 10.1021/ie071321n (cit. on p. 132).

(265) P. J. Marteney and L. J. Spadaccini, "Thermal Decomposition of Aircraft Fuel", *Journal of Engineering for Gas Turbines and Power*, 1986, **108**, 648–653, DOI: 10.1115/1.3239960 (cit. on pp. 132, 134, 137).

(266) R. Clark and P. Stevenson, "The Thermal degredation of aviation fuels in jet engine injector feed arms: results from a half scale rig", *Symposium on the stability and oxidation chemistry of middle distillate fuels*, 1990, **August**, 1302–1340 (cit. on p. 132).

(267) J. D. Smith, "Fuel for the Supersonic Transport. Effects of Deposits on Heat Transfer to Aviation Kerosine", *Industrial & Engineering Chemistry Process Design and Development*, 1969, **8**, 299–308, DOI: 10.1021/i260031a003 (cit. on pp. 132, 134, 135).

(268) M. Sicard, J. Boulicault, K. Coulon, C. Thomasset, J. Ancelle, B. Raepsaet and F. Ser, "Oxidation stability of jet fuel model molecules evaluated by rapid small scale oxidation tests.", *IASH, 13th International Conference on Stability, Handling and Use of Liquid Fuels, Rhodes, Greece*, 2013, 1–13 (cit. on p. 133).

(269) S. Siouris, S. Blakey and C. W. Wilson, "Investigation of deposition in aviation gas turbine fuel nozzles by coupling of experimental data and heat transfer calculations", *Fuel*, 2013, **106**, 79–87, DOI: https://doi.org/10.1016/j.fuel.2012.12.006 (cit. on p. 135).

(270) R. L. McCormick and S. R. Westbrook, "Storage Stability of Biodiesel and Biodiesel Blends", *Energy & Fuels*, 2010, **24**, 690–698, DOI: 10.1021/ef900878u (cit. on p. 135).

(271) Z. Hamadache and A. Spencer, "Fuel Gallery Residence Time and Heat Transfer Experimental Technique Development for Gas Turbine Fuel Injectors", *17th International Symposium on Applications of Laser Techniques to Fluid Mechanics*, 2014 (cit. on p. 135).

(272) J. S. Chin and A. H. Lefebvre, "Influence of Flow Conditions on Deposits From Heated Hydrocarbon Fuels", *Turbo Expo: Power for Land, Sea, and Air*, 1992, V003T06A011, DOI: 10.1115/92-GT-114 (cit. on p. 136).

(273) C. Moses, "Effect of Reynolds Number on Deposition in Fuels Flowing Over Heated Surfaces", *Journal of Engineering for Gas Turbines and Power*, 2013, **135**, 121503, DOI: 10.1115/1.4025147 (cit. on pp. 137, 138).

(274) P. Gadsby and S. G. Blakey, "Wall Roughness Effects on Deposition of Thermally Stressed Aviation Fuel", *IASH, 15th International Conference on Stability, Handling and Use of Liquid Fuels, Rome, Italy*, 2017 (cit. on p. 138).

(275) R. C. Striebich, L. M. Shafer, R. K. Adams, Z. J. West, M. J. DeWitt and S. Zabarnick, "Hydrocarbon Group-Type Analysis of Petroleum-Derived and Synthetic Fuels Using Two-Dimensional Gas Chromatography", *Energy & Fuels*, 2014, **28**, 5696–5706, DOI: 10.1021/ef500813x (cit. on p. 143).

(276) D. C. Mielczarek, M. Matrat, A. B. Amara, Y. Bouyou, P. Wund and L. Starck, "Toward the Accurate Prediction of Liquid Phase Oxidation of Aromatics: A Detailed Kinetic Mechanism for Toluene Autoxidation", *Energy and Fuels*, 2017, **31**, 12893–12913, DOI: 10.1021/acs.energyfuels.7b00416 (cit. on p. 143).

(277) A. International, *D7545-14 - Standard Test Method for Oxidation Stability of Middle Distillate Fuels—Rapid Small Scale Oxidation Test (RSSOT)*, tech. rep., ASTM International, 2019, p. 7 (cit. on p. 144).

(278) B. Pütz, *Product Information - Verification fluid*, tech. rep., Anton Paar, 2018, p. 4 (cit. on p. 147).

(279) D. R. Hardy and M. a. Wechter, "Insoluble sediment formation in middle-distillate diesel fuel: the role of soluble macromolecular oxidatively reactive species", *Energy & Fuels*, 1990, **4**, 270–274, DOI: 10.1021/ef00021a009 (cit. on p. 153).

(280) E. Pensa, E. Cortés, G. Corthey, P. Carro, C. Vericat, M. H. Fonticelli, G. Benítez, A. A. Rubert and R. C. Salvarezza, "The Chemistry of the Sulfur–Gold Interface: In Search of a Unified Model", *Accounts of Chemical Research*, 2012, **45**, 1183–1192, DOI: 10.1021/ar200260p (cit. on pp. 156, 250).

(281) P. M. Rawson, C.-a. Stansfield, R. L. Webster, D. Evans and U. Yildirim, "The oxidative stability of synthetic fuels and fuel blends with monoaromatic blending components", *Fuel*, 2015, **161**, 97–104, DOI: 10.1016/j.fuel.2015.08.038 (cit. on p. 167).

(282) M. Badertscher, P. Bühlmann and E. Pretsch, *Structure Determination of Organic Compounds*, Springer, Berlin, Heidelberg, 2009, DOI: `https://doi.org/10.1007/978-3-540-93810-1` (cit. on pp. 170, 186).

(283) Q. Ma, M. Schwilk, C. Köppl and H.-J. Werner, "Scalable Electron Correlation Methods. 4. Parallel Explicitly Correlated Local Coupled Cluster with Pair Natural Orbitals (PNO-LCCSD-F12)", *Journal of Chemical Theory and Computation*, 2017, **13**, 4871–4896, DOI: `10.1021/acs.jctc.7b00799` (cit. on p. 195).

(284) Q. Ma and H.-J. Werner, "Scalable Electron Correlation Methods. 5. Parallel Perturbative Triples Correction for Explicitly Correlated Local Coupled Cluster with Pair Natural Orbitals", *Journal of Chemical Theory and Computation*, 2018, **14**, 198–215, DOI: `10.1021/acs.jctc.7b01141` (cit. on p. 195).

(285) G. F. Mangiatordi, E. Brémond and C. Adamo, "DFT and Proton Transfer Reactions: A Benchmark Study on Structure and Kinetics", *Journal of Chemical Theory and Computation*, 2012, **8**, PMID: 26605719, 3082–3088, DOI: `10.1021/ct300338y` (cit. on p. 195).

(286) A. Galano and J. R. Alvarez-Idaboy, "Kinetics of radical-molecule reactions in aqueous solution: A benchmark study of the performance of density functional methods", *Journal of Computational Chemistry*, 2014, **35**, 2019–2026, DOI: `10.1002/jcc.23715` (cit. on p. 195).

(287) W. H. Green, R. H. West and Various, *Reaction Mechanism Generator*, 2019, `https://rmg.mit.edu/` (visited on 08/27/2019) (cit. on p. 196).

(288) Various, *NIST kinetic database 17*, 2015, `https://kinetics.nist.gov/kinetics/index.jsp` (visited on 08/27/2019) (cit. on p. 196).

(289) A. Mahler, B. G. Janesko, S. Moncho and E. N. Brothers, "Why are GGAs so accurate for reaction kinetics on surfaces? Systematic comparison of hybrid vs. nonhybrid DFT for representative reactions", *The Journal of Chemical Physics*, 2017, **146**, 234103, DOI: `10.1063/1.4986404` (cit. on p. 196).

(290) (Cit. on p. 196).

(291) B. Chan, A. T. B. Gilbert, P. M. W. Gill and L. Radom, "Performance of Density Functional Theory Procedures for the Calculation of Proton-Exchange Barriers: Unusual Behavior of M06-Type Functionals", *Journal of Chemical Theory and Computation*, 2014, **10**, PMID: 26588522, 3777–3783, DOI: `10.1021/ct500506t` (cit. on p. 196).

(292) Y. Zhao and D. G. Truhlar, "The M06 suite of density functionals for main group thermochemistry, thermochemical kinetics, noncovalent interactions, excited states, and transition elements: two new functionals and systematic testing of four M06-class functionals and 12 other functionals", *Theoretical Chemistry Accounts*, 2008, **120**, 215–241, DOI: `10.1007/s00214-007-0310-x` (cit. on p. 196).

(293) J. S. Heyne, A. L. Boehman and S. Kirby, "Autoignition Studies of trans- and cis-Decalin in an Ignition Quality Tester (IQT) and the Development of a High Thermal Stability Unifuel/Single Battlefield Fuel", *Energy & Fuels*, 2009, **23**, 5879–5885, DOI: `10.1021/ef900715m` (cit. on p. 199).

(294) G. A. Russell, "Deuterium-isotope Effects in the Autoxidation of Aralkyl Hydrocarbons. Mechanism of the Interaction of Peroxy Radicals1", *Journal of the American Chemical Society*, 1957, **79**, 3871–3877, DOI: `10.1021/ja01571a068` (cit. on pp. 210, 234).

(295) T. S. Dibble, "Failures and limitations of quantum chemistry for two key problems in the atmospheric chemistry of peroxy radicals", *Atmospheric Environment*, 2008, **42**, Selected Papers from the First International Conference on Atmospheric Chemical Mechanisms, 5837 –5848, DOI: `https://doi.org/10.1016/j.atmosenv.2007.11.005` (cit. on pp. 210, 234, 250).

(296) B. Cordero, V. Gómez, A. E. Platero-Prats, M. Revés, J. Echeverría, E. Cremades, F. Barragán and S. Alvarez, "Covalent radii revisited", *Dalton Trans.*, 2008, **0**, 2832–2838, DOI: `10.1039/B801115J` (cit. on p. 217).

(297) E. Alborzi, P. Gadsby, M. S. Ismail, A. Sheikhansari, M. R. Dwyer, A. J. H. M. Meijer, S. G. Blakey and M. Pourkashanian, "Comparative Study of the Effect of Fuel Deoxygenation and Polar Species Removal on Jet Fuel Surface Deposition", *Energy & Fuels*, 2019, **33**, 1825–1836, DOI: `10.1021/acs.energyfuels.8b03468` (cit. on pp. 230, 239–241, 256, 259).

(298) Q. Niu and G. D. Mendenhall, "Structural effects on the yields of singlet molecular oxygen (1.DELTA.gO2) from alkylperoxyl radical recombination", *Journal of the American Chemical Society*, 1990, **112**, 1656–1657, DOI: `10.1021/ja00160a070` (cit. on p. 234).

(299) Q. J. Niu and G. D. Mendenhall, "Yields of singlet molecular oxygen from peroxyl radical termination", *Journal of the American Chemical Society*, 1992, **114**, 165–172, DOI: `10.1021/ja00027a024` (cit. on p. 234).

(300) R. R. Valiev, G. Hasan, V.-T. Salo, J. Kubečka and T. Kurten, "Intersystem Crossings Drive Atmospheric Gas-Phase Dimer Formation", *The Journal of Physical Chemistry A*, 2019, **123**, 6596–6604, DOI: `10.1021/acs.jpca.9b02559` (cit. on p. 234).

(301) E. Alborzi, M. R. Dwyer, C. M. Parks, A. Sheikhansari, A. J. H. M. Meijer, S. G. Blakey and M. Pourkashanian, "Construction of Reduced Chemical Kinetic Mechanism for Autoxidation of n-Paraffininc Solvent - A Model for Aviation Fuel", *Submitted to Fuel*, 2020 (cit. on pp. 239, 241–245, 256, 259).

(302) S. Grimme and P. R. Schreiner, "Computational Chemistry: The Fate of Current Methods and Future Challenges", *Angewandte Chemie International Edition*, 2018, **57**, 4170–4176, DOI: `10.1002/anie.201709943` (cit. on p. 255).

(303) M. R. Dwyer, S. G. Blakey, E. Alborzi and A. J. H. M. Meijer, "Investigating the autoxidation accelerating reactions of peroxides and peroxyl radicals using quantum chemistry calculations", *IASH, 16th International Conference on Stability, Handling and Use of Liquid Fuels, Long Beach, USA*, 2019, 1–14 (cit. on p. 259).

(304) R. Iten, T. Metger, H. Wilming, L. Rio and R. Renner, "Discovering physical concepts with neural networks", *Phys. Rev. Lett.*, 2019, 1–21 (cit. on p. 262).

(305) K. T. Schütt, M. Gastegger, A. Tkatchenko, K.-R. Müller and R. J. Maurer, "Unifying machine learning and quantum chemistry with a deep neural network for molecular wavefunctions", *Nature Communications*, 2019, **10**, 5024, DOI: `10.1038/s41467-019-12875-2` (cit. on p. 262).

Appendices

9.1 Experimental data

PetroOxy data of blends of pure hydrocarbons
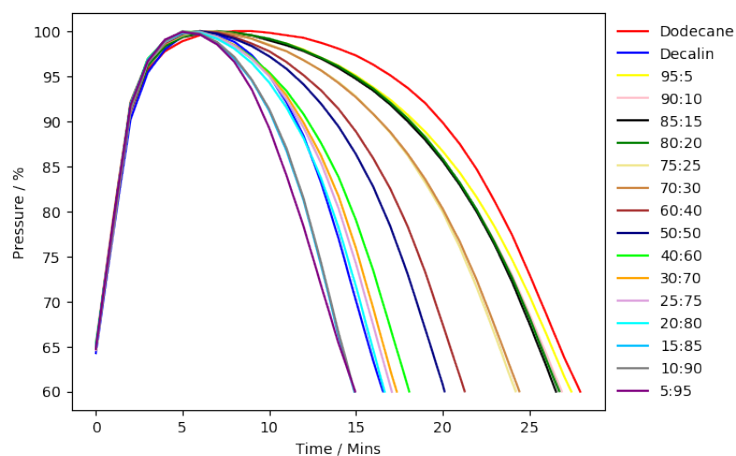
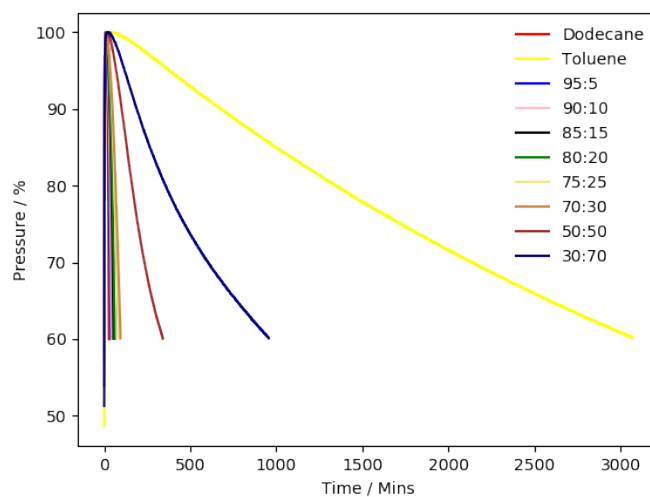**Fig. 9.1:** PetroOxy plot of increasing Dodecane:Decalin mixture.

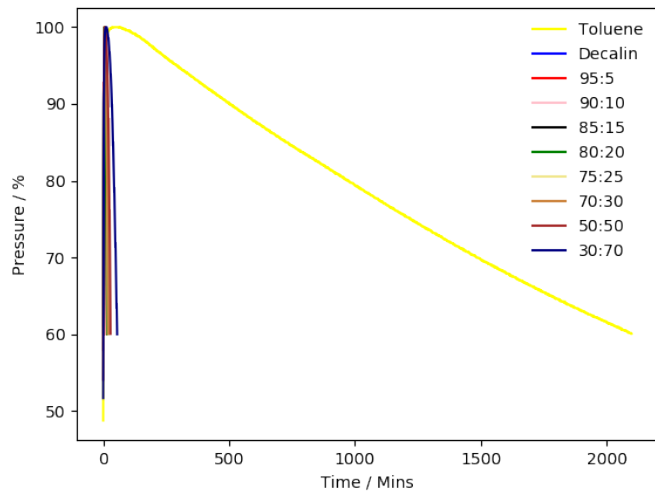**Fig. 9.2:** PetroOxy plot of increasing Dodecane:Toluene mixture.

Fig. 9.3: PetroOxy plot of increasing Decalin:Toluene mixtures.

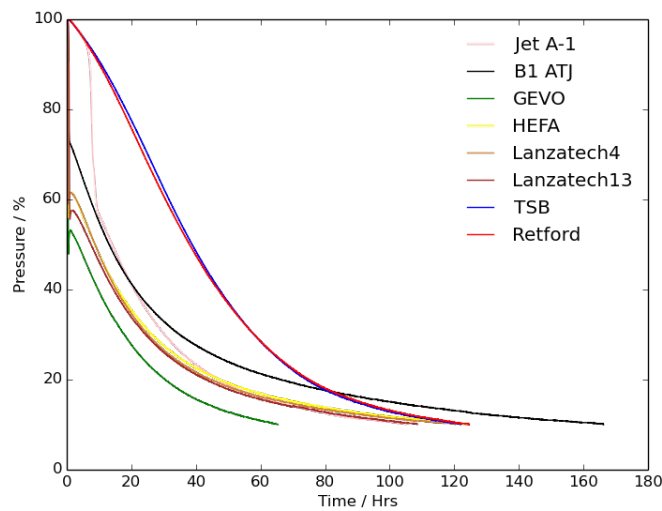## PetroOxy testing of aviation fuels with unknown chemical composition

Fig. 9.4: PetroOxy plot of the 90% pressure drop for a selection of fuels with unknown chemical composition, with B1-AtJ and Base Jet A1 for comparison.

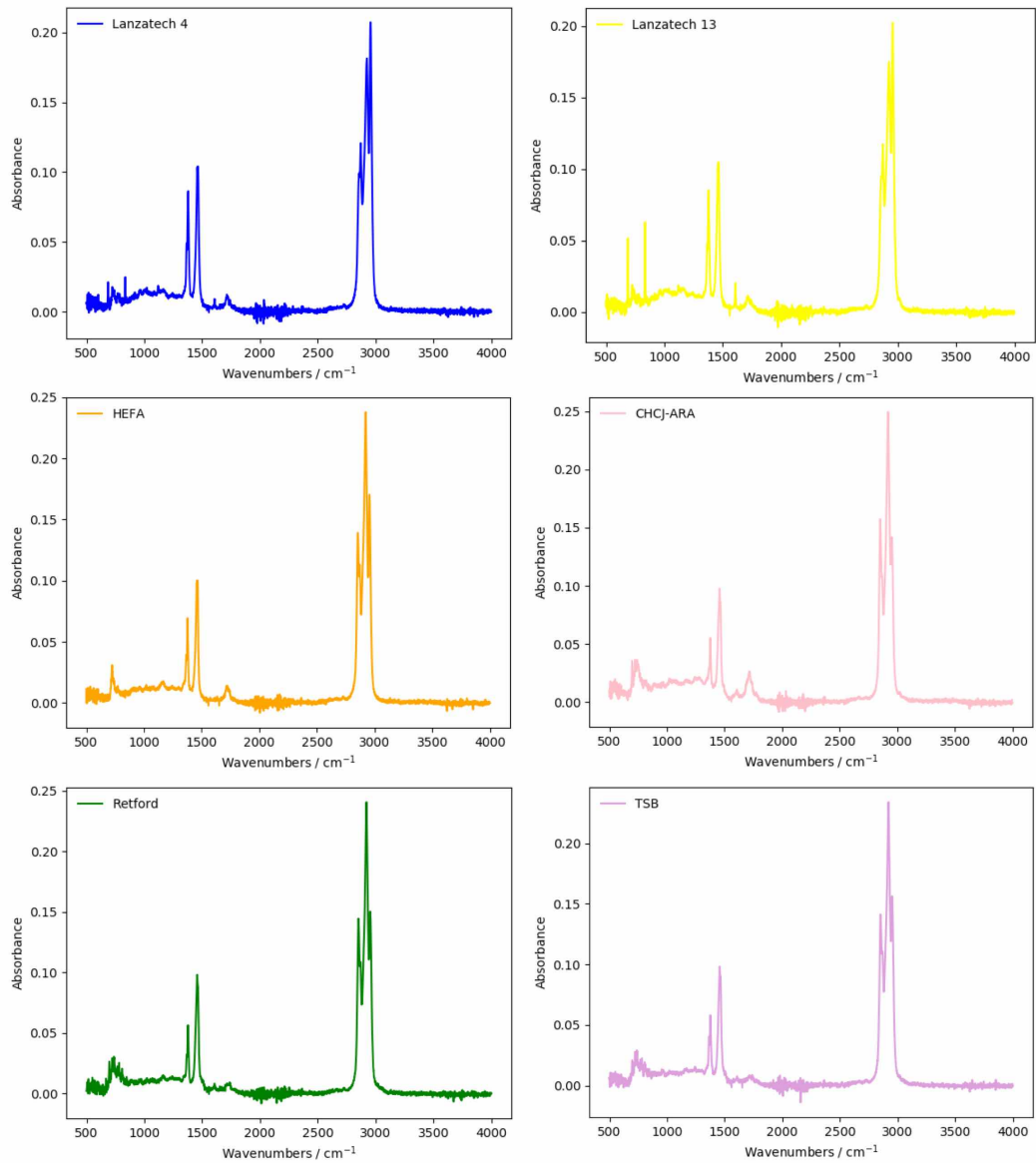# FTIR spectra of fuels with unknown chemical composition

Fig. 9.5: Infrared absorbance spectrums for thermally stressed fuels with unknown chemical composition.

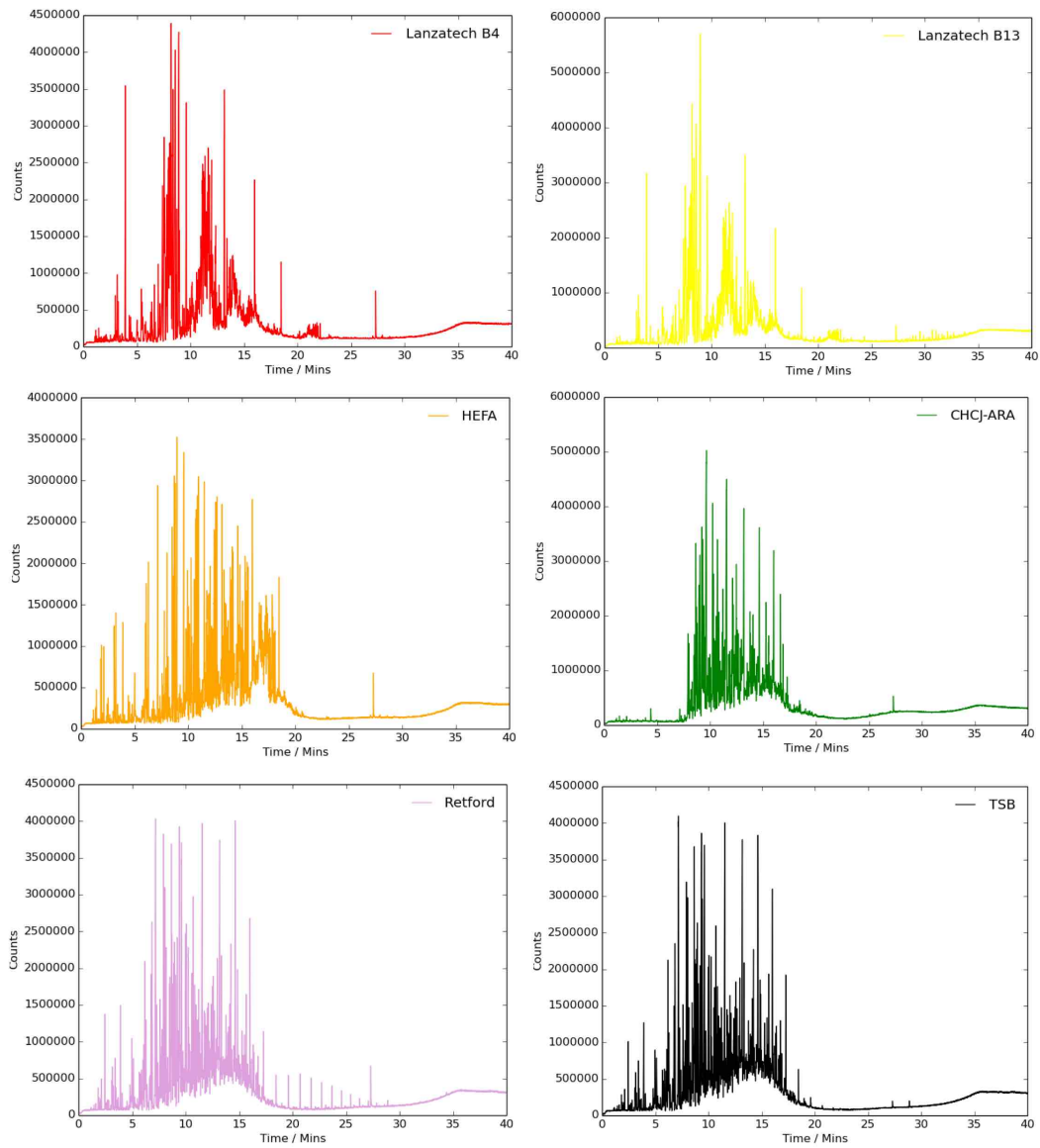**GCMS trace of fuels with unknown chemical composition**

Fig. 9.6: GCMS traces for the thermally stressed fuels with unknown chemical composition.
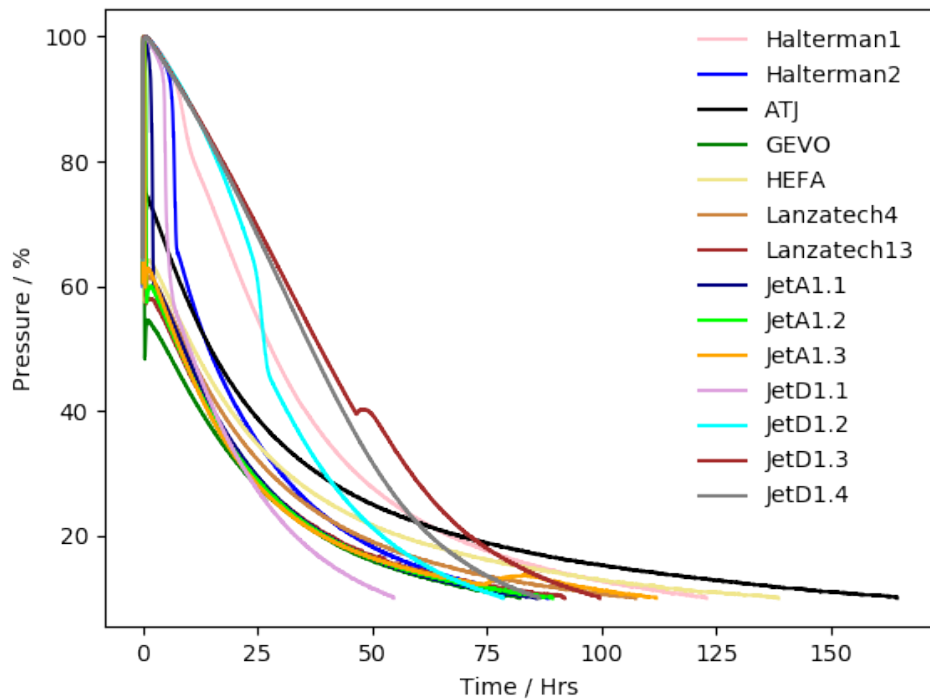
Experimental data from PetroOxy1

Fig. 9.7: PetroOxy plot of all fuels and model hydrocarbons building blocks tested using the PetroOxy1 device. The Retford and TSB fuel were not tested, as the PetroOxy1 device developed a malfunction, where it would pull through oxygen into the chamber during testing when the oxygen value was opened to start testing on the other PetroOxy device. This can be seen in the PetroOxy trace for fuel D1.3.

9.2 Example calculation inputs for multi-reference methods

Gaussain09 BS-UDFT input

Example transition state optimisation using BS-UDFT

****
Gaussian 09: EM64L-G09RevD.01 24-Apr-2013
19-Jul-2018
****
%nprocshared=4
Will use up to 4 processors via shared memory.
%mem=6GB
_____

# opt=(calcall,qst3) freq=noraman ub3lyp/cc-pvtz scrf=(solvent=heptane)
guess=mix geom=connectivity
_____

```
1/5=1,10=4,14=-1,18=20,26=3,27=203,38=1,57=2/1,3;
2/9=110,12=2,17=6,18=5,40=1/2;
3/5=16,6=1,11=2,16=1,25=1,30=1,70=2201,71=2,72=16,74=-5,116=2,140=1/1,2,3;
4/13=-1/1;
5/5=2,38=5,53=16/2;
8/6=4,10=90,11=11/1;
11/6=1,8=1,9=11,15=111,16=1/1,2,10;
10/6=1/2;
6/7=2,8=2,9=2,10=2,18=1,28=1/1;
7/10=1,25=1/1,2,3,16;
1/5=1,10=4,14=-1,18=20,26=3,27=203/3(3);
2/9=110/2;
7/8=1,9=1,25=1,44=-1/16;
99//99;
2/9=110/2;
3/5=16,6=1,11=2,16=1,25=1,30=1,70=2205,71=2,72=16,74=-5,116=2,140=1/1,2,3;
4/5=5,16=3,69=1/1;
5/5=2,38=5,53=16/2;
8/6=4,10=90,11=11/1;
```

11/6=1,8=1,9=11,15=111,16=1/1,2,10;
10/6=1/2;
7/10=1,25=1/1,2,3,16;
1/5=1,10=4,14=-1,18=20,26=3,27=203/3(-8);
2/9=110/2;
6/7=2,8=2,9=2,10=2,18=1,19=2,28=1/1;
7/8=1,9=1,25=1,44=-1/16;
99//99;
————————-

Title Card Required

————————-

Symbolic Z-matrix:
Charge = 0 Multiplicity = 1
C 2.86232 0.70652 0.
H 2.45341 1.46647 -0.66675
H 2.87164 1.08098 1.02662
H 2.25667 -0.19964 -0.0588
C 7.69724 1.50072 -0.103
H 7.64493 2.25066 0.68714
H 6.97996 1.736 -0.89127
H 8.70793 1.46312 -0.51024
O 7.37429 0.27326 0.53774
O 7.5117 -0.77211 -0.4601
H 6.57599 -1.00446 -0.60033
O 4.1736 0.47594 -0.48231
O 4.74029 -0.58125 0.33875
H 5.454 -0.09436 0.79307

————————-

Title Card Required

————————-

Symbolic Z-matrix:
Charge = 0 Multiplicity = 1
C 0.72464 3.31522 0.
H 0.06076 2.68251 -0.60049
H 1.37038 3.95823 -0.61145
H 0.08693 4.01725 0.57254
C 8.21146 3.03645 0.48265
H 8.74628 3.04292 1.42875

H 8.6817 3.69982 -0.23973
H 8.12804 2.02775 0.08435
O 6.8869 3.53439 0.78608
O 6.13424 3.5692 -0.29253
H 4.34452 4.37097 0.36686
O 1.43825 2.622 0.93572
O 3.52184 4.72449 0.72893
H 3.05448 3.95469 1.07744

――――――――

Title Card Required

――――――――

Symbolic Z-matrix:
Charge = 0 Multiplicity = 1
C 0.60385 -1.13871 -0.01491
H 0.88927 -0.61092 0.90607
H -0.47629 -1.57032 0.28016
H 0.36268 -0.49816 -0.87383
C -3.62774 -2.13253 -0.07839
H -4.30544 -2.15441 -0.93158
H -3.50541 -1.10359 0.26908
H -4.02305 -2.75152 0.72914
O -2.40858 -2.65764 -0.57159
O -1.49012 -2.67206 0.52441
H -0.59133 -3.35643 0.17787
O 1.3941 -2.15481 -0.31207
O 0.48212 -3.78408 -0.17815
H 1.00871 -4.06293 0.58101

Molpro CASPT2 input

Example CASPT2 scan in Molpro

```
***,CH3OOH SCAN CAS calculations
memory,600,m
gprint,orbitals


angstrom
geometry={
c1
o2, c1, rCO
o3, o2, r, c1, aCOO
h4, c1, rCH4, o2, aCO2H4, o3, dH4COO
h5, c1, rCH5, o2, aCO2H5, o3, dH5COO
h6, c1, rCH6, o2, aCO2H6, o3, dH6COO
h7, o3, rOH7, o2, aHOO, c1, dH7OOC
}

rCO=1.4145
r=1.00
rCH4=1.09331
rCH5=1.09068
rCH6=1.09191
rOH7=0.9666
aCOO=106.492
aCO2H4=111.633
aCO2H5=104.677
aCO2H6=111.235
aHOO=100.389
dH4COO=-64.01
dH5COO=177.299
dH6COO=58.983
dH7OOC=116.08
i=0

basis= { default,def2-SVP }
```

```
do i=1,51
rOO(i)=r
{ hf;wf,26,1,0 };
e_hf(i)=energy

Optg;inactive,r

{ mp2;natorb,orbprint };
e_mp2(i)=energy

{multi;closed,7;occ,15;
wf,26,1,0;
wf,26,1,2;
canonical,ci };
e_mcscf0(i)=energy(1)
e_mcscf2(i)=energy(2)

{rs2,NOCHECK;
wf,26,1,0;
wf,26,1,2;
orbital,ignore_Error};
e_pt0(i)=energy(1)
e_pt2(i)=energy(2)

r=r+0.05

enddo

{table,rOO,e_hf,e_mp2,e_mcscf0,e_mcscf2,e_pt0,e_pt2
head,rOO,EHF,EMP,EMCSCFsing,EMCSCFtrip,EPTsing,EPTtrip
save,ROOHfullcanpt-10-8.tab}
```